



Optimization of beta-lactamase inhibitors belonging to the diazabicyclo-octane family and design of a mass spectrometry-based approach for exploring peptidoglycan polymerization

Heiner Atze

► To cite this version:

Heiner Atze. Optimization of beta-lactamase inhibitors belonging to the diazabicyclo-octane family and design of a mass spectrometry-based approach for exploring peptidoglycan polymerization. Biochemistry, Molecular Biology. Sorbonne Université, 2021. English. NNT : 2021SORUS159 . tel-03531105

HAL Id: tel-03531105

<https://theses.hal.science/tel-03531105>

Submitted on 18 Jan 2022

HAL is a multi-disciplinary open access archive for the deposit and dissemination of scientific research documents, whether they are published or not. The documents may come from teaching and research institutions in France or abroad, or from public or private research centers.

L'archive ouverte pluridisciplinaire **HAL**, est destinée au dépôt et à la diffusion de documents scientifiques de niveau recherche, publiés ou non, émanant des établissements d'enseignement et de recherche français ou étrangers, des laboratoires publics ou privés.

Sorbonne Université

Ecole doctorale 515 Complexité du Vivant

Structures Bactériennes Impliquées dans la Modulation
de la Résistance aux Antibiotiques

Centre de Recherche des Cordeliers, UMRS 1138, Equipe 12

**Optimization of β -lactamase inhibitors belonging to the
diazabicyclo-octane family and design of a mass spectrometry-based
approach for exploring peptidoglycan polymerization**

Par **Heiner E. G. Atze**

Thèse de doctorat de Biochimie

Dirigée par Michel Arthur

Présentée et soutenue publiquement le 29 septembre 2021

Devant un jury composé de :

Pr. Alexandra Aubry, Sorbonne Université

Présidente

Dr. Marie-Pierre Chapot-Chartier, Institut Micalis

Rapporteure

Dr. Thierry Touzé, Université Paris Saclay

Rapporteur

Dr. Séverine Zirah, MNHN

Examinatrice

Dr. Michel Arthur, INSERM

Directeur de thèse

Acknowledgements

I would like to start by thanking the members of my jury: Alexandra Aubry, Marie-Pierre Chapot-Chartier, Thierry Touzé, Séverine Zirah, and my doctoral advisor Michel Arthur.

The experiments for this work have been performed from June 2018 to April 2021 in the laboratory of team 12 "Bacterial structures implicated in the modulation of antibiotic resistance" at the Centre de Recherche des Cordeliers in the historic Latin Quarter of Paris where the scholars of the past seem to have passed on their knowledge and some of their furniture.

I thank all the people whom I had the pleasure to work with at my host laboratory. Not to forget our collaborators at the University of Paris - called "the chemists" -, in particular Flavie Bouchet, Laura Iannazzo and Mélanie Ethève-Quelquejeu, Lionel Dubost and Arul Marie at the mass spectrometry platform of the National Museum of Natural History, and Filippo Rusconi (a biochemist turned software developer) whose work inspired me to take a similar path.

Striving for a PhD is challenging by itself, but even more so in a foreign country - as close as it may seem to your home and your beloved ones. When facing the unknown - personally, culturally, professionally, scientifically - what we need most (besides trust in our own instincts and capabilities) is guidance, support, understanding, encouragement and kindness of the people we know and especially of those who we meet on this journey. We learn that the things we need cannot always be found where we are expecting them.

Writing a dissertation means to take inventory of scientific accomplishments and one more time letting pass by the milestones of the last three years: More than once, I was about to quit. More than once I decided to stay - surrounded by supportive, sympathetic and encouraging people. Anne, Lauriane, David, Mathieu, Inès, Delphine, Philipp, Marc, Julia, Sabine, Hilbert, Hartwig, Luise, Lola, Erika, Edeltraut, Gerd.

What more could I say than a heartfelt and humble *Thank you* ?

Remerciements

Je voudrais commencer par remercier les membres de mon jury: Alexandra Aubry, Marie-Pierre Chapot-Chartier, Thierry Touzé, Séverine Zirah et mon directeur de thèse Michel Arthur.

Les expériences de ma thèse ont été réalisées entre juin 2018 et avril 2021 dans le laboratoire d'équipe 12 "Structures bactériennes impliquées dans la modulation de la résistance aux antibiotiques" au Centre de Recherche des Cordeliers situé dans l'historique Quartier Latin de Paris où les savants du passé semblent nous avoir cédé à la fois leur savoir et une partie de leur mobilier.

Je remercie tous les membres du laboratoire avec lesquels j'ai eu le plaisir de travailler. Je remercie également nos collaborateurs à l'Université de Paris - dit "les chimistes" - notamment Flavie Bouchet, Laura Iannazzo et Mélanie Ethève-Quelquejeu, Lionel Dubost et Arul Marie de la plateforme de spectrométrie de masse au Muséum National d'Histoire Naturelle, et Filippo Rusconi (un biochimiste et massiste devenu développeur de logiciels scientifiques) qui m'a inspiré de suivre un parcours similaire.

La poursuite d'une thèse est un défi en soi, encore plus dans un pays étranger - aussi proche qu'il peut paraître de chez soi et ses proches. Quand on fait face à l'inconnu - personnellement, culturellement, professionnellement, scientifiquement - on a le plus besoin des conseils, du soutien, de la compréhension et de la bienveillance des gens qu'on connaît et surtout des gens qu'on rencontre sur ce chemin. On apprend aussi qu'on ne trouve pas forcément ce dont a besoin là où on s'y attendait.

L'écriture du mémoire conduit à faire le bilan des accomplissements scientifiques et de revenir sur les moments clés des dernières trois années : Plus qu'une fois j'ai failli arrêter, plus qu'une fois je suis resté - entouré par des gens à l'écoute qui m'ont soutenu et encouragé. Anne, Lauriane, David, Mathieu, Inès, Delphine, Philipp, Marc, Julia, Sabine, Hilbert, Hartwig, Luise, Lola, Erika, Edeltraut, Gerd.

Qu'est-ce que je pourrais vous dire plus qu'un sincère et humble *Merci* ?

Contents

Abbreviations	iii
List of Figures	iv
List of Tables	v
I Introduction	1
1 Ultrastructure of the cell envelope of Gram-negative bacteria	2
1.1 The outer membrane	2
1.2 The inner membrane	3
1.3 The periplasm	4
2 Peptidoglycan of <i>Escherichia coli</i>	5
2.1 Structure and function	5
2.2 Biosynthesis	7
2.2.1 Precursor biosynthesis	7
2.3 PG polymerisation	8
2.3.1 Periplasmic reactions of PG assembly	8
2.3.2 PG crosslinking enzymes	12
2.3.3 Peptidoglycan hydrolases	15
2.3.4 Spatio-temporal organization of PG synthesis	18
2.4 Recycling and turnover	22
2.5 Diversity of peptidoglycan structure in Gram-positive bacteria	22
3 β-lactam antibiotics	25
3.1 Targets, molecular mode of action and molecular determinants	25
3.2 Structural classes of β -lactam antibiotics	27
3.3 Resistance to β -lactam antibiotics	31
4 β-lactamases	34
4.1 Classification	35
4.2 Serine β -lactamases	36
4.2.1 Characteristic motifs	37
4.2.2 Molecular catalytic mechanism	38

4.3	Metallo β -lactamases	42
4.4	Regulation of chromosomal β -lactamases in Gram-negative bacteria	43
5	β-lactamase inhibitors	47
5.1	Serine β -lactamase inhibitors	47
5.1.1	β -lactam based β -lactamase inhibitors	47
5.1.2	Diazabicyclooctanes	49
5.1.3	Boronic-acid derivatives	53
5.2	Inhibitors of class B β -lactamases	54
II	Optimization of β-lactamase inhibitors belonging to the diazabicyclo-	
	octane family	56
6	Introduction	57
7	Publication I	59
8	Publication II	76
9	Discussion	81
III	Design of a mass-spectrometry-based approach for exploring peptido-	
	glycan polymerization	86
10	Objectives	87
11	Publication III	89
Annex		192
Publication IV		193
References		201

Abbreviations

OM	Outer membrane
IM	Inner membrane
OMP	Outer membrane protein
IMP	Inner membrane protein
LPS	Lipopolysaccharide
PG	Peptidoglycan
GlcNAc	N-Acetylglucoseamine
MurNAc	N-Acetylmuramic acid
Lac	Lactoyl, lactic acid
UDP	Uridine-5'-diphosphate
ESBL	Extended spectrum β -lactamase
BLI	β -lactamase inhibitor
MIC	Minimal inhibitory concentration

Amino acids are indicated using their three letter code preceded by a stereochemical identifier (D/L) where necessary.

List of Figures

1	The bacterial cell envelope	2
2	Strucutre of PG and its subunits; cytoplasmic steps of PG synthesis	5
3	PG polymerization	9
4	Structure of RodA in complex with PBP2	11
5	Transpeptidation by PBPs and LDTs	12
6	Structure of PBP1b of <i>E. coli</i>	13
7	Reaction catalyzed by lytic transglycosylases	16
8	Model for initiation of PG synthesis by PBP2 binding	21
9	Recycling and turnover of 1,6-anhydro-tripeptide	23
10	Examples of modifications in the peptidoglycan of Gram-positive bacteria	24
11	Structure of penicillin G	25
12	Reactions of PBPs with substrate and β -lactam antibiotics	26
13	Comparison of tertiary amide and β -lactam carbonyl groups	27
14	General mechanism for reaction of β -lactams with β -lactamases and PBPs	35
15	Classification of β -lactamases	36
16	Representative structures of β -lactamases	37
17	General mechanism of β -lactam hydrolysis by serine β -lactamases	39
18	Alternative acylation mechanisms in class A β -lactamases	41
19	Deacylation mechanism in class C β -lactamases	42
20	Proposed catalytic mechanism for class D β -lactamases	43
21	Catalytic mechanism of metallo- β -lactamases	44
22	Regulation of chromosomal β -lactamases in Gram-negative bacteria	45
23	Representative structures of β -lactamase inhibitors	48
24	Binding mode of first generation β -lactamase inhibitors	49
25	Formation of various covalent species after β -lactamaseacylation by penam sulfones	50
26	Molecular mechanism for acylation of TEM-1 β -lactamse by avibactam	51
27	Structure of CPD4	53
28	Crystal structure of NDM-1 in complex with a boronic acid inhibitor	54
29	Modeling of non-covalent complexes formed by DBOs and KPC-2	85
30	Models for the insertion of new PG units into the existing PG layer	87

List of Tables

1	Sequences of major muropeptides found in <i>E. coli</i>	7
2	Protein composition of the elongasome and the divisom	19
3	Structural classes of β -lactam antibiotics	28
4	Structural motifs of class A β -lactamases	38
5	Acylation efficacy of triazole-containing DBOs and 2'-amide DBO constitutional isomers in comparison to avibactam	85

Part I

Introduction

"MU-RE-IN!"

- A German Professor

1 Ultrastructure of the cell envelope of Gram-negative bacteria

The envelope of Gram-negative bacteria comprises a complex cell wall located at the surface of the inner membrane. The cell wall includes two main structures, the outer membrane and the peptidoglycan layer (Fig. 1a). The space between the inner and outer membrane, which contains the peptidoglycan layer, is referred to as the periplasm. Due to its structure, the cell wall constitutes a remarkable barrier against physicochemical variations in the external medium, provides the cell with mechanical stability, and enables it to tightly regulate interaction with the environment [Zerbib, 2017].

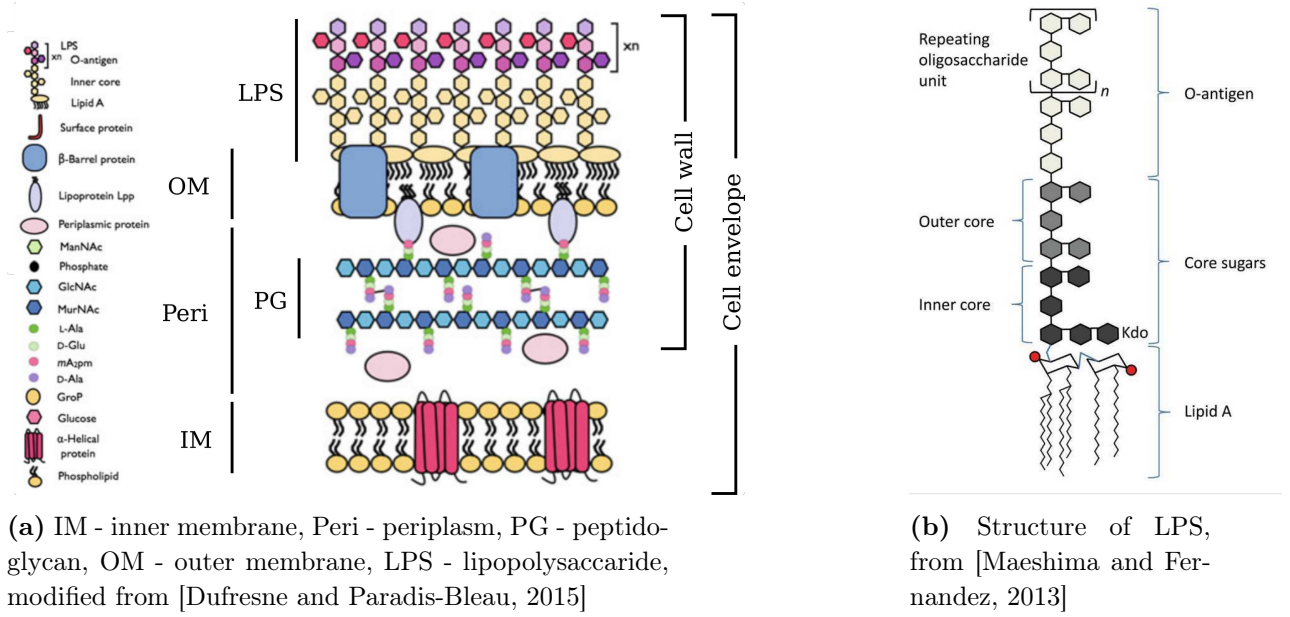


Figure 1: The bacterial cell envelope

1.1 The outer membrane

Lipids. The outer membrane is a distinctive feature of Gram-negative bacteria. It is asymmetric with respect to the lipid composition of its two leaflets. While the inner leaflet contains phospholipids, the outer leaflet is composed of lipopolysaccharide (LPS). This glycolipid is the main determinant of the permeation barrier properties of the cell envelope. Additionally, it is implicated in the host-pathogen interaction as it represents a virulence factor and is detected by the innate immune system [Dufresne and Paradis-Bleau, 2015].

The structure of LPS comprises three domains (Fig. 1b): Lipid A, the oligosaccharide core and the *O*-antigen. The Lipid A moiety consists of a phosphorylated *N*-acetyl-glucosamine disaccharide acylated by up to seven saturated fatty acids at the remaining hydroxyl and amine groups. The aliphatic side-chains, which constitute the outer leaflet of the OM, create a strongly

lipophilic environment exhibiting very low fluidity. This leads to high free energy barriers for penetration of hydrophilic molecules into the OM and to the accumulation of hydrophobic molecules in the outer leaflet [Carpenter et al., 2016].

Lipid A is covalently attached to the oligosaccharide core of LPS. The inner core often contains heptose and deoxy-octose residues and shows high inter-strain and inter-species variability compared to Lipid A. This is even more the case for the outer core (see [Holst, 2007] for review). The distal *O*-antigen is composed of repeating subunits comprising one to six carbohydrate residues. It represents the most variable part of LPS. Its role seems to be mainly protective, assisting the bacterial cell to evade recognition and attack by the host immune system [Raetz and Whitfield, 2002].

Proteins. The majority of proteins associated with the outer membrane are either lipoproteins or integral β -barrel transmembrane proteins [Silhavy et al., 2010]. Lipoproteins are inserted into the inner leaflet of the outer membrane by lipid chains, which are attached via a modification of a conserved cysteine residue [Konovalova and Silhavy, 2015]. The most abundant lipoprotein in *E. coli* is Braun’s Lipoprotein ($\sim 10^6$ copies per cell), Lpp, of which approximately one-third is covalently linked to the peptidoglycan (PG) layer in the periplasm [Braun and Hantke, 2019]. Besides conferring structural stability to the cell envelope, it is implicated in size control of the periplasm [Asmar et al., 2017].

Outer membrane proteins (OMPs) adopt conformations in which β -sheets are arranged into a cylinder that spans the OM. The most abundant OMPs, OmpF and OmpC, form trimeric porins that allow non-specific passive diffusion of small molecules of upto 700 Da, *e.g.* mono- and disaccharides and amino acids into the periplasm. Uptake of larger nutrients such as iron-chelates and vitamins is assured by larger, less abundant porins [Nikaido, 2003]. The predominant paradigm that lipoproteins of the OM exclusively face the periplasm, has been challenged by recent identification of surface exposed lipoproteins, homomeric complexes of lipoproteins and heteromeric complexes between lipoproteins and other outer membrane proteins [Konovalova and Silhavy, 2015].

1.2 The inner membrane

Metabolic functions are located at the inner membrane, similar to organelle membranes of eukaryotic cells. These comprise catabolic and metabolic processes such as protein synthesis and folding, lipid biosynthesis as well as carbohydrate metabolism [Silhavy et al., 2010].

Lipids. In contrary to the outer membrane, the inner membrane is a phospholipid bilayer which contains 75% of phosphatidylethanolamine and 20% of phosphatidylglycerol [Dufresne and Paradis-Bleau, 2015]. Recent results indicate an asymmetric phospholipid distribution between the inner and the outer leaflet in *E. coli* [Bogdanov et al., 2020]. Minor amounts of isoprenoid phosphate carriers found in the IM are implicated in the translocation of hydrophilic metabolites important for envelope biogenesis, *e.g.* peptidoglycan precursors ([Silhavy et al., 2010], see also Section 2.2).

Proteins. Integral membrane proteins are anchored in the IM by their hydrophobic α -helical transmembrane domains (Fig. 1a). Translation is initiated in the cytoplasm. Upon recognition of the highly hydrophobic N-terminus by the signal recognition particle (SRP), the ternary complex of ribosome, oligopeptide chain and SRP binds to FtsY at the inner leaflet of the IM. With the help of the Sec-translocase complex, the nascent peptide chain is inserted into the IM. For a review of the wide variety of functions exerted by inner membrane proteins see [Weiner et al., 2001].

1.3 The periplasm

The periplasm is the space enclosed by the inner and outer membrane (Fig. 1). It is a gel-like matrix due to the high concentration of solutes. A variety of functions are located in the periplasmic space [Miller and Salama, 2018]. Proteins present in the periplasm can be assigned to three functional classes: (i) enzymes implicated in catabolism and detoxification (RNase, alkaline phosphatase, β -lactamases and others [Silhavy et al., 2010]), (ii) chaperones and (iii) high affinity binding proteins facilitating the transport of nutrients to and across the cytoplasmic membrane [Seltmann and Holst, 2002, Zerbib, 2017]. The periplasm is a transit space for lipoproteins and OMPs that are assembled at the cytoplasmic membrane and then translocated to the outer membrane with the help of their chaperones for further processing and membrane insertion [Dalbey and Kuhn, 2012]. Early studies suggested that the outer and inner membranes are connected in defined zones during exponential growth [Bayer, 1968] and recent results imply that sensing of outer membrane damages is mediated by proteins spanning the entire periplasm [Cohen et al., 2017]. The peptidoglycan layer, which is located in the periplasm will be extensively described in chapter 2.

2 Peptidoglycan of *Escherichia coli*

2.1 Structure and function

The peptidoglycan is located between the inner and the outer membrane of diderm bacteria and completely surrounds the bacterial cell. Its width is in the low nanometer range (10 nm or less) [Matias et al., 2003] and by counteracting the enormous internal turgor pressure of the cytoplasm (approximately 3 atm [Cayley et al., 2000]), peptidoglycan ensures the structural integrity and shape of the bacterial cell. Damage to the PG layer, *e.g.* by lysozyme can therefore severely impair growth and survival of cells [Delhaye et al., 2019]. This makes PG an attractive and validated target for antibiotics. Indeed, the β -lactam antibiotics interfere with PG biosynthesis [KONG et al., 2010].

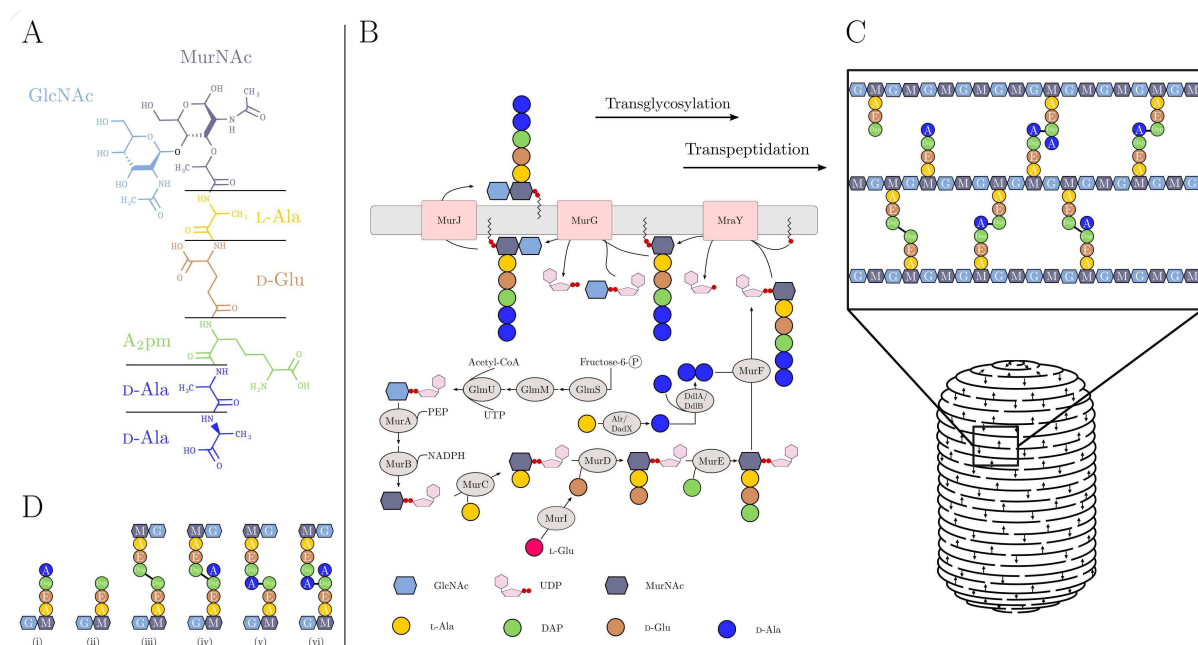


Figure 2: **A** - Structure of GlcNAc-MurNAc-pentapeptide **B** - Schematic representations of mucopeptides commonly found after muramidase treatment of sacculi, (i) Tri, (ii) Tetra, (iii) Tri(3→3)Tri, (iv) Tri(3→3)Tetra, (v) Tetra(4→3)Tri, (vi) Tetra(4→3)Tetra **C** - Cytoplasmic steps of PG precursor synthesis, details see text, adapted from [Dufresne and Paradis-Bleau, 2015] **D** - Schematic representation of the PG layer

Chemical structure. Peptidoglycan contains glycan chains crosslinked by short peptide stems (Fig. 2D). The glycan chains are composed of alternating of *N*-acetylglucosamine (GlcNAc) and *N*-acetylmuramic acid (MurNAc). All glycosidic bonds are β -(1→4). The lengths of glycan chains have a broad distribution, from a few disaccharide subunits (3 to 4) up to a hundred [Vollmer and Bertsche, 2008]. The disaccharide units of adjacent glycan strands are cross-linked via peptide stems which are attached to the lactoyl moiety of MurNAc via their N-terminus.

The pentapeptide stem in Gram-negative bacteria typically consists of L-alanine- γ -D-glutamic acid-2,6-diaminopimelic acid (A₂pm)-D-alanine-D-alanine (Fig. 2A).

Number of layers. Several studies using different biophysical approaches determined the width of peptidoglycan to be between 6 and 7 nm [Vollmer and Seligman, 2010]. However, there is no conclusive evidence as to whether PG is a strictly single-layered or a partially multi-layered structure in *E. coli*: Results from neutron small-angle scattering using purified sacculi are compatible with 20% of PG being triple-layered and the remaining parts monolayered. [Labischinski et al., 1991]. However, another group found no evidence of multi-layered PG from cryo-transmission electron microscopy of frozen-hydrated sections of bacterial cells [Matias et al., 2003].

Glycan strand orientation Another point that has been widely disputed is the orientation of glycan chains with respect to the long axis of the cell and the inner membrane. Elasticity of purified sacculi has been mainly attributed to the peptide stems and was shown to be anisotropic, with facilitated deformability found in the long direction of the cell. Based on these findings, the "layered model of peptidoglycan architecture" suggests that glycan chains are oriented perpendicular to the long cell axis and parallel to the inner membrane. In contrary, the "scaffold model of peptidoglycan architecture" suggests an orientation of glycan chains perpendicular to the inner membrane [Dmitriev et al., 1999]. However, the width of the periplasm was deemed too narrow to accommodate PG chains in a vertical orientation [Vollmer and Bertsche, 2008].

Torsion angle and periodicity of peptide side chains. The conformation of the β -(1 \rightarrow 4)-glycosidic bonds between GlcNAc and MurNAc induces a shifted orientation of peptide-stems with respect to main axis of the glycan strand [Vollmer et al., 2008]. The orientation of the stem is crucial for PG synthesis and architecture. Generally, a periodicity of 90° is assumed, which would lead to every fourth peptide-stem pointing in the same direction [Vollmer et al., 2008], which has been supported by results from molecular modeling [Gumbart et al., 2014]. However, studies based on NMR measurements of a PG fragment comprising two disaccharide-pentapeptide subunits, found a torsion angle of 120° between peptide-stems [Meroueh et al., 2006].

Major muropeptides and cross-link types In general, the muropeptide composition of PG is characterized after digestion of extracted sacculi by muramidases (*e.g.* lysozyme or mutanolysin) and subsequent separation by HPLC [Glauner, 1988]. The obtained muropeptides

Table 1: Sequences of major muropeptides found in *E. coli*, numbering as in Fig. 2D

	Sequence	Abbreviation
(i)	GlcNAc-MurNAc-L-Ala-D-Glu-A ₂ pm	Tri
(ii)	GlcNAc-MurNAc-L-Ala-D-Glu-A ₂ pm-D-Ala	Tetra
(iii)	GlcNAc-MurNAc-L-Ala-D-Glu-A ₂ pm(3→3)A ₂ pm-D-Glu-L-Ala-MurNAc-GlcNAc	Tri-Tri
(iv)	GlcNAc-MurNAc-L-Ala-D-Glu-A ₂ pm(3→3)A ₂ pm(-D-Ala)-D-Glu-L-Ala-MurNAc-GlcNAc	Tri-Tetra
(v)	GlcNAc-MurNAc-L-Ala-D-Glu-A ₂ pm-D-Ala(4→3)A ₂ pm-D-Glu-L-Ala-MurNAc-GlcNAc	Tetra-Tri
(vi)	GlcNAc-MurNAc-L-Ala-D-Glu-A ₂ pm-D-Ala(4→3)A ₂ pm(-D-Ala)-D-Glu-L-Ala-MurNAc-GlcNAc	Tetra-Tetra

can be distinguished into two groups: uncross-linked disaccharide peptide units (*i.e.* monomers, Fig. 2D (i) and (ii)) and cross-linked (*i.e.* dimers, Fig. 2D (iii)-(vi), and less abundant, higher order multimers). Muropeptide dimers are cross-linked via the C-terminal amino acid of a donor stem (D-Ala or A₂pm) and A₂pm of the acceptor stem. Cross-links are referred to as (4→3) in case of D-Ala → A₂pm and (3→3) in case of A₂pm → A₂pm. Major muropeptides are listed in Table 1.

The predominant muropeptides found in PG extracted from *E. coli* are the Tetra monomer (more than 30%) and the Tetra(4→3)Tetra dimer (20%) [Glauner, 1988]. Accordingly, the majority of crosslinks is of the 4→3-type. Relative abundances of muropeptides and relative contributions of crosslink types vary with growth conditions and the metabolic state of the culture (*e.g.* stationary culture or biofilms) with a notable switch towards 3→3-crosslinks (from about 5% to 40%, [unpublished data from the host laboratory]). Of note, a high amount of 3→3-crosslinks is implicated in antibiotic resistance [Hugonnet et al., 2016].

2.2 Biosynthesis

2.2.1 Precursor biosynthesis

PG biosynthesis is a multistep, compartmentalized process. Biosynthesis of the precursor uridine-diphosphate-*N*-acetyl muramic acid (UDP-MurNAc) pentapeptide is located in the cytoplasm (Fig. 2B). Its starting point is the conversion of fructose-6-phosphate into uridine-diphosphate-*N*-acetylglucosamine (UDP-GlcNAc) by the successive actions of the GlmS, GlmM, and GlmU enzymes. Subsequently, MurA catalyzes the addition of enolpyruvate to the 3-hydroxy group of UDP-GlcNAc. This side chain is then reduced by MurB, yielding UDP-MurNAc.

De novo synthesis of the peptide stem involves the addition of L-Ala, D-Glu, A₂pm, and the D-Ala-D-Ala dipeptide to the D-lactoyl moiety of UDP-MurNAc. These sequential reactions are ATP-dependent and are catalyzed by four distinct enzymes: MurC, MurD, MurE and MurF. L-Ala and L-Glu are racemized by Alr or DadX and MurI, respectively. The dipeptide substrate for MurF is provided by two D-Ala:D-Ala ligases DdlA and DdlB (Fig. 2B). Alternatively, the

L-Ala-D-Glu-A₂pm tripeptide issued from existing peptidoglycan can be directly transferred to UDP-MurNAc by Mpl ([Herve et al., 2007], see also section 2.4).

The membrane steps of peptidoglycan synthesis are initiated by the transfer of the phospho-MurNAc-pentapeptide moiety of UDP-MurNAc-pentapeptide to membrane-bound lipid carrier undecaprenylphosphate by MraY affording undecaprenyl-pyrophospho-MurNAc-pentapeptide (Lipid I). In the following, MurG transfers GlcNAc from UDP-GlcNAc to Lipid I resulting in undecaprenyl-pyrophosphate-MurNAc(GlcNAc)-pentapeptide, commonly referred to as Lipid II.

Given the hydrophilic nature of GlcNAc-MurNAc-pentapeptide, translocation over the IM into the periplasm necessitates an auxiliary mechanism. In fact attachment to the lipid carrier is a prerequisite for flipping the PG precursor across the inner membrane. Two proteins have been suggested to have the required flippase activity, FtsW and MurJ. Evidence concerning these two proteins has been controversial: MurJ was suggested as Lipid II flippase in 2008 based on genetic analysis [Ruiz, 2008]. In contrast, results from *in vitro* experiments using fluorescently labeled Lipid II inserted into liposomes argued in favor of FtsW [Mohammadi et al., 2011]. Using a different *in vivo* approach, which involved the *in situ* cleavage of freshly flipped Lipid II in the periplasm by the colicin M phosphatase, led to the conclusion that only MurJ was essential [Sham et al., 2014].

2.3 PG polymerisation

2.3.1 Periplasmic reactions of PG assembly

Following flipping the Lipid II precursor to periplasm, the disaccharide subunit is assembled into peptidoglycan. The periplasmic steps of PG synthesis rely on two major enzymatic processes: (i) transglycosylation for glycan strand elongation and (ii) transpeptidation for cross-linking glycan strand via their peptide stems. While transpeptidation occurs only simultaneously with transglycosylation, the latter can proceed independently. These functions are exerted by interacting monofunctional enzymes and/or bi-functional enzymes. Moreover, a variety of enzymatic activities needs to be coordinated with PG synthesis in order to ensure structural integrity of the cell during expansion of the PG layer upon growth. These comprise endopeptidases, lytic transglycosylases and amidases.

Transglycosylation. Glycosyltransferases (GT) transfer the growing side-chain linked to the lipid carrier by a diphospho bond at its reducing end to a newly translocated Lipid II precursor [Perlstein et al., 2007, Heijenoort, 2001]. This reaction leads to the release of the di-phospho-

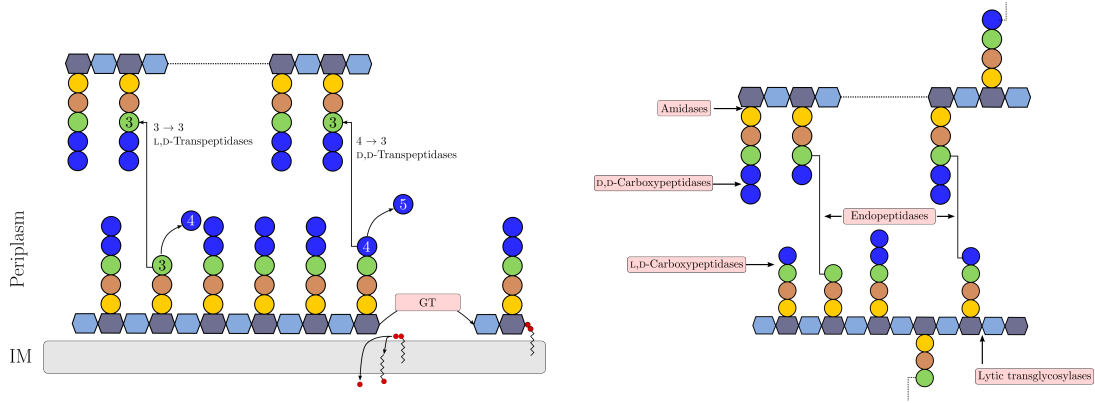


Figure 3: Peptidoglycan polymerization. (A) Glycan chains are polymerized by glycosyltransferases (TG) and cross-linked by transpeptidases of the D,D-, and L,D-specificities that form 4→3 and 3→3 cross-links. (B) Hydrolases involved in peptidoglycan polymerization and maturation.

undecaprenyl lipid carrier and to the addition of one subunit to the growing glycan chain. The reaction proceeds for several rounds yielding a glycan polymer. The polymerization of glycan chains is terminated by lytic glycosyltransferases that release glycan chains by forming an anhydro-MurNAc residue at their reducing end and released of undecaprenyl-pyrophosphate. The released undecaprenyl-pyrophosphate molecules are flipped back into the cytoplasm, dephosphorylated, and the resulting undecaprenyl-phosphate molecules are then available for charging new disaccharide-peptide units by MraY.

GT activity is found in monofunctional glycosyltransferases (MtgA), the SEDS proteins (RodA and FtsW), and the N-terminal domain of bi-functional class A Penicillin Binding Proteins (aPBPs) [Egan et al., 2020]. The catalytic domains of these proteins belong to two families of unrelated enzymes, the Glycosyltransferase 51 (GT51) family and the *Shape-Elongation-Division-Sporulation* (*SEDS*) family.

Glycosyltransferase family 51 (GT51) enzymes. In *E. coli* there are four members of the GT51 family, which contain either a GT51 domain only (MtgA) or a GT51 domain in combination with a penicillin-binding transpeptidase module (PBP1A, PBP1B, PBP1C) (GlycosylTransferase Family 51, n.d.; Lombard et al., 2014). Enzymes capable of polymerizing PG lipid intermediates without simultaneous transpeptidation were reported as early as 1984 [Hara and Suzuki, 1984]. In *E. coli*, the product of the *mtg* locus, MtgA, was identified as a monofunctional glycosyltransferase. It shares high sequence similarity with the transglycosylase domain of the class A PBPs (aPBPs) PBP1a, PBP1b, and PBP1c). Class A PBPs are bi-functional enzymes, which contain an additional penicillin-binding transpeptidase module. In contrast to MtgA, the TG activity of aPBPs is sensitive to inhibition by the phosphoglycolipid-antibiotic moenomycin [Di Berardino et al., 1996]. The low conservation of the sequence of monofunctional

transglycosylases in various species and the absence of phenotypes associated with the deletion of the corresponding genes led to consider that aPBPs are the main transglycosylases. However, the construction of mutants of *Bacillus subtilis*, *Enterococcus faecium*, and *Enterococcus faecalis* that grow in spite of the deletion of all genes encoding GT51-family members [McPherson and Popham, 2003] led to reconsider this conclusion. Experiments performed in *E. coli* [Cho et al., 2016], *Bacillus subtilis* [Meeske et al., 2016], and *P. aeruginosa* [Taguchi et al., 2019] recently led to the proposal that transglycosylation could not only be performed by GT51-family members but also by SEDS proteins.

SEDS proteins RodA, the first member of the SEDS protein family to be identified, had already been identified as an important partner in PG synthesis 35 years ago [Ishino et al., 1986]. Overproduction of bPBP2 and RodA was sufficient to sustain PG synthetic activity in membrane fractions of *E. coli* with other PBPs inhibited by antibiotics. However, the glycosyltransferase activity was attributed to bPBP2 in light of what was known about PBPs at that time. Both RodA and FtsW, another member of the SEDS family, have recently been extensively purified and shown to display glycosyltransferase activity [Taguchi et al., 2019, Cho et al., 2016, Meeske et al., 2016]. Together with their respective cognate transpeptidase partner (PBP2 for RodA and PBP3 for FtsW), they provide the core synthetic activity in multi-enzyme complexes responsible for PG synthesis during cell elongation (RodA/PBP2) and division (FtsW/PBP3). Deletion of either gene is associated with phenotypes that resemble depletion of the respective bPBP partner: round cells upon depletion of RodA or PBP2, [Matsuzawa et al., 1973, Spratt, 1975] and filamentous growth upon depletion of FtsW or PBP3 [Boyle et al., 1997, Spratt, 1975]. Enzymatic activity of RodA and FtsW resembles that of GT51-domain containing enzymes, *i.e.* they elongate nascent glycan strands at the reducing end [Welsh et al., 2019]. As for MtgA, the GTase activity of RodA and FtsW is not sensitive to inhibition by moenomycin [Taguchi et al., 2019, Meeske et al., 2016]. SEDS proteins are more conserved than aPBPs over a variety of species [Meeske et al., 2016]. GTase activity of RodA and FtsW is dependent on the presence of their cognate bPBP partner [Taguchi et al., 2019, Sjødt et al., 2020].

The structure of RodA has recently been elucidated, both alone [Sjødt et al., 2018] and in complex with PBP2 (Fig. 4A), [Sjødt et al., 2020]. Both studies were performed using proteins from *Thermus thermophilus*. RodA is embedded in the inner membrane via its α -helical transmembrane domains. Interaction with PBP2 is mediated via transmembrane (TM) domains 8 and 9 of RodA and TM domain of PBP2 (Fig. 4B Interface I), as well as the extracellular loop 4 (ECL4) of RodA and the pedestal domain of PBP2 (Fig. 4B Interface II). Upon complex formation, structural shifts in RodA lead to opening of a cavity that is sufficiently

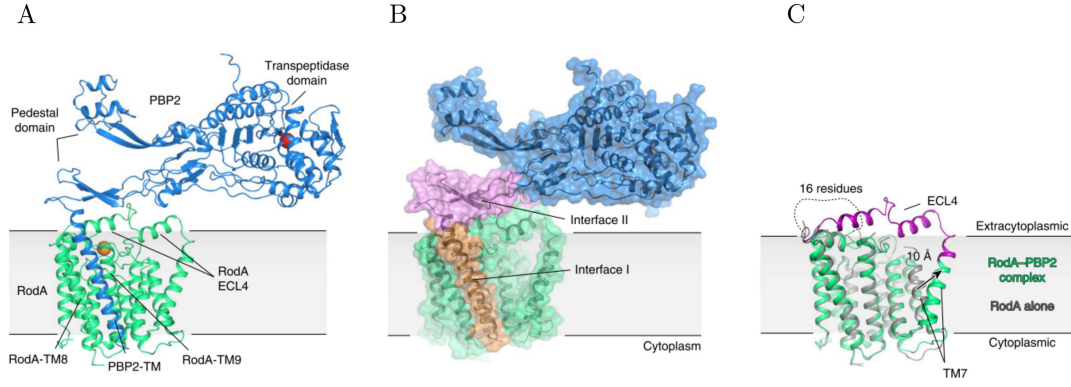


Figure 4: Structure of RodA in complex with PBP2. (A) Structure of the RodA–PBP2 complex viewed parallel to the membrane plane. The active site residue (Ser308) in the transpeptidase domain of PBP2 and Asp255 in RodA are shown as red and orange spheres, respectively. (B) Surface view showing two distinct interfaces. Interface I (orange) is within the membrane plane, while interface II (pink) lies above the membrane (C) Comparison of the structure of RodA in isolation (PDB code: 6BAR; grey) and RodA in complex with PBP2 (green); adapted from [Sjodt et al., 2020]

large to accommodate a Lipid II molecule (Fig. 4C).

Transpeptidation. The majority of peptide cross-links is formed by D,D-transpeptidases, resulting in cross-links of the 4→3-type (Fig. 5A). The only accepted donor substrate in this reaction is a pentapeptide, as the energy released during cleavage of the terminal D-Ala⁴-D-Ala⁵ bond drives the formation of the crosslink. Requirements for the acceptor substrate are less strict, as tri-, tetra-, and pentapeptide stems can be utilized. The first step in the transpeptidation reaction is a nucleophilic attack of the active site serine on the carbonyl carbon of D-Ala⁴, leading to formation of an acylenzyme intermediate and the release of D-Ala⁵. The reaction proceeds via nucleophilic attack on the ester bond of the acyl enzyme by the free amino group of A₂pm in the acceptor peptide stem. This leads to the release of the cross-linked dimer and the free-enzyme. D,D-transpeptidases are the targets of the β -lactam antibiotics and thus referred to as penicillin binding protein or PBPs.

Formation of 3→3-cross-links is catalyzed by a structurally unrelated group of enzymes, the L,D-transpeptidases (Fig. 5B). This family of enzymes has been characterized in the early 2000s, providing the rationale for 3→3-cross-links, that had already been detected in small amounts by chemical analyses [Glauner, 1988]. L,D-transpeptidases are dependent on available tetrapeptide stems as donor substrate and exert their catalytic function via a cysteine residue.

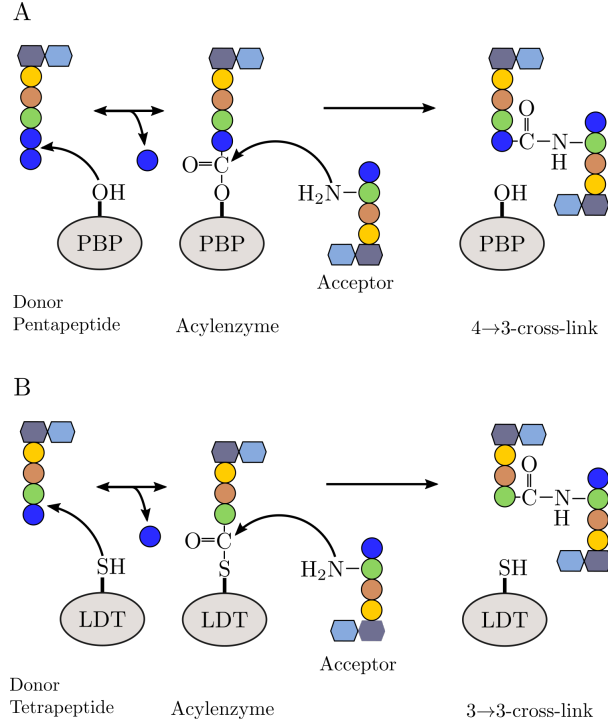


Figure 5: Transpeptidation reaction catalyzed by PBPs (A) and L,D-transpeptidases (B).

2.3.2 PG crosslinking enzymes

PBPs. *E. coli* contains a total of 13 PBPs grouped into class A, class B, and class C [Sauvage et al., 2008, Dik et al., 2018]. Class A and class B comprise peptidoglycan synthetases, while the class C PBPs are implicated in PG remodeling and recycling (see section 2.3.3).

Class A PBPs, also referred to as aPBPs. The three class A PBPs of *E. coli* are bi-functional enzymes, exerting both glycosyltransferase and transpeptidase activity. aPBPs are peripheral membrane proteins anchored to the inner membrane by an N-terminal transmembrane helix (Fig. 6). The N-terminal GT51-domain is located in proximity to the membrane anchor and is connected to the C-terminal TP-domain via a linker region. Additionally, small non-catalytic domains (ODD in PBP1a, UB2H in PBP1b), located between the GT and TP domain, bind to the cognate lipoprotein regulators LpoA and LpoB, respectively.

LpoA stimulates the transpeptidase activity of PBP1a. However, structural insights into the interaction of the two proteins as well as mechanistic understanding is lacking as of today. The picture is different for PBP1b and LpoB. LpoB is a lipoprotein, that protrudes from the inner leaflet of the outer membrane into the periplasm. Interaction occurs via the globular C-terminal domain of LpoB and the UB2H domain of PBP1b. This induces conformational changes in the regulatory domain that transduce to both the GT and TP domains of PBP1b, thereby enhancing both enzymatic activities. CpoB is a modulator of PBP1b regulation by LpoB [Gray et al., 2015],

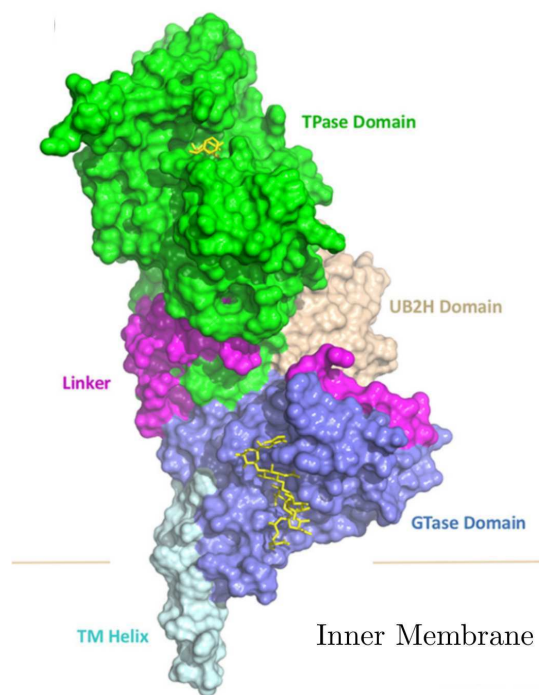


Figure 6: Structure of PBP1b of *E. coli*. The structure of PBP1B is shown in surface representation. The transmembrane (TM) helix, the glycosyltransferase (GTase) domain, the linker, the UB2H domain, and the transpeptidase (TPase) domain are colored cyan, beige, blue, pink, and green, respectively. Moenomycin and ampicillin are shown as yellow sticks in the GTase and TPase domains, respectively. From [King et al., 2017b]

by selectively abolishing LpoB mediated enhancement of the TP activity of PBP1b. Amongst others, CpoB mediates coordination of PBP1b activity with the outer-membrane constriction machinery during cell division [Egan et al., 2020]. Further protein-protein-interactions of PBP1b with other PG synthases and regulatory proteins, especially during cell division will be discussed in section 2.3.4.

The cellular role of the third class A PBP, PBP1c, remains elusive [Schiffer and Höltje, 1999], PBP1a and PBP1b are responsible for a substantial part of PG synthesis. Either PBP1a or PBP1b is necessary for cell viability, while PBP1c is dispensable for normal growth [Schiffer and Höltje, 1999]. PBP1a and PBP1b are able to substitute for each other [Yousif et al., 1985, Derouaux et al., 2008], with certain growth conditions requiring expression of specific class A PBP, *e.g.* PBP1a in alkaline pH and PBP1b in acidic pH [Delhaye et al., 2019].

Class B PBPs, also referred to as bPBPs. Class B PBPs are monofunctional enzymes containing a C-terminal transpeptidase domain [Sauvage et al., 2008]. No enzymatic activity has been described for the N-terminal domain of class B PBPs so far. This domain has been proposed to be important for protein-protein-interactions [Höltje, 1998], an idea corroborated by the most recent elucidation of the structure of the PBP2/RodA complex [Sjodt et al., 2020]. The N-terminal transmembrane helix serves as membrane anchor and the adjacent pedestal domain mediates interaction with its glycosyltransferase partner RodA. *E. coli* expresses two class B PBPs: PBP2 and PBP3, which are the main transpeptidases during lateral growth and cell division, respectively [Zhao et al., 2017]. Accordingly, inhibition or depletion of PBP2 and PBP3 is associated with distinct phenotypes: insufficient PBP2 activity causes cells to grow spherically while PBP3 inhibition or depletion leads to filamentation due to the inability of cells to divide [Spratt, 1975].

LDTs. Historically, L,D-transpeptidases (LDTs) were first identified in an ampicillin-resistant strain of *Enterococcus faecium* whose peptidoglycan was shown to exclusively contain 3→3-cross-links [Mainardi et al., 2005]. This strain relied solely on its L,D-transpeptidase for PG cross-linking, accounting for ampicillin resistance since the enzyme is not inhibited by the drug. LDTs are structurally unrelated to PBPs and are insensitive to inhibition by all classes of β -lactams except the carbapenems.

The genome of *E.coli* contains genes encoding six LDT paralogues: ErfK (LdtA), YbiS (LdtB), YcfS (LdtC), YcbB (LdtD), YnhG (LdtE), and YafK (LdtF). ErfK, YcfS and YbiS attach the Braun lipoprotein (Lpp) to peptidoglycan. Attachment occurs via linking A₂pm of a donor peptide to the ϵ -amino group of Lys58 of Lpp [Magnet et al., 2007]. The activity of

these three proteins is redundant and simultaneous deletion of all three genes causes phenotypes resembling deletion of *lpp*, with an impaired barrier function of the outer membrane [Sanders and Pavelka, 2013].

YcbB and YnhG catalyze formation of 3→3 cross-links [Magnet et al., 2008]. The increase in the proportion of 3→3-cross-links upon change from the exponential to the stationary phase of growth implies a role of the two proteins mainly in the stationary phase. Both proteins are non-essential and deletions are not associated with any particular phenotype during growth in laboratory conditions [Sanders and Pavelka, 2013]. Recently it has been shown that YcbB (but not YnhG) is able to confer resistance to β -lactams upon overproduction of the enzyme and the (p)pGpp alarmone. In the presence of otherwise lethal doses of ampicillin YcbB completely bypasses PBPs for peptidoglycan cross-linking [Hugonnet et al., 2016]. This particular phenotype requires constitutive synthesis of the (p)pGpp, the alarmone inducing the stringent response. The phenotype also depends on the transpeptidase activity of YcbB, the glycosyltransferase activity of PBP1b, and D,D-carboxypeptidase activity of PBP5. PBP5 is essential as it catalyzes the formation of tetrapeptide stems required by YcbB for L,D-transpeptidation. Furthermore, the Cpx-mediated cell envelope stress response involves upregulation of the *ldtD* gene (coding for YcbB) [Morè et al., 2019]. The entry into the stationary phase is accompanied by expression of the *ldtE* and *ldtF* genes. When outer membrane assembly is impaired, *ldtD*, *ldtE*, and *ldtF* become essential [Morè et al., 2019].

2.3.3 Peptidoglycan hydrolases

PG synthesis is carried out in tight coordination with altering the structure of the already existing peptidoglycan. This ensures orderly insertion of new material into the sacculus. These alterations are catalyzed by a variety of enzymes, which are also involved in autolysis, maturation, and turnover, and recycling of PG. PG hydrolases are grouped according to the bond they cleave into *N*-acetylmuramoyl-L-alanine amidases, carboxypeptidases, endopeptidases, and lytic transglycosylases (Fig. 3).

Amidases. Amidases catalyze the cleavage of the amide bond connecting the D-Lac moiety of MurNAc and L-Ala¹, thereby removing the peptide stems from the glycan strands. *E. coli* contains five amidases: AmiA, AmiB, AmiC, AmpD, and AmiD. The first three enzymes selectively cleave peptide stems off MurNAc substrates while AmpD and AmiD also process 1,6-anhydro-MurNAc-containing substrates (issued from the activity of lytic transglycosylases, see below) [Vollmer and Bertsche, 2008]. The released tri-, tetra-, or pentapeptide stems are either released to the culture medium or reimported into the cytoplasm via the Mpp/Opp system (see also

2.4). AmiA, AmiB, and AmiC are periplasmic enzymes, AmiD is a lipoprotein anchored into the inner leaflet of the outer membrane, and AmpD is located in the cytoplasm. During cell division, AmiA and AmiB are recruited to the division site, while AmiC stays dispersed over the entire periplasm. However, construction of all combinations of double deletions in the genes encoding AmiA, AmiB, and AmiC showed that each of these three enzymes can compensate for the absence of the other two. The triple mutant $\Delta amiABC$ grows as chains of bacteria, highlighting the role of the three amidases in daughter cell separation after the completion of septum synthesis [Heidrich et al., 2001]. Periplasmic amidases are regulated by the outer membrane lipoproteins EnvC (AmiA and AmiB) [Uehara et al., 2010] and NlpD (AmiC) [Uehara et al., 2010].

AmpD is a cytoplasmic amidase that selectively cleaves peptide stems off 1,6-anhydro-MurNAc containing muropeptides (mono- and disaccharide peptide units) after their reimport into the cytoplasm. Accordingly, inactivation of *ampD* results in the accumulation of recycled muropeptides [Uehara and Park, 2008]. The products of the reaction catalyzed by AmpD, free peptide stems and amino-mono- and disaccharides, are further metabolized and can re-enter the synthesis of PG precursors (see also 2.4).

AmiD is a homologue of AmpD acting on peptidoglycan and muropeptides in the periplasm. This enzyme acts on muropeptides with and without 1,6-anhydro-MurNAc residues as well as intact peptidoglycan. The amidase activity of AmiD is not required for cell division [Park and Uehara, 2008].

Lytic transglycosylases. Lytic transglycosylases (LTs) are *N*-acetylmuramidases that catalyze the cleavage of the β -1,4-glycosidic bond between MurNAc and GlcNAc units. During the reaction, LTs perform an intramolecular glycosyl transfer linking C₁ and C₆ of MurNAc, which yields 1,6-anhydro-MurNAc at the reducing end of glycan chains [van Heijenoort, 2011] (Fig 7).

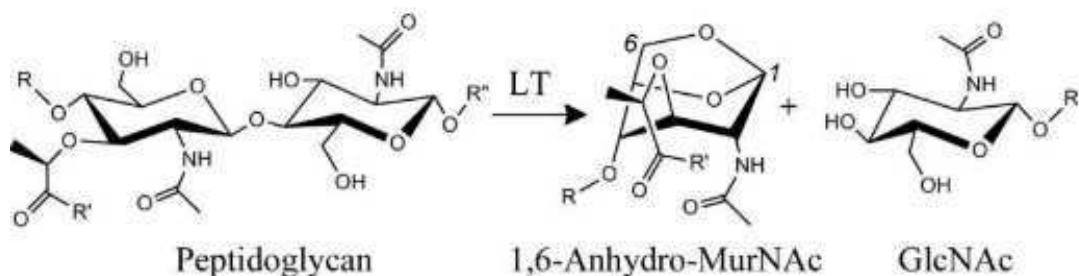


Figure 7: LTs catalyze the cleavage of the β -1,4-glycosidic bonds between MurNAc and GlcNAc residues in PG, with the concomitant formation of a 1,6-anhydro-MurNAc residue, from [Madoori and Thunnissen, 2010]

Hydrolysis can take place either at the end of glycan strands (exolytic activity) or within the polymer (endolytic activity). *E. coli* contains a total of eight lytic transglycosylases (MltA-MltG and SltY). SltY is a soluble enzyme located in the periplasm (hence the name Soluble Lytic Transglycosolase). The remaining LTs are either lipoproteins anchored to the outer membrane (MltA-F) or α -helical proteins bound to the outer leaflet of the inner membrane (MltG) [Alcorlo et al., 2017, Yunck et al., 2016]. LTs exert redundant activities, a mutant deficient in six of the eight enzymes is viable but grows in chains of unseparated cells, indicating impaired daughter cell separation [Heidrich et al., 2002]. *In vitro* characterization using digestion of purified sacculi by LTs revealed exolytic activity for all LTs and additional endolytic activity for MltE and MltG [Lee et al., 2013, Yunck et al., 2016]. SltY is a target of the antibiotic bulgecin [Templin et al., 1992]. In cells challenged with mecillinam, a β -lactam specifically active on PBP2, SltY is responsible for hydrolyzing uncrosslinked glycan strands resulting from a futile cycle of PG synthesis [Cho et al., 2014]. Inactivation of SltY induces hypersensitivity to mecillinam [Templin et al., 1992]. In affinity chromatography experiments using immobilized SltY, PG synthases PBP1b, PBP1c, PBP2, and PBP3, as well as the endopeptidase PBP7 were identified as binding partners of SltY [von Rechenberg et al., 1996].

Endopeptidases. Endopeptidases cleave peptide cross-links in the peptidoglycan layer (Fig. 3). PBP4, PBP7, and AmpH are penicillin-binding proteins that specifically cleave 4 \rightarrow 3 crosslinks. MepA, MepH, MepK, MepM, and MepS are penicillin-insensitive enzymes that cleave both 4 \rightarrow 3 and 3 \rightarrow 3-crosslinks. Single mutants of these proteins are not associated with any particular phenotype. PBP4, PBP7, AmpH, and MepA are soluble periplasmic proteins. Except PBP7, which does not hydrolyze soluble mucopeptides, these four proteins act on both intact sacculi and purified mucopeptides. In addition to D,D-endopeptidase activity, PBP4 and AmpH display D,D-carboxypeptidase activity.

Simultaneous deletion of MepA, PBP4, and PBP7 aggravates the filamentous phenotype associated with triple amidase deletion [Heidrich et al., 2002]. MepS, MepM, and MepH are redundantly essential meaning that deletion of all three genes causes cells to lyse [Singh et al., 2012]. Several endopeptidases have been described to interact with the outer-membrane-anchored protein NlpI [Banzhaf et al., 2020]. NlpI delivers MepS to the periplasmic protease Prc for degradation, while interaction with PBP4, PBP7 and MepM does not alter abundance of these endopeptidases. NlpI has been suggested to serve as an adaptor protein promoting the localization of endopeptidases to the cell elongation machinery [Egan et al., 2020]. Recently, MepK has been identified as a new L,D-endopeptidase in *E. coli* which is essential for cell viability when the L,D-transpeptidase YcbB is overproduced [Chodiseti and Reddy, 2019].

Carboxypeptidases. Carboxypeptidases cleave the C-terminal amino acid off free peptide stems (Fig. 3). The substrates are pentapeptides for D,D-carboxypeptidases and tetrapeptides for L,D-carboxypeptidases. Both groups of enzymes release D-Ala. In *E. coli*, six D,D-carboxypeptidases have been described so far - PBP4, PBP4b, PBP5, PBP6, PBP6b and AmpH, some of which also show D,D-endopeptidase activity (PBP4 and AmpH). The main D,D-carboxypeptidase of *E. coli* is the class C PBP5. PBP5 is anchored to the outer leaflet of the cytoplasmic membrane via its C-terminal helix. Albeit PBP5 not being essential, inactivation leads to aberrant cell morphology and to an accumulation of pentapeptide subunits in the PG. This indicates a role of PBP5 in regulating the amount of available pentapeptide stems for D,D-transpeptidation by PBPs. Overproduction of PBP5 is lethal and associated with round cell shape before lysis. When the PBP pathway for PG crosslinking is bypassed by overproduction of YcbB in the presence of ampicillin, PBP5 becomes essential for providing tetrapeptide stems for L,D-transpeptidation [Hugonnet et al., 2016]. PBP5 is found in sites of ongoing PG synthesis, during both cell elongation and division. This localization depends on the amphiphatic C-terminal helix of the protein [Potluri et al., 2010].

L,D-carboxypeptidase activity has been described for two proteins, YcbB [Hugonnet et al., 2016] and LdcA [Templin et al., 1999]. LdcA is a cytoplasmic enzyme, which is involved in processing recycled muropeptides (see section 2.4). The cellular role of the L,D-carboxypeptidase activity of YcbB is not known.

2.3.4 Spatio-temporal organization of PG synthesis

The cell cycle of *E. coli* proceeds via two main phases, cell elongation and cell division. For both phases it has been suggested, that the necessary synthetic and hydrolytic enzymatic activities for PG synthesis are provided by multi-protein complexes [Höltje, 1998]: the elongasome for elongation and the divisome for division. According to recent results from studies using single-molecule-tracking of putative components of the suggested complexes, these complexes have to be more thought of as groups of proteins that are functionally dependent, rather than complexes. Direct interactions do occur but may be transient.

The elongasome and the divisome are constituted by proteins with largely equivalent functions (see Table 2). Both contain a cytoskeletal protein, PBPs with transpeptidase and/or glycosyltransferase activity and the cognate SEDS partners of the respective bPBPs with glycosyltransferase activity. Besides these core functions, regulatory and adaptor proteins control and direct the synthetic activities from the cytoplasm, the periplasm, and the outer membrane (for example LpoA and LpoB which control the activities of PBP1a and PBP1b).

Table 2: Protein composition of the elongasome and the divisome

Role	Elongasome	Divisome
Cytoskeletal protein	MreB	FtsZ
Transpeptidase	PBP2, PBP1a(TPase)	PBP3, PBP1b(TPase)
Glycosyltransferase	RodA, PBP1a(GTase)	FtsW, PBP1b(GTase)
Class A PBP regulator	LpoA	LpoB

Elongasome. The cytoskeletal protein associated with insertion of new PG subunits into the lateral wall of rod shaped bacteria during elongation is the actin-homologue MreB [Egan et al., 2020]. MreB polymerization depends on ATP and yields double antiparallel filaments [van den Ent et al., 2014]. Polymerization takes place at the inner leaflet of the cytoplasmic membrane and localization was described to depend on membrane curvature [Garner et al., 2011], a view that was questioned by a recent study [Ozbaykal et al., 2020], that attributed correlations between MreB localization and curvature to persistent motion of MreB. Membrane interaction of MreB is mediated by its N-terminal amphiphatic helix [Salje et al., 2011]. Monomers of MreB are found throughout the cytoplasm, but the lipid composition of cell poles (enriched in cardiolipin and phosphatidylglycerol) prevents polymerization, which is thus restricted to the cylindrical part of the cell wall [Kawazura et al., 2017]. MreB polymerization can be inhibited by A22 which competes for the ATP binding pocket. Inhibition results in homogenous distribution of MreB in the cytoplasm and eventually in a spherical cell phenotype, similar to *mreB* deletion [Kruse et al., 2005]. Early localization studies found MreB in static helical structures spanning the whole cylindrical part of the cell [Shih et al., 2003]. However, techniques enabling higher resolution imaging revealed that MreB filaments were not continuous over the entire circumference of the cell. The MreB filaments moved circumferentially around the cylindrical part of the cell in arc-like patches [van Teeffelen et al., 2011]. This motion depended on the transpeptidase activity of PBP2 but was independent of the enzymatic activity of class A PBPs [Cho et al., 2016]. MreB interacts with the membrane associated proteins MreC and MreD. MreC interacts with PBP2 and induces conformational changes which putatively regulate the transpeptidase activity of PBP2 [Rohs et al., 2018]. MreD also interacts with PBP2, but its role in cell elongation is unknown [Egan et al., 2020]. Another binding partner of MreB is RodZ, a transmembrane protein mediating interactions of MreB with RodA, PBP2, PBP1a, and PBP1b [Egan et al., 2020]. RodZ exhibits motion similar to MreB and is essential for proper cell shape in *E. coli*. The absence of RodZ diminishes MreB circumferential motion and results in spherical cells [Morgenstein et al., 2015]. Deletions of *mreCD* or *rodZ* can be compensated for by mutations in PBP2, RodA, or MreB [Shiomi et al., 2013]. Together with sustained elongation in the absence of a class A PBP (albeit at approx. 20% activity) [Cho et al., 2016], these findings emphasize

the core roles of RodA, PBP2, MreB in the elongasome.

A generally accepted model for elongation suggested that MreB is the pedestal protein for the remaining proteins of the elongasome thereby determining the localization of the enzymatic activities of aPBPs and bPBPs [Zhao et al., 2017]. As mentioned above, this view has been questioned by numerous studies, which investigated the motions of putative members of the elongasome by single-molecule imaging of fluorescent fusion constructs. Class A PBPs show a bimodal motion pattern in *B. subtilis*, with one subpopulation engaged in free two-dimensional diffusion in the membrane and another subpopulation engaged in directed motion at a speed an order of magnitude lower [Cho et al., 2016]. The motion of aPBPs was reported not to overlap with those of MreB or RodA/PBP2, indicating that class A PBPs activities are spatially independent of the core proteins of the elongasome. However, another study identified a MreB subpopulation showing diffusive motion similar to that of class A PBPs [Billaudeau et al., 2017], raising to possibility of direct association of MreB and class A PBPs. Of note, there has been evidence of such an association using bacterial two-hybrid and protein pull-down assays [Kawai et al., 2009]. Seemingly contradictory results have been obtained concerning the trajectories of MreB and RodA/PBP2: Cho *et al.* found similar trajectories for the three proteins [Cho et al., 2016], while a previous study revealed differences in the velocities of MreB and PBP2 [Lee et al., 2014]. In line with the findings from [Lee et al., 2014], a subpopulation of PBP2 showed immobile behaviour [Ozbaykal et al., 2020]. The authors concluded that the latter PBP2 subpopulation was bound to PG either directly or through an unknown binding partner. Binding occurred independently from MreB. Immobile PBP2 molecules transitioned to a state of persistent motion whose trajectories overlapped with those of MreB. Based on these results, the authors suggested that the first step in initiation of PG synthesis is binding of PBP2 to a target site of unknown nature, which is followed by association with MreB and subsequent PG synthesis [Ozbaykal et al., 2020].

Divisome. Formation of the septum involves at least 30 proteins of which 12 are essential or conditionally essential: FtsZ, FtsA, ZipA, FtsE, FtsX, FtsK, FtsQ, FtsL, FtsB, FtsW, FtsI (PBP3) and FtsN [Du and Lutkenhaus, 2017]. FtsZ is a tubulin homologue which relies on GTP hydrolysis for polymerization. FtsZ filaments adopt curved conformations and are attached to the inner leaflet of the cytoplasmic membrane by the proteins FtsA and ZipA [Pazos and Peters, 2019]. Similar to MreB, results from early studies using immunostaining techniques led to the conclusion that FtsZ forms a continuous ring-like structure located at future division sites. Higher resolution imaging revealed that FtsZ assembles into short filaments, which use treadmilling for circumferential inward motion. The motion of FtsZ is independent of PG

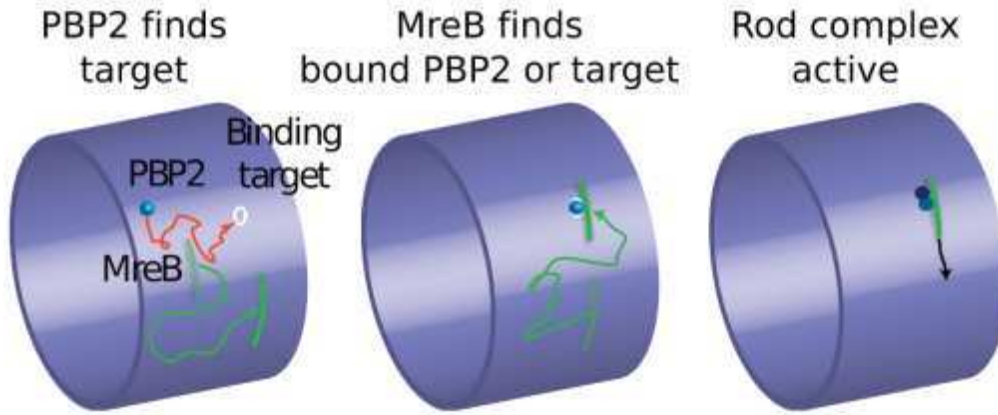


Figure 8: Model for initiation of PG synthesis by PBP2 binding, from [Ozbaykal et al., 2020]

synthesis [Yang et al., 2017]. However, FtsZ motion alone is not sufficient to initiate membrane constriction in the absence of cell wall synthesis [Daley et al., 2016].

Divisome assembly in *E. coli* proceeds in two phases. Proteins that are recruited to midcell early during division include FtsZ, FtsA, ZipA, ZapA-D, and FtsEX. Localization of these proteins occurs before any constriction is visible and coincides with so-called preseptal PG synthesis [Egan and Vollmer, 2013]. Preseptal PG synthesis was first detected in synchronized cells with inactivated PBP3 (hence the synonym PBP3-Independent-Peptidoglycan-Synthesis or PIPS for short) [Wientjes and Nanninga, 1989]. While the cells were not able to complete septation and thus grew as filaments, constriction was clearly visible. Autoradiography revealed a high level of incorporation of [^3H]DAP into PG at the constriction sites. These results were markedly different from studies using cells which were conditionally deficient in cell division due to expression of a temperature sensitive FtsZ mutant [WOLDRINGH et al., 1987]. Cells labeled after culture at the restrictive temperature, showed a diffuse pattern of [^3H]DAP incorporation. Other imaging based on the exchange of D-Ala by D-Cys, subsequent biotinylation of the Cys residues and subsequent immunolabeling showed that synthesis of preseptal PG depends upon FtsZ but not upon PBP3 [de Pedro et al., 1997, Varma et al., 2007], in agreement with the early studies mentioned above [Wientjes and Nanninga, 1989]. Besides FtsZ, only the enzymatic activities of a class A PBP and the presence of ZipA are essential for PIPS [Potluri et al., 2012]. ZipA is a transmembrane protein spanning the cytoplasmic membrane and mediating interactions of the FtsZ ring with periplasmic components of the divisome, *e.g.* PBP1b. Maturation of the divisome is marked by arrival of another set of proteins: FtsK, FtsQ, FtsL, FtsB, FtsW, PBP3 (FtsI), PBP1b, and FtsN (for an extensive review of protein-protein interactions between divisome components see [Egan and Vollmer, 2013]). The trimeric complex FtsQLB

exerts inhibitory effects on the glycosyltransferase activity of PBP1b and the transpeptidase activity of PBP3. Eventually, the late arrival of FtsN overrides inhibition of PBPs by FtsQLB and triggers septation [Egan et al., 2020]. FtsZ filaments disassemble before septum completion [Söderström et al., 2014], while FtsN and PBP3 do not leave the division site until completion of septum synthesis [Söderström et al., 2016]. The activity of PBP3 is necessary for septum closure [Coltharp et al., 2016]. Of the three amidases of *E. coli* only AmiB and AmiC are implicated directly in cell division. The two amidases and their respective regulator proteins (EnvC for AmiB, NlpD for AmiC) are recruited independently to the division site. Arrival of AmiB and NlpD depends on FtsN [Peters et al., 2011]. Localisation of EnvC is coordinated by FtsE and FtsX [Yang et al., 2011].

2.4 Recycling and turnover

Peptidoglycan turnover is defined as loss of peptide stems into the culture medium and recycling refers to a process during which muropeptides are reimported into the cytoplasm where they reenter into biosynthesis of the cytoplasmic peptidoglycan precursors (Fig. 9). Lytic transglycosylases hydrolyse glycan strands from their reducing end yielding mainly disaccharide tripeptide units containing a 1,6-anhydro-MurNAc residue. The main permease implicated in PG recycling is AmpG. In the cytoplasm, the anhydro muropeptides are processed by the glucosaminidase NagZ and the amidase AmpD resulting in free tripeptide stems and aminosugars. The tripeptide stem is used in PG precursor synthesis without further processing. The anhydro-MurNAc units undergo several metabolic reactions before they reenter PG precursor synthesis [Johnson et al., 2013].

2.5 Diversity of peptidoglycan structure in Gram-positive bacteria

The peptidoglycan of Gram-positive bacteria shows marked differences compared to that of Gram-negative bacteria. In contrary to Gram-negative bacteria, there is a large variability in the amino acid composition of the stem peptides [Quintela et al., 1995] (Fig. 10). Amidation of carboxyl groups is a common chemical modification, as found for example for DAP residues in *B. subtilis* and D-iGlu residues in *S. aureus* [Pazos and Peters, 2019].

The peptide stems of Gram-positive bacteria generally contain a lysine residue at position 3 of the peptide stems, which often bears an additional side-chain linked to its ϵ -amino group. The N-terminus of this side-chain acts as an acyl-acceptor in the cross-linking reaction. The peptidoglycan of *S. aureus* contains penta-glycine interpeptide bridges, which are added to intracellular PG precursors by the successive actions of the transferases FmhB, FemA, and

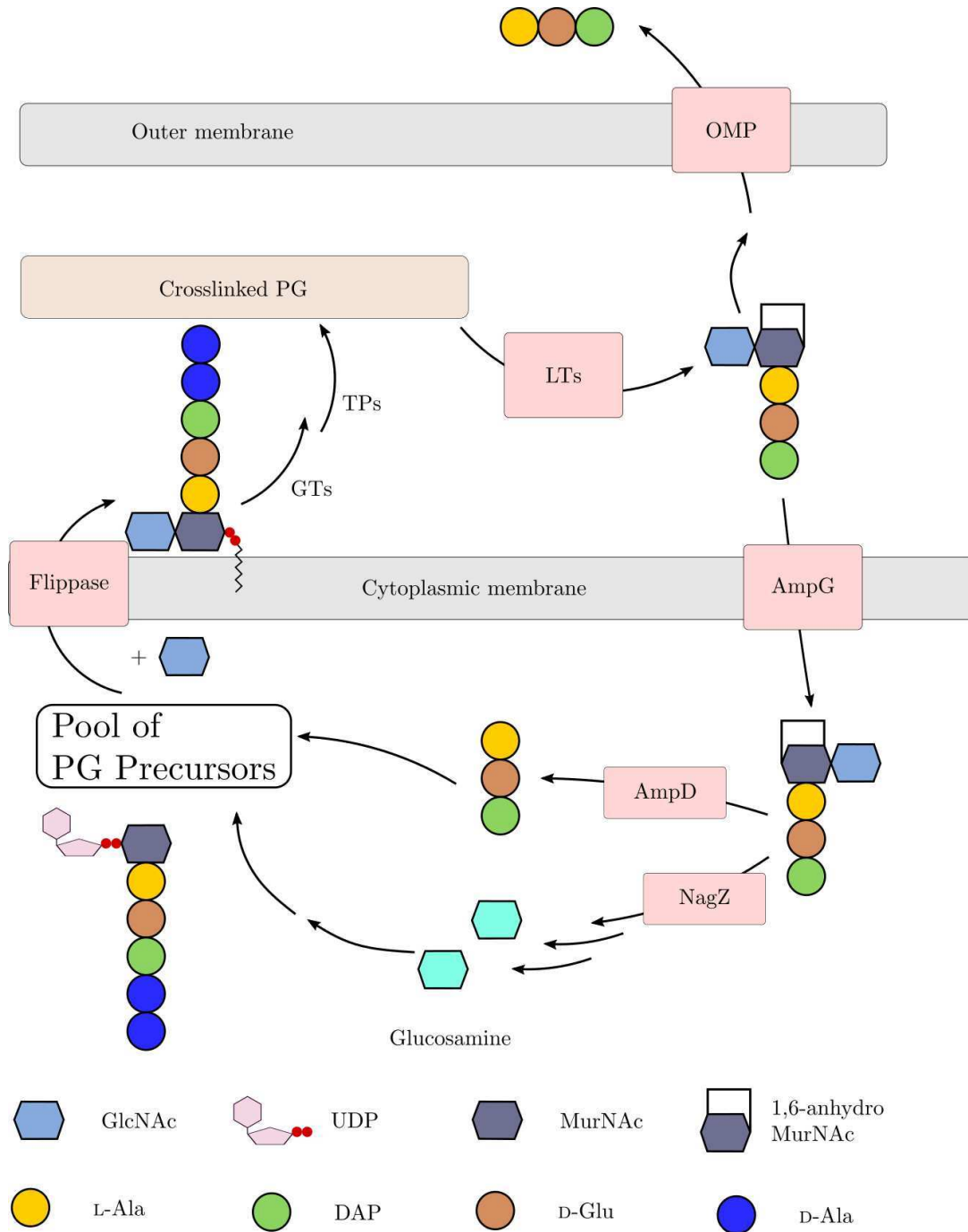


Figure 9: Recycling and turnover of 1,6-anhydro-tripeptide. LTs - Lytic transglycosylases, OMP - Outer membrane porin, GTs - Glycosyltransferases, TP - Transpeptidase

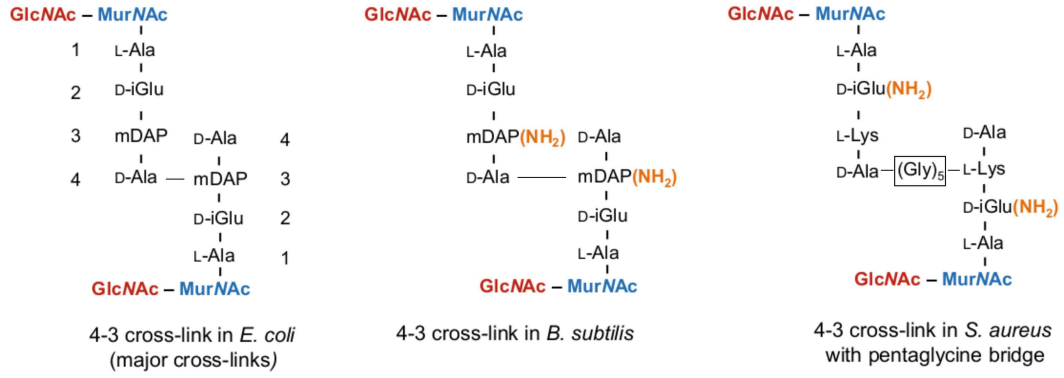


Figure 10: Examples of peptides and cross-link types in the peptidoglycan PG of different species. Amidation of residues is depicted in orange. Interpeptide bridges are framed with a square; from [Pazos and Peters, 2019]

FemB [Rietmeyer et al., 2021]. *O*-acetylation, *N*-deacetylation and *N*-glycolation have been described as secondary modifications of the glycan building blocks. These modifications are often associated with increased resistance to PG hydrolyzing enzymes [Vollmer, 2008]. The PG of Gram-positive bacteria can be up to 100 nm thick [Rohde, 2019], due to a higher number of layers in comparison to diderm bacteria (*ca.* 10 *vs.* 1).

3 β -lactam antibiotics

Bacterial cell wall synthesis is the target of several groups of antibiotics.

However, the most widely used group of antibiotics targeting synthesis of peptidoglycan are the β -lactam antibiotics which inhibit the transpeptidation reaction catalyzed by PBPs [Bush and Bradford, 2016]. These compounds are named after their common structural core, the four-membered β -lactam ring (Fig. 11).

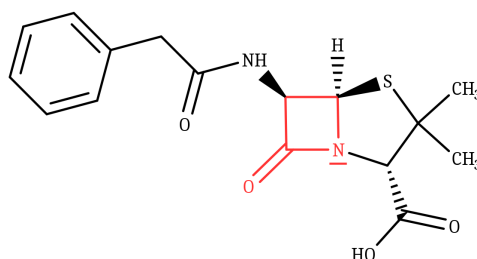


Figure 11: Structure of Penicillin G, β -lactam core highlighted in red

3.1 Targets, molecular mode of action and molecular determinants

The molecular targets of β -lactam antibiotics comprise the transpeptidase domains of aPBPs, bPBPs and peptidoglycan hydrolases. Proteins which are inhibited by β -lactam antibiotics are grouped together as Penicillin-Binding-Proteins (PBPs) as some of them have historically been characterized due to inhibition by the first identified β -lactam antibiotics, the penicillins. In *E. coli*, targets of β -lactam antibiotics include the aPBPs PBP1a and PBP1b, the bPBPs PBP2 and PBP3, and the PG hydrolases PBP4, PBP4b, PBP5, PBP5, PBP6, PBP6b, PBP8 and AmpH [Bhattacharjee, 2016, Pazos and Peters, 2019]. β -lactams show various selectivity profiles for PBPs which can be used to study the roles of specific PBPs [Kocaoglu and Carlson, 2015].

The transpeptidation reaction catalyzed by class A and class B PBPs proceeds via nucleophilic attack of the catalytic serine on the C-terminal peptide bond of the donor pentapeptide stem leading to the formation of a tetrahedral intermediate (Fig. 12A(i)). Release of D-Ala yields the acylenzyme complex between the PBP and a tetrapeptide stem (Fig. 12A(ii)). The ester bond is attacked by the ϵ -amino group of the DAP residue in the acceptor peptide (Fig. 12A(iii)), which leads to the formation of a second tetrahedral intermediate. In the last step, free enzyme and crosslinked peptide stems are released (Fig. 12A(iv)).

Inhibition of PBPs by β -lactams relies on acylation of the catalytic serine residue in the active site of PBPs. The mechanism of inhibition shows strong similarities to the first steps of the physiological transpeptidation reaction catalyzed by PBPs. The reaction is initiated by nucleophilic attack of the hydroxyl group of the catalytic serine on the carbonyl carbon of the

β -lactam ring, yielding a tetrahedral intermediate similar to the one formed in the physiological reaction (Fig. 12B(i)). In a second step, the β -lactam ring is opened, resulting in the acylenzyme complex (Fig. 12B(ii)). Nucleophilic attack by either a peptide stem or a water molecule on the acylenzyme is prevented by steric hindrance which results from bulky residues bound to the β -lactam ring, *e.g.* a second ring structure found in most classes of β -lactam antibiotics.

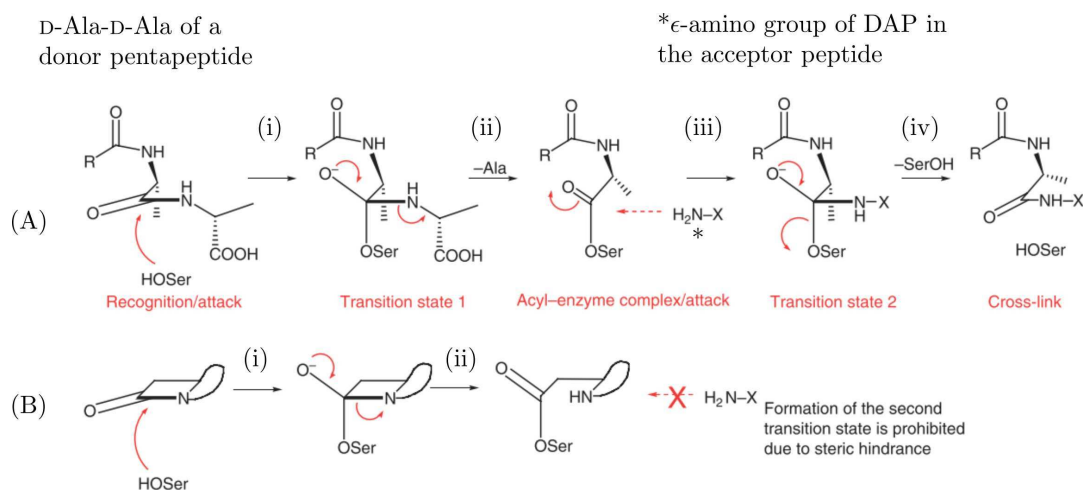


Figure 12: Reactions of PBPs with substrate and β -lactam antibiotics (A) Mechanism of transpeptidation reaction catalyzed by PBPs (B) Suicide inhibition of PBPs by β -lactam antibiotics, adapted from [Hubschwerlen, 2007]

The inhibition of PBPs by β -lactam antibiotics is attributed to similarity of the compounds to the C-terminal D-Ala-D-Ala dipeptide of disaccharide pentapeptide stems, the natural substrate of PBPs [Tipper and Strominger, 1965, Boyd, 1979].

The carbonyl group of the β -lactam ring is susceptible to nucleophilic attack, an unusual finding for tertiary amides. In tertiary amides, inductive effects enhance the delocalization of the free pair of electrons of the amide nitrogen. This reduces the electrophilic character of the amide carbon, which leads to a reduced activity towards nucleophiles. Reactivity of β -lactam antibiotics relies on the electrophilic character of the carbonyl carbon and is ensured by two effects occurring alone or in combination [Hubschwerlen, 2007]:

- (1) **A second ring fused to the β -lactam ring.** Presence of a fused ring system adjacent to the azetidinone ring blocks delocalization of the free pair of electrons of the lactam nitrogen. Upon delocalization in unconstrained tertiary amides, the sp^2 -hybridization of the nitrogen results in bond angles of 120° . However, the constrained bicyclic structure of β -lactams, would impose a bond angle of 90° which would result in extreme ring strain (Fig. 13).

- (2) **Electron-withdrawing groups bound to the β -lactam nitrogen.** Groups directly bound to the β -lactam nitrogen exerting either a negative inductive or a negative mesomeric effect or both, decrease electron density at the lactam nitrogen and accordingly enhance the electrophilic character of the carbonyl carbon.

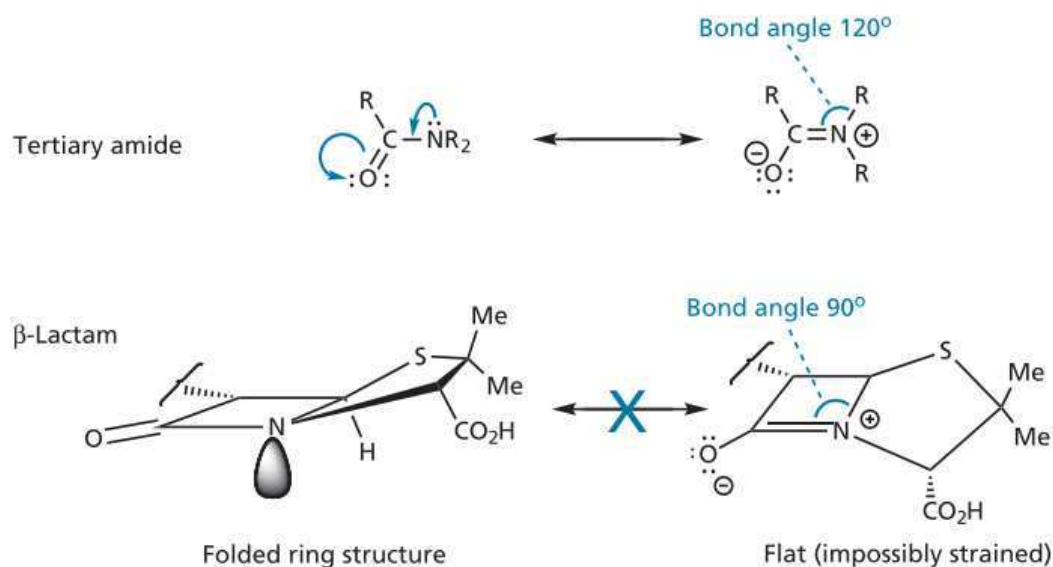


Figure 13: Comparison of tertiary amide and β -lactam carbonyl groups; from [Patrick, 2013]

3.2 Structural classes of β -lactam antibiotics

Table 3 gives the core structures and a representative of the various classes of β -lactam antibiotics which will be discussed in the following sections.

Penams. The first identified β -lactam antibiotics belonged to the penam group. As they were found in species of the *Penicillium* mould, they are also referred to as penicillins. Penams contain a thiazolidine ring fused to the β -lactam core. Early X-ray crystallography studies revealed the strained structure of benzylpenicillin, a major determinant of its reactivity as discussed above [Crowfoot et al., 1949]. Penams are often obtained by semi-synthesis starting from 6-Aminopenicillanic acid (6-APA, $R = -NH_2$ for the penam core structure shown in Table 3) [Nayler, 1991]. After the introduction of naturally occurring penams into clinical use, these semi-synthetic molecules were further improved with respect to oral availability, extension of antimicrobial spectrum to gram-negative species and β -lactamase stability [Page, 2012]. β -lactams are prone to ring opening under acidic conditions, which limits oral bioavailability. Electron-withdrawing groups within residues attached to the 6' position have been shown to be beneficial for acid stability [Page, 2012]. Amino groups in the α -position of a 6'-acylamino-sidechain, as

Table 3: Structures of classes of β -lactam antibiotics and representatives of each class.

β -lactam class (fused ring)	Core structure	Representative
Penam (thiazolidine)		Amoxicillin R =
Cephem (1,3-dihydrothiazine)		Cefuroxime R1 = R2 =
Carbapenem (2-pyrroline)		Imipienem R1 = R2 = H
Penem (thiazoline)		Faropenem R =
Monobactam (N.A.)		Aztreonam R1 = R2 = SO ₃ H

N.A. not applicable

found for example in amoxicillin and ampicillin, simultaneously extend the antibacterial spectrum to gram-negative species and enhance acid stability [Hubschwerlen, 2007]. Bulky lipophilic substituents at the 6' position confer stability against staphylococcal penicillinases, β -lactam hydrolyzing enzymes, which emerged in the 1950s due the clinical use of penicillins. In today's clinical practice, β -lactam antibiotics are often co-administered with a β -lactamase inhibitor due to the wide spread of strains producing β -lactamases (see chapters 4 and 5).

Cephems. Cephems, also called cephalosporins, were first identified when Cephalosporin C was isolated from the eponymous *Cephalosporium acremonium* in 1948 [Turck, 1982]. Cephems contain a 1,3-dihydrothiazine ring fused to the azetidinone ring. The distinctive feature of cephems compared to penams is, besides the six-membered ring, the 2,3-double bond which is required for antibacterial activity [Holden, 1984]. The double bond is in resonance with the nitrogen lone pair which reduces electron density at the lactam nitrogen and enhances the electrophilic character of the carbonyl carbon. The importance of combining an electron withdrawing group and a strained bicyclic ring system is highlighted by the finding that isomerization of the double bond to the 3,4-position leads to loss of activity. This indicates that the strain induced by fusing a six-membered ring is not enough to maintain a sufficiently reactive β -lactam molecule [Indelicato et al., 1974]. Modifications of the cephem scaffold are introduced mainly at the 3' and 7' positions. Substituents at 7' influence antibacterial activity while substituents at 3' mainly alter pharmacokinetic properties. Cephalosporins with a methoxy group at the 7α position are called cephamycins [Hubschwerlen, 2007]. The majority of Cephalosporins are obtained via semi-synthesis starting from 7-aminocephalosporinic acid (7-ACA). 7-ACA is obtained by chemical modification of Cephalosporin C produced by fermentation of *Cephalosporium acremonium* [Holden, 1984]. When cephems were first introduced into the clinic in the 1960s, they were more stable towards acid hydrolysis and the at that time predominant staphylococcal β -lactamase. Continuous development since then led to discovery of five generations of cephalosporins. Main focus of these campaigns were the improvement of coverage of Gram-negative bacteria and an increased stability towards hydrolysis by an ever increasing number of β -lactamases which are especially problematic in these bacteria. Of all β -lactams in clinical use today, the cephalosporins are the most prescribed ones [Bush and Bradford, 2016, Hubschwerlen, 2007].

Carbapenems. Carbapenems contain a 2-pyrroline ring, which combines the high strain of five-membered rings with the effect of the electron withdrawing double bond in the 2,3-position [Hubschwerlen, 2007]. In all clinically used carbapenems, the substituent at position 6 is a hydroxyethyl side-chain, in contrast to the aminoacyl substituents found in cephems and penams.

The hydroxyethyl side-chain was suggested to be important for β -lactamase resistance. Substituents in positions 5 and 6 are in *trans*-configuration. Position 3 is substituted with varying thioether sidechains. Carbapenems have a very broad spectrum covering both Gram-positive and Gram-negative bacteria with minor differences between the substances [Bradley et al., 1999] and they show a high level of stability towards β -lactamases with the exception of the emerging carbapenemases [Bush and Bradford, 2016] (see also chapter 4). Thienamycin, produced by the bacterium *Streptomyces cattleya*, was the first carbapenem to be identified in the 1970s. However, it was chemically unstable and was therefore not suitable for clinical use [Kahan et al., 1979]. Minor modifications of the 3' side-chain of thienamycin yielded imipenem. Imipenem is susceptible to hydrolysis by the renal enzyme dehydropeptidase-I (DHP-I) and is therefore administered in combination with the DHP-I inhibitor cilastatin [Kahan et al., 1983]. Discovery programs since the introduction of imipenem focused on improved stability against DHP-I, improved chemical stability, and on enhanced antibacterial activity against increasingly resistant strain of *P. aeruginosa* and *S. aureus*. Introduction of a 4 β -methyl substituent confers stability to hydrolysis by DHP-1, as realized in all clinically used carbapenems developed after imipenem (meropenem, biapenem, doripenem, ertapenem) [Bush and Bradford, 2016]. Due to their broad antibacterial spectrum and high potency, carbapenems are last resort antibiotics for treating infections caused by otherwise resistant bacteria.

Penems. The penem core contains a thiazolidine ring instead of the 2-pyrroline of carbapenems. Penems are synthetic compounds, which were first designed bearing the aminoacyl sidechains as found penams and cepems [Woodward, 1980]. However, prototypes with this type of sidechain were chemically unstable. The hydroxyethyl sidechain of carbapenems provided stable molecules. The antibacterial spectrum of penems is comparable to that of carbapenems with the exception of *P. aeruginosa* [Hubschwerlen, 2007]. Faropenem is the only compound with market authorization as of today, with several others in clinical development [Hamilton-Miller, 2003, ARCAMONE et al., 2000].

Monobactams. Monobactam antibiotics contain only the monocyclic β -lactam ring. Nucleophilic reactivity is therefore assured by derivatising the lactam nitrogen with highly electron withdrawing substituents, *e.g.* sulfonic acid groups as found in aztreonam. Aztreonam is the only monobactam in clinical use. Monobactams lack antibacterial activity against Gram-positive bacteria [Hubschwerlen, 2007]. Their therapeutic use has been compromised by the emergence of β -lactamases. Of note, monobactams are only weakly hydrolysed by metallo- β -lactamases for which currently no inhibitor is available for clinical use [Bush and Bradford, 2016] (see also chap-

ters 4 and 5). Current research in the monobactam field includes exploration of siderophores, iron-chelating moieties, which allow the antibiotic to hijack iron-transporters to enter the bacterial cell. Of note, a siderophore bearing monobactam has shown antibacterial activity superior to that of carbapenems [Page et al., 2010].

3.3 Resistance to β -lactam antibiotics

Bacterial defense against β -lactam antibiotics was described even before the first penicillins entered clinical use. Indeed, *Abraham and Chain* (1940) provided the first account of penicillinase activity in crude cell preparations of *E. coli* [Abraham and Chain, 1940]. This early report underlines that already at the beginning of the antibiotic era, the development of new antibacterial drugs was a question of keeping up with the pace of new mechanisms of antibiotic resistance. The selective pressure exerted by the abundant use of antibiotics in medicine and agriculture over the last decades favored the emergence of multidrug-resistance bacterial strains encountered in the clinic, which are extremely difficult and sometimes impossible to treat. It remains not a single β -lactam antibiotic for which no resistance has been described. Resistance to β -lactams can be attributed to three groups of mechanisms, which are generally found in combination in resistant bacterial strains: (i) Altered structure and expression of PBPs, (ii) modification of β -lactam transport, and (iii) enzymatic degradation of β -lactams [King et al., 2017a].

Alteration of target structure and expression. A first hallmark of antibiotic resistance was the identification of methicillin resistant S. aureus (MRSA) in the 1960s [Chambers and DeLeo, 2009]. Methicillin had previously been developed to combat resistance in *S. aureus* due to the production of a penicillinase. The resistance of MRSA against methicillin and all other β -lactams available at that time was attributed to the production of a low-affinity PBP, PBP2a. This PBP2 is the product of the *mec* locus, which codes for a class B PBP, which shows tremendously decreased reactivity towards β -lactams [King et al., 2017a]. The active site of the apo form of PBP2a adopts a closed conformation compared to other PBPs. While the initial non-covalent binding of β -lactams to PBP2a is only weakly affected in comparison to other PBPs, the rate constant of the chemical step of the reaction, acylation of the catalytic serine, is three orders of magnitude lower [Lambert, 2005]. This finding was rationalized by structural studies which showed that the active site of PBP2a has to undergo substantial and energetically costly rearrangements for acylation [Lim and Strynadka, 2002]. Co-incubation of PBP2a with nitrocefin (a chromogenic β -lactam) and peptidoglycan fragments revealed allosteric regulation of the active site leading to enhanced acylation of PBP2a by β -lactams upon binding of PG fragments [Fuda et al., 2005]. The fifth-generation cephalosporin ceftaroline binds to the al-

losteric site, thereby inducing the necessary active site rearrangement for effective acylation a second ceftaroline molecule [Otero et al., 2013]. Expression of the *mecA* locus is regulated by the MecI/MecR system. MecR1 is a transmembrane sensor/transducer protein located in the cytoplasmic membrane. It comprises an extracellular β -lactam sensor domain and a Zn^{2+} -dependent metalloprotease domain. Acylation of the sensor domain by β -lactams triggers cleavage of MecI, the repressor of the *mecA* locus leading to derepression and expression of *mecA* [Marrero et al., 2006]. The presence of β -lactams does not alter the expression level of the remaining four native PBPs of *S. aureus*. Under these conditions, PBP2a adopts the role of the main transpeptidase, which however depends on the glycosyltransferase activity of the class A PBP2 and on the presence of the class B PBP1 [Zapun et al., 2008].

The intrinsic moderate resistance of enterococci to β -lactams has been attributed to low-affinity PBPs, PBP5 in *E. faecium*, and PBP4 in *E. faecalis*. PBP5_{*E. faecium*} and PBP2a of *S. aureus* are found in the same subgroup of class B PBPs [El Kharroubi et al., 1991]. As for PBP2a, acylation of PBP5_{*E. faecium*} is lowered by two to three orders of magnitude compared to high-affinity PBPs [Zapun et al., 2008]. Recently, the crystal structure of the apo forms of PBP4_{*E. faecalis*} and PBP5_{*E. faecium*} were solved [Moon et al., 2018]. Comparison of the apo enzymes with the β -lactam complexes revealed rearrangements in the active site of PBP5_{*E. faecium*} and PBP4_{*E. faecalis*}, similar to those described for PBP2a. Overproduction of low-affinity PBPs in enterococci is not sufficient for high-level β -lactam resistance, which necessitates additional amino acid substitutions [Rybkin et al., 1998, Rice et al., 2018]. This combination is commonly found in clinical isolates [Klare et al., 1992].

Besides acquisition of additional genes, low-affinity PBPs can arise from intra- or interspecies recombination events of different alleles resulting in so-called mosaic genes [King et al., 2017a]. Genetic analyses of *Streptococcus pneumoniae* revealed a high degree of polymorphism in the transpeptidase domain in four of six PBPs in resistant strains compared to susceptible strains [Hakenbeck et al., 1991, Zapun et al., 2008].

Modification of β -lactam transport. Especially Gram-negative bacteria have shown adaptability of their outer membrane physiology in response to β -lactam exposure. General porins in the outer membrane provide the main entry route for many antibiotics as they cannot passively diffuse through the outer membrane due to their hydrophilicity [King et al., 2017a]. Porin mediated resistance to antibiotics is normally associated with mutations in the porin genes or in genes coding for porin regulatory elements. In *E. coli*, β -lactam resistance can be linked to complete loss of OmpF or amino acid substitution in the constriction zone of OmpC [Harder et al., 1981, Lou et al., 2011]. Multidrug resistance caused by antibiotic efflux is largely conferred

by proteins of the resistance-nodulation-cell division (RND) superfamily [King et al., 2017a]. Ternary complexes, which span the entire periplasm, are composed of a pump protein in the cytoplasmic membrane, an adapter unit, and an outer membrane channel. These complexes can export compounds from the periplasm, including β -lactams, to the external medium [Nikaido and Takatsuka, 2009]. Such export systems have been described in wide variety of clinically relevant bacterial species, such as *P. aeruginosa*, *A. baumannii*, and *K. pneumoniae* [King et al., 2017a]. Inhibitors of antibiotic efflux pumps have been developed, but success in restoring the therapeutic activity of β -lactams has not been achieved, mainly due to the presence of a combination of resistance mechanisms in clinical strains [Kourtesi et al., 2013].

Enzymatic degradation of β -lactams The most prevalent mechanism of resistance against β -lactams is the expression of hydrolytic enzymes, the β -lactamases. These enzymes render β -lactams ineffective by opening of the β -lactam ring before the drugs can reach their targets. Virtually since the first use of β -lactam antibiotics to treat patients, these enzymes have been a threat to therapeutic effectiveness and indeed, emergence of new types of β -lactamases has repeatedly triggered drug design efforts over the last decades. Their structure and function will be discussed in the next chapter.

4 β -lactamases

Production of antibiotics by microorganisms (*e.g.* β -lactam production in fungal and bacterial species) confers advantages to producers over non-producers occupying the same ecological niche. A particularly rich source of antibiotics are soil actinomycetes [Peterson and Kaur, 2018]. Producers of antibiotics need to be adapted to the exposure to their own metabolites, a characteristic called self-resistance. This could be the absence of targets as for β -lactam-producing fungi or production of β -lactamases, enzymes capable of hydrolyzing the four-membered β -lactam ring, in the case of β -lactam producing bacteria [Ogawara, 2016]. How exactly the production of a degrading enzyme is compatible with β -lactam production, is not fully understood [Peterson and Kaur, 2018]. Forty years ago, emergence of β -lactamases was attributed to selective pressure exerted by the ubiquitous use of antibiotics and their appearance was thought to have coincided with introduction of β -lactams into the clinic [Hamilton-Miller, 1979]. While there is no doubt that therapeutic (over)use of β -lactam antibiotics accelerated the dissemination of β -lactamase-mediated antibiotic resistance [Bush, 2018], phylogenetic analyses estimate the age of β -lactamases to be about 2 billion years and the transfer of their genes to plasmids to have happened approximately 400 million years ago [Hall and Barlow, 2004]. Additionally, β -lactamase activity has repeatedly been detected in bacterial samples from environmental niches, that had been isolated from human presence from several thousands up to millions of years [Sari et al., 2011, Segawa et al., 2013, Jae et al., 2005]. Transfer of self-resistance genes to clinical pathogens can occur directly, however it is deemed more likely that resistance genes are transferred from producers to clinical strains via increasingly distant non-producing strains [Peterson and Kaur, 2018]. Mechanisms for gene transfer include conjugation of mobile genetic elements or transformation. Production of plasmid-encoded β -lactamases constitute today's single most prevalent mechanism of resistance to β -lactam antibiotics [King et al., 2017a].

The majority of known β -lactamases contains a catalytic serine residue and are structurally related to PBPs both in terms of fold and conservation of amino acid motifs comprising catalytic residues. It has been suggested that β -lactamases evolved from PBPs [Bush, 2018]. In the time course of this evolution, structural alterations in the active site of β -lactamases abolished binding and recognition of peptidoglycan donor and acceptor stems, while retaining binding of β -lactams and developing effective hydrolysis of the resulting acylenzymes [Meroueh et al., 2003].

The general mechanism for the reaction of β -lactams with PBPs and β -lactamases shows striking similarities (Fig. 14). The reaction is initiated by formation of a non-covalent complex (E•S) followed by acylation of the active site serine. The main difference between β -lactamases and PBPs lies in the deacylation step, characterized by the kinetic constant k_3 which generally is

very low for PBPs implying that half-lives of the acylenzyme complexes exceed several generation times for PBPs *versus* less than one second for β -lactamases [Zapun et al., 2008]. Interestingly, site-directed mutagenesis of *S. pneumoniae* PBP2x showed that the P450D substitution led to a 100-fold increase in k_3 [Chesnel et al., 2002]. The authors suggested that the negatively charged Asp residue could activate a deacylating water molecule, an event frequently described for β -lactamases. Although this substitution was not detected in clinical isolates, certain PBPs from *S. pneumoniae* display increased values for k_3 (70 to 80 fold) in comparison to PBP2x from susceptible isolates [Lu et al., 2001]. These findings indicate a subtle structural delineation of PBPs and β -lactamases.

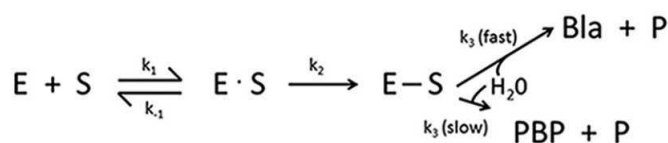


Figure 14: General reaction mechanism for binding of a β -lactam substrate (S) to a PBP (E) or a serine β -lactamase (E). Reversible formation of a Michaelis complex ($\text{E} \cdot \text{S}$) which proceeds to a stable acyl enzyme ($\text{E}-\text{S}$) caused by reaction with the active-site serine. Hydrolysis occurs to form the microbiologically inactive ring-opened β -lactam (P) and either enzymatically active PBP (slow hydrolysis of acylenzyme) or β -lactamase (Bla, high hydrolysis rate), from [Bush, 2018]

4.1 Classification

An ever growing number of β -lactamases is being identified. The β -lactamase database [Naas et al., 2017] (www.bldb.eu) lists over 7000 enzymes as of the time of writing and this number is growing exponentially [Bush, 2018]. Since the discovery of β -lactamases, efforts were undertaken to classify β -lactamases into meaningful groups. Classification was based on substrate profile, sequence and structure similarity, characteristic sequence motifs, and inhibition profile. Classification of β -lactamases today relies on a combination of two classification schemes: the Ambler system, based on sequence information [Ambler, 1980] and the functional classification by Bush, Jacoby and Medeiros [Bush et al., 1995]. The Ambler classification captures the major mechanistic differences between β -lactamases, which contain an active site serine (Ambler classes A, C, and D) and enzymes containing metal ions in their active site (Ambler class B) (Fig. 15). At time of their proposal, the Ambler classes of serine β -lactamases roughly correlated with their substrate spectrum. This was captured by a first attempt of functional classification [Bush, 1989], which was based on substrate and inhibition profiling. With the continuous emergence of new enzymes, sequence based classification was not sufficient anymore to provide a clinically

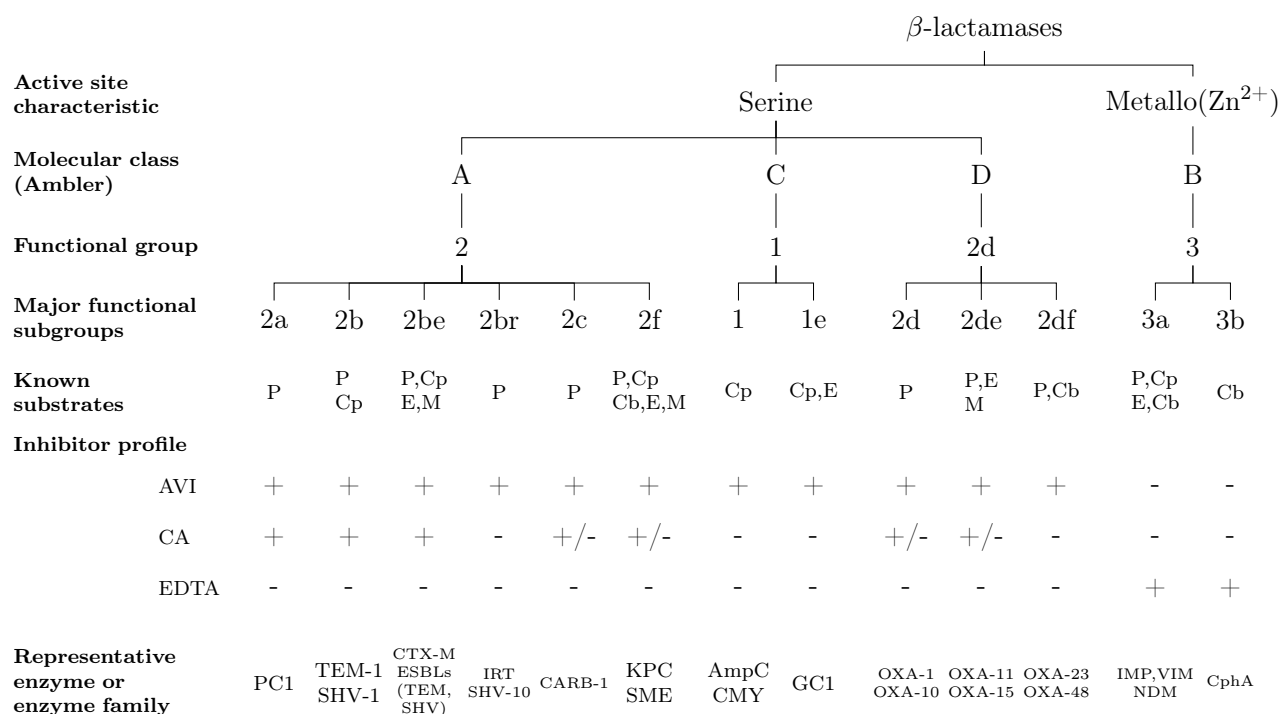


Figure 15: Molecular and functional relationships among β -lactamases. AV, avibactam; CA, clavulanic acid; Cb, carbapenem; Cp, cephalosporin; E, expanded-spectrum cephalosporin; M, monobactam; P, penicillin; ESBL, extended-spectrum β -lactamase; redrawn from [Bush, 2018]

useful grouping exemplified by the heterogeneity of Ambler class A enzymes comprising "simple" penicillinases (functional groups 2a and 2c, Fig. 15) and enzymes capable of hydrolyzing the majority of clinically used β -lactams (KPC family of enzymes, functional subgroup 2f). Therefore the original functional classification is continuously updated in order to provide support for therapeutic decisions [Bush et al., 1995, Bush and Jacoby, 2010].

Another sometimes confusing aspect of β -lactamase classification is the high number of seemingly redundant allele designations. "Seemingly redundant", because new alleles sometimes only differ in a single amino acid. Suggestions have been made to only assign new gene names if there is at least at 2% divergence in nucleotide sequence [Hall and Schwarz, 2016]. However, this proposal was rejected by clinicians. Indeed, changes seeming too subtle to justify assignment of a new gene name can result in a change in substrate and inhibitor profile of clinical importance, as for example is the case for acquisition of a broader substrate spectrum in the TEM enzymes, which necessitates a different therapeutic approach [Bush, 2018].

4.2 Serine β -lactamases

Enzymes with a catalytic serine residue constitute the largest group among β -lactamases and are also the most heterogenous in terms of substrate spectrum [Bush, 2018] (Fig. 15). Structure

and function of these enzymes will be discussed in the following sections.

4.2.1 Characteristic motifs

Serine β -lactamases are grouped into the molecular classes A, C, and D. Conserved characteristic sequence motifs are given in Table 4. The active site serine is found in the SXXK motif, also present in PBPs [Massova and Mobashery, 1998]. The SXN triad in class A β -lactamases, the YXN triad in class C and the SXV triad in class D β -lactamases are important for protonation of the β -lactam nitrogen during hydrolysis [King et al., 2016b]. The residues in the K-T/S-G motif form a positively charged subcavity in the active site responsible for binding the carboxylate group of β -lactams [Strynadka et al., 1992]. Class A β -lactamases harbor a glutamine residue in position 166, which was shown to activate a water molecule during both acylation and deacylation [Escobar et al., 1991, Tooke et al., 2019]. Structures of representatives of each class of serine β -lactamase are shown in Fig. 16.

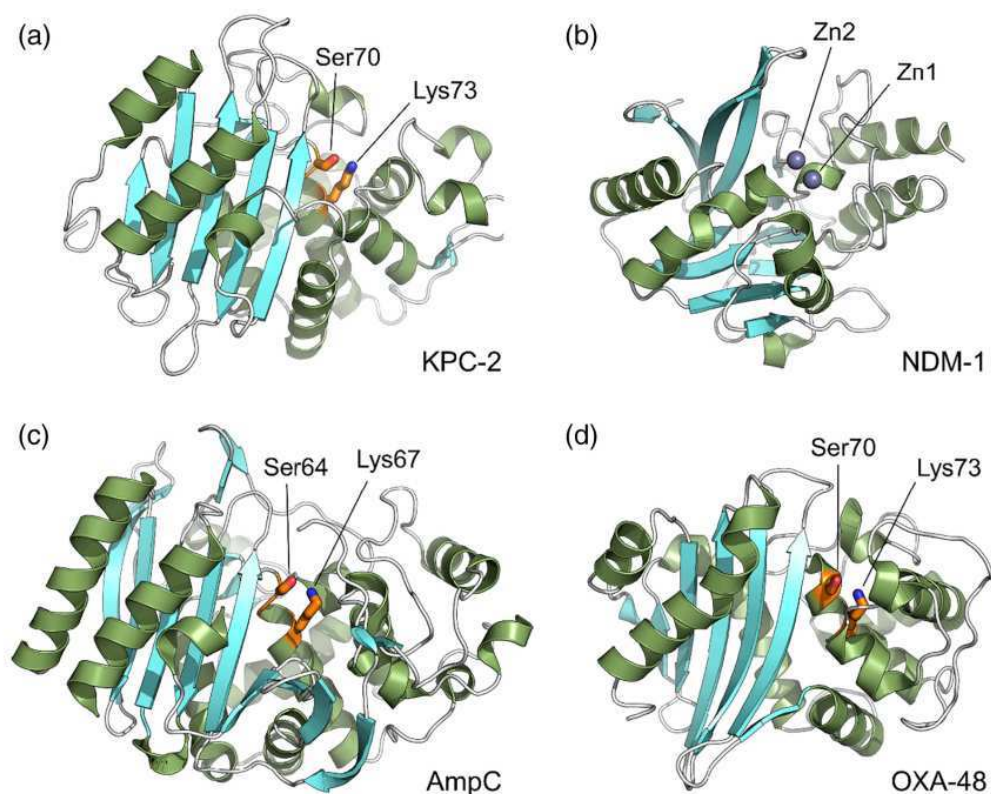


Figure 16: Overall structure of representative β -lactamases from each Ambler class. Catalytic important residues of serine- β -lactamases (serine 64/70 and lysine 67/73, labeled) are colored orange, and the metallo- β -lactamase zinc ions are shown as gray spheres. (a) Class A KPC-2 (PDB 5ul8). (b) Class B NDM-1 (PDB 5zgy). (c) Class C AmpC (PDB 1ke4). (d) Class D OXA-48 (PDB 3hbr), from [Tooke et al., 2019]

Table 4: Distinguishing characteristics of the three major molecular classes of serine β -lactamases; The most common motifs are shown in bold; alternative sequences are shown in parentheses, with X representing sequences that can accommodate multiple substitutions; S in SXXK is the catalytic serine residue; modified from [Bush, 2013]

Molecular Class	Characteristic amino acid motifs				
A	S⁷⁰TSK (SXXK)	S¹³⁰DN (SXN)	-	E¹⁶⁶XXLN	K²³⁴TG
C	S⁶⁴TSK (SXXK)	Y¹⁵⁰AN (YXN)	-	-	K^{315p}TG (KSG)
D	S⁷⁰TSK	S¹¹⁸XV	Y¹⁴⁴GN (FGN)	-	K²¹⁶TG (KSG)

4.2.2 Molecular catalytic mechanism

General mechanism. Despite minor sequence similarities, the general catalytic mechanism is very similar among serine β -lactamases of classes A, C, and D [Tooke et al., 2019] (Fig. 17). After formation of a non-covalent complex, the β -lactam carbon undergoes nucleophilic attack by the hydroxyl group of the catalytic serine, which is activated by a general base B1. The reaction proceeds via a tetrahedral oxyanion transition state and yields the acylenzyme intermediate. Nucleophilic attack of a water molecule activated by general base B2 yields a second tetrahedral intermediate, from which free enzyme and the hydrolyzed β -lactam are released.

Class A β -lactamases. While the mechanism as described above is generally accepted, there is ongoing research to elucidate which residues exert the function of the general base during acylation and deacylation. For class A β -lactamases, it is widely accepted that Glu166 acts as general base during deacylation [Tooke et al., 2019]. For the acylation step, two alternative mechanisms have been put forward, in which either Glu166 or Lys73 (part of SXXK motif) acts as proton acceptor (Fig. 18). Studies addressing the acylation pathway are normally employing one of the three following methods: (i) site-directed mutagenesis of residues in question, (ii) high level molecular simulations (Quantum Mechanics/Molecular Mechanics), and (iii) high resolution structure determination allowing to determine protonation states of residues of interest.

Results from high resolution X-ray and neutron diffraction studies of apo structures of class A β -lactamases revealed a hydrogen bonding network in their active site indicating Glu166 is deprotonated and is suitably positioned to activate the catalytic serine via a water molecule. Lys73 was found to be present in the protonated form, which is incompatible with a role as general base [Chen et al., 2007, Tomanicek et al., 2011] (Intermediate (b) in Fig. 18). These findings were corroborated by molecular modeling studies, which found that the Glu166-mediated acyla-

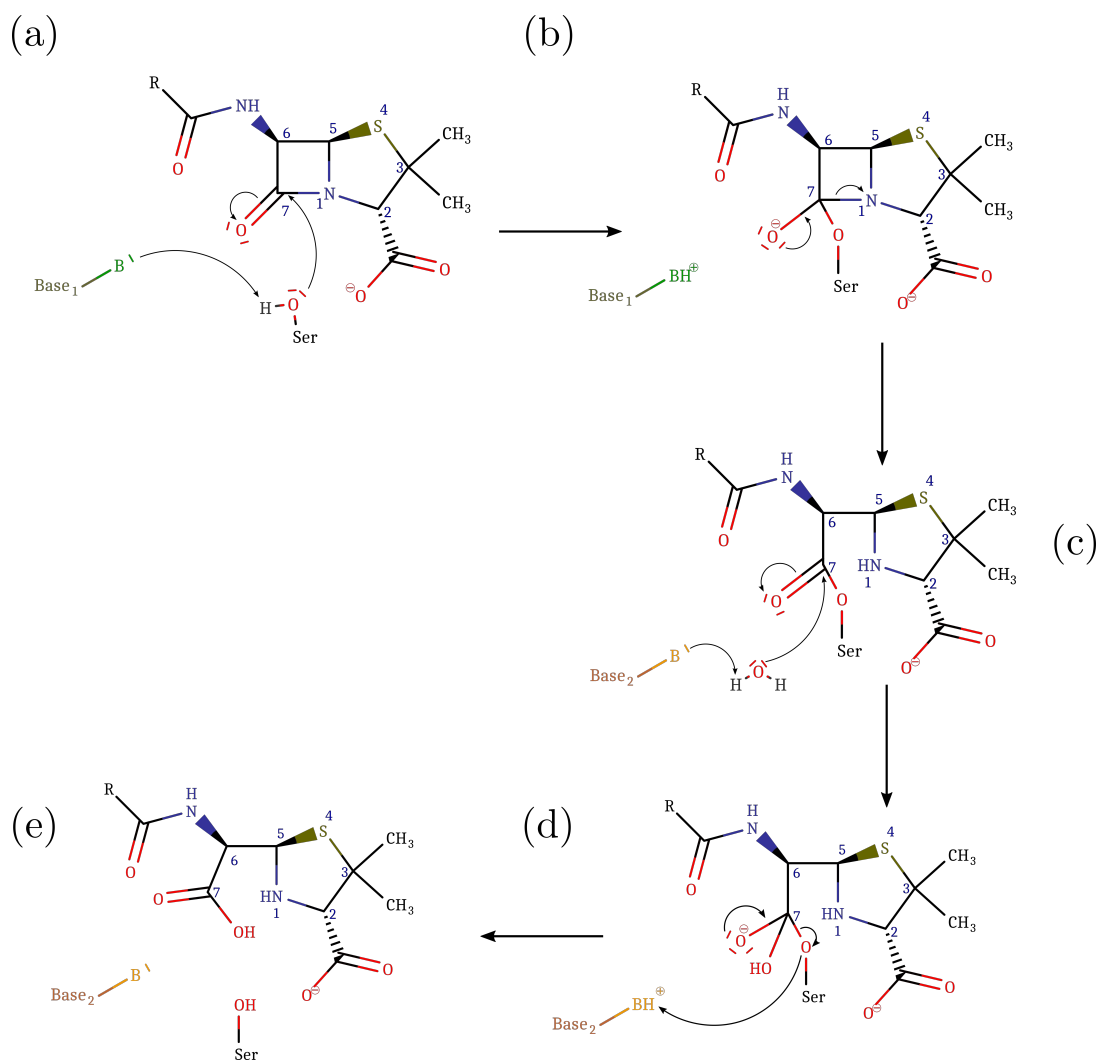


Figure 17: General mechanism of β -lactam hydrolysis by serine β -lactamases. (a) General base B1 activates Ser for nucleophilic attack on the amide carbonyl carbon (C7) generating covalent acyl-enzyme (c) via tetrahedral oxyanionic acylation transition state (b). General base B2 activates incoming deacylating water molecule for nucleophilic attack on the acyl-enzyme carbonyl liberating penicilloate product (e) via tetrahedral deacylation transition state (d). For clarity, details of proton transfers to N1 and Ser are omitted. Note that the identities of bases B1 and B2 vary between β -lactamase classes; redrawn from [Tooke et al., 2019]

tion mechanism is energetically favored [Hermann et al., 2003, Hermann et al., 2005, Hermann et al., 2009]. Alternatively, Lys73 was proposed to mediate activation of the catalytic serine since Lys73 mutants provided a means to trap the initial non-covalent complex of the reaction [Tremblay et al., 2010] (Intermediate (c) in 18). This is also supported by the retained acylation of Glu166-mutants by β -lactams [Chen and Herzberg, 2001]. Combined results from X-ray, neutron diffraction studies and QM/MM simulations indicate that substrate binding alters the pK_a values of active site residues [Meroueh et al., 2005, Langan et al., 2018, Pemberton et al., 2020]. This allowed to reconcile models based on the structure of the apo form of the enzymes and on the characterization of Glu166 and Lys73 mutants. Accordingly, *Meroueh et al.* (2005) suggested that Glu66 and Lys73 mediated acylation are both energetically favourable and could occur competitively to each other. Another mechanistic proposal involves proton transfer from Lys73 to Glu166 *via* the catalytic serine upon substrate binding [Langan et al., 2018, Pemberton et al., 2020]. The deprotonated Lys73 can then act as general base in the acylation reaction.

Class C β -lactamases. The catalytic mechanism of class C β -lactamases is less well characterized [Tooke et al., 2019]. Lys67 and Tyr150 are candidate residues for being the general base in acylation. Molecular modeling, based on the first solved crystal structure of a class C β -lactamase, proposed that Tyr150 in its tyrosinate form acts as a general base during acylation [Oefner et al., 1990]. In contrast, NMR titration experiments found no indication of the existence of the Tyr150 tyrosinate in an apo class C β -lactamase over a wide range of pH values [KATO-TOMA et al., 2003]. Additionally, further computational studies designated Lys67 as the general base for the acylation step, with an impact of substrate binding on pK_a values of Lys67 and Tyr150 [Díaz et al., 2006, Tripathi and Nair, 2013]. Two mechanistic proposals for deacylation in class C β -lactamases have been put forward (Fig. 19): (i) the "conjugate base" mechanism and (ii) the "substrate assisted" mechanism. The former is based on QM/MM simulations [Gherman et al., 2004] and site-directed mutagenesis of Lys67 [Chen et al., 2009]. In this mechanism Lys64 needs to be deprotonated in order to abstract a proton from Tyr150, which in turn activates the deacylating water molecule for nucleophilic attack on the acylenzyme ester bond (Fig. 19(a)). In the substrate-assisted mechanism, the nitrogen of the former β -lactam ring deprotonates the deacylating water molecule, which is additionally activated by Tyr450 (Fig. 19(b)). This mechanism is supported by structural data [Patera et al., 2000, Chen et al., 2006] and by the observation that structural analogs of β -lactams lacking the ring nitrogen act as irreversible inhibitors [Bulychev et al., 1997].

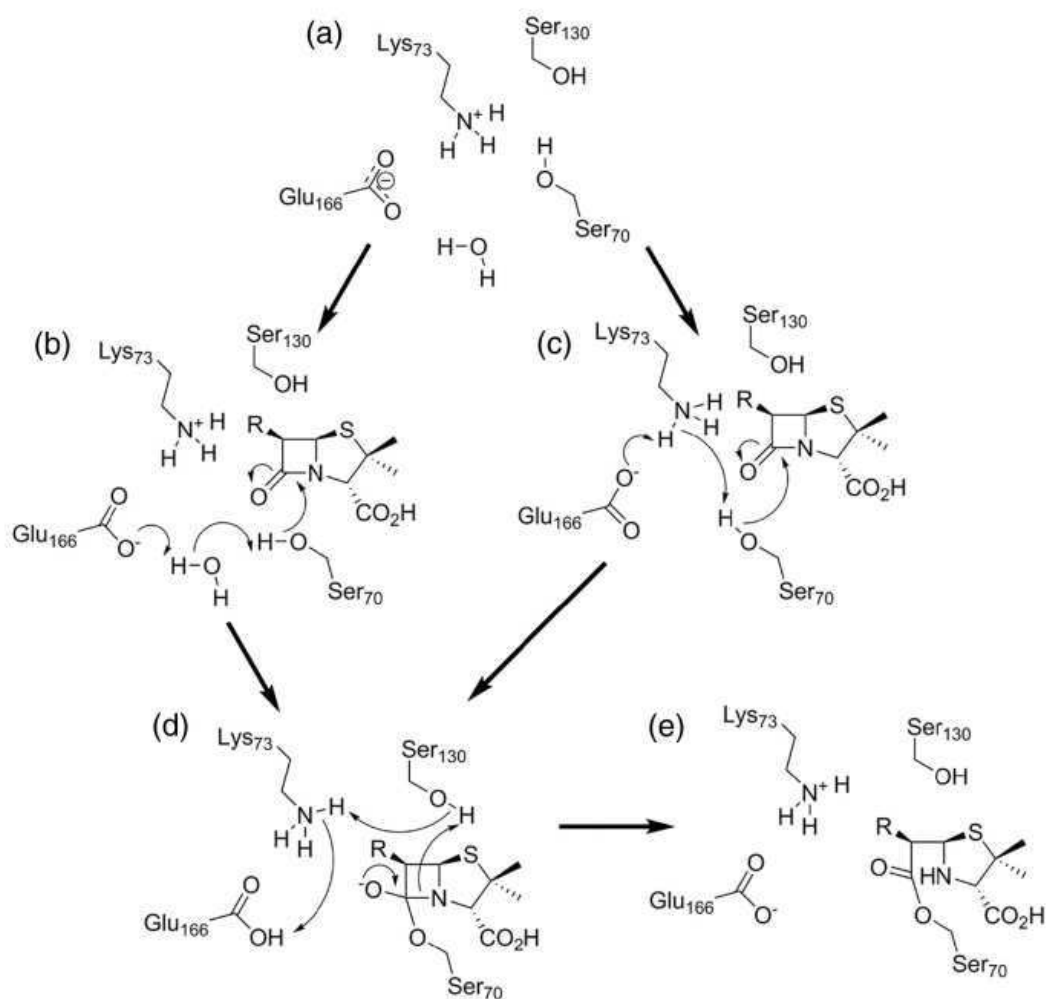


Figure 18: (a) Apoprotein active site shows Lys73 protonated and Glu166 deprotonated. (b) Ser70 may be activated for nucleophilic attack upon the β -lactam carbonyl by Glu166 via a water molecule. (c) Alternatively, substrate binding reorganizes protonation in the active site such that neutral Lys73 activates Ser70. The transition state (d) resolves to the acylenzyme intermediate (e) by protonation of the amide nitrogen from Ser130; from [Tooke et al., 2019]

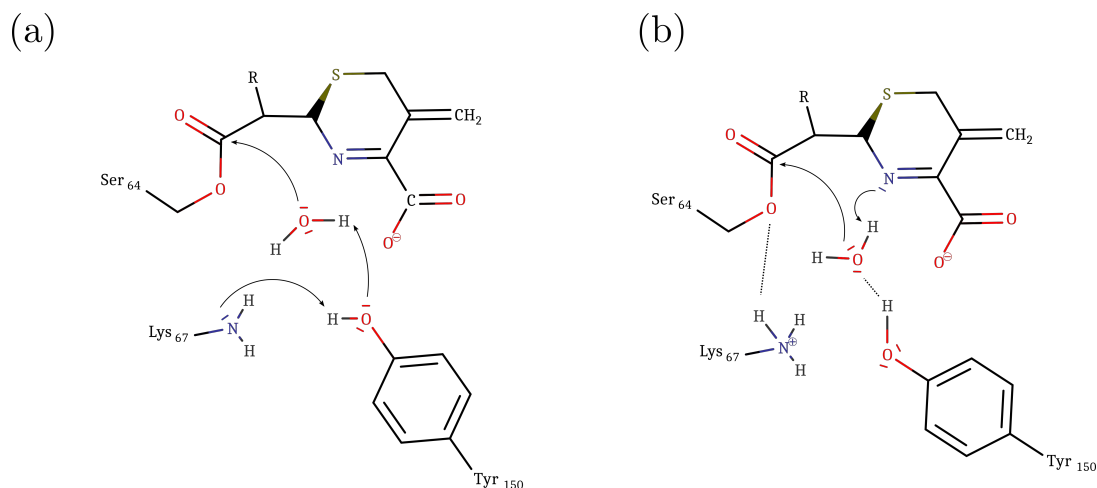


Figure 19: Proposed deacylation mechanisms in class C β -lactamases depicted with a generic cephalosporin substrate. (a) Conjugate base mechanism. Sequential proton abstraction of Lys67 and Tyr150 leads to the activation of the deacylation water molecule. (b) Substrate assisted mechanism. Tyr150 activates the deacylating water molecule for proton abstraction by a substrate nitrogen atom.

Class D β -lactamases. The active site of class D β -lactamases has a more hydrophobic character than those of classes A and C due to a high number of conserved hydrophobic residues [Leonard et al., 2013]. This is further emphasized by replacement of the Asn to Val or Ile in the SXN motif [Poirel et al., 2010]. The hydrophobic active site environment was proposed to sufficiently lower the pK_a of Lys73 resulting in the formation of a carbamate functional group by carboxylation of the primary amine [Sun, 2003]. Structural superposition of class A and class D enzymes aligns the carboxylated lysine residue with Glu166, suggesting that the carboxylate acts as the general base during both acylation and deacylation [Maveyraud et al., 2002] (Fig. 20). Stabilization by hydrogen bonds and salt bridges prevents spontaneous decomposition of the carbamate into carbon dioxide and free amine [Golemi et al., 2001].

4.3 Metallo β -lactamases

The Ambler class B β -lactamases comprises enzymes that rely on two Zn^{2+} ions in their activate site for β -lactam hydrolysis with the exception of the class B2 enzymes (metallo-carbapenemases) [Bush, 2013]. Class B β -lactamases are not related to PBPs, but belong to a superfamily also comprising thioesterases, phosphodiesterases, and oxydoreductases [Bebrone, 2007]. Conserved residues and motifs such as the characteristic HXHXAH are mostly implicated in metal coordination [Bebrone, 2007, Palzkill, 2013].

Molecular catalytic mechanism. As for serine β -lactamases, major questions for mechanistic understanding of the catalytic mechanism of metallo- β -lactamases are the identity of the

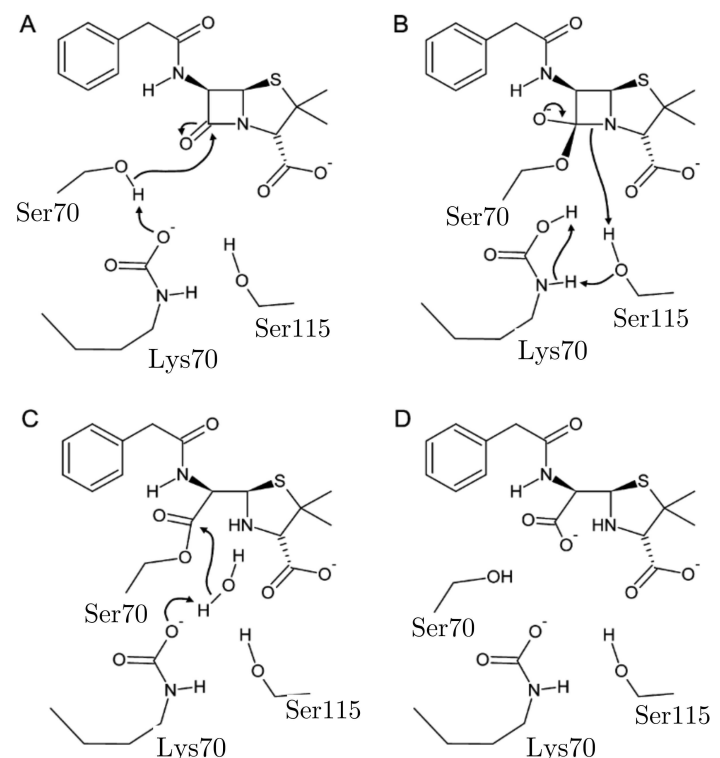


Figure 20: Proposed mechanism for class D β -lactamases. The initial acylation step is aided by carboxy-lysine-mediated deprotonation of S67. The carbamate also activates the deacylating water in the second step, modified from [Leonard et al., 2013]

nucleophile for attack on the carbonyl carbon of the β -lactam ring and the origin of the proton found on the product after ring opening. The mechanism of penam hydrolysis depicted in Fig. 21 has been proposed based on studies using enzymes in which Zn^{2+} has been replaced by Co^{2+} . This replacement enabled the characterization of the ligands of the active site metal ions using UV-Vis-spectrophotometry [Llarrull et al., 2008]. In the apo state, the active site zinc ions bind a bridging hydroxyl anion (W1) and a water molecule (W2). Substrate binding induces a shift of W2 to the bridging position and W1 positions for nucleophilic attack on the β -lactam carbonyl carbon. The β -lactam carboxyl group interacts with a lysine residue via electrostatic interactions. Hydrogen bonding of Asp120 with W2 in the bridging position decreases the pK_a of W2 and enables protonation of the β -lactam nitrogen upon ring opening. Intermediate ES^1 can convert into the non-productive intermediate ES^2 in which the β -lactam carboxyl group displays bidentate coordination to one of the zinc atoms. Catalytic mechanisms for the hydrolysis of cephalosporins and carbapenems are reviewed in [Meini et al., 2015].

4.4 Regulation of chromosomal β -lactamases in Gram-negative bacteria

It has been discovered in the 1980s that the genomes of enterobacteria and *P. aeruginosa* encode for a class C β -lactamase [Fisher and Mobashery, 2014]. While expression in *E. coli* is low

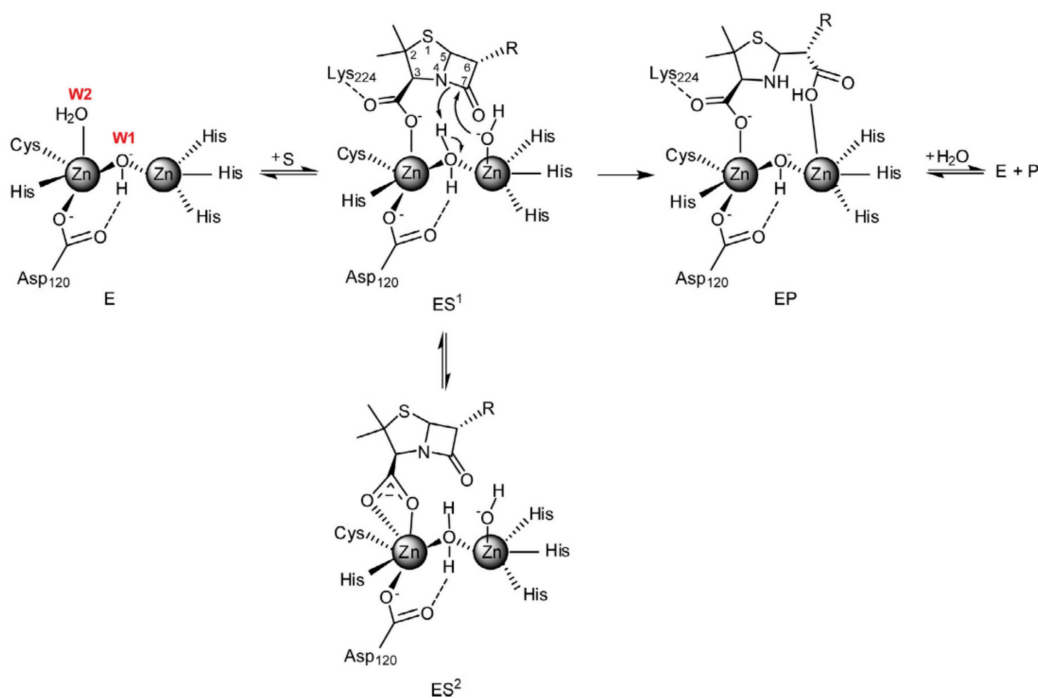


Figure 21: Catalytic mechanism of penam hydrolysis by metallo- β -lactamases, from [Meini et al., 2015].

and constitutive, expression in other Gram-negative enterobacterial species (*e.g.* *Citrobacter freundii*) was shown to increase when cells are challenged with β -lactam antibiotics [Lindberg et al., 1985].

In the aftermath of these results, induction of chromosomally encoded β -lactamses has been linked to peptidoglycan metabolism via the *ampR* gene [Fisher and Mobashery, 2014]. AmpR is a transcription regulator of the *ampC* β -lactamase gene. During growth in the absence of antibiotics, AmpR is in complex with major cytosolic peptidoglycan precursor, UDP-MurNAc-pentapeptide. This interaction negatively regulates AmpR [Jacobs et al., 1997] leading to a very low basal level of β -lactamase production [Honoré et al., 1986].

Under such conditions, peptidoglycan monomers containing a 1,6-anhydro-MurNAc unit are produced in the periplasm by the activity of PG lytic transglycosylases (Fig. 22A). The periplasmic anhydro muropeptides reach the cytoplasm via the AmpG permease, where they are further metabolized by the AmpD amidase and re-enter PG precursor synthesis [Johnson et al., 2013].

Upon β -lactam-mediated inhibition of PBPs, the equilibrium between PG synthesis and hydrolysis is tilted towards hydrolysis [Cho et al., 2014], leading to an accumulation of anhydro-turnover products in the cytoplasm due to substrate saturation of AmpD (Fig. 22B) [Jacobs et al., 1994]. Simultaneously, the pool of the UDP-MurNAc-pentapeptide is depleted under β -lactam treatment [Lara et al., 2005]. Under these conditions, anhydro-muropeptides displace

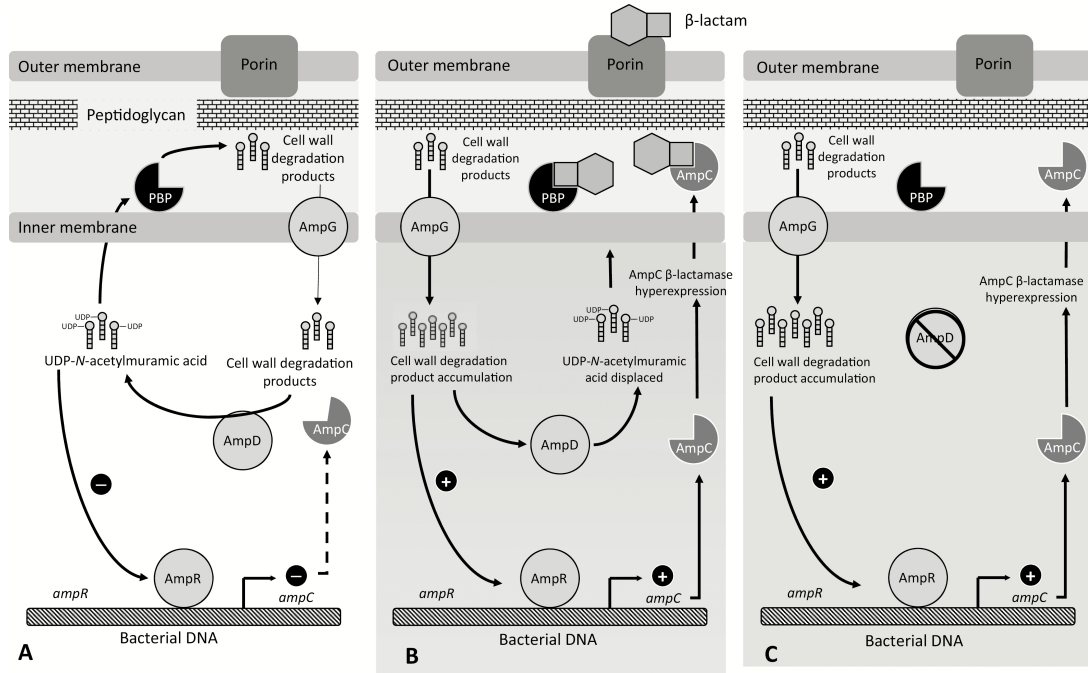


Figure 22: A simplified illustration of AmpC β -lactamase expression. (A) Basal AmpC β -lactamase production. (B) Increased transcription of *ampC* in the presence of an inducing β -lactam antibiotic that increases cell-wall degradation production to levels beyond the capacity of AmpD cleavage. Cell-wall degradation products accumulate and compete with UDP-N-acetylmuramic acid peptides for binding to AmpR. With decreased binding of UDP-N-acetylmuramic acid to AmpR, AmpR undergoes conformational changes resulting in increased AmpC production. (C) An AmpD mutation resulting in inactivation and subsequent stable derepression of AmpC. Abbreviations: PBP, penicillin binding protein; UDP, uridine diphosphate; from [Tamma et al., 2019]

UDP-MurNAc-pentapeptide in the AmpR binding site, which induces conformational changes activating AmpR and leads to enhanced transcription of the *ampC* gene [Jacobs et al., 1997].

Transition from inducible to constitutive expression of AmpC is often caused by mutations of genes implicated in sensing peptidoglycan turnover products (Fig. 22C). Clinical isolates of ceftazidime resistant *Enterobacter cloacae* with high β -lactamase activity harboured mutations in either *ampD* or *ampR* [Kaneko et al., 2005]. AmpG is essential for AmpD-mediated β -lactam resistance as in there is no accumulation peptidoglycan turnover products in its absence [Zhang et al., 2010]. It therefore represents a putative target in antibacterial therapy as inhibition could abolish β -lactamase overexpression and thereby restore activity of β -lactam antibiotics [Collia et al., 2018]. .

5 β -lactamase inhibitors

The emergence of β -lactamases was initially met with the development of β -lactamase-stable β -lactams [Bush and Bradford, 2019]. In the 1980s, the additional concept of administering β -lactams in combination with compounds restoring their activity in presence of β -lactamases led to the introduction of the first β -lactamase inhibitor (BLI), clavulanic acid, into the clinic [Reading and Cole, 1977]. In recent years, the field of β -lactamase inhibitors has seen major discovery efforts due to the dissemination of broad-spectrum inhibitor-resistant β -lactamases. New chemotypes have been granted market authorization or are in clinical trials [Wang et al., 2016, Bush and Bradford, 2019].

5.1 Serine β -lactamase inhibitors

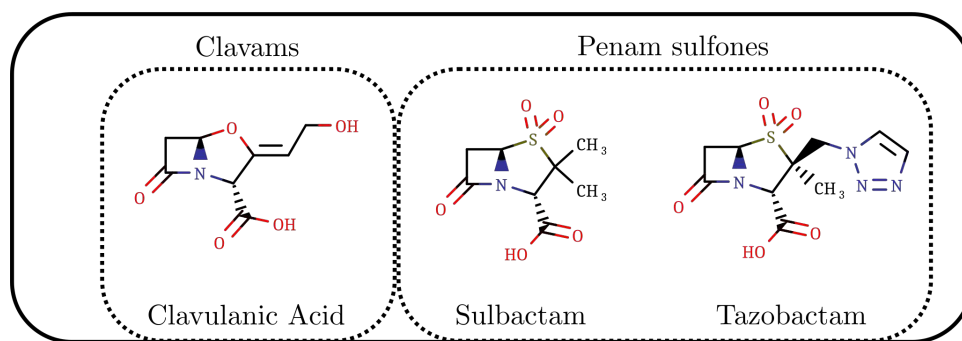
The structures of representatives of different structural classes of serine β -lactamase inhibitors are shown in Fig. 23 (A)-(C).

5.1.1 β -lactam based β -lactamase inhibitors

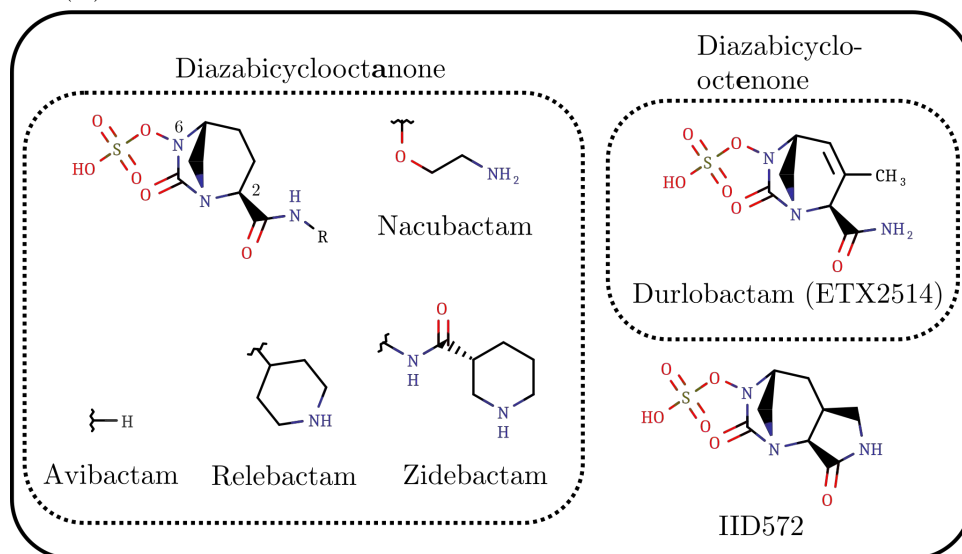
The first β -lactamase inhibitors were developed to encounter the increasing spread of β -lactamases, especially plasmid encoded TEM-1 [Bush and Bradford, 2019]. Natural product screening led to the discovery of clavulanic acid (CA) in *Streptomyces clavuligerus* (Fig. 23(A)) [Reading and Cole, 1977]. CA displays only limited intrinsic antibacterial activity [Finlay, 2003] and shows structural similarity to the classical β -lactamase substrates. Based on mechanistic insights from CA-mediated β -lactamase inhibition, the penam sulfones sulbactam (SUL) and tazobactam (TZB) (Fig. 23(A)) were developed. While tazobactam has no antibacterial activity, sulbactam is sufficiently active to warrant its clinical development in combination with a second generation β -lactamase inhibitor against multidrug-resistant strains of *Acinetobacter spp.* [Barnes et al., 2019].

The binding modes of first generation β -lactamase inhibitors are reminiscent of those observed in the formation of β -lactam- β -lactamase complexes. In particular, the carboxyl moiety of the inhibitors is positioned in the electropositive cavity and is stabilized by hydrogen bonds. The β -lactam carbonyl group of the inhibitors occupies the oxyanion hole [van den Akker and Bonomo, 2018] (Fig. 24). Inhibition of β -lactamases by CA, SUL and TZB relies on acylation of the active site serine (Fig. 25) [Marchand-Brynaert and Brulé, 2008]. Secondary rearrangement leads to opening of the thiazolidine ring and formation of the iminium species E-I' which can undergo an additional covalent reaction with Ser130 (with the loss of a portion of the molecule) leading to irreversible inhibition. E-I' can also tautomerize to its *cis*-enamine form which itself

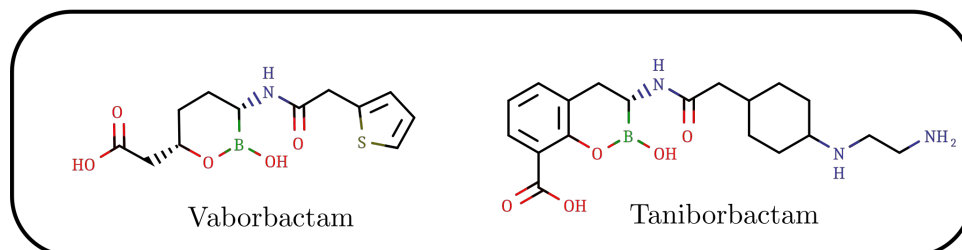
(A) β -lactam based BLIs



(B) DBOs



(C) Boronic-acid-based serine BLIs



(D) Metallo- β -lactamase inhibitor

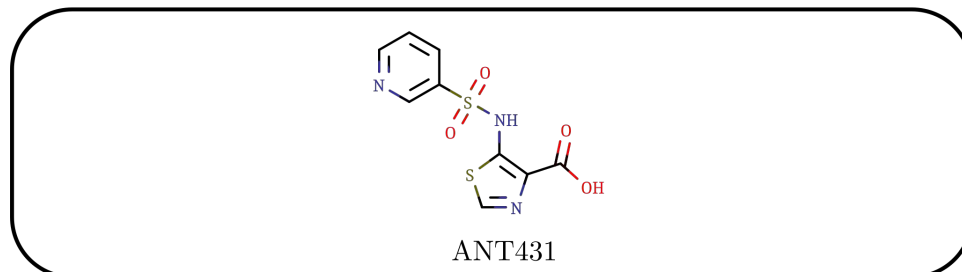


Figure 23: Structures of β -lactamase inhibitors. (A) First generation β -lactam based β -lactamase inhibitors (B) Second generation β -lactamase inhibitors with diazabicyclo[3.2.1]octan (DBO) scaffold (C) Second generation β -lactamase inhibitors serine β -lactamase inhibitors derived from boronic acid (D) Lead compound for recently discovered thiazole-4-carboxylic acid-based metallo- β -lactamase inhibitors

undergoes isomerization to the *trans* form. The vinylogous amide is deemed responsible for the stability of the enamine adduct as the electron density at the carbonyl carbon is increased due to conjugation. The increased electron density hinders nucleophilic attack of a deacylating water molecule. The *trans*-enamine adduct is very slowly hydrolyzed and its stabilization has been exploited to rescue inhibitory activity of penam sulfones against β -lactamases bearing a S130G mutation [Ke et al., 2012]. Hydrolysis and rearrangements leading to stable adducts occur concomitantly. In the case of TEM-1, 115 molecules of CA are hydrolyzed for one irreversibly inactivated molecule of TEM-1 [Bush and Bradford, 2019].

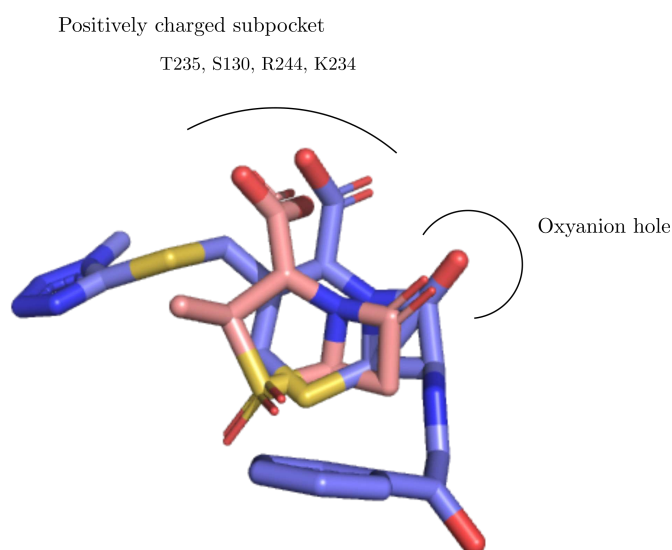


Figure 24: Binding mode of first generation β -lactamase inhibitors. Binding poses of cefamandole (blue sticks) and sulbactam (beige sticks) extracted from superposed K73A BlaC (class A β -lactamase of *M. tuberculosis*, PDB code 3NY4) and S70C SHV-1 (PDB code 4FH2), respectively. Figure created with PyMOL.

First generation BLIs inhibit Ambler class A β -lactamases of the functional groups 2a, 2b, and 2be, including Extended-Spectrum-Beta-Lactamases (ESBLs). ESBLs hydrolyze third generation extended spectrum cephalosporins, such as ceftriaxone, ceftazidime, and cefotaxime [Bush and Bradford, 2019]. CA, SUL and TZB show no or only minor activity against class A and class D carbapenemases [Leonard et al., 2013] and no activity against class C cephalosporinases [Jacoby, 2009]. Ongoing preclinical and clinical research addresses inhibition of serine carbapenemases by penam sulfones [Vázquez-Ucha et al., 2020].

5.1.2 Diazabicyclooctanes

In light of the limited inhibition spectrum of β -lactam based BLIs and the continuing spread of class A and D carbapenemases as well as strains harbouring multiple β -lactamases, a dire

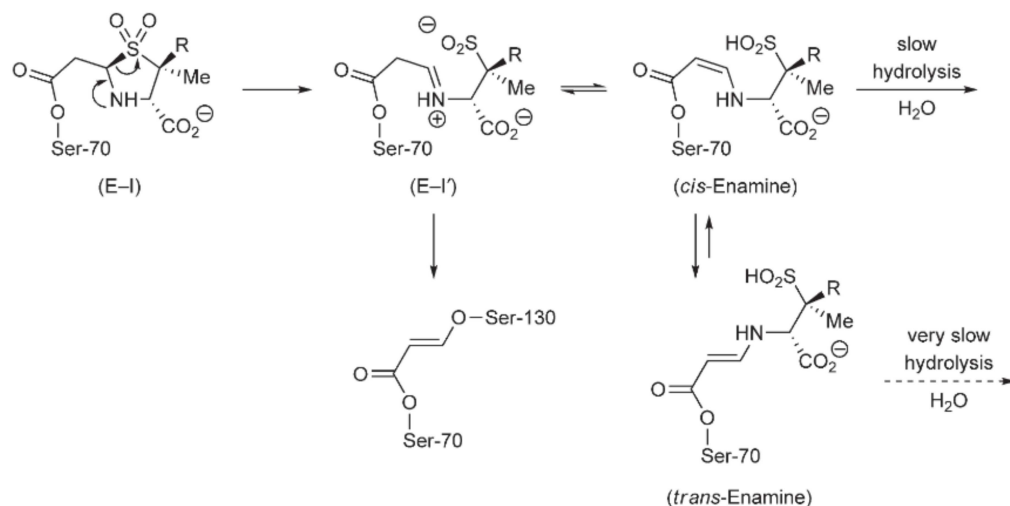


Figure 25: Formation of various covalent species after β -lactamase acylation by penam sulfones, from [Marchand-Brynaert and Brulé, 2008]

need for new inhibitors has arisen [Drawz and Bonomo, 2010]. Avibactam, a non- β -lactam BLI, was the first representative of BLIs based on a diazabicyclo[3.2.1]octane (DBO) scaffold that was granted market access in combination with the 3rd-generation cephalosporin ceftazidime [Bonney, 2004, Bush and Bradford, 2019] (Fig 23(B)). Since then, several pharmaceutical companies have launched development programs of β -lactam/DBO combinations [Yahav et al., 2020].

Avibactam is a slow-binding reversible β -lactamase inhibitor [Ehmann et al., 2012]. Formation of a non-covalent complex is followed by nucleophilic attack of the active site serine on the carbonyl carbon of the cyclic urea group. The sulfate group occupies the carboxyl binding region and the carbonyl group is positioned in the oxyanion hole. Avibactam adopts a similar conformation in acylenzyme-complexes with β -lactamases of classes A, C and D [Lahiri et al., 2013, Lahiri et al., 2015]. The molecular reaction mechanism for acylation of class A β -lactamases is similar to that of classical β -lactamase substrates (Fig. 26). Based on QM/MM simulations, Glu166 abstracts the proton via a water molecule and a tetrahedral intermediate is formed after nucleophilic attack of the Ser70 sidechain on the carbonyl carbon of the cyclic urea group. Ring opening occurs upon protonation of the urea nitrogen by Ser130 yielding the acylenzyme complex [Sgrignani et al., 2014].

A distinctive feature of DBO BLIs is the reversibility of the acylation reaction, which has first been established for Avibactam using mass spectrometry [Ehmann et al., 2012]. Avibactam was incubated with TEM-1, the acylenzyme was purified and incubated with apo-CTX-M-15. Detection of the CTX-M-15-avibactam acylenzyme by mass spectrometry implied recyclicalisation

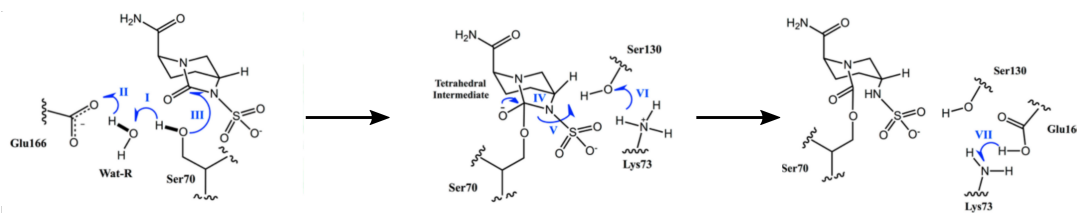


Figure 26: Molecular mechanism for acylation of TEM-1 β -lactamases by avibactam, modified from [Sgrignani et al., 2014]

of avibactam in the active site of TEM-1 followed by release of an intact avibactam molecule.

The ability of avibactam to reversibly acylate β -lactamases is generally attributed to reduced strain in the five-membered ring of avibactam compared to the four-membered ring of β -lactams which is thought to lower the energy barrier for recyclisation [Drawz et al., 2014]. Additionally, in the acylenzymes complexes the formerly connected carbon and nitrogen atoms remain positioned in close proximity [Choi et al., 2016]. Hydrolysis of the acylenzyme complex is disfavored since the deacylating water molecule is not appropriately positioned for nucleophilic attack on the carbamoyl group. In addition, the carbonyl of the carbamate is less electrophilic compared to an ester group due to resonance with the lone pair of the carbamate nitrogen [Lahiri et al., 2013]. However, desulfation of avibactam in the KPC-2-avibactam acylenzyme was reported to be followed by hydrolysis of the carbamoyl bond and release of the active carbapenemase [Ehmann et al., 2013].

Inhibition profile. Avibactam restores the activity of its β -lactam partner ceftazidime against strains harbouring one or several clinically relevant class A and C β -lactamases. Avibactam is also active against certain D β -lactamases but lacks activity against class B metallo-enzymes [Ehmann et al., 2013, Livermore et al., 2018]. The ceftazidime/avibactam combination (Avycaz) is approved for the treatment of complicated urinary tract and intra-abdominal infections as well as nosocomial infections. The combination is currently evaluated for respiratory tract infections caused by *P. aeruginosa* in patients with cystic fibrosis [Vázquez-Ucha et al., 2020]. Avycaz is of limited use against infections caused by *Acinetobacter* spp. since these bacteria often produce chromosomally encoded class D OXA variants, which are poorly inhibited by avibactam.

Avibactam is currently evaluated in a phase III clinical trial in combination with the monobactam aztreonam, which is a poor substrate for metallo- β -lactamases. The combination should provide a treatment option for Gram-negative bacteria producing multiple β -lactamases including metallo-enzymes [Marshall et al., 2017].

Relebactam is the second DBO, which entered the market. It is formulated in combination with imipenem/cilastatin. It is used to treat infections caused by carbapenem-resistant *Enter-*

obacteriaceae (CRE) and *P. aeruginosa*, including strains producing ESBLs, carbapenemases, and class C cephalosporinsases [Bush and Bradford, 2019]. Relebactam’s ability to restore the activity of imipenem in strains of *K. pneumoniae* and *Enterobacter* spp. is not affected by the loss of porins as an additional mechanism of resistance [Lapuebla et al., 2015]. Relebactam evades efflux from resistant strains of *P. aeruginosa* [Young et al., 2019], a characteristic that has been attributed to the positively charged secondary amino group in the 2’-sidechain (Fig. 23B) [Blizzard et al., 2014]. Interestingly, the presence of sterically unhindered amines has been more generally linked to enhanced penetration of small molecules into cells of Gram-negative bacteria [Richter et al., 2017]. Relebactam does not inhibit class D OXA enzymes [Tsivkovski et al., 2020]. Thus, the combination relebactam/imipenem is not a therapeutic option for OXA-48 producing enterobacteria and *Acinetobacter* spp. infections [Lapuebla et al., 2015].

Durlobactam (formerly ETX2514, Fig. 23B) has been specifically developed for the inhibition of class D β -lactamases since avibactam was only active on a few enzymes of this class including OXA-48. Optimization included evaluation of new compounds in biochemical assays against representative serine β -lactamases of classes A, C, and D. Simultaneously, determination of Minimal inhibitory concentrations (MICs) of piperacillin in presence of the new compounds against isogenic strains of *P. aeruginosa* producing the same β -lactamases was carried out, accompanied by estimation of chemical reactivity of the cyclic urea warhead. It was shown that small hydrophobic substituents in the 3’-position are favorable for inhibition of class D β -lactamases. Durlobactam restores the activity of meropenem and piperacillin against clinical isolates of *P. aeruginosa* and *A. baumannii*. [Durand-Réville et al., 2017]. Durlobactam is currently evaluated in combination with sulbactam as a narrow-spectrum treatment option for infections due to resistant strains *A. baumannii*, which are often producing OXA-type carbapenemases [Barnes et al., 2019]. In this combination, durlobactam protects sulbactam from hydrolysis by β -lactamses and thereby enables it to inhibit PBP1a and PBP3 of *A. baumannii*. Additionally, durlobactam complements the activity of sulbactam by inhibiting PBP2 of *A. baumannii* [Penwell et al., 2015, Barnes et al., 2019].

Additional targets of DBOs The main incentive in the development of DBO based inhibitors was the inhibition of β -lactamases. However, avibactam was shown to bind, albeit weakly, to PBPs of Gram-positive and Gram-negative bacteria [Asli et al., 2016]. Rational design efforts led to the discovery of CPD4 (Fig. 27), with improved *in vitro* activity against PBP2 of *E. coli* and enhanced intrinsic antibacterial activity. β -lactamase inhibition was reduced for CPD4 [Levy et al., 2019]. Zidebactam and Nacubactam display intrinsic antibacterial activity while retaining clinically useful β -lactamase inhibitory activity and are therefore called β -lactam enhancers

[Morinaka et al., 2015, Moya et al., 2017].



Figure 27: Structure of CPD4. The oxazole moiety in combination with the double bond enables formation of new hydrophobic and pi-pi-stacking interactions, the aminomethyl substituent at position 2' enhances antibacterial activity, from [Levy et al., 2019]

Avibactam and triazole-based DBOs were shown to inhibit L,D-transpeptidases from enterobacteria and *Mycobacterium tuberculosis* and to reduce the MIC of amoxicillin against *M. tuberculosis* [Edoo et al., 2018, Munnik et al., 2020]. *M. tuberculosis* relies mainly on L-D-transpeptidases for peptidoglycan crosslinking [Lavollay et al., 2008] and expresses a class A β -lactamase. As the class A β -lactamase of *M. tuberculosis* is only weakly inhibited by DBOs [Soroka et al., 2016], these findings indicate inhibition of additional targets by DBOs in *M. tuberculosis*.

5.1.3 Boronic-acid derivatives

Boronic acids are alkylated or arylated boric acid derivatives. Boronic acids act as strong Lewis acids and electrophiles due to their open *p* shell. They have been first recognized as inhibitors of serine proteases [Smoum et al., 2012]. These findings triggered the rational design of the first boronic acid-based inhibitor of TEM-1 [Martin and Jones, 1995]. Boronic acid- β -lactamase inhibitors reversibly form covalent adducts with the catalytic serine residue. X-ray crystallographic studies revealed that these adducts mimic the deacylation transition state [Strynadka et al., 1996]. Vaborbactam (Fig. 23C) has recently been approved in combination with meropenem for treatment of urinary tract infections [Bush and Bradford, 2019]. Vaborbactam inhibits class A carbapenemases and class C cephalosporinases but shows no activity against class B and class D enzymes [González-Bello et al., 2020]. Efforts to extend the inhibition spectrum of vaborbactam led to discovery of taniborbactam (Fig. 23C) which additionally inhibits some class D enzymes and a panel of clinically relevant metallo- β -lactamases and is currently in clinical development in combination with cefepime [Krajnc et al., 2019]. QPX7728 is a novel boronic acid based β -lactamase inhibitor with a remarkable coverage of all classes of β -lactamases including class B metallo- β -lactamases [Tsivkovski et al., 2020]. QPX7728 is also effective as a β -lactamase

inhibitor against ESBL producing enterobacteria, carbapenem resistant enterobacteria and *A. baumannii*, as well as against a large collection of *P. aeruginosa* clinical isolates. The compound is not affected by porin modifications nor drug efflux [Hecker et al., 2020].

5.2 Inhibitors of class B β -lactamases

Metallo- β -lactamases (MBLs) represent an unmet medical need as they hydrolyze all clinically used β -lactams with the exception of the monobactam aztreonam. MBLs are insensitive to inhibition by DBO-based BLIs.

As mentioned in the previous section, boronic acid derivatives provide a promising pharmacophore for pan- β -lactamase inhibition [González-Bello et al., 2020]. Inhibition of Zn^{2+} -containing metallo- β -lactamases relies on coordinative covalent bonds formed between the boron atom and the catalytic water molecule as well as between oxygen atoms in the boronic acid and carboxylate groups and the active site zinc ions (Fig. 28).

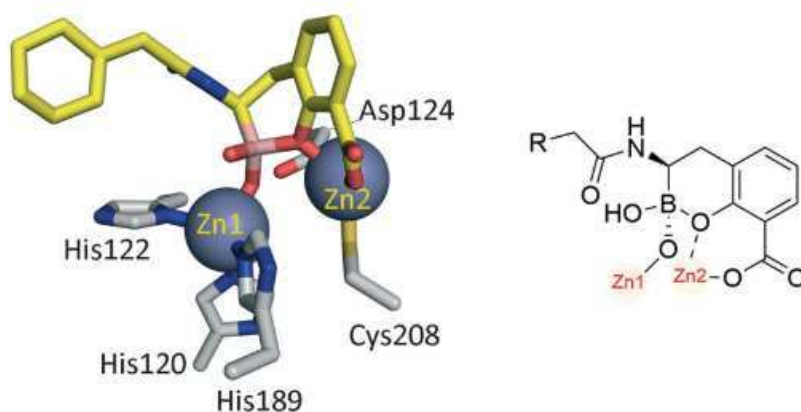


Figure 28: Crystal structure of NDM-1 in complex with a boronic acid inhibitor, relevant side chain residues are shown and labeled. Zn^{2+} ions are shown as spheres, boron atoms are colored in pink, from [González-Bello et al., 2020]

Other classes of metallo- β -lactamases inhibitors also exploit chelation of the active site zinc ions. Dipicolinic acid derivatives have been identified as inhibitors of MBLs [Chen et al., 2017]. While the lead compound from this study was not further developed due to non-selectivity and safety concerns [González-Bello et al., 2020], the thiazole-4-carboxylic acid inhibitor ANT431 (Fig. 23D) was based on these prior findings [Leiris et al., 2019]. Bioisosteric replacement of the picolinic acid moiety by a thiazole-4-carboxylic acid in combination with an aryl-sulfonamide substituent was found to improve *in vitro* inhibition of metallo- β -lactamases. Although, ANT431 was able to potentiate the activity of meropenem in a mouse thigh infection model, coverage of MBL producing strains, as determined against a wide panel of clinical isolates, was deemed insufficient for further clinical development [Everett et al., 2018]. ANT431 served as a template in

a recent medicinal chemistry campaign, which resulted in the discovery of a thiazole-4-carboxylic acid-inhibitor with suitable antibacterial, physicochemical, and pharmacokinetic properties to warrant clinical development in combination with meropenem [Davies et al., 2020a].

Part II

Optimization of β -lactamase inhibitors belonging to the diazabicyclo-octane family

"Soyons rationnels.

N'exagérons pas les choses."

- Mick Boyle, *Youth*

6 Introduction

In 2017, the WHO prioritized bacteria according to the need for new antibiotics for treatment of infections caused by multi-drug resistant strains. Critical priority pathogens comprise *Acinetobacter baumannii*, *Pseudomonas aeruginosa* and *Enterobacteriaceae*, all of which have been classified as such due to their resistance to β -lactam antibiotics, especially to carbapenems [Taccconelli et al., 2017]. This report came during a period of decreasing market entries of new antibiotics, as many major pharmaceutical companies closed their antibiotic development programs in the last decades [Plackett, 2020]. Of the ten antibacterial drugs approved by the FDA in the years 2015 to 2019, four were either β -lactams (Cefiderocol) or β -lactam/ β -lactamase inhibitor combinations (ceftazidime/avibactam, meropenem/vaborbactam, imipenem/relebactam) [Andrei et al., 2018, Andrei et al., 2019]. Resistance to the ceftazidime/avibactam combination (Avycaz) has already been described in patients under treatment with this combination [Shields et al., 2016]. The resistant strain had acquired mutations in genes coding for KPC β -lactamases [Shields et al., 2017]. Resistance was mainly due to poor inhibition of the enzymes by avibactam (as opposed to improved hydrolysis of ceftazidime) [Compain and Arthur, 2017]. These findings emphasize the ongoing need for new β -lactamase inhibitors with the potential to overcome acquired resistance in β -lactamases.

In this context, our objective was to obtain additional DBOs with improved characteristics in the framework of a collaboration with the team of Mélanie Ethève-Quelquejeu for chemical synthesis of new compounds. I performed the evaluation of their activity both with respect to inhibition of purified β -lactamases and antibacterial activity of β -lactam/inhibitor combinations.

In the first publication we characterized a series of new DBO-based β -lactamase inhibitors. Our collaborators, namely Flavie Bouchet and Lauro Iannazzo from the team of Mélanie Ethève-Quelquejeu, have developed an optimized synthetic route giving access to an azido-DBO intermediate which can easily be functionalized using click-chemistry [Edoo et al., 2018]. A series of 15 compounds, substituted with diverse functional groups was synthesized and tested against a panel of five clinically relevant β -lactamases, including the emerging carbapenemases KPC-2 (class A) and OXA-48 (class D), CTX-M-15 a representative of class A extended spectrum β -lactamases, and AmpC from *Enterobacter cloacae* (AmpC_{clo}), a representative of class C β -lactamases from aerobic Gram-negative bacteria. This enzyme panel covers all molecular classes of serine β -lactamases and major functional groups. Spectrophotometric assays were used to obtain the kinetic constants of inhibition for all compounds against all enzymes. Five isogenic strains of *E. coli* harboring one of the β -lactamases on a plasmid under control of an inducible promoter were constructed and the ability of the compounds to restore activity of β -lactams

was evaluated. For each β -lactamase, we choose a β -lactam, which is effectively hydrolyzed to monitor various extents of inhibition by the β -lactamases by the compounds. We show that the triazole substituent is compatible with a DBO scaffold and β -lactamase inhibition. However, in this first series, none of compounds proved superior to the reference DBO inhibitors avibactam and relebactam. Modeling performed with class A β -lactamases suggested that introduction of the triazole ring prevented formation of a crucial hydrogen bond involving asparagine at position 132 (Ambler numbering). The large set of data collected with five β -lactamases and 17 inhibitors enabled me to explore the correlation between *in vitro* inhibition of the purified β -lactamases and the antibacterial activity of β -lactam/inhibitor combinations in the cellular assay. The two indicators of efficacy were generally correlated, indicating that impaired penetration was not the major determinant of the lessened activity of our compounds. A more detailed analysis of the data revealed that certain functional groups are associated with better (primary amines) or worse (bulky sidechain substituents) translation of *in vitro* activity into activity in the cellular assay.

In the second publication we explored the potential benefit of combining relebactam with either imipenem or amoxicillin on the *in vitro* and intracellular efficacy against *Mycobacterium abscessus* and compared the results to those obtained with Avibactam. I contributed to this study by characterizing the *in vitro* inhibition by relebactam of Bla_{Mab}, the class A β -lactamase intrinsically found in all *M. abscessus* isolates. *M. abscessus* is an opportunistic pathogen commonly found in patients suffering from pulmonary diseases such as cystic fibrosis and chronic obstructive pulmonary disease (COPD) [Park and Olivier, 2015]. Imipenem is recommended for the treatment of infections due to *M. abscessus* in patients suffering from cystic fibrosis in spite of hydrolysis of this drug by Bla_{Mab} with a moderate but significant activity [Soroka et al., 2014, Floto et al., 2016]. We evaluated the impact of the inhibition of Bla_{Mab} by relebactam on the activity of imipenem by means of MIC determination, time-kill curves and intracellular proliferation in a macrophage model of infection. While the inhibition of Bla_{Mab} by relebactam was less potent compared to avibactam, results from cellular assays were equivalent. Based on these data and the fact, that avibactam is exclusively available in combination with ceftazidime, which is inactive against *M. abscessus*, we propose that the imipenem/relebactam combination should be considered for treatment of infections due to *M. abscessus*.

I also participated in a study aimed at characterizing the basis for the variations in fluorescence intensity associated with acylation of β -lactamases and transpeptidases by β -lactams and DBOs. Since this study corresponds to a side project with a minor contribution I have included the publication in the annexes.

Publication I

Bouchet, F.; **Atze, H.**; Fonvielle, M.; Edoo, Z.; Arthur, M.; Ethève-Quelquejeu, M.; Iannazzo, L. Diazabicyclooctane Functionalization for Inhibition of β -Lactamases from Enterobacteria. *J. Med. Chem.* 2020, 63 (10), 5257–5273.
<https://doi.org/10.1021/acs.jmedchem.9b02125>.

Publication II

Le Run, E.; **Atze, H.**; Arthur, M.; Mainardi, J. L. Impact of Relebactam-Mediated Inhibition of Mycobacterium Abscessus BlaMab β -Lactamase on the in Vitro and Intracellular Efficacy of Imipenem. *J. Antimicrob. Chemother.* 2020, 75 (2), 379–383.
<https://doi.org/10.1093/jac/dkz433>.

9 Discussion

Medicinal chemistry challenges of DBO-based β -lactamase inhibitors. The abundance of characterized β -lactam derivatives allowed to derive comprehensive structure-activity-relationships for their primary targets, the PBPs, and also for β -lactamases [Hubschwerlen, 2007]. While structural data for approved DBO-based β -lactamase inhibitors useful to rationalize changes in inhibitory activity upon altered inhibitor structure is available, actually very few complete structure-activity-relationship (SAR) series have been published in the peer-reviewed literature. The small pharmaceutical company Antabio (Toulouse) published a series of DBO compounds obtained during the rational optimization of inhibition of class D β -lactamases, starting from avibactam. The authors anticipated a positive impact of lipophilic substituents at the 2'-position of the DBO scaffold, based on analysis of the the OXA-48/avibactam structure. They found that a fluorine substituent retained activity against known β -lactamase targets of avibactam and extended the inhibition spectrum to new class D carbapenemases. Accordingly, the new compound (ANT3310) was able to potentiate the activity of meropenem against *A. baumannii* clinical isolates producing class D enzymes [Davies et al., 2020b]. Another series explored the impact of substituting the 2'-carboxamide of avibactam with sulfur containing groups, such as sulfoxides and sulfones in order to increase the electron-withdrawing character of the 2' substituent. In addition, the impact of substitutions in position 6' were investigated in the background of a methyl-sulfone in position 2'. Results indicated that a suitable combination of substituents with respect to electron-withdrawing properties in positions 2' and 6' is necessary for activity [Fujiu et al., 2020].

Comparison of our study with *Davies et. al* (2020) and *Fujiu et. al* (2020) highlights some of the medicinal chemistry challenges in the design of β -lactamase inhibitors with covalent mechanisms of inhibition. DBOs have been shown to act as reversible two-step slow-binding inhibitors of β -lactamases [Ehmann et al., 2012]. As the name implies, the formation of the equilibrium between inhibitor and the enzyme occurs slowly compared to reaction of the enzyme with the substrate. Thus, inhibition is time-dependent with consequences on classical determination of IC_{50} s [Copeland, 2005]. Indeed, measuring the IC_{50} for this type of inhibitors is ambiguous as results depend on the duration of preincubation of the enzyme with the inhibitor prior to the addition of the substrate (10 min *vs.* 0 min in [Davies et al., 2020b] and [Fujiu et al., 2020], respectively) and on readout time after addition of substrate (10 min *vs.* 20 min). While still useful to compare activities within a series of inhibitors, these differences in assay conditions prohibit direct comparison of the datasets presented in the two references cited in the previous sentence. In contrast, full kinetic characterization does allow for such comparisons. In addition,

such data enable the conversion into IC_{50} s if needed for comparison with inhibitors exhibiting a different mode of action [Lebeaux et al., 2019]. Apart from the fact that determination of drug binding kinetics does not fit well with screening efforts due to the need for comprehensive mechanistic data analysis, it has been advocated based on theoretical considerations that kinetic characterization is beneficial even in the early drug discovery process [Keighley, 2011]. In the case of slow-binding inhibitors it is evident that affinity based screening is prone to overlooking potent inhibitors. The kinetics of drug binding is also important to assess *in vivo* target selectivity. Indeed, a drug may be selective for one target, even among a group of targets for which it displays similar affinities, as measured by the equilibrium inhibition constant K_i . This is the case when selectivity is governed by the on- and off-rate constants for the different targets rather than by the K_i [Tonge, 2018]. Thus, off-target effects may be more accurately identified by kinetic rather than by thermodynamic selectivity determination.

Correlation of kinetic parameters and the post-antibiotic effect (PAE) have been investigated for a series of slow-binding inhibitors [Walkup et al., 2015]. The authors found that the residence time (the inverse of the overall off-rate) correlated best with PAE values. The authors also proposed a new pharmacodynamics (PD) model explicitly incorporating slow-binding kinetics, which showed superior predictive performance of drug effects compared to standard PD models exclusively based on equilibrium affinity. Interestingly, using the new model for dose finding would result in significant lower doses, which clearly emphasizes the importance of kinetic characterization early during the drug discovery process [Tonge, 2018].

Pros and cons of developing a standalone β -lactamase inhibitor. Pharmaceutical companies prioritize the development a pan- β -lactamase inhibitor (in the best of all cases) in combination with a β -lactam partner, which is active against the majority of critical priority pathogens. This strategy is justified from a regulatory perspective. Independent development of a BLI has no precedent and thus no model for regulatory approval exists [Yahav et al., 2020]. Additionally, proof had to be established that the BLI is able to restore the activity of a variety of β -lactams. This would include an inhibition spectrum covering relevant β -lactamses, which are able to hydrolyse the β -lactam partner and most importantly from a clinical perspective, compatible pharmacokinetic properties. It has however been argued from a clinical perspective that access to standalone BLI would be beneficial [Abodakpi et al., 2019], a view supported by our study since avibactam is effective in inhibiting the *M. abscessus* β -lactamase although the partner drug (ceftazidime) has no antibacterial activity against this mycobacterium (Publication 2). Use of stand-alone BLIs would require that the dosing of the BLI and the combined β -lactam is coordinated by the clinical infectious disease specialist according to the pharmacokinetic characteristics of the two

drugs. One can easily imagine a situation where a strain expresses a β -lactamase resistant to avibactam but susceptible to relebactam and which hydrolyzes ceftazidime (the β -lactam partner of avibactam). These resistance determinants could be identified by diagnostic tools such as antibiograms of β -lactams in the presence of several BLIs or whole genome sequencing. In order to limit the use of carbapenems (relebactam is available only in combination with imipenem), a suitable option would be the combination of ceftazidime and relebactam. However, due to the current approval situation, the clinician has to resort to imipenem/relebactam. In at least one case (MK-6183) the pharmaceutical industry has considered development of an inhibitor without a fixed β -lactam partner. This inhibitor developed by Merck showed promising results in a one-compartment *in vitro* infection model for combination with several β -lactams [Ambrose et al., 2017]. The compound restored activity of four β -lactam partners in varying dosing regimen and intervals against a panel of *Enterobacteriaceae* producing eight serine-carbapenemases, alone or in combination. The authors concluded that MK-6183 is a suitable candidate for development as standalone BLI. However, the current state of development is unknown and the compound is not listed in the current Merck pipeline [Papp-Wallace, 2019].

Critical role of hydrogen bonding to Asn132 for effective inhibition of class A β -lactamases by DBOs. The asparagine at position 132 (Ambler numbering) is part of the canonical SDN motif commonly found in class A β -lactamases [Bush, 2013]. Crystal structures of acylenzymes revealed hydrogen bonding of the side-chain of Asn132 with the carbonyl oxygen of the 6 β -side-chain of β -lactams [Strynadka et al., 1992] and of the 2'-amide of DBOs [Lahiri et al., 2013]. The catalytic role of Asn132 in β -lactam hydrolysis is not well understood. *Jacobs et al.* (1990) studied the impact of the N132S and N132A substitutions on protein stability and catalytic activity [Jacob et al., 1990]. While the authors found only a minor impact on protein melting temperatures, the catalytic efficiency for hydrolysis of penams ($k_{\text{cat}}/K_{\text{m}}$) was severely impaired for N¹³²A (residual catalytic efficiency less than 1% compared to the wild-type enzyme) and partially retained for the N¹³²S mutant (>15%). Since the decrease in the catalytic efficiency observed for N¹³²A was mainly due to a decrease in the rate constant for the catalytic step (k_{cat}) the authors concluded that Asn132 stabilizes the transition state rather than the non-covalent complex.

This hypothesis is corroborated by structural studies employing TEM-1 and an acylation transition state analogue (TSA) inhibitor, which revealed interaction of the 6 β -sidechain equivalent of the TSA inhibitor with Asn132 [Maveyraud et al., 1998]. Asn132 is a highly conserved residue in class A β -lactamases (>99.9% conservation in 661 analyzed sequences of class A β -lactamases) [Lahiri et al., 2016]. The broad-spectrum class A β -lactamase of *Mycobacterium*

tuberculosis (BlaC) harbors Gly rather than Asn at Ambler position 132 and is poorly inhibited by avibactam whereas clavulanate acts as potent irreversible inhibitor [Soroka et al., 2016]. Introduction of asparagine at position 132 of BlaC improves inhibition by avibactam and impairs inhibition by clavulanate. Introduction of a N¹³²G substitution in other class A β -lactamases results in a BlaC-like inhibition profile [Soroka et al., 2016, Ourghanlian et al., 2017]. However these results were not in agreement with another study [King et al., 2016a], which reported that introduction of N¹³²A in CTX-M-15 did not affect the inhibition of this class A β -lactamase by avibactam. In several class A β -lactamases, including CTX-M-15 and KPC-2, the 2'-carboxamide of avibactam interacts with Asn170 in addition to Asn132. These interactions are absent in the PER class β -lactamases against which avibactam shows less activity [Lahiri et al., 2016, Ruggiero et al., 2017].

In order to further investigate the role of the 2'-amide group in DBO-based β -lactamase inhibitors and to corroborate the findings from our study (Publication I), we evaluated the acylation efficacy of constitutional isomers of 2'-amide DBOs differing only in the position of the amide carbonyl group (FBC159 vs. FBC111 in Table 5). As can be deduced from the data presented in Table 5, the inversion of the amide group in the 2'-sidechain of DBOs leads to significant loss of inhibitory activity against class A and C β -lactamases, similar to introduction of the 2'-triazole-methylene substituent (compound FBC069 (10b)) in Table 5. Thus, modifications of the structure of DBOs indicate that loss of the critical hydrogen bond involving Asn132 and the carbonyl group of the 2'-carboxamide of the inhibitor is crucial for effective inhibition of class A β -lactamases, in agreement with data based on substitutions at position 132 presented in the preceding paragraph. Figure 29 illustrates the interactions of Asn132 of KPC-2 with avibactam and triazole-containing DBOs 7b and 10b. Modelling revealed loss of the critical hydrogen bond for 7b and 10b. The figure also illustrates that 7b can form additional hydrophobic interactions with the enzyme that partially compensate for loss of hydrogen bonding with N132. This may account for the higher efficacy of 7b in comparison to 10b (Table 5).

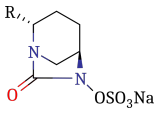
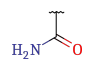
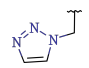
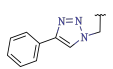
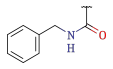
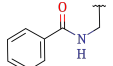
		TEM-1	KPC-2	CTX-M-15	AmpC _{clo}	OXA-48
	Avibactam	88,000 ± 2,000	26,000 ± 1,000	130,000 ± 10,000	18,000 ± 1,000	980 ± 60
	FBC069 (10b)	1,200 ± 1,000	280 ± 30	280 ± 10	210 ± 20	140 ± 20
	FBC049 (7b)	4,700 ± 1,000	930 ± 40	6,900 ± 2,000	200 ± 10	110 ± 30
	FBC159	47,000 ± 1,350	54,600 ± 4,200	34,400 ± 2,500	250,000 ± 41,000	380 ± 52
	FBC111	1,250 ± 115	120 ± 40	3070 ± 170	28 ± 6	660 ± 81

Table 5: Acylation efficacy of triazole-containing DBOs and 2'-amide DBO constitutional isomers in comparison to avibactam

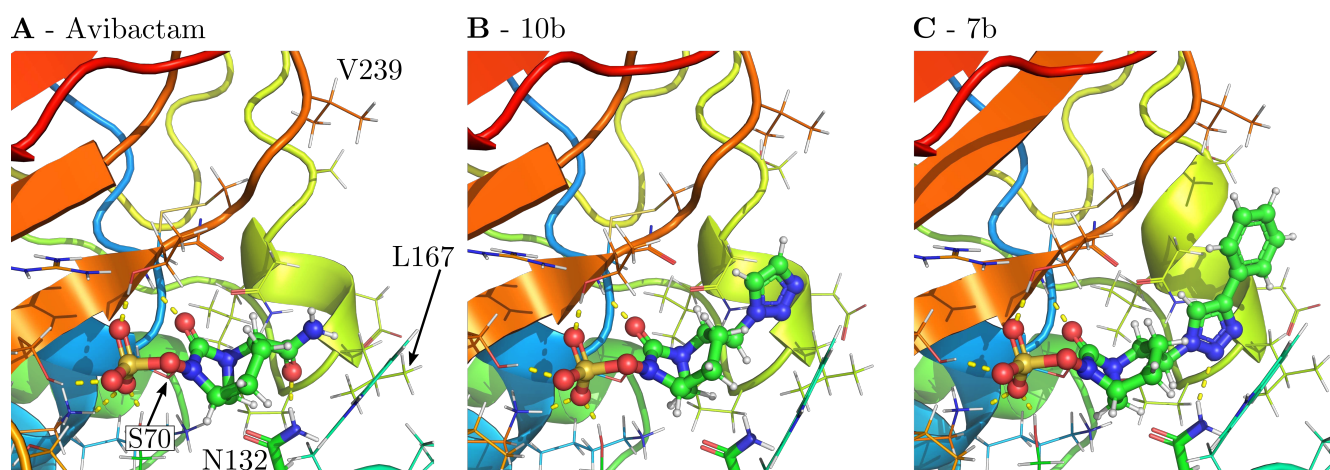


Figure 29: Modeling of non-covalent complexes formed by DBOs and KPC-2. (A) Avibactam; (B) DBO 10b; (C) DBO 7b. The enzyme is shown as cartoon, ligands as ball and stick and active site residues in proximity to the DBOs as wireframe or stick. Putative hydrogen bonds are indicated by yellow dashed lines. Solvent molecules have been omitted. To construct the models, the crystal structure of KPC-2 carbamoylated by avibactam was retrieved from RSCB protein databank (accession code 4ZBE). Closure of the avibactam ring and protonation of Ser70 were performed manually. Protonation states of ionizable groups were assigned using the H++ webserver [Anandakrishnan et al., 2012] in accordance with previous studies [Sgrignani et al., 2014]. The model was placed in a box of water ensuring a minimum distance of 7 Å between any protein atom and the box boundary. The system was minimized with a convergence criterion of 0.1 kJ/mol. The model of the KPC-2:avibactam complex generated by this approach was used as a template to manually model DBOs 10b and 7b into the enzyme active site. Energy was subsequently minimized using the procedure described above. Modeling and visualization of complexes and compounds were performed with PyMol [Schrödinger, 2015]. For minimization, we used OpenMM [Eastman et al., 2017] with the Amber ff14SB [Maier et al., 2015] (protein), Parsley [Mobley, 2019] (ligand), and TIP3P (solvent) parameter sets.

Part III

Design of a mass-spectrometry-based approach for exploring peptidoglycan polymerization

*"Per me l'unica scena jazz
interessante è quella etiope."*

- Viola, *La Grande Bellezza*

10 Objectives

The chemical composition of the PG layer has been reported for a wide range of bacterial species [Quintela et al., 1995]. However, the dynamics of its expansion during growth and maturation are less well understood. A range of models for the insertion of new subunits into the existing PG layer have been proposed (for a commented selection of models see Fig. 30).

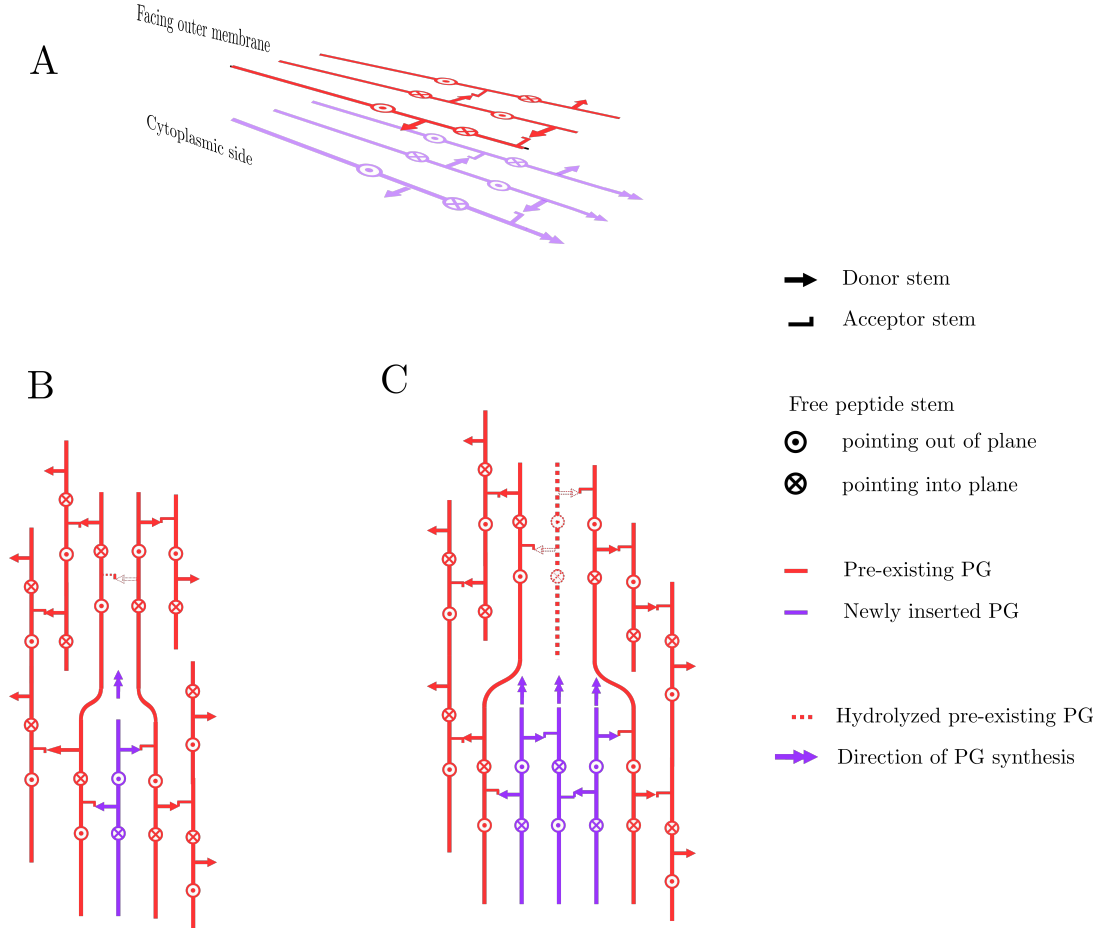


Figure 30: Models for the insertion of new PG units into the existing PG layer, adapted from [Höltje, 1998] **(A)** Neo-synthesized (new) material is not attached to pre-existing (old) material, crosslinks should exclusively link newly synthesized material **(B) One strand at a time**, all crosslinks are expected to contain old and new material **(C) Three-for-one**, three strands are polymerized simultaneously and replace a docking strand which is removed; crosslinks are expected to occur both between new and preexisting subunits and between new subunits

Experiments investigating the insertion of new subunits into PG and the fate of PG during growth have historically been based on pulse labeling of cultures of *E. coli* with [^3H]- or [^{14}C]-labeled DAP [Wientjes et al., 1985, Burman and Park, 1984, Glauner and Holtje, 1990]. The usage of DAP as tracer molecule is challenging. While DAP residues are exclusively found in PG, a large proportion of DAP is converted into L-lysine. Efficient labeling of PG with DAP necessitates an adjustment of the metabolic fluxes in *E. coli*, namely (i) deletion of *lysA* (coding for

the diaminopimelate decarboxylase) in order to prevent conversion of DAP to L-lysine (ii) inactivation of *dapF* (coding for the diaminopimelate epimerase) to abolish endogenous biosynthesis of DAP, and (iii) adding L-lysine and DAP to the culture medium, due the auxotrophy for these amino acids induced by the aforementioned gene deletions. *E. coli* W7 (*dapF*, *lysA*), which was used in various studies [Goodell, 1985, Burman et al., 1983, Burman and Park, 1984, Glauner and Holtje, 1990] harbors a large intracellular pool of DAP when grown in the media supplemented with DAP (usually 2 µg/ml). This DAP pool induces a lag between the addition of radioactive DAP and appearance of the label in the metabolites of interest, such as intracellular peptidoglycan precursors and muropeptides of the PG layer. The duration of the lag depends on the amount of DAP present in the growth medium [Wientjes et al., 1985].

Because of this limitation, we aimed at developing a new labeling method using heavy stable isotopes of carbon [^{13}C] and nitrogen [^{15}N] and mass spectrometry that would not require any specific genetic background to enable fast labeling kinetics. We compared our method to radioactive DAP-based techniques in terms of lag time prior to the detection of newly synthesized material and their ability to distinguish muropeptides issued from recycling and from *de novo* synthesis. Our method was also used to characterize differences between the modes of PG cross-linking mediated by PBPs and LDTs. The results are presented in the form of a an article in preparation for submission the the journal eLife.

Our MS-based approach necessitated (i) the calculation of theoretical mass spectra of muropeptides containing combinations of labeled and unlabeled residues starting from their isotopic composition and chemical formula and (ii) the development of custom data preprocessing and analysis tools, comprising batch analysis of data files, automated peak annotation in mass spectra and comparison of experimental data to theoretical fragmentation patterns of muropeptides. Calculation of theoretical mass spectra was performed using IsoTool [Atze, 2021], which provides a graphical user interface for the IsoSpec algorithm for isotopic cluster calculations [Lacki et al., 2017] (available at <https://github.com/kantundpeterpan/IsoTool>). Tools for MS data analysis have been grouped into MassElTOF package (<https://gitlab.com/kantundpeterpan/masseltof>), which contains example applications in its documentation.

11 Publication III

Exploring bacterial cell wall metabolism by mass spectrometric analysis of peptidoglycan labeled with stable isotopes

Heiner Atze, Filippo Rusconi, and Michel Arthur

Centre de Recherche des Cordeliers, Sorbonne Université, INSERM, Université de Paris,
F-75006, Paris, France

Manuscript in preparation

Abstract

Peptidoglycan, the major component of bacterial cell walls, is a giant net-like macromolecule made of glycan strands cross-linked by short peptides. Since peptidoglycan is essential to sustain the osmotic pressure of the cytoplasm and is only found in bacteria the enzymes involved in its synthesis are attractive targets for drug development. This is the case for D,D-transpeptidases belonging to the penicillin-binding protein (PBP) family that catalyze the last cross-linking step of peptidoglycan polymerization and are inactivated by drugs of the β -lactam family such as ampicillin. These enzymes form 4 \rightarrow 3 cross-links connecting the 4th and 3rd positions of acyl donor and acceptor stem peptides located in adjacent glycan chains. In *Escherichia coli*, bypass of PBPs through formation of 3 \rightarrow 3 cross-links by L,D-transpeptidase YcbB results in ampicillin resistance. Here, the mode of insertion of neo-synthesized peptidoglycan subunits into the expanding peptidoglycan macromolecule was investigated based on labeling with heavy isotopes and mass spectrometry. This new approach offered several advantages over previously used labeling with a radioactive precursor since it enabled analysis of peptidoglycan synthesis and recycling in a single experiment and did not require metabolic engineering for labeling optimization. In the absence of ampicillin, PBPs and YcbB participated in similar modes peptidoglycan polymerization mainly involving single-strand insertion of glycan chains into the expanding side walls. The absence of any transpeptidase-specific signature suggests that the mode of insertion of glycan chains might be determined by other components of the peptidoglycan polymerization complexes. In the presence of ampicillin, YcbB mediated insertion of multiple strands that were exclusively cross-linked to tripeptide-containing acceptors present in the preexisting peptidoglycan. We propose that this unique mode of insertion depends upon accumulation of linear glycan chains due to PBP inhibition by ampicillin and formation of tripeptide acceptors due to cleavage of pre-existing 3 \rightarrow 3 cross-links by a β -lactam-insensitive endopeptidase.

1 Introduction

The peptidoglycan is an essential component of the bacterial cell wall that provides a mechanical barrier against the turgor pressure of the cytoplasm, thereby preventing cells from bursting and lysing [1]. The peptidoglycan also determines the shape of bacterial cells and is intimately integrated into the cell division process because the barrier to the osmotic pressure needs to be maintained during the entire cell cycle. These functions depend upon the net-like structure of the peptidoglycan macromolecule (*ca.* 4.2×10^9 Da in *Escherichia coli*) consisting of glycan strands cross-linked by short peptides (Fig. 1A) [2]. It is assembled from *ca.* 4.7×10^6 disaccharide-peptide subunits consisting of β -1 \rightarrow 4 linked *N*-acetylglucosamine (GlcNAc) and *N*-acetyl muramic acid (MurNAc) and a stem peptide linked to the D-lactoyl group of MurNAc

(Fig. 1B) [2]. Polymerization of the subunits is mediated by glycosyltransferases for the elongation of glycan chains and by transpeptidases for cross-linking stem peptides carried by adjacent glycan chains.

Peptidoglycan biosynthesis is initiated in the cytoplasm by the production of UDP-MurNAc from UDP-GlcNAc followed by the sequential addition of L-Ala, D-Glu, *meso*DAP, and the D-Ala-D-Ala dipeptide to form UDP-MurNAc-pentapeptide (Supplementary Fig. S1) [3]. The following steps involve precursors inserted into the inner leaflet of the cytoplasmic membrane. These steps are initiated by the transfer of the phospho-MurNAc-pentapeptide moiety of UDP-MurNAc-pentapeptide to the C₅₅ lipid transporter (undecaprenyl-phosphate) followed by the addition of the GlcNAc moiety of UDP-GlcNAc generating Lipid I and Lipid II, respectively. The complete disaccharide-pentapeptide subunit linked to the lipid carrier is then translocated to the outer surface of the cytoplasmic membrane by the flippase MurJ and/or FtsW and polymerized.

Following the polymerization of glycan chains by glycosyltransferases, the last cross-linking step of peptidoglycan polymerization is catalyzed by two types of structurally unrelated transpeptidases [4], the D,D-transpeptidases [5], which belong to the penicillin-binding protein (PBP) family, and the L,D-transpeptidases (LDTs) [6]. PBPs (Fig. 1C) and LDTs (Fig. 1D) harbor different catalytic nucleophiles (Ser *versus* Ala), use different acyl donor substrates (pentapeptide *versus* tetrapeptide, resulting in the formation of 4→3 *versus* 3→3 cross-links), and are inhibited by different classes of β -lactams (potentially all β -lactams *versus* members of the carbapenem class), respectively [7, 8]. In wild type *E. coli*, LDTs are fully dispensable for growth, at least in laboratory conditions [9]. Accordingly, these enzymes have a minor contribution to peptidoglycan cross-linking, as 3→3 cross-links account for 11% and 16% of the cross-links present in the peptidoglycan extracted from bacteria in the exponential and stationary phases of growth, respectively [10, 1]. However, selection of mutants resistant to ceftriaxone, a β -lactam of the cephalosporin class, results in a full bypass of PBPs by the YcbB L,D-transpeptidase [8]. The bypass requires overproduction of the (p)ppGpp alarmone and of YcbB [8]. The peptidoglycan of the mutant grown in the presence of ceftriaxone exclusively contains cross-links of the 3→3 type due to full inhibition of the D,D-transpeptidase activity of PBPs [8].

D,D-carboxypeptidase and L,D-carboxypeptidase activities sequentially remove D-Ala residues at the 5th and 4th positions of stem peptides containing a free carboxyl end, which are present in the acceptor position of dimers and in monomers. D,D-carboxypeptidases (DDCs), which belong to the PBP family, hydrolyze the D-Ala⁴-D-Ala⁵ amide bond of stem pentapeptides to generate stem tetrapeptides in mature peptidoglycan [11]. Since that reaction is nearly total in *E. coli*,

stem pentapeptides are found in very low abundance unless DDCs are inactivated by β -lactams. The L,D-carboxypeptidase activity of LDTs is responsible for hydrolysis of the DAP³-D-Ala⁴ amide bond, thus converting tetrapeptide stems into tripeptide stems [9]. Since this reaction is incomplete, the peptidoglycan contains combinations of tetrapeptide and tripeptide stems in monomers and in the acyl acceptor position of dimers. The hydrolysis of stem peptides catalyzed by DDCs and LDTs, which occurs before or after the cross-linking reactions, leads to the polymorphism in the acceptor position of dimers depicted in Fig. 1C and 1D.

By removing D-Ala⁵ from pentapeptide stems, DDCs eliminate the essential pentapeptide donor of PBPs and generate the essential tetrapeptide donor of LDTs [8, 12]. By removing D-Ala⁴ from tetrapeptide stems, LDCs eliminate their essential tetrapeptide donor stems. Thus, the DDC and LDC activities of PBPs and LDTs regulate both the extent of peptidoglycan cross-linking and the relative contributions of D,D-transpeptidases and L,D-transpeptidases to this process at the substrate level.

The interconversion between monomers and dimers involves not only PBPs and LDTs in the biosynthetic direction but also hydrolytic enzymes, referred to as endopeptidases, that cleave the cross-links. Endopeptidases belonging to the PBP family are specific of 4→3 cross-links whereas other endopeptidases cleave both 4→3 and 3→3 cross-links [13, 14]. Among eight endopeptidases with partially redundant functions, at least one enzyme is essential in the context of the formation of 4→3 cross-links whereas two endopeptidases, MepM and MepK, are required in the context of 3→3 cross-links [14].

Morphogenesis of *E. coli* cells depends upon controlled expansion of the peptidoglycan and requires scaffolding proteins, homologues of tubulin (MreB) and of actin (FtsZ) [15]. These proteins are involved in the localization of peptidoglycan polymerases and in the coordination of their activities with that of hydrolases [16]. The cell cycle involves two phases corresponding to the MreB-dependent elongation of the side wall at a constant diameter followed by FtsZ-dependent formation of the septum at mid cell. These processes are thought to involve two distinct multienzyme complexes, the elongasome and the divisome, and specific enzymes, in particular PBP2 and PBP3 (class B PBPs), that mediate peptidoglycan cross-linking in the side wall and in the septum, respectively [17]. Accordingly, specific inhibition of PBP2 or PBP3 by the β -lactam mecillinam or aztreonam results in the growth of *E. coli* as spheres or as filaments, respectively.

The average chemical composition of the peptidoglycan is well known. Most enzymes involved in the formation or cleavage of glycosidic and amide bonds have been identified (at least one enzyme and generally several enzymes for each bond kind). However, the spatial arrangement of

glycan strands is still a matter of debate. Most models propose a regular arrangement of glycan strands parallel to the cell surface and perpendicular to the long axis of the cell as depicted in Fig. 1A [18], perhaps with an helical arrangement to account for the helical nature of MreB filaments. Alternatively, it has been proposed that the glycan strands protrude perpendicularly to the surface of the cytoplasmic membrane [19, 20]. The lack of direct experimental evidence originate from the heterogeneity of the peptidoglycan macromolecule that prevents the analysis of the polymer by radiocrystallography. NMR also failed to determine the structure of the polymer due to its heterogeneity and its important flexibility as measured by NMR relaxation for Gram-positive and Gram-negative bacteria [21]. The mode of insertion of new glycan strands in the growing peptidoglycan is also not fully characterized. Murein enlargement according to the ‘three-for-one’ growth model involves the insertion of three neosynthesized glycan strands to the detriment of the hydrolysis of one preexisting strand, which acts as a docking strand [16]. Other models propose that glycan strands are inserted either one or two at a time, the latter possibility being supported by the dimeric nature of certain D,D-transpeptidases [22]. These models postulate that expansion of the peptidoglycan layer requires cleavage of cross-links by endopeptidases and obey to the ‘make-before-break’ principle, that proposes that cross-links present in the preexisting peptidoglycan are hydrolyzed by endopeptidases only if the newly synthesized glycan strands are cross-linked and can sustain the osmotic pressure of the cytoplasm.

At each generation, about half of the disaccharide-peptide units making the peptidoglycan is released by the combined action of endopeptidases and lytic glycosyltransferases [23, 24]. The latter enzymes catalyze a non-hydrolytic cleavage of the β -1 \rightarrow 4 MurNAc-GlcNAc glycosylic bond and generate GlcNAc-anhydro-MurNac-peptide fragments via cyclisation at positions 1 and 6 of MurNAc. These fragments are transported into the cytoplasm by the AmpG permease and recycled according to the pathway depicted in supplementary Fig. S1. The key features of the recycling pathway are that the L-Ala- γ -D-Glu-DAP tripeptide is directly recycled whereas the glucosamine moiety of GlcNAc and MurNAc reenter into the peptidoglycan biosynthesis pathway at the level of glucosamine-1-phosphate. The relationships between peptidoglycan synthesis and recycling are poorly understood. The ‘three-for-one’ growth model predicts that the docking strand is recycled, while the “one-or-two-strand-at-a-time” models do not predict that recycling is a consequence of peptidoglycan synthesis.

Pulse-labeling of peptidoglycan with radioactive DAP provides a means for experimentally exploring these models since the ratio of radioactivity in acceptor stems to that in donor stems varies as a function of the model (acceptor-to-donor radioactive ratio or ADRR) (Fig. S2) [25]. Alternatively, the decay of radioactive DAP from labeled peptidoglycan was used to follow

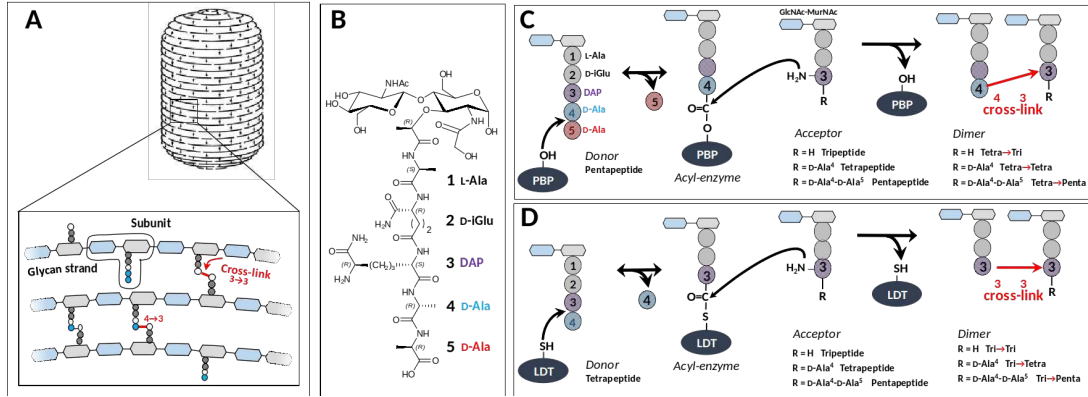
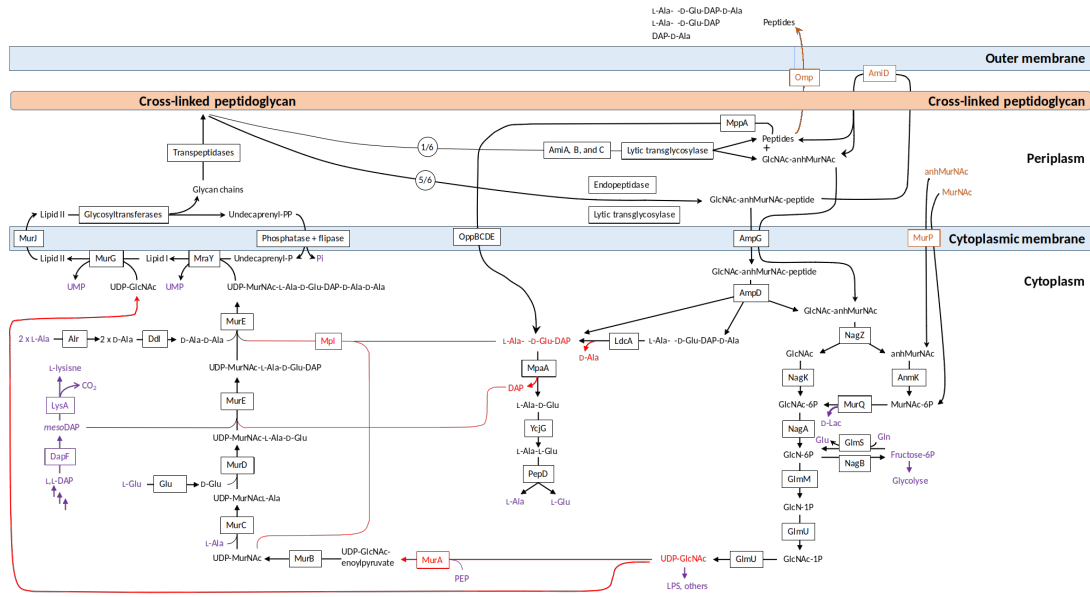


Figure 1: Structure and biosynthesis of *E. coli* peptidoglycan (A) Structure of peptidoglycan. The net-like macromolecule is made of glycan strands cross-linked by short peptides. The polymerization of peptidoglycan involves glycosyltransferases that catalyze the elongation of glycan strands and transpeptidases that form 4→3 or 3→3 cross-links. (B) Structure of the peptidoglycan subunit. The stem peptide is assembled in the cytoplasm as a pentapeptide, L-Ala¹-D-iGlu²-DAP³-D-Ala⁴-D-Ala⁵, in which D-iso-glutamic acid (D-iGlu) and meso-diaminopimelic acid (DAP) are connected by an amide bond between the γ -carboxyl of D-iGlu and the L stereo-center of DAP. (C) Formation of 4→3 cross-links. Active-site Ser transpeptidases belonging to the penicillin-binding protein (PBP) family catalyze the formation of 4→3 cross-links connecting the carbonyl of D-Ala at the 4th position of an acyl donor stem peptide to the side-chain amino group of DAP at the 3rd position of an acyl acceptor stem peptide. A pentapeptide stem is essential in the donor substrate to form the acyl enzyme intermediate. The acyl acceptor potentially harbor a pentapeptide, a tetrapeptide, or a tripeptide stem leading to the formation of Tetra-Tri, Tetra-Tetra, or Tetra-Penta dimers, respectively. (D) Formation of 3→3 cross-links. Active-site Cys transpeptidase belonging to the L,D-transpeptidase (LDT) family catalyze the formation of 3→3 cross-links connecting two DAP residues. LDTs are specific of tetrapeptide-containing donors.



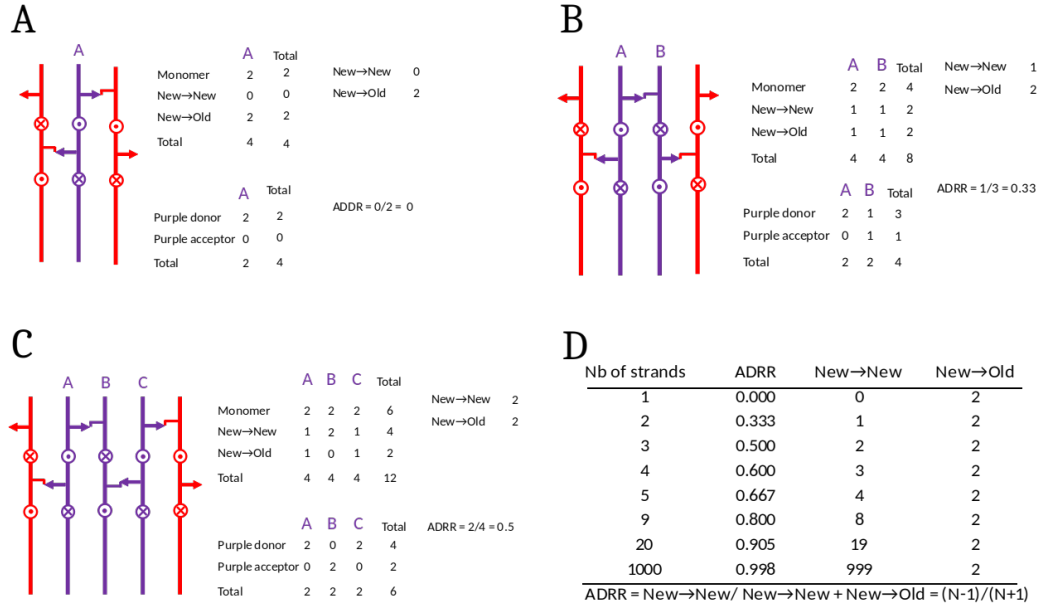
Supplementary Figure S1: Synthesis and recycling of peptidoglycan in *E. coli*. Key intermediates connecting synthesis (on the left) to recycling (on the right) are figured in red. Metabolites common to peptidoglycan metabolism and to other metabolic pathways are figured in purple. Effective incorporation of DAP from the culture medium requires inactivation of the genes encoding DapF and LysA generating lysine auxotrophy. Peptidoglycan turnover refers to the release of peptidoglycan fragments (<600 Da) into the culture medium. PG fragments cross the outer membrane through porins.

peptidoglycan turnover. In this study, we show that the use of stable isotopes of carbon and nitrogen in combination with mass spectrometry (MS) has several advantages over the labeling techniques based on radioactive DAP because it enables following peptidoglycan synthesis and recycling in a single experiment. In addition, the MS-based technique is not limited to the fate of DAP but covers all sugar and amino acid constituents of peptidoglycan. Using this approach, we also report the mode of peptidoglycan cross-linking by LDTs which has not been previously investigated.

2 Materials and Methods

Sample preparation and analysis

Strains. *E. coli* M1.5 [8, 14] is a derivative of *E. coli* BW25113 [26] harboring (i) plasmid pJEH12 for IPTG inducible expression of the *ycbB*-transpeptidase gene, (ii) deletions of the *erfK*, *ynhG*, *ycfS*, and *ybiS* L,D-transpeptidase genes, (iii) a 13-bp deletion lowering the translation level of the gene encoding the isoleucyl-tRNA synthase (IleRS) resulting in increased synthesis of the (p)ppGpp alarmone, and (iv) a chromosomal mutation inactivating the *slt* lytic transglycosylase gene enabling growth in the presence of ampicillin in liquid media. Upon



Supplementary Figure S2: (A) One strand at a time. (B) Two strands at a time. (C) Three strands at a time (applies to the three for one model). (D) Calculation for various number of strands. Preexisting and neo-synthesized strands are figures in red and in purple, respectively. Donor and acceptor stems are represented by an arrow and by an L, respectively. Uncross-linked peptide stems that protrude above and below the plan are indicated by circles with a dot or an X, respectively.

induction of *ycbB* by IPTG, *E. coli* M1.5 expresses high-level resistance to ampicillin and ceftriaxone following production of YcbB and (p)ppGpp. Deletion of the *erfK*, *ycfS*, and *ybiS* genes abolishes the anchoring of the Braun lipoprotein and simplifies the *rpHPLC* mucopeptide profile because stem peptides substituted by a Lys-Arg dipeptide are absent [27].

The *ampG* permease gene [24] of *E. coli* BW25113 M1.5 was deleted using the two-step procedure described by Datzenko and Wanner [26]. The kanamycin resistance gene used for allelic exchange was amplified with oligonucleotides 5'-CCAAAACTATCGTGCCAGC and 5'-AGAGTGACAACTGGGTGATG.

E. coli $\Delta 6ldts$ is a derivative of strain BW25113 obtained by deletion of the six L,D-transpeptidase genes present in *E. coli* (*erfK*, *ynhG*, *ycfS*, *ybiS*, *yafK*, and *ycbB*) [27, 9, 28, 29].

Growth conditions and determination of the generation time. *E. coli* strains were grown in M9 minimal medium composed of 2 mM MgSO₄, 0.00025% FeSO₄, 12.8 g/l Na₂HPO₄, 3 g/l KH₂PO₄, 0.5 g/l NaCl, 1 g/l NH₄Cl, 1 μ g/l thiamine, 1 g/l glucose (unlabeled M9 minimal medium). Labeling was performed in the same medium except for replacement of NH₄Cl and glucose by [¹⁵N]NH₄Cl (Cambridge Isotope Laboratories; 99% labeling) and uniformly labeled [¹³C]glucose (Euriso-top; 99% labeling) at the same concentrations, respectively (labeled M9

minimal medium). The growth media were sterilized by filtration (Millex-LG 0.2 μm , Merck Millipore).

Bacteria were grown on brain heart infusion (BHI) agar plates (Difco) to initiate the experiment with an isolated colony that was inoculated in 25 ml of labeled minimal medium. The pre-culture was incubated for 18 h at 37 °C with aeration (180 rpm). The entire pre-culture (25 ml) was inoculated into one liter of labeled M9 medium and the resulting culture was incubated until the optical density at 600 nm (OD₆₀₀) reached 0.4. Bacteria were collected by centrifugation (8,200 x g, 7 min, 22 °C), resuspended in 1 liter of prewarmed (37 °C) unlabeled M9 medium, and incubation was continued in the same conditions. Samples (200 ml) were withdrawn at various times and bacteria were collected by centrifugation (17,000 x g, 5 min, 4 °C) and stored at -55 °C. The generation time was deduced from the inverse of the slope of semi-logarithmic plots (log of OD₆₀₀ as a function of time).

Peptidoglycan preparation and purification of mucopeptides. Peptidoglycan was extracted by the hot SDS procedure and treated with pronase and trypsin [30]. Mucopeptides were solubilized by digestion with lysozyme and mutanolysin, reduced with NaBH₄, and separated by rpHPLC in a C18 column (Hypersil GOLD aQ 250 x 4.6, 3 μm ; ThermoFisher) at a flow rate of 0.7 ml/min. A linear gradient (0% to 100%) was applied between 11.1 min and 105.2 min at room temperature (Buffer A: TFA 0.1%; Buffer B: TFA 0.1% acetonitrile 20%; v/v). Absorbance was monitored at 205 nm and peaks corresponding to the major monomers and dimers were individually collected, lyophilized, solubilized in 30 μl of water, and stored at -20 °C.

Calculation of the molar ratios of mucopeptides. HPLC analysis of sacculi digested by muramidases provided relative areas for peaks detected by the absorbance at 205 nm. In order to evaluate the relative molar abundance of mucopeptides we used the correction factors reported by Glauner [10], which take into account the number of disaccharide units, amide bonds, 1,6-anhydro-ends, and Lys-Arg residues. Since the relative amount of the mucopeptides did not vary upon growth (*i.e.* between samples collected at various times following the medium switch), or between samples from independent experiments, (*i.e.* between biological repeats obtained for the same strain in the same growth conditions) an average molar composition of the sacculi was deduced from the HPLC chromatograms and the correction factors reported by Glauner [10].

Mass spectrometry. For routine identification of mucopeptides, samples were diluted (10 μl plus 50 μl of water) and 2 μl were injected into the mass spectrometer (Maxis II ETD, Bruker,

France) at a flow rate of 0.1 ml/min (acetonitrile / water (50:50) acidified with 0.1% formic acid, v/v). Mass spectra were acquired in the positive mode with a capillary voltage of 3,500V, pre-storage pulse 18 μ s, Funnel 1 RF 300 Vpp. The m/z scan range was from 300 to 1850 at a speed of 2 Hz. Stepping mode was enabled with the following parameters: RF values 400 and 1200 V; transfer time 30 μ s and 90 μ s; timing 50% and 50%. MS/MS spectra were obtained using a collision energy of 50 eV in the m/z range of 150 - 1,000 for mucopeptide monomers and 150 - 2,000 for mucopeptide dimers with isolation width of 1. The collision energy was varied between 77 to 100% with timings of 33% and 67%, respectively.

Structural characterization of the labeled GlcNAc-MurNAc-tetrapeptide isotopologues was performed on a ThermoFisher Orbitrap Fusion Lumos instrument operated in nanospray mode. The 50% acetonitrile in water analyte solution was acidified to 1% formic acid and introduced in the instrument using conventional nanospray glass emitter tips. The source voltage was set to 3,000-3,500V and the sample was introduced without pneumatic assistance. The ions under each one of the peaks that made the isotopic cluster were fragmented individually by tune-mode quadrupole-selection of the corresponding ions in a 0.4 m/z -width selection window centered on the peak apex. That narrow selection window proved to be selective enough to only fragment the ions under each isotopic cluster peak of interest (from most intense to less intense: m/z 986.52, m/z 985.51, m/z 984.51). The fragmentation was obtained for a collision-induced dissociation energy of 10 eV. The MS/MS data were acquired in 200-1000 m/z -range spectra (at least 50 MS/MS scans were acquired). Raw MS/MS data files were converted to the standard mzML file format using ProteoWizard’s msconvert tool [31]. The obtained data files were scrutinized using the mineXpert software version 2 [32].

Mass spectrometric data analysis

Simulation of high resolution mass spectra to determine the isotopic composition of mucopeptides and the extent of ^{13}C and ^{15}N labeling. Mass spectral data analyses were carried over by performing matches between simulated and observed isotopic clusters for mucopeptides recovered from bacteria grown in labeled and unlabeled media. The approach used to generate the simulated spectra was adapted from a recent publication [33] as detailed below. Data are presented below for the reduced disaccharide-tripeptide (GlcNAc-MurNAc-L-Ala- γ -D-iGlu-DAP), which was taken as an example.

Isotopologue abundance The first step in obtaining simulations of high resolution mass spectra is the calculation of the abundance of all possible isotopomers, *i.e.* molecules defined by the presence of a specific isotope at each position. Table 1 provides the mass and abundance of the

Table 1: Mass and relative abundance of H, C, N, and O isotopes used for isotopic cluster simulations

Isotope	Mass ^a	Relative abundance in the growth media	
		Unlabeled	Labeled
¹² C	12.000 000 000 000	0.9893 ^b	0.01 ^c
¹³ C	13.003 354 835 071	0.0107 ^b	0.99 ^c
¹ H	1.007 825 032 231	0.999885 ^b	0.999885 ^b
² H	2.014 101 778 120	0.000115 ^b	0.000115 ^b
¹⁴ N	14.003 074 004 426	0.99636 ^b	0.01 ^c
¹⁵ N	15.000 108 898 884	0.00364 ^b	0.99 ^c
¹⁶ O	15.994 914 619 566	0.99757 ^b	0.99757 ^b
¹⁷ O	16.999 131 756 500	0.00038 ^b	0.0038 ^b
¹⁸ O	17.999 159 612 858	0.00205 ^b	0.00205 ^b

^a Mass of atoms (u) as reported by Wang *et al.* (2012)[34]

^b Isotopic abundance in terrestrial materials as reported by Meija *et. al* [35]

^c Isotopic abundance reported by the manufacturers of [¹³C]glucose and [¹⁵N]NH₄Cl

C, H, N, and O isotopes that were used for these calculations. There is a total of nine isotopes: two for carbon, hydrogen, and nitrogen and three for oxygen. The elemental composition of the $[M+H]^+$ pseudo molecular ion is C₃₄H₅₈N₆O₂₀•H⁺ for the reduced disaccharide-tripeptide. According to the elemental composition of the mono-charged disaccharide-tripeptide (59 hydrogens), there are 2.21×10^{39} isotopomers ($2^{34} * 2^{59} * 2^6 * 3^{20}$) but 3,395,700 ($35 * 60 * 7 * 231$) distinct isotopologues (*i.e.* isotopomers with the same mass) because isotopomers with the same isotopic composition have the same mass irrespective of the position of the isotopes in the molecules.

For the disaccharide-tripeptide, the isotopic composition of the isotopologues is defined by five numbers (n_1 to n_5) according to the number of ¹²C (n_1) and ¹³C ($34 - n_1$) nuclei for carbon, the number of ¹H (n_2) and ²H ($59 - n_2$) nuclei for hydrogen, the number of ¹⁴N (n_3) and ¹⁵N ($6 - n_3$) nuclei for nitrogen, and the number of ¹⁶O (n_4), ¹⁷O (n_5), and ¹⁸O ($20 - n_4 - n_5$) nuclei for oxygen.

The abundance of the isotopologues with a defined isotopic composition depends upon the abundance of the isotopes listed in Table 1 and is the product of four relative abundances ($RA_C * RA_H * RA_N * RA_O$) independently calculated for the four elements.

For carbon: $RA_C = 0.9893^{n_1} * 0.0107^{(35-n_1)}$ * the number of combinations of n_1 objects among 35 (C_{35, n_1});

For hydrogen: $RA_H = 0.999885^{n_2} * 0.000115^{(59-n_2)}$ * (C_{59, n_2});

For nitrogen: $RA_N = 0.99636^{n_3} * 0.00364^{(6-n_3)}$ * (C_6, n_3);

For oxygen: $RA_O = 0.99757^{n_4} * 0.00038 * n_5 * 0.00205^{(20-n_4-n_5)}$ * (C_{20, n_4, n_5}).

Figure 2A provides the general formula for molecules composed of any combination of elements and isotopes. Fig. 2B provides, as an example, the application of this formula to the

calculation of the abundance of the disaccharide-tripeptide isotopologue containing light isotopes except for two ^{13}C and one ^{15}N atoms. The formula is valid under the assumption that the incorporation of an isotope at a specific position of a muropeptide solely depends upon the average abundance of this isotope in the culture medium. This requires, but is not guaranteed by, a uniform distribution of ^{12}C and ^{13}C nuclei at the six positions of labeled glucose used as the sole source of carbon in the labeled medium. Minor deviations from this assumption may occur since the rate of enzymatic reactions is known to be marginally affected by the isotopic composition of substrates and products [36].

Figure 2C shows the mass and abundance of the 25 most abundant isotopologues calculated for the unlabeled medium using the terrestrial abundance of the isotopes (Table 1). The cumulative abundance of these isotopologues was 99.9009% indicating that the remaining isotopologues did not significantly contribute to the intensity of the peaks in the actual mass spectra. In practice, computing the relative abundance of the full complement of the 3,353,560 distinct isotopologues is time-consuming but the algorithm described by Lacki *et al.* [33] provides an efficient means to limit calculations to the most abundant isotopologues by setting a limit for the cumulative abundance (a limit of 99.99% was used in this study). Note that the most abundant isotopologue (64.2053%) exclusively contained the light isotopes of the four elements (^{12}C , ^1H , ^{14}N , and ^{16}O). The second and third most abundant isotopologues (23.6105% and 4.2135%) contained light isotopes of the four elements except for one and two ^{13}C carbon atoms, respectively. This was accounted for by the relatively high terrestrial abundance of the ^{13}C isotope (1.07%) and the important contribution of carbon to the total number of atoms present in the disaccharide-tripeptide (34 out of 119 atoms). In comparison, nitrogen only contributed to 6 of the 119 atoms accounting for the modest contribution of isotopologues containing a single ^{15}N nucleus to the isotopologue pool (1.4074%) despite the relatively high terrestrial abundance of ^{15}N (0.364%).

Figure 2D shows the mass and abundance of the 25 most abundant isotopologues calculated for the labeled medium (Table 1), which contains the terrestrial abundance of hydrogen and oxygen isotopes and predominantly the ^{13}C (99%) and ^{15}N (99%) isotopes of carbon and nitrogen according to analyses provided by the manufacturers of $[^{13}\text{C}]$ glucose and $[^{15}\text{N}]\text{NH}_4\text{Cl}$, respectively. The cumulative abundance of these isotopologues was 99.9009% indicating that they should be the major contributors to isotopic clusters. The most abundant isotopologue was “uniformly labeled” as it exclusively contained the ^{13}C and ^{15}N nuclei. The next most abundant isotopologues contained a single unlabeled nucleus, ^{12}C (21.7356%) or ^{14}N (3.8357%), reflecting the similar relative abundance of these isotopes (1%) and the elemental composition of the

A		B	
$P = \prod_{e \in E} X((n_e(i_1) = k_{i_1}) \cap (n_e(i_2) = k_{i_2}) \cap \dots \cap (n_e(i_m) = k_{i_m}))$		Isotopic composition	Contribution of each element (C ₃₄ H ₅₈ N ₆ O ₂₀ •H ⁺)
$X((n_e(i_1) = k_{i_1}) \cap (n_e(i_2) = k_{i_2}) \cap \dots \cap (n_e(i_m) = k_{i_m})) =$ $\frac{t_e!}{k_{i_1}!k_{i_2}!\dots k_{i_m}!} * p_e(i_1)^{k_{i_1}} * \dots * p_e(i_m)^{k_{i_m}}$		¹² C n=32 ¹³ C n=2	0.9893 ³² * 0.0107 ² * $\frac{34!}{32! * 2!}$ 0.70875525 * 0.00011449 * 561 = 0.04552256
<i>P</i> :	relative abundance (isotopologue)	¹ H n=59	0.999885 ⁵⁹ = 0.99323758
<i>E</i> :	set of elements	¹⁴ N n=5 ¹⁵ N n=1	0.99636 ⁶ * 0.00364 ² * $\frac{6!}{5! * 1!}$ 0.98193201 * 0.00364 * 6 = 0.02144540
<i>X</i> :	Joint probability of finding defined number of atoms of each isotope of element <i>e</i>	¹⁶ O n=20	0.99757 ²⁰ = 0.95250574
<i>n_e(i_m)</i> :	number of atoms of isotope <i>m</i> of element <i>e</i>	Relative abundance of the isotopologue	
<i>p_e(i_m)</i> :	relative abundance of isotope <i>m</i> within element <i>e</i>	0.04552256 * 0.99323758 * 0.02144540 * 0.95250574 = 0.00092359 = 0.09%	
<i>t_e</i> :	total number of atoms of element <i>e</i> (=∑ ^{<i>m</i>} <i>n</i> (<i>i_m</i>))		

C Unlabeled medium			D Labeled medium		
Isotopic composition	Exact mass	Abundance %	Isotopic composition	Exact mass	Abundance %
<i>All</i> ¹² C ¹ H ¹⁴ N ¹⁶ O	871.3779	64.2053	<i>All</i> ¹³ C ¹ H ¹⁵ N ¹⁶ O	911.4741	63.2890
1 ¹³ C	872.3812	23.6105	1 ¹² C	910.4708	21.7356
2 ¹³ C	873.3846	4.2135	1 ¹⁴ N	910.4771	3.8357
1 ¹⁸ O	873.3821	2.6388	2 ¹² C	909.4674	3.6226
1 ¹⁵ N	872.3749	1.4074	1 ¹⁸ O	913.4784	2.6012
1 ¹³ C 1 ¹⁸ O	874.3855	0.9704	1 ¹² C 1 ¹⁴ N	909.4737	1.3173
1 ¹³ C 1 ¹⁵ N	873.3783	0.5175	1 ¹² C 1 ¹⁸ O	912.4750	0.8933
1 ¹⁷ O	872.3821	0.4891	1 ¹⁷ O	912.4784	0.4822
3 ¹³ C	874.3879	0.4861	1 ² H	912.4804	0.4295
1 ² H	872.3841	0.4357	3 ¹² C	908.4641	0.3903
1 ¹³ C 1 ¹⁷ O	873.3854	0.1799	2 ¹² C 1 ¹⁴ N	908.4704	0.2196
2 ¹³ C 1 ¹⁸ O	875.3888	0.1732	1 ¹² C 1 ¹⁷ O	911.4750	0.1656
1 ² H 1 ¹³ C	873.3875	0.1602	1 ¹⁴ N 1 ¹⁸ O	912.4813	0.1576
2 ¹³ C 1 ¹⁵ N	874.3816	0.0924	2 ¹² C 1 ¹⁸ O	911.4717	0.1489
1 ¹⁵ N 1 ¹⁸ O	874.3791	0.0578	1 ² H 1 ¹² C	911.4771	0.1475
2 ¹⁸ O	875.3864	0.0515	2 ¹⁴ N	909.4801	0.0969
4 ¹³ C	875.3913	0.0407	1 ¹² C 1 ¹⁴ N 1 ¹⁸ O	911.4780	0.0541
2 ¹³ C 1 ¹⁷ O	874.3888	0.0321	2 ¹⁸ O	915.4826	0.0508
1 ² H 2 ¹³ C	874.3909	0.0286	1 ¹² C 2 ¹⁴ N	908.4767	0.0333
1 ¹³ C 1 ¹⁵ N 1 ¹⁸ O	875.3825	0.0213	4 ¹² C	907.4607	0.0306
3 ¹³ C 1 ¹⁸ O	876.3922	0.0200	1 ¹⁴ N 1 ¹⁷ O	911.4813	0.0292
1 ¹⁷ O 1 ¹⁸ O	874.3863	0.0191	2 ¹² C 1 ¹⁷ O	910.4716	0.0276
1 ¹³ C 2 ¹⁸ O	876.3897	0.0189	1 ² H 1 ¹⁴ N	911.4834	0.0260
1 ² H 1 ¹⁸ O	874.3884	0.0179	1 ² H 2 ¹² C	910.4737	0.0246
2 ¹⁵ N	873.3719	0.0129	3 ¹² C 1 ¹⁴ N	907.4670	0.0237
Sum: 99.9009			Sum: 99.8326		

Figure 2: (A) General formula for molecules composed of any combination of elements and isotopes. (B) Example of the calculation of the abundance of a mono-charged ($[M+H]^+$) GlcNAc-MurNAc-tripeptide molecular ion ($C_{34}H_{58}N_6O_{20}\bullet H^+$) exclusively containing light isotopes (^{12}C , 1H , ^{14}N , ^{16}O) except for two ^{13}C and one ^{15}N heavy isotopes. (C and D) Mass and relative abundance of the 20 most abundant GlcNAc-MurNAc-tripeptide isotopologues ($C_{34}H_{58}N_6O_{20}\bullet H^+$), calculated for the unlabeled and labeled media, respectively, and sorted by decreasing abundance. The arrow points to the example of calculation detailed in panel B.

disaccharide tripeptide (34 carbons versus 6 nitrogens), respectively.

Shaping isotopic clusters using the calculated abundance of isotopologues The calculated abundance of isotopologues cannot be easily compared to experimental mass spectra because the former provides relative abundance for discrete (centroid) m/z values whereas the latter provides fully profiled peaks, the shape of which is defined by the resolution of the mass spectrometer, the treatment of the signal, and the convolution of signals from isotopologues with almost identical masses. The effect of signal convolution is illustrated by the distribution of the masses of the most abundant isotopologues listed in Figures 2C and 2D but sorted, this time, by increasing masses (Figures 3A and 3B, respectively). This analysis shows that the masses expected to generate the peaks of the isotopic cluster differ by approximately, but not exactly, one unit. This is due to the fact that the gain of a neutron by different nuclei does not lead to exactly the same mass increment as the gain in energy in the resulting nuclei is not exactly the same. For example, the gain of a neutron by the ^{12}C and ^{14}N nuclei results in mass increments of 1.00335 and 0.99703, respectively. Thus, the distribution of the relative abundances can only be visualized as a centroids (Figure 3C). To enable comparison of the calculated isotopic clusters with experimental mass spectra, a Gaussian peak was modeled for each isotopic composition according to equations 1 and 2,

$$\mu = \frac{m_{\text{iso}} + z * m_{H^+}}{z} \quad (1)$$

$$\sigma = \frac{FWHM}{2.355} \quad (2)$$

where m_{H^+} is the mass of a proton (H^+), z the net charge of the analyte, and $FWHM$ the full width at half maximum. The value of $FWHM$ used in this study (40,000) was chosen to match the resolving power of the mass spectrometer deduced from experimental spectra. Each peak was subsequently scaled by the relative abundance of the isotopologues and overlaid (Figure 3D). In order to obtain simulated mass spectra that could effectively be compared to experimental data, the modeled peaks were binned with a bin size of 0.002 m/z corresponding to the binsize used for the experimental mass spectra (Figure 3E).

Estimation of the relative increase in the amount of peptidoglycan upon bacterial growth. Since the amount of peptidoglycan per cell remains constant during exponential growth, the amount of peptidoglycan $f_{PG}(t)$ was considered to increase with time according to equation 3:

A Unlabeled medium

Isotopic composition	Exact mass	Abundance %
Cluster 1 (35.0000)	871.3779	64.2053
<i>All</i> ^{12}C ^1H ^{14}N ^{16}O	871.3779	64.2053
Cluster 2 (13.9922)	872.3809	25.9427
$1\ ^2\text{H}$	872.3841	0.4357
$1\ ^{17}\text{O}$	872.3821	0.4891
$1\ ^{13}\text{C}$	872.3812	23.6105
$1\ ^{15}\text{N}$	872.3749	1.4074
Cluster 3 (4.1290)	873.3834	7.7497
$1\ ^2\text{H}\ 1\ ^{13}\text{C}$	873.3875	0.1602
$1\ ^{13}\text{C}\ 1\ ^{17}\text{O}$	873.3854	0.1799
$2\ ^{13}\text{C}$	873.3846	4.2135
$1\ ^{18}\text{O}$	873.3821	2.6388
$1\ ^{13}\text{C}\ 1\ ^{15}\text{N}$	873.3783	0.5175
Cluster 4 (0.9102)	874.3859	1.7184
$1\ ^2\text{H}\ 2\ ^{13}\text{C}$	874.3909	0.0286
$2\ ^{13}\text{C}\ 1\ ^{17}\text{O}$	874.3888	0.0321
$3\ ^{13}\text{C}$	874.3879	0.4861
$1\ ^{13}\text{C}\ 1\ ^{18}\text{O}$	874.3855	0.9704
$2\ ^{13}\text{C}\ 1\ ^{15}\text{N}$	874.3816	0.0924
$1\ ^{15}\text{N}\ 1\ ^{18}\text{O}$	874.3791	0.0578
Cluster 5 (0.1682)	875.3883	0.3195
$4\ ^{13}\text{C}$	875.3913	0.0407
$2\ ^{13}\text{C}\ 1\ ^{18}\text{O}$	875.3888	0.1732
$2\ ^{18}\text{O}$	875.3864	0.0515
$1\ ^{13}\text{C}\ 1\ ^{15}\text{N}\ 1\ ^{18}\text{O}$	875.3825	0.0213

B Labeled medium

Isotopic composition	Exact mass	Abundance %
Cluster A (0.0301)	907.4644	0.0598
$4\ ^{12}\text{C}$	907.4607	0.0306
Cluster B (0.3316)	908.4669	0.6445
$1\ ^{12}\text{C}\ 2\ ^{14}\text{N}$	908.4767	0.0333
$2\ ^{12}\text{C}\ 1\ ^{14}\text{N}$	908.4704	0.2196
$3\ ^{12}\text{C}$	908.4641	0.3903
Cluster C (2.6356)	909.4693	5.0479
$2\ ^{14}\text{N}$	909.4801	0.0969
$1\ ^{12}\text{C}\ 1\ ^{14}\text{N}$	909.4737	1.3173
$2\ ^{12}\text{C}$	909.4674	3.6226
Cluster D (13.7225)	910.4717	25.6702
$1\ ^{14}\text{N}$	910.4771	3.8357
$1\ ^{12}\text{C}$	910.4708	21.7356
Cluster E (35.0000)	911.4742	63.8643
$1\ ^{12}\text{C}\ 1\ ^{14}\text{N}\ 1\ ^{18}\text{O}$	911.4780	0.0541
$1\ ^2\text{H}\ 1\ ^{12}\text{C}$	911.4771	0.1475
$1\ ^{12}\text{C}\ 1\ ^{17}\text{O}$	911.4750	0.1656
<i>All</i> $^{13}\text{C}\ ^1\text{H}\ ^{15}\text{N}\ ^{16}\text{O}$	911.4741	63.2890
$2\ ^{12}\text{C}\ 1\ ^{18}\text{O}$	911.4717	0.1489
Cluster F (1.0413)	912.4775	1.9658
$1\ ^{14}\text{N}\ 1\ ^{18}\text{O}$	912.4813	0.1576
$1\ ^2\text{H}$	912.4804	0.4295
$1\ ^{17}\text{O}$	912.4784	0.4822
$1\ ^{12}\text{C}\ 1\ ^{18}\text{O}$	912.4750	0.8933
Cluster G (1.6892)	913.4784	2.6264
$1\ ^{18}\text{O}$	913.4784	2.6012
Cluster I (0.0277)	915.4826	0.0508
$2\ ^{18}\text{O}$	915.4826	0.0508

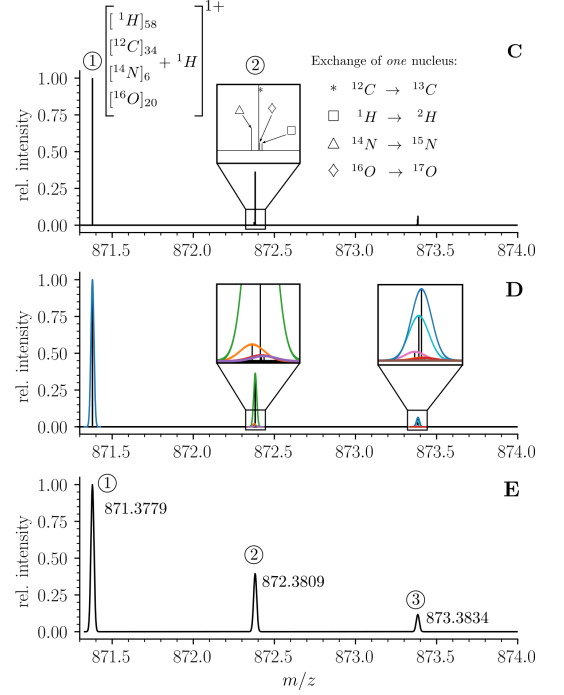


Figure 3: Shaping mass spectra. (A) and (B) Mass and abundance of GlcNAc-MurNAc-tripeptide isotopologues ($\text{C}_{34}\text{H}_{58}\text{N}_6\text{O}_{20}\bullet\text{H}^+$) calculated for the unlabeled and labeled media, respectively. Data are sorted by increasing mass to highlight clusters of isotopologues that fall within very narrow mass intervals. Abundances and masses for clusters were calculated using the whole set of isotopologues obtained in calculations using a cumulative abundance cutoff of 0.9999. Thus, cluster abundances differ slightly from the sum of abundances of the isotopologues shown in panels A and B.

(C) Abundance of isotopologues (for the unlabeled medium) visualized as a centroid spectrum. The magnification shows individual peaks within the cluster. Cluster 1 consists of a single isotopologue exclusively containing light isotopes (^1H , ^{12}C , ^{14}N , or ^{16}O). Cluster 2 consists of four isotopologues exclusively containing light isotopes except for one ^2H , ^{13}C , ^{15}N , or ^{17}O nucleus. Cluster 3 consists of eleven isotopologues (5 of which are shown in Panel A) exclusively containing light isotopes except for one ^{18}O nucleus or combinations of two nuclei among ^2H , ^{13}C , ^{15}N , and ^{17}O .

(D) Modeling of Gaussian peaks for each cluster according to equations 1 and 2.

(E) Simulated mass spectrum. The mass, which was used for comparison of simulated and experimental mass spectra is indicated at the peak apex. These values are reported in panel A for each cluster along with the cumulative abundance of the isotopologues belonging to the same cluster. The maximum intensity of the simulated peaks (arbitrary units) is also shown in parenthesis.

$$f_{PG}(t) = PG_0 * 2^{\frac{t}{g}} \quad (3)$$

in which PG_0 is the amount of peptidoglycan at $t=0$ (normalized to 1), g is the generation time and $t=0$ corresponds to the time of the medium switch. Since the relative amount of the muropeptides did not vary (above) the normalized molar amount of muropeptide m , $f_m(t)$, was considered to increase with time according to equation 4:

$$f_m(t) = m_0 * 2^{\frac{t}{g}} \quad (4)$$

in which m_0 is the relative molar amount of muropeptide at $t=0$. This approach enables monitoring the increase in the amount of muropeptides during exponential growth relative to the amount present at $t=0$.

Estimates of the molar abundance of muropeptide isotopologues. The relative molar abundance of muropeptide isotopologues detected in the same mass spectrum was deduced from the relative maximal current intensity (A_{mi}) for m/z values corresponding to the $[M+H]^+$ and $[M+H]^{2+}$ ions of isotopologues for the monomers and dimers, respectively. These estimates are robust since that they are based on the detection of chemically identical molecular ions in the same injection, which is standard practice in quantitative mass spectrometry. The increase in the normalized amount of isotopologue i of muropeptide m , $f_{m_i}(t)$, was deduced from the normalized molar amount of muropeptide m (equation 4) and from A_{m_i} , the relative current intensity of the isotopologue i (above) according to equation 5:

$$f_{m_i}(t) = A_{m_i} * m_0 * 2^{\frac{t}{g}} \quad (5)$$

3 Results

Muropeptide composition of the peptidoglycan from *E. coli* M1.5. Strain M1.5 was chosen for initial experiments because D,D-transpeptidases and L,D-transpeptidases both have major contributions to peptidoglycan polymerization offering the possibility to study 4→3 and 3→3 cross-linked dimers from the same peptidoglycan preparation. Strain M1.5 was grown in labeled M9 minimal medium containing $[^{15}\text{N}]\text{NH}_4\text{Cl}$ and $[^{13}\text{C}]\text{glucose}$ as the sole sources of nitrogen and carbon, respectively. *E. coli* M1.5 was also grown in unlabeled M9 minimal

Supplementary Table S1: Muropeptide composition of the peptidoglycan of strains BW25113 $\Delta 6ldt$ and M1.5

Strain β -lactam ^b	Muropeptide (%) ^a							
	Tri	Tetra	Penta	Tri→Tri	Tri→Tetra	Tri→Penta	Tetra→Tri	Tetra→Tetra
BW25113 $\Delta 6ldt$								
None (9) ^e	ND	74 ± 2	ND	ND	ND	ND	ND	26 ± 2
AZT (5) ^e	ND	77 ± 1	ND	ND	ND	ND	ND	23 ± 1
MEL (5) ^e	ND	70 ± 2	ND	ND	ND	ND	ND	30 ± 2
M1.5								
None (12) ^e	31 ± 3	36 ± 4	ND	7 ± 1	8 ± 1	ND	7 ± 1	12 ± 1
AMP (10) ^e	29 ± 2	21 ± 3	6 ± 2	13 ± 2	24 ± 1	6 ± 0.2	1 ± 0.3	ND

^a Data are the mean ± standard deviation from independent experiments (see note c)

^b β -lactam added to the growth medium. AZT, aztreonam at 12 µg/ml; MEL, mecillinam at 2.5 µg/ml; AMP, ampicillin at 16 µg/ml.

^c The number peptidoglycan analyses is indicated in parenthesis.

Abbreviations: ND, not detected; Tri, tripeptide monomer; Tetra, tetrapeptide monomer; Penta, pentapeptide monomer; Tri→Tri, Tri→Tetra, and Tri→Penta, 3→3 cross-linked dimers; Tetra→Tri and Tetra→Tetra, 4→3 cross-linked dimers. The inter-peptide cross-link direction is indicated using the donor→acceptor conventional notation.

medium. Peptidoglycan was extracted from exponentially growing cultures and digested by muramidases, which generate soluble disaccharide-peptides. The resulting muropeptides were reduced with NaBH₄ and purified by *rp*HPLC. Mass spectrometric analyses (see below) were performed to determine the structure of the six predominant muropeptides. These muropeptides included two monomers containing either a tripeptide (L-Ala¹-D-iGlu²-DAP³) or a tetrapeptide (L-Ala¹-D-iGlu²-DAP³-D-Ala⁴) stem, both linked to a reduced GlcNAc-MurNAc disaccharide. The remaining four muropeptides were dimers containing a 3→3 or a 4→3 cross-link with a tripeptide or a tetrapeptide stem in the acceptor position in all four combinations. As expected, growth in the labeled *versus* unlabeled medium did not alter the muropeptide composition of peptidoglycan. The average abundance of the six predominant muropeptides is reported in Supplementary Table S1.

Determination of the isotopic composition of the unlabeled monomers. The mass spectra of monomers from *E. coli* grown in unlabeled M9 minimal medium displayed the conventional isotopic clusters (Fig. 4A, B, and C and Supplementary Fig. S3 for the disaccharide-tripeptide and -tetrapeptide, respectively), as expected for the natural abundances of carbon, hydrogen, nitrogen, and oxygen isotopes (Table 1). For the disaccharide-tripeptide, the most abundant isotopologue (64.382%) only contained the light isotopes of the four chemical elements (Fig. 2C). The second peak of the isotopic cluster was composed of isotopologues containing only light isotopes except for either one ¹³C (23.497%), ²H (0.437%), ¹⁵N (1.411%), or ¹⁷O (0.492%)

isotope, together representing 25.877% of the relative abundance of the most abundant isotopologues (Cluster 2 in Fig. 3A). The overlay of the experimental and simulated spectra (Fig. 4C) confirmed the expected isotopologue composition.

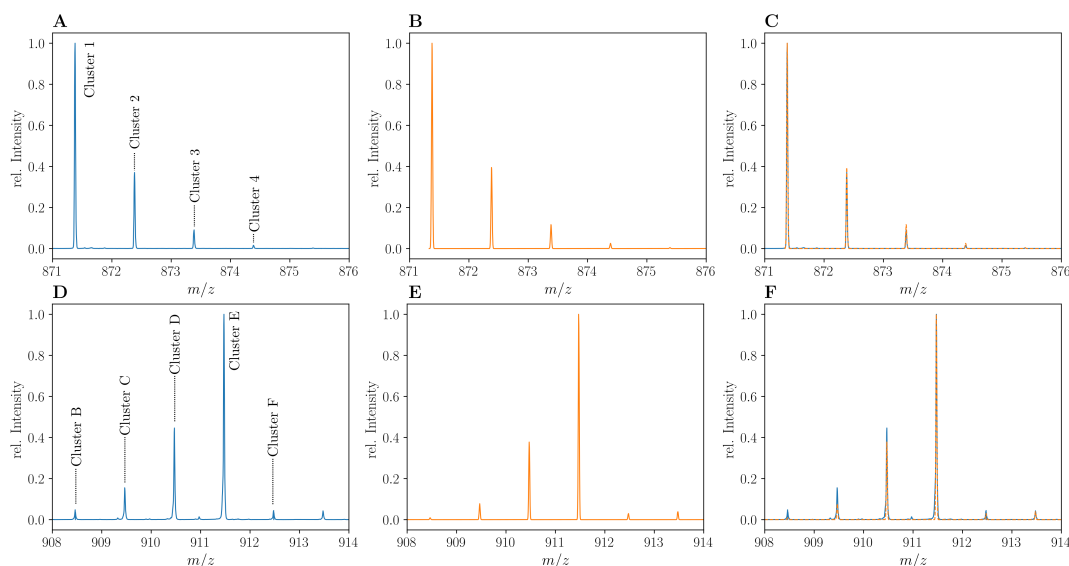
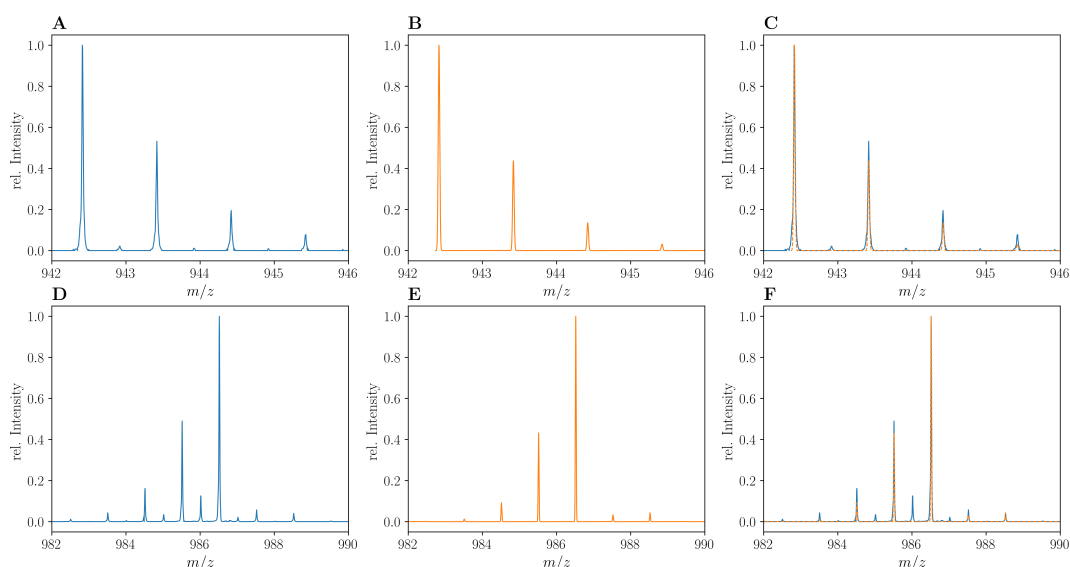


Figure 4: Mass spectra of the unlabeled and uniformly labeled disaccharide-tripeptide monomers. (A) Experimental mass spectrum of the mono-protonated ($[M+H]^{1+}$) disaccharide-tripeptide ($C_{34}H_{58}N_6O_{20} \bullet H^+$) extracted from *E. coli* M1.5 grown in unlabeled M9 minimal medium. (B) Simulated spectrum obtained for the natural abundance of carbon and nitrogen isotopes. (C) Overlay of the spectra in A and B. (D) Observed mass spectrum of the GlcNAc-MurNAc-tripeptide purified from the peptidoglycan of *E. coli* M1.5 grown in the labeled M9 minimal medium. (E) Simulated mass spectrum obtained for 99% ^{13}C and ^{15}N labeling. (F) Overlay of spectra in D and E.

Determination of the isotopic composition of the labeled monomers. Mass spectrometric analyses were performed on the reduced disaccharide-tripeptide monomer purified from the peptidoglycan of strain M1.5 grown in the labeled medium (Fig. 4D). The theoretical mass spectra were simulated as described in the Materials and Method section (Fig. 4E) and overlaid to the experimental spectra (Fig. 4F), revealing a good match between the two types of spectra. For the labeled tripeptide, the most intense peak at m/z 911.473 ($z = 1$) (Fig. 4D) corresponds to cluster peak E (Fig. 3B), which is mainly accounted for by the uniformly labeled disaccharide-tripeptide (m/z value of 911.4741; Fig. 2D). Additional cluster peaks at m/z values of 908.463, 909.467, and 910.469 (Fig. 4D), correspond to clusters B, C, and D (m/z values of 908.4669, 909.4693, and 910.4717; Fig. 3B). These peaks correspond to uniformly labeled species except for the presence of combinations of 3, 2, and 1 light ^{12}C or ^{14}N nuclei, respectively. The presence of these peaks fits the simulated spectra that were calculated with the extent of $[^{15}N]NH_4Cl$ and $[^{13}C]glucose$ labeling reported by the manufacturers (99% for each isotope) Fig. 3B). The same



Supplementary Figure S3: Mass spectra of the unlabeled and uniformly labeled disaccharide-tripeptide monomers. (A) Experimental mass spectrum of the mono-protonated ($[M+H]^+$) disaccharide-tetrapeptide ($C_{37}H_{63}N_7O_{21} \bullet H^+$) extracted from *E. coli* M1.5 grown in unlabeled M9 minimal medium. (B) Simulated spectrum obtained for the natural abundance of carbon and nitrogen isotopes. (C) Overlay of the spectra in A and B. (D) Observed mass spectrum of the GlcNAc-MurNAc-tetrapeptide purified from the peptidoglycan of *E. coli* M1.5 grown in the labeled M9 minimal medium. (E) Simulated mass spectrum obtained for 99% ^{13}C and ^{15}N labeling. (F) Overlay of spectra in D and E. The additional peaks of low intensity in the experimental spectra, in particular for the labeled disaccharide-tetrapeptide, correspond to the $[2M+2H]^{2+}$ ion.

conclusion was drawn from the comparison of the simulated and experimental spectra of the labeled disaccharide-tetrapeptide (Supplementary Fig. S3).

Qualitatively, it is worth noting that the mass spectra of the unlabeled and labeled disaccharide-tripeptide presented in Fig. 4 are almost mirror images. This reflects the preponderance of the isotopologue containing only “light” isotopes in the unlabeled mucopeptide followed (to the right) by peaks of decreasing intensity resulting from incorporation of a few rare heavy isotopes. In contrast, the peak of the fully labeled disaccharide-tripeptide is preceded (to the left) by peaks of decreasing masses due to incorporation of a few rare ^{12}C and ^{14}N nuclei. The same conclusions apply to the spectrum of the unlabeled disaccharide-tetrapeptide monomer (supplementary Fig. S3).

The structure of the isotopologues was determined by tandem mass spectrometry. As an example, Table 2 presents the MS/MS data obtained for mono-protonated isotopologue ions of the labeled disaccharide-tetrapeptide ($\text{C}_{37}\text{H}_{63}\text{N}_7\text{O}_{21}\bullet\text{H}^+$) under isotopic cluster peaks at m/z_{obs} 986.519 and 985.516. These values match the calculated m/z_{cal} values for isotopologues either exclusively containing the ^{13}C and ^{15}N isotopes (m/z 986.518) or bearing a single light isotope of either element (m/z_{cal} 985.515 or 985.521 for a ^{12}C or ^{14}N isotope, respectively). Fragmentation of the isotopologues under the peak at m/z_{obs} of 986.519 resulted in the expected set of product ions for a uniformly labeled disaccharide-tetrapeptide, while two sets of product ions, differing by approximately one mass unit, were observed for the fragmentation of isotopologues bearing a single light isotope under the peak at m/z_{obs} of 985.516. The fragments in the lower-mass ion set had retained their single light nucleus (^{12}C or ^{14}N) while the fragments in the higher-mass ion set had lost their single light nucleus and were uniformly labeled (these higher-mass fragments matched exactly those obtained for the uniformly labeled disaccharide-tetrapeptide). Thus, each fragment was present in the spectrum as a pair of peaks that reflected the presence or the absence of the light isotope. Table 2 provides the relative intensity of these two peaks for each fragment of the isotopologues. The relative intensity of the peak containing the light isotope decreased with the mass of the fragment. This result is expected for a uniform distribution of the light isotope in both the sugar and peptide moieties of the disaccharide-tetrapeptide because a smaller number of nuclei (smaller mass) makes it more probable to lose the single light nucleus during fragmentation.

Taken together, these results show that we successfully achieved extensive peptidoglycan labeling, the extent of which was only limited by the extent (99%) of the labeling of glucose and NH_4Cl in the labeled growth medium. Thus, isotopic dilution due to atmospheric N_2 and CO_2 was not an issue, as expected from the metabolic fluxes of *E. coli* grown in minimal medium.

Table 2: Tandem mass spectrometry analysis of isotopologues of the GlcNAc-MurNAc-tetrapeptide.

Structure	Isotopologue	m/z_{calc}	Uniformly labeled		One light nucleus	
			m/z_{obs}	Intensity (%)	m/z_{obs}	Intensity (%)
GlcNAc-MurNAc-L-Ala- γ -D-Glu-DAP-D-Ala ^a	Uniformly labeled	986.52	986.52	100	ND	0
	One light nucleus	985.52	ND	0	985.60	100
MurNAc-L-Ala- γ -D-Glu-DAP-D-Ala	Uniformly labeled	774.42	774.42	100	774.45	18
	One light nucleus	773.41	ND	0	773.45	82
MurNAc-L-Ala- γ -D-Glu-DAP	Uniformly labeled	681.36	681.36	100	681.40	12
	One light nucleus	680.36	ND	0	680.40	88
L-Ala- γ -D-Glu-DAP-D-Ala	Uniformly labeled	485.27	485.27	100	485.30	35
	One light nucleus	484.26	ND	0	484.30	65
γ -D-Glu-DAP-D-Ala	Uniformly labeled	410.22	410.22	100	410.25	47
	One light nucleus	409.22	ND	0	409.25	53
L-Ala- γ -D-Glu-DAP	Uniformly labeled	392.21	392.21	100	392.25	48
	One light nucleus	391.21	ND	0	391.25	52
γ -D-Glu-DAP	Uniformly labeled	317.17	317.17	100	317.20	54
	One light nucleus	316.16	ND	0	316.20	46

^a Mono-protonated precursor ion: $\text{C}_{37}\text{H}_{63}\text{N}_7\text{O}_{21}\bullet\text{H}^+$.

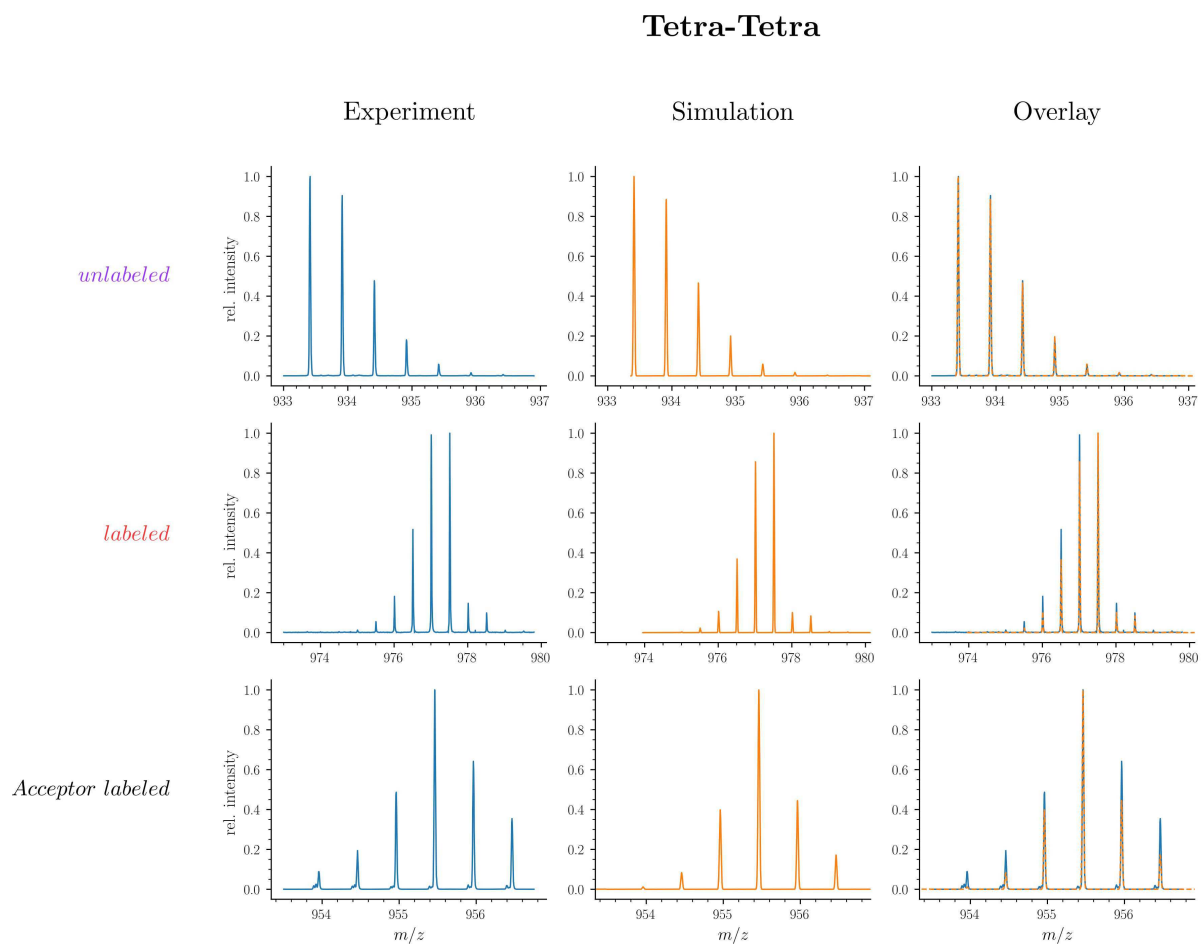
Abbreviations: m/z_{cal} , calculated m/z ; m/z_{obs} , observed m/z ; ND, not detected.

Note that the pre-culture and the culture were both performed in labeled M9 medium to avoid any contribution of the initial inoculum to the final isotopic composition of the peptidoglycan. Simulation of high-resolution mass spectra was successfully used to assign isotopologues of defined structure and isotopic composition to the corresponding peaks in experimental mass spectra (Fig. 4 and Supplementary Fig. S3). These assignments were confirmed by tandem mass spectrometry for two isotopologues (Table 2).

Mass spectra of the four dimers Peptidoglycan dimers do not harbor any symmetry axis as one peptide stem acts as an acyl donor in the transpeptidation reaction whereas the other acts as an acyl acceptor and retains the single free carboxyl extremity of the peptide moiety (Fig. 1). By convention, the structure of dimers is represented by placing the donor on the left separated from the acceptor by an arrow (donor→acceptor). In *E. coli* M1.5, the YcbB L,D-transpeptidase catalyzes the formation of DAP³→DAP³ cross-links connecting two diaminopimelyl residues (DAP³) located at the third position of a donor stem (a tripeptide) and of an acceptor stem (a tripeptide or a tetrapeptide), thus generating Tri→Tri and Tri→Tetra dimers, respectively. These dimers only differ by the presence or absence of D-Ala at the C-terminal end of the acceptor stem. The D,D-transpeptidases of *E. coli* M1.5 catalyze the formation of D-Ala⁴→DAP³ cross-links connecting a tetrapeptide donor stem to an acceptor stem containing either a tripeptide (Tetra→Tri dimer) or a tetrapeptide (Tetra→Tetra dimer). In these dimers, D-Ala at the fourth position of the donor stem is engaged in the D-Ala⁴→DAP³ cross-link and DAP³ or D-Ala⁴ occupies the C-terminal position of the acceptor stem. The Tri→Tetra and Tetra→Tri isomers formed by YcbB and the D,D-transpeptidases can be discriminated by tandem mass spectrometry based on the dissociation of the DAP³→DAP³ and D-Ala⁴→DAP³ cross-links, respectively, and on the loss of a C-terminal D-Ala only present in the acceptor stem of the dimer generated by YcbB (Supplementary Data). As detailed above for monomers, the comparison of the experimental and simulated mass spectra showed that the observed isotopic clusters of the dimers can be accounted for by the isotopic composition of the growth media (see Supplementary Fig. S4 for the Tetra→Tetra dimer). The structure of all dimers was confirmed by tandem mass spectrometry (Supplementary Data).

Muropeptide composition of the peptidoglycan of M1.5 and labeling procedure.

To investigate the mode of insertion of peptidoglycan precursors into sacculi, *E. coli* M1.5 was grown in minimal medium to an OD₆₀₀ of 0.4. Bacteria were collected by centrifugation and resuspended in the unlabeled medium. Incubation was continued in the same conditions and samples were collected at 5, 30, 45, 65, and 85 min after the medium switch (Fig. 5A)



Supplementary Figure S4: Mass spectra of unlabeled and uniformly labeled Tetra→Tetra dimer.

representing a little less than an generation (90 min; Supplementary Table S2). Peptidoglycan was extracted and the six predominant muropeptides, two monomers and four dimers, were purified by *rp*HPLC (Fig. 5B to 5F), and identified by mass spectrometry (Fig. 5G). The relative abundance of these six muropeptides remained similar in all samples indicating, as expected, that the medium switch did not alter the overall peptidoglycan composition (Fig. 5G and 5H).

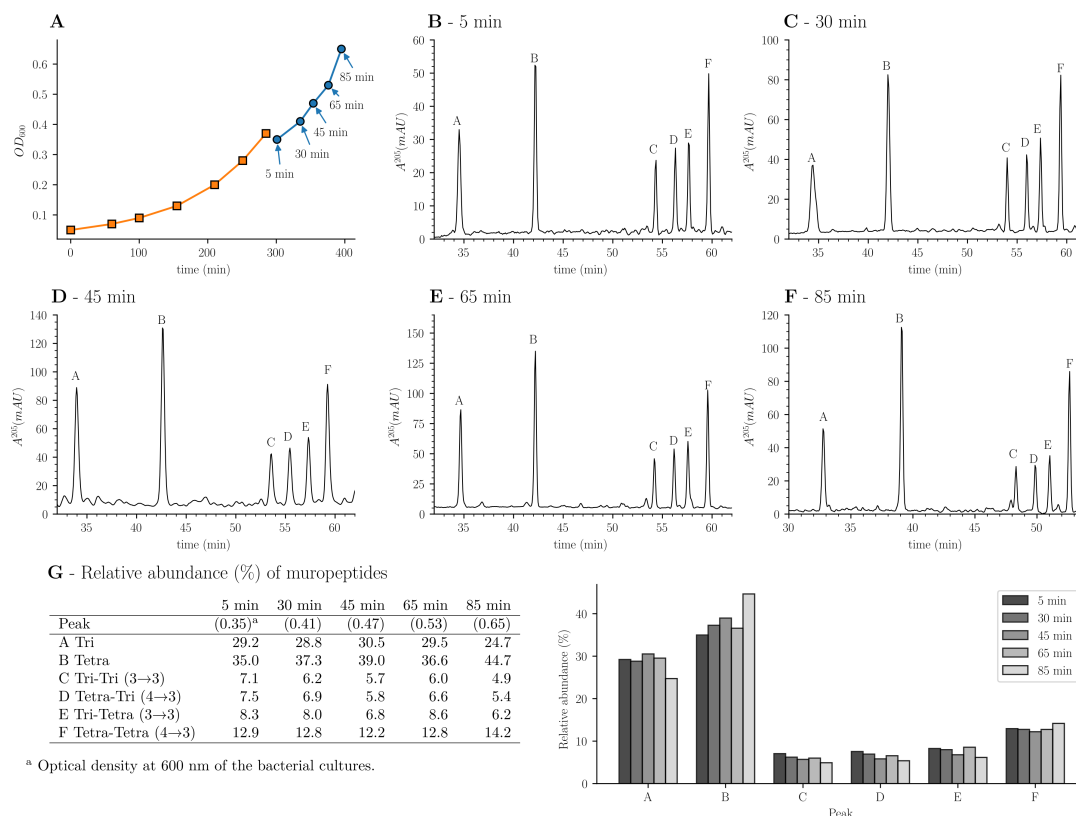


Figure 5: Muropeptide profile of peptidoglycan extracted from *E. coli* M1.5 after the medium switch. (A) *E. coli* M1.5 was inoculated in the labeled minimal medium and bacterial growth was monitored by determining the OD₆₀₀ (orange curve, squares). When the optical density reached 0.4, bacteria were collected by centrifugation, resuspended in the unlabeled minimum medium, incubation was continued (blue curve), and samples were withdrawn at 5, 30, 45, 65, and 85 min (circles). (B to F) Peptidoglycan was extracted from these five culture samples, digested with muramidases, and the resulting muropeptides were separated by *rp*HPLC. (G) and (H) Identification and relative abundance of muropeptides in the major chromatographic peaks.

Impact of the medium switch on the isotopic composition of monomers. Mass spectrometry revealed that growth in the unlabeled medium after the switch led to the appearance of disaccharide-tripeptide isotopologues of natural isotopic composition (Fig. 6A). These isotopologues were exclusively assembled from unlabeled glucose and NH₄Cl after the medium switch. In addition, minor amounts of hybrids containing both labeled and unlabeled moieties were

Supplementary Table S2: Generation time for growth of BW25113 derivatives in M9 minimal medium

Strain	Generation time (min)	
	Experiment 1	Experiment 2
β-lactam ^a		
M1.5		
None	90 \pm 2	85 \pm 3
AMP	163 \pm 9	165 \pm 13
BW25113 Δ6ldt		
None	67 \pm 1	66 \pm 1
AZT ^b	64 \pm 1	63 \pm 1
MEL ^b	63 \pm 1	65 \pm 1

^a β -lactam added to the growth medium. AZT, aztreonam at 12 μ g/ml; MEL, mecillinam at 2.5 μ g/ml; AMP, ampicillin at 16 μ g/ml.

^b For growth in the presence of aztreonam and mecillinam, the generation time was estimated from the variation in OD₆₀₀ during 90 min.

detected (named h1, h2, and h3 in Fig. 6A).

Tandem mass spectrometry (Supplementary Data) indicated that hybrid h1 consists of two types of isotopologues containing a labeled hexosamine moiety either in the GlcNAc or MurNAc residue). Hybrid h2 contained a labeled stem peptide and an unlabeled disaccharide. Hybrid h3 was uniformly labeled except for GlcNAc. Hybrids h1, h2, and h3 could originate from the incorporation of recycled fragments of preexisting (labeled) peptidoglycan. This requires digestion of the preexisting peptidoglycan by hydrolases and import of the digested fragments by specialized permeases (AmpG and Opp) [24]. Alternatively, the hybrids could originate from an intracellular pool of labeled precursors present prior to the medium switch. The structures of h1 and h2 were fully accounted for by the known peptidoglycan recycling pathway of *E. coli* [24] (Supplementary Fig. S1). Indeed, GlcNAc and MurNAc are recycled into glucosamine-6-phosphate, a common precursor of UDP-GlcNAc and UDP-MurNAc. This pathway could therefore account for the incorporation of a recycled (labeled) hexosamine into the GlcNAc or MurNAc residues of the h1 isotopomer. Regarding h2, the peptide moiety of peptidoglycan fragments is recycled as a tripeptide, which is added to UDP-MurNAc by the Mpl synthetase [37]. This pathway could be responsible for formation of the h2 hybrid containing a labeled (recycled) tripeptide and an unlabeled GlcNAc-MurNAc disaccharide. In contrast, the formation of the h3 hybrid did not depend upon recycling since MurNAc-peptide moieties are not selectively recycled as single molecules. Thus, the h3 hybrid originated from moieties that were assembled after (unlabeled GlcNAc) or prior to (labeled MurNAc-peptide) the medium switch. GlcNAc is incorporated into the peptidoglycan by the MurG transferase that catalyzes the transfer of the GlcNAc residue from UDP-GlcNAc to the late peptidoglycan precursor undecaprenyl-pyrophospho-MurNAc-pentapeptide

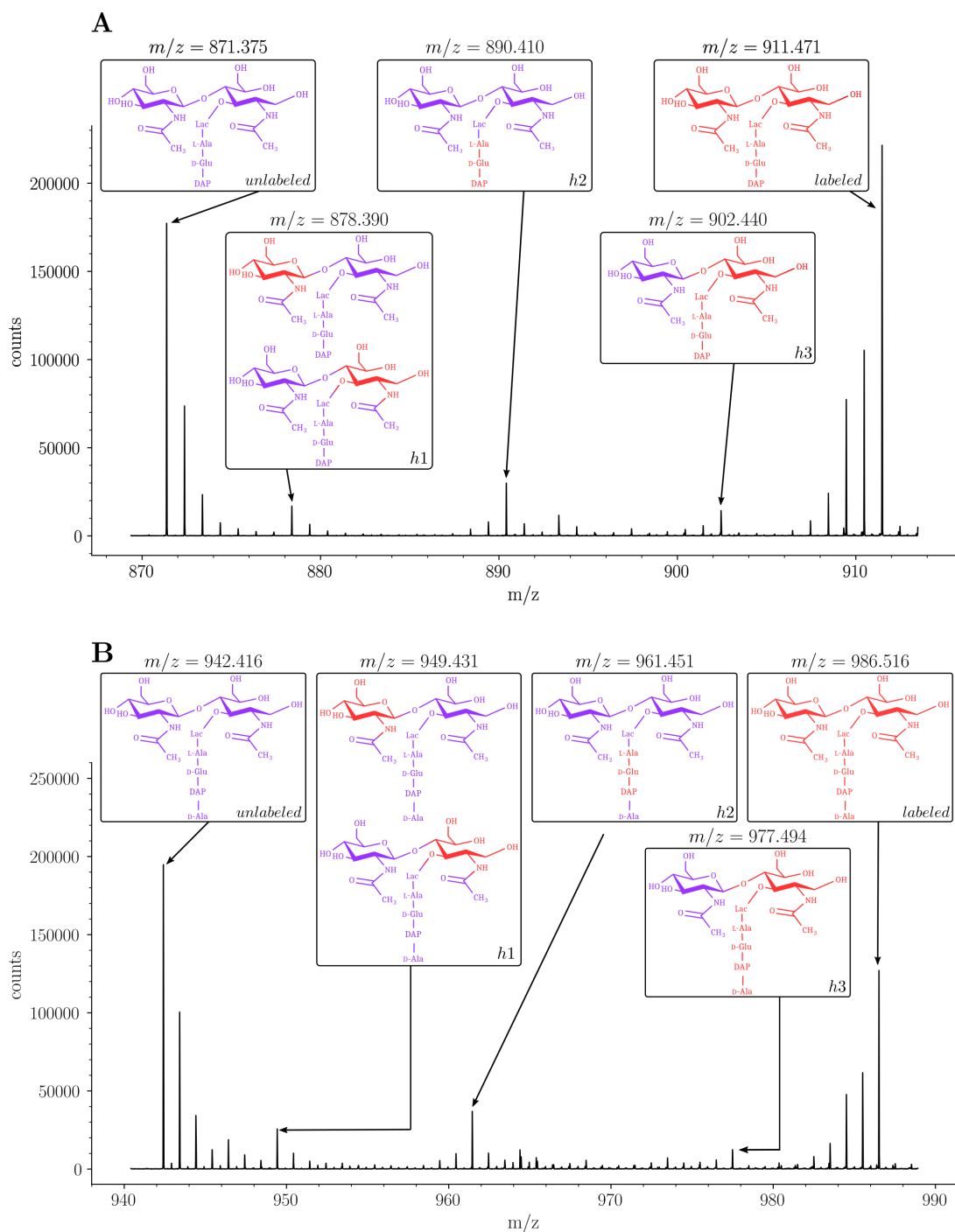
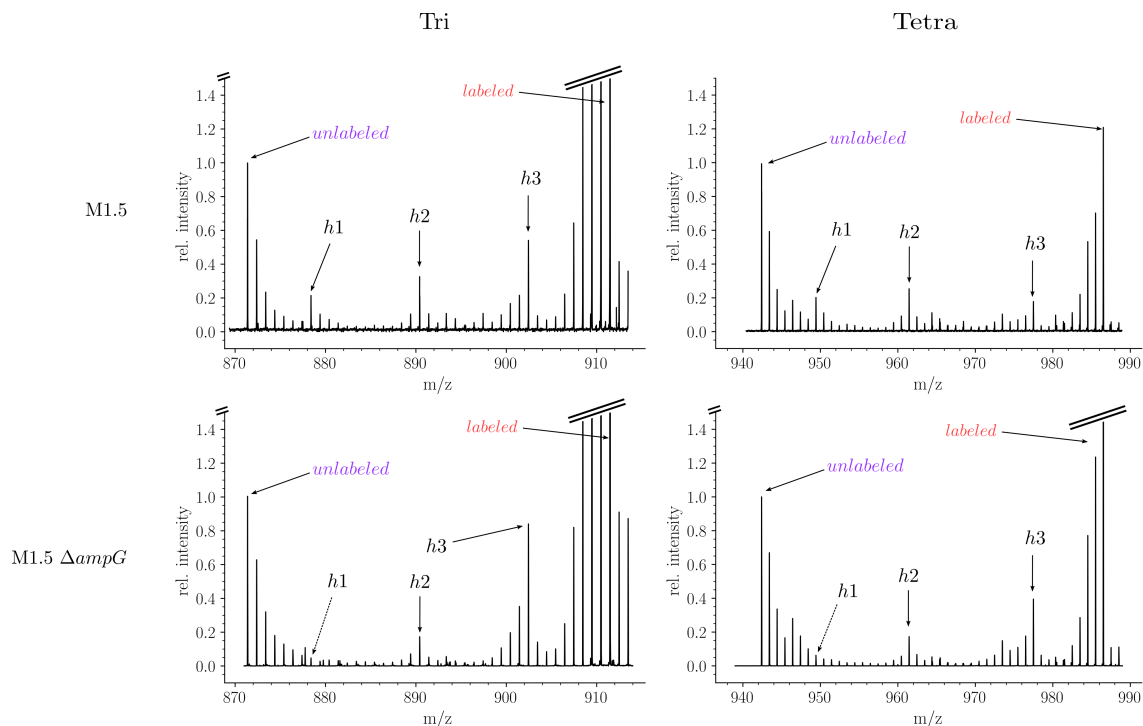


Figure 6: Isotopic composition of monomers isolated from the peptidoglycan of *E. coli* M1.5 after the medium switch. (A) Mass spectrum obtained for the GlcNAc-MurNAc-tripeptide monomer recovered in peak A of the chromatogram in Fig. 5D. (B) Mass spectrum obtained for the GlcNAc-MurNAc-tetrapeptide monomer recovered in peak B of the chromatogram in Fig. 5D. Purple and red colors indicate the unlabeled (^{12}C and ^{14}N) or labeled (^{13}C and ^{15}N) isotopic content of the amino acid and sugar moieties of the monomers, respectively.

(Supplementary Fig. S1). UDP-GlcNAc is expected to be rapidly synthesized from glucose and NH_4Cl (via glutamine; five biosynthetic steps) and rapidly consumed as it participates in various biosynthetic pathways. In contrast, the assembly of undecaprenyl-pyrophospho-MurNAc-pentapeptide from UDP-GlcNAc requires eight additional biosynthetic steps plus those required for production of the amino acids incorporated into the stem pentapeptide. The cytoplasm of *E. coli* contains an important pool of UDP-MurNAc-pentapeptide (an estimate of 120,000 molecules per bacterial cell), which is the immediate precursor of undecaprenyl-pyrophospho-MurNAc-pentapeptide [2]. The pool of UDP-MurNAc-pentapeptide represents *ca.* 3% of the total number of stem peptides present in the cell wall. These observations indicate that h3 is the sole hybrid assembled independently from recycling since it consists of labeled (preexisting) UDP-MurNAc-pentapeptide and unlabeled (synthesized *de novo*) GlcNAc moieties.

The role of recycling in the formation of the isotopologues was further investigated by constructing a derivative of *E. coli* M1.5 deficient in peptidoglycan recycling following deletion of the *ampG* permease gene. In this mutant, h1 hybrids were not detected indicating that they originated from incorporation of recycled glucosamine (Supplementary Fig. S5). Hybrids h2 and h3 were present in the peptidoglycan of the $\Delta\textit{ampG}$ mutant as expected from the metabolic chart presented in Supplementary Fig. S1. Indeed, recycling of the tripeptide (hybrid h2) involves both the transport of anhydroMurNAc-peptides by AmpG and the transport of the tripeptide by the Opp permease [24]. Deletion of the *ampG* gene is therefore expected to reduce rather than abolish formation of the h2 hybrid. The h3 hybrid was proposed to originate from preexisting UDP-MurNAc-pentapeptide and *de novo* synthesized GlcNAc moieties (above). Accordingly, the *ampG* deletion did not prevent formation of the h3 hybrid.

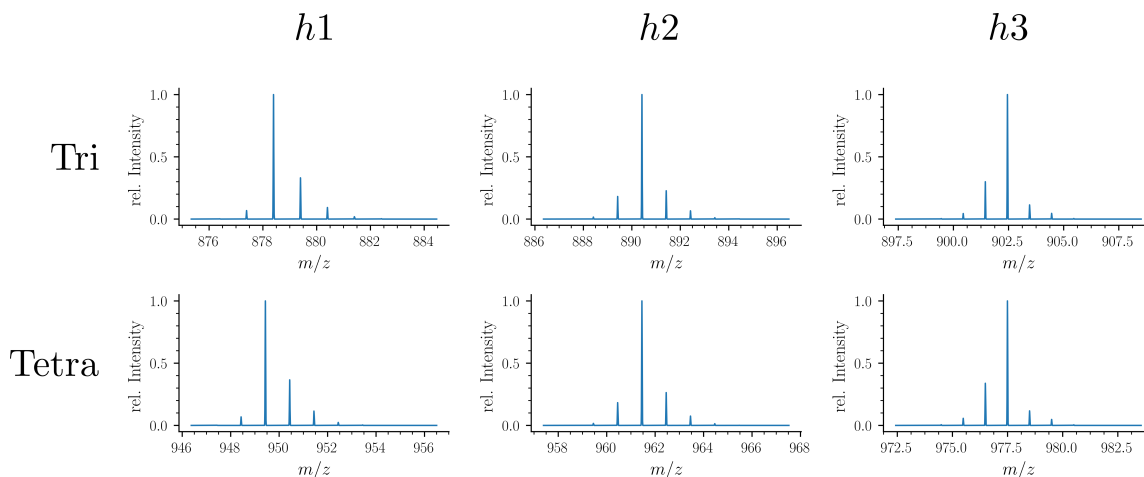
Analysis of the disaccharide-tetrapeptide (Fig. 6B and Supplementary Data) revealed a pattern of incorporation of unlabeled moieties very similar to that described above for the disaccharide-tripeptide. After the medium switch, the bulk of the ^{12}C and ^{14}N nuclei were incorporated into uniformly unlabeled disaccharide-tetrapeptides. Hybrid molecules retained labeled glucosamine moieties in GlcNAc or MurNAc (h1), a labeled tripeptide moiety in the tetrapeptide stem (h2), or labeling of the entire molecule except for GlcNAc (h3). As expected, the h1 hybrid originated from peptidoglycan recycling as it was not detected in the $\Delta\textit{ampG}$ mutant (Supplementary Fig. S5). The h1 hybrid could be accounted for by incorporation of recycled hexosamine, as described above for the disaccharide-tripeptide. The hybrid tetrapeptide stem present in h2 is also in full agreement with the *E. coli* recycling pathway as the tripeptide and the terminal D-Ala are expected to have different origins. Indeed, the terminal D-Ala of recycled tetrapeptide stems is cleaved off by a cytoplasmic L,D-carboxypeptidase to form a



Supplementary Figure S5: Isotopic composition of monomers isolated from the peptidoglycan of *E. coli* M1.5 and a recycling-deficient derivative obtained by deletion of the *ampG* permease gene.

tripeptide that is added to MurNAc by the Mpl synthetase [38]. In the following step, MurF, adds the D-Ala-D-Ala dipeptide to generate the complete pentapeptide stem. Thus, hybrid h2 originated from recycled (labeled) tripeptides while the other components (GlcNAc, MurNAc, and D-Ala⁴) were synthesized from unlabeled glucose and NH₄Cl introduced at the medium switch. Hybrid h3 was present in the peptidoglycan preparation of the $\Delta ampG$ mutant indicating that it was assembled from unlabeled GlcNAc and labeled MurNAc-pentapeptide moieties, as described above for the disaccharide-tripeptide.

Each of the five isotopomers discussed above generated the isotopic clusters expected from the isotopic composition of the culture media. The basis for the mirror image of the isotopic clusters of muropeptides exclusively generated from either labeled or unlabeled glucose and NH₄Cl has already been introduced in the text and in Fig. 4. The major h2 isotopologue mass peak had minor mass peaks both at lower and higher m/z values generating a seemingly symmetrical cluster (Fig. 6A and 6B; Supplementary Fig. S6 for simulated spectra). Peaks at lower m/z values mostly originated from the presence of rare ¹²C and ¹⁴N nuclei in the labeled moiety of the molecule. Peaks at higher m/z values mostly originated from the presence of rare ¹³C and ¹⁵N nuclei in the unlabeled moiety of the molecule. The contribution of these two effects shaped a nearly symmetrical isotopic cluster centered on the major isotopologue mass



Supplementary Figure S6: Simulated spectra of hybrid monomers

peak exclusively containing (i) ^{12}C and ^{14}N nuclei in the unlabeled moiety of the molecule, (ii) ^{13}C and ^{15}N nuclei in the labeled moiety, and (iii) ^1H and ^{16}O nuclei in the entire molecule.

Kinetics of incorporation of unlabeled nuclei into mucopeptide monomers. Our next objective was to compare the evolution of the ratios of uniformly labeled and unlabeled monomers following the culture medium switch. This analysis was based on the mass spectra of mucopeptides isolated from culture samples withdrawn at various times after the medium switch as described in Fig. 5. The mass spectra obtained for the disaccharide-tripeptide and disaccharide-tetrapeptide are displayed in Fig. 7A and 7C, respectively. Variations in the relative abundance of the uniformly labeled and unlabeled isotopologues deduced from mass spectral ion intensities are presented in Fig. 7B and 7D. For the disaccharide-tripeptide, replacement of the uniformly labeled isotopomer by its unlabeled counterpart reached *ca.* 50% in 85 min (Fig. 7B). In contrast, the replacement was more rapid for the disaccharide-tetrapeptide (*ca.* 94% in 85 min) (Fig. 7D). Thus, the isotopic labeling method was able to resolve different kinetics of accumulation of the neo-synthesized monomers (Fig. 7) although their relative proportions in the peptidoglycan remained similar (Fig. 5). The tetrapeptide and tripeptide stems may originate from sequential hydrolytic reactions involving the removal of D-Ala⁵ from free (uncross-linked) pentapeptide stems by D,D-carboxypeptidases, followed by the removal of D-Ala⁴ from the resulting tetrapeptide by the L,D-carboxypeptidase activity of YcbB [9]. The sequential nature of these reactions may explain, at least in part, the delayed accumulation of the disaccharide-tripeptide, as it derives from the disaccharide-tetrapeptide.

Kinetics of accumulations of hybrids revealed that hybrids h1 and h2, which originated from peptidoglycan recycling, were virtually absent at 5 min and increased between 5 and 85 min for the disaccharide-tripeptide and between 5 and 30 min for the disaccharide-tetrapeptide (Fig.

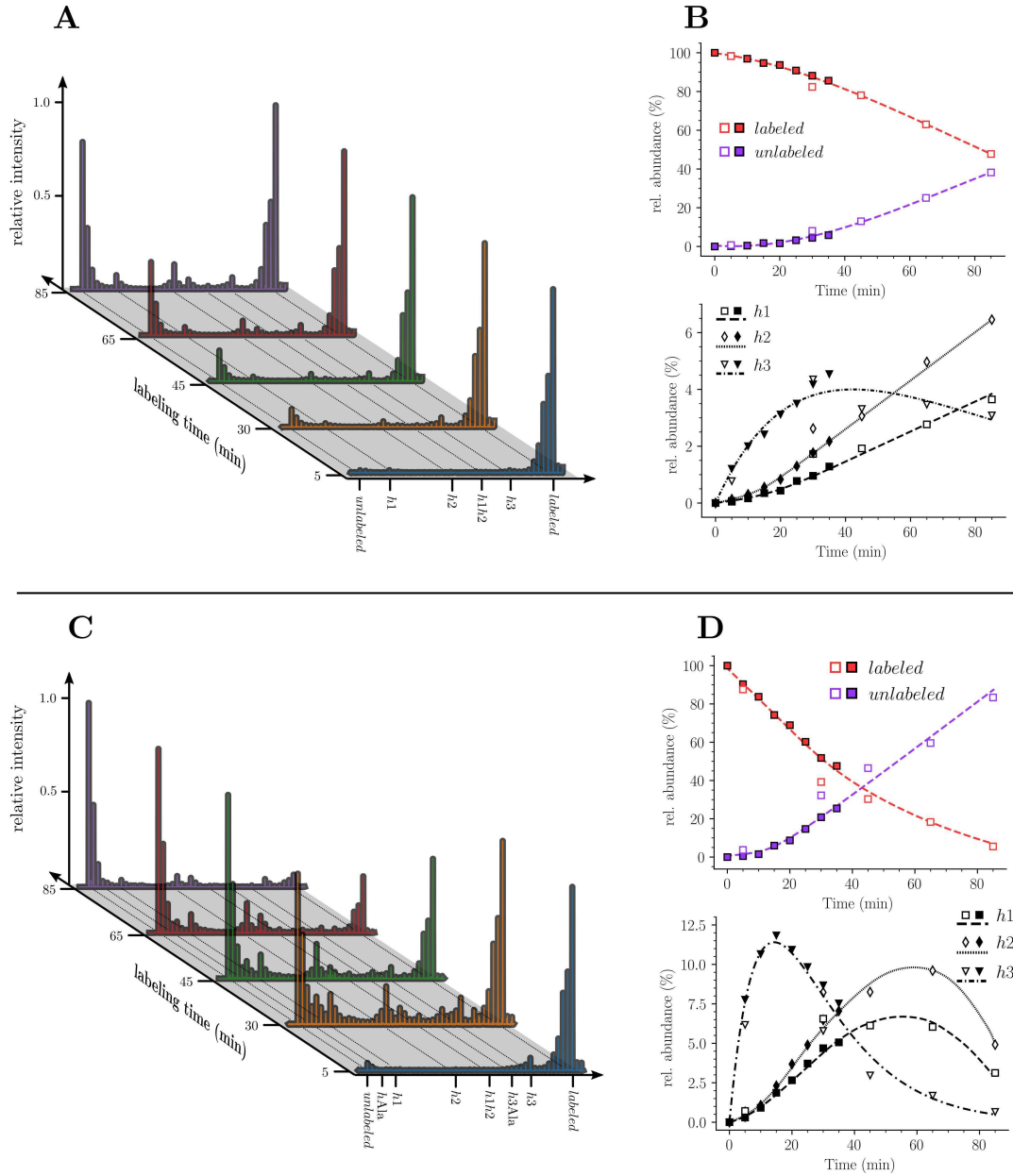
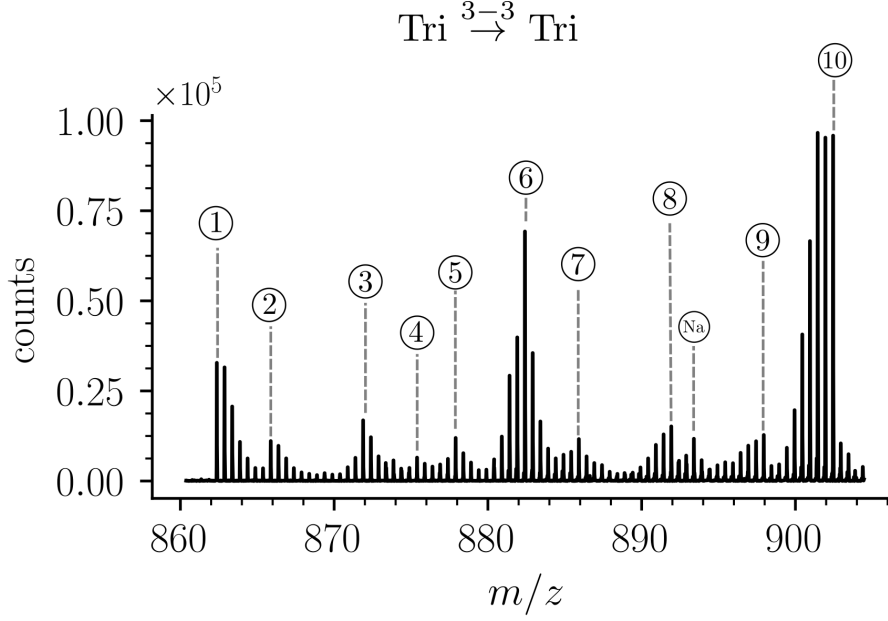


Figure 7: Kinetic analysis of the proportion of isotopologue monomers in the peptidoglycan of strain M1.5. (A) and (C), mass spectra of disaccharide-tripeptide and disaccharide-tetrapeptide from bacteria collected at 5, 30, 45, 65, and 85 min after the medium switch. (B) and (D), kinetic analysis of the ratios of isotopologues calculated from relative ion current intensities for the disaccharide-tripeptide and disaccharide-tetrapeptide, respectively. The upper panels show the evolution of the relative abundance of uniformly labeled and unlabeled monomers. The lower panels present the evolution of the relative abundance of hybrids relative to the complete set of monomers. The open and solid symbols are the results from two biological repeats. See Supplementary Data for the complete assignment of hybrid structures.

7). This is expected since recycled building blocks (glucosamine and tripeptide for h1 and h2, respectively) originated from a peptidoglycan that was fully labeled at the time of the medium switch and remained partially labeled during the time course of the experiment. In contrast, h3 hybrids were already present at 5 min, and reached a maximum at *ca.* 18 and 30 min for tetrapeptide and tripeptide, respectively, as expected for their synthesis from a cytoplasmic pool of labeled UDP-MurNAc-pentapeptide present at the time of the medium switch.

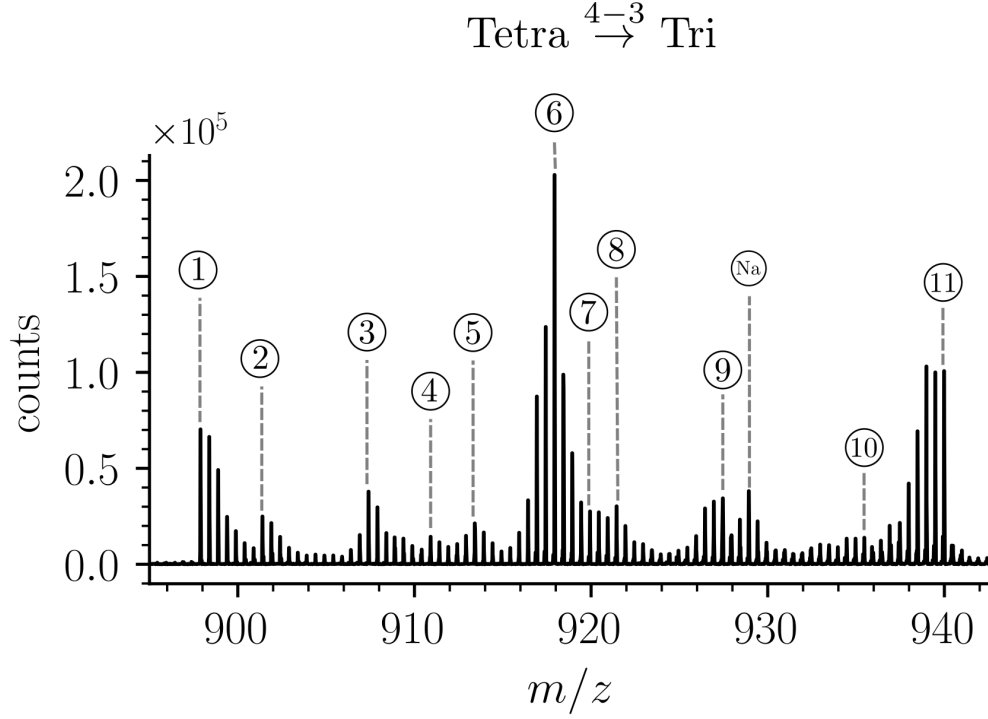
Impact of the medium switch on the isotopic composition of dimers. Three main types of isotopologues were observed after the medium switch for each of the four dimers (Fig. 8 for the Tri→Tri dimer and Supplementary Fig. S7, S8, and S9 for the Tetra→Tri, Tri→Tetra, Tetra→Tetra dimers, respectively). The first type of isotopologues were uniformly labeled. These dimers were generated by the cross-linking of stems peptides assembled before the medium switch. Thus, they correspond to fragments of the pre-existing peptidoglycan. These dimers are referred to as old→old isotopologue dimers. The second type of isotopologues was generated by the cross-linking of a donor stem assembled after the medium switch to an acceptor stem assembled prior to the medium switch (referred to as new→old isotopologue dimers). These isotopologue dimers correspond to a *de novo* synthesized donor stem attached to the pre-existing peptidoglycan, which provided the acceptor. The third type of isotopologue dimers was generated by the cross-linking of two neo-synthesized stem peptides (new→new). The h1, h2, and h3 hybrid depicted in Fig. 6 were assigned to the neo-synthesized type of disaccharide-peptides since they contained unlabeled moieties implying their assembly after the medium switch. The absence of old→new dimers (see Supplementary data for MS/MS analyses) indicated that the peptide stems present in the pre-existing peptidoglycan were not used as donors for cross-linking to neo-synthesized acceptors. For 4→3 cross-linked dimers, this result is expected since D,D-transpeptidases belonging to the PBP family use pentapeptide-containing donors, which are almost completely absent from mature peptidoglycan due to the hydrolysis of the D-Ala⁴-D-Ala⁵ amide bond by D,D-carboxypeptidases (See Introduction section and Fig. 1). For the 3→3 cross-linked Tri→Tetra dimer, tetrapeptide stems present in the pre-existing peptidoglycan could potentially be used as donors by the YcbB L,D-transpeptidase although this was not observed. Thus, the absence of old→new 3→3 cross-linked Tri→Tetra dimer indicates that YcbB discriminates neo-synthesized tetrapeptide stems (used as donors) from pre-existing tetrapeptide stems (used as acceptors) by an unknown mechanism that does not depend upon the structure of the disaccharide-peptide but upon the presence of the donor in a neo-synthesized glycan chain and of the acceptor in the preexisting peptidoglycan. The absence of old→new 3→3 cross-linked Tri→Tri dimers could be accounted for by the same mechanism.



m/z					Isotopologue	Origin (MS)	
	obs	calc	Ion	ppm	Donor→Acceptor	Donor→Acceptor	%
①	862.3683	862.3731	[M+2H] ²⁺	5.6	D→A	new→new	11.6
②	865.8808	865.8817	[M+2H] ²⁺	1.1	D _{h1} →A, D→A _{h1}	new→new	3.9
③	871.8916	871.8924	[M+2H] ²⁺	0.9	D _{h2} →A, D→A _{h2}	new→new	5.9
④	875.4014	875.4009	[M+2H] ²⁺	0.5	D _{h1} →A _{h2} , D _{h2} →A _{h1}	new→new	2.3
					D _{h2Hex} →A, D→A _{h2Hex}		
⑤	877.9063	877.9093	[M+2H] ²⁺	3.4	D _{h3} →A, D→A _{h3}	new→new	4.2
⑥	882.4187	882.4213	[M+2H] ²⁺	3.0	D→A	new→old	24.4
⑦	885.9268	885.9298	[M+2H] ²⁺	3.5	D _{h1} →A	new→old	4.1
⑧	891.9388	891.9405	[M+2H] ²⁺	1.9	D _{h2} →A	new→old	5.3
Na	893.4058	893.4122	[M+H+Na] ²⁺	7.2	D→A	new→new	NA
⑨	897.9538	897.9575	[M+2H] ²⁺	4.1	D _{h3} →A	new→old	4.5
⑩	902.4651	902.4694	[M+2H] ²⁺	4.8	D→A	old→old	19.2

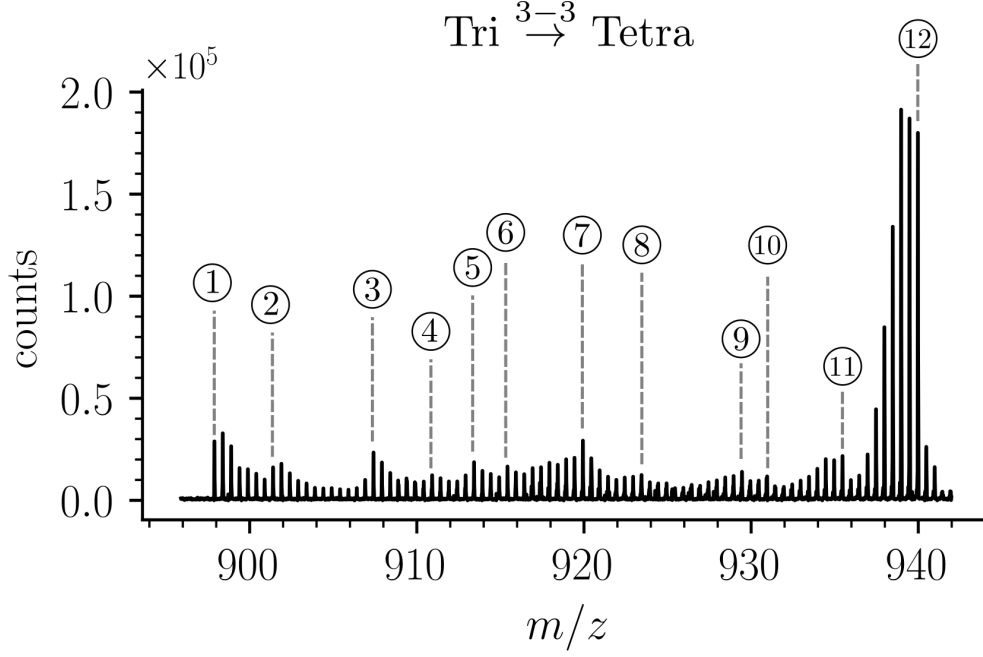
Figure 8: Structure of Tri→Tri isotopologues in the peptidoglycan of strain M1.5 grown in the absence of β -lactams. (A) Mass spectrum highlighting the 10 major isotopologues. (B) Structure of the 10 major isotopologues. The observed (obs) and calculated (cal) m/z values of the molecular ions (ion) and the difference in part per million (ppm) between these values are indicated. New (neo-synthesized) unlabeled moieties of isotopologues are indicated in purple. Old (preexisting) labeled moieties of isotopologues are indicated in red. h1, h2, and h3 (in red) refer to recycled moieties originating from pre-existing labeled peptidoglycan (h1 and h2) or from the pre-existing (labeled) UDP-MurNAc-pentapeptide pool as described in Fig. 6. The origin of the donor and acceptor participating in the cross-linking reaction, new (neo-synthesized) or old (preexisting in the cell wall) are indicated in purple and red, respectively. The relative abundance of the isotopologues (%) was deduced from the relative intensity of peaks corresponding to $[M+2H]^{2+}$ ions as labeled in A.

Abbreviations: h1, hybrid containing a recycled glucosamine moiety; h2, hybrid containing a recycled tripeptide moiety; h3, hybrid containing a labeled MurNAc-tripeptide moiety originating from the preexisting UDP-MurNAc-pentapeptide pool.



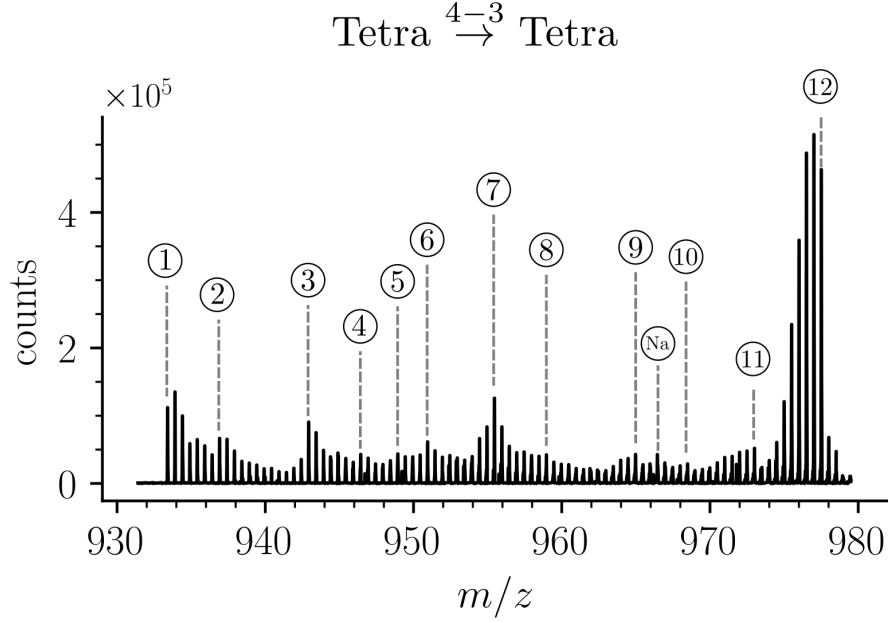
m/z		Isotopologue			Origin (MS)		
	obs	calc	Ion	ppm	Donor→Acceptor	Donor→Acceptor	%
①	897.8935	897.8917	[M+2H] ²⁺	2.1	D→A	new→new	11.0
②	901.3974	901.4003	[M+2H] ²⁺	-3.2	D _{h1} →A, D→A _{h1}	new→new	4.2
③	907.4109	907.4109	[M+2H] ²⁺	0.1	D _{h2} →A, D→A _{h2}	new→new	6.4
④	910.9203	910.9195	[M+2H] ²⁺	0.9	D _{h1} →A _{h2} , D _{h2} →A _{h1} D _{h2Hex} →A, D→A _{h2Hex}	new→new	2.5
⑤	913.4263	913.4279	[M+2H] ²⁺	-1.8	D _{h3} →A, D→A _{h3}	new→new	4.3
⑥	917.9383	917.9398	[M+2H] ²⁺	-1.7	D→A	new→old	35.8
⑦	919.9430	919.9434	[M+2H] ²⁺	-0.4	D _{hAla} →A	new→old	4.9
⑧	921.4472	921.4484	[M+2H] ²⁺	-1.3	D _{h1} →A	new→old	5.6
⑨	927.4563	927.4591	[M+2H] ²⁺	-3.0	D _{h2} →A	new→old	6.7
Ⓝa	928.9263	928.9308	[M+H+Na] ²⁺	5.2	D→A	new→new	NA
⑩	935.4768	935.4796	[M+2H] ²⁺	-3.0	D _{h3} →A	new→old	2.4
⑪	939.9917	939.9915	[M+2H] ²⁺	0.2	D→A	old→old	16.2

Supplementary Figure S7: Structure of Tetra→Tri isotopologues in the peptidoglycan of strain M1.5 grown in the absence of β -lactams.



m/z		Isotopologue			Origin (MS)		
	obs	calc	Ion	ppm	Donor→Acceptor	Donor→Acceptor	%
①	897.8935	897.8917	$[M+2H]^{2+}$	2.5	$D \rightarrow A$	new→new	8.2
②	901.3974	901.4003	$[M+2H]^{2+}$	0.4	$D_{h1} \rightarrow A, D \rightarrow A_{h1}$	new→new	4.7
③	907.4109	907.4109	$[M+2H]^{2+}$	2.1	$D_{h2} \rightarrow A, D \rightarrow A_{h2}$	new→new	6.3
④	910.9203	910.9195	$[M+2H]^{2+}$	0.4	$D_{h1} \rightarrow A_{h2}, D_{h2} \rightarrow A_{h1}$ $D_{h2Hex} \rightarrow A, D \rightarrow A_{h2Hex}$	new→new	3.1
⑤	913.4263	913.4279	$[M+2H]^{2+}$	1.1	$D_{h3} \rightarrow A$	new→new	4.8
⑥	915.4293	915.4314	$[M+2H]^{2+}$	1.7	$D_{h3} \rightarrow A_{hAla}, D \rightarrow A_{h3}$	new→new	4.9
⑦	919.9430	919.9434	$[M+2H]^{2+}$	3.1	$D \rightarrow A$	new→old	7.0
⑧	923.4492	923.4520	$[M+2H]^{2+}$	2.9	$D_{h1} \rightarrow A$	new→old	3.2
⑨	929.4594	929.4626	$[M+2H]^{2+}$	3.5	$D_{h2} \rightarrow A$	new→old	3.6
⑩	930.9651	930.9676	$[M+2H]^{2+}$	2.7	$D_{h3} \rightarrow A_{h3}$	new→new	2.8
⑪	935.4768	935.4796	$[M+2H]^{2+}$	2.5	$D_{h3} \rightarrow A$	new→old	5.6
⑫	939.9917	939.9915	$[M+2H]^{2+}$	0.8	$D \rightarrow A$	old→old	45.8

Supplementary Figure S8: Structure of Tri→Tetra isotopologues in the peptidoglycan of strain M1.5 grown in the absence of β -lactams.



m/z		Isotopologue			Origin (MS)		
	obs	calc	Ion	ppm	Donor→Acceptor	Donor→Acceptor	%
①	933.4097	933.4102	[M+2H] ²⁺	0.6	D→A	new→new	8.2
②	936.9174	936.9188	[M+2H] ²⁺	1.5	D _{h1} →A, D→A _{h1}	new→new	4.7
③	942.9261	942.9295	[M+2H] ²⁺	3.6	D _{h2} →A, D→A _{h2}	new→new	6.3
④	946.4369	946.4381	[M+2H] ²⁺	1.2	D _{h1} →A _{h2} , D _{h2} →A _{h1}	new→new	3.1
					D _{h2Hex} →A, D→A _{h2Hex}		
⑤	948.9410	948.9464	[M+2H] ²⁺	5.8	D _{h3} →A, D→A _{h3}	new→new	4.8
⑥	950.9477	950.9500	[M+2H] ²⁺	2.5	D _{h3} →A _{hAla} , D _{hAla} →A _{h3}	new→new	4.9
⑦	955.4594	955.4619	[M+2H] ²⁺	2.6	D→A	new→old	7.0
⑧	958.9658	958.9705	[M+2H] ²⁺	4.9	D _{h1} →A	new→old	3.2
⑨	964.9772	964.9812	[M+2H] ²⁺	4.1	D _{h2} →A	new→old	3.6
Ⓝa	966.4509	966.4529	[M+H+Na] ²⁺	1.8	D→A	new→new	NA
⑩	968.4868	968.4897	[M+2H] ²⁺	3.0	D _{h3} →A _{h3}	new→new	2.8
⑪	973.0004	973.0017	[M+2H] ²⁺	1.3	D _{h3} →A	new→old	5.6
⑫	977.5101	977.5136	[M+2H] ²⁺	3.6	D→A	old→old	45.8

Supplementary Figure S9: Structure of Tetra→Tetra isotopologues in the peptidoglycan of strain M1.5 grown in the absence of β -lactams.

Kinetic analyses revealed that the Tri→Tri and Tetra→Tri dimers were almost exclusively of the new→old type rather than of the new→new type (Fig. 9). Thus, cross-linking of neo-synthesized donor stems to tripeptide acceptor stems present in the preexisting peptidoglycan had a significant contribution to peptidoglycan polymerization by PBPs and YcbB. Strikingly, the kinetics of formation of Tri→Tri and Tetra→Tri dimers containing a tripeptide stem in the acceptor position were similar for both types of transpeptidases. Similarity between the transpeptidases was also detected for the kinetics of synthesis of Tri→Tetra and Tetra→Tetra dimers containing a tetrapeptide stem in the acceptor position.

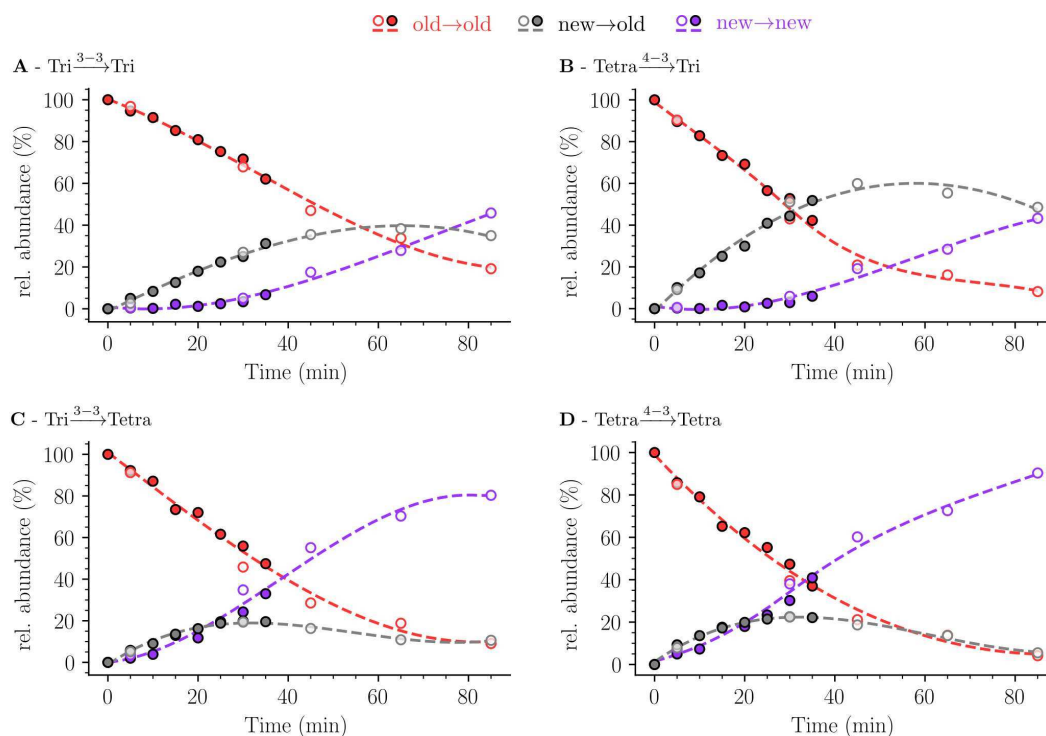


Figure 9: Mode of cross-linking of *de novo* synthesized peptidoglycan subunits in *E. coli* M1.5 grown in the absence of β -lactam. For each dimer (A, B, C, and D), the relative abundance (rel. abundance) was calculated for isotopologues originating from cross-linking of (i) two pre-existing stems (old→old; red), (ii) a new donor stem (*i.e.* a stem synthesized after the medium switch) and a pre-existing acceptor stem (new→old; grey), and (iii) two new stems (new→new; purple). The calculations take into account the contribution of *de novo* synthesized stems originating from recycled moieties and from the labeled UDP-MurNAc-pentapeptide pool as described in Figure 8 and in Supplementary Fig. S7, S8, and S9 for the Tri→Tri, Tetra→Tri, Tri→Tetra, and Tetra→Tetra dimers, respectively. The open and closed symbols correspond to data from two independent experiments.

In contrast, strikingly distinct kinetics were observed between dimers containing a stem tripeptide or tetrapeptide in the acceptor position irrespective of the transpeptidase responsible for their formation. The former (tripeptide acceptor) were almost exclusively of the new→old type (above) whereas the latter (tetrapeptide acceptor) were accounted for by similar amounts

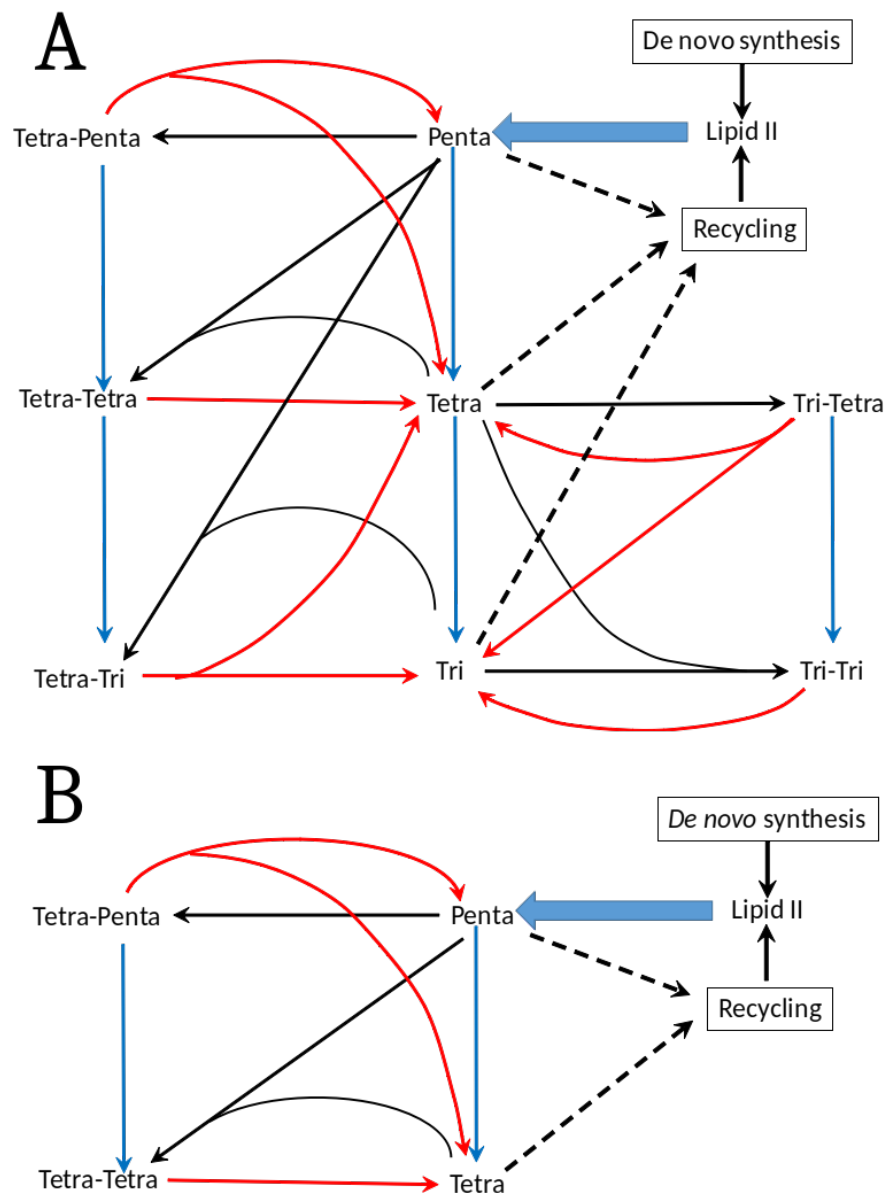
of isotopologues of the new→old and new→new types in the first 25 min of the kinetics. Thus, the mode of insertion of peptidoglycan subunits depended upon the structure of the acceptor stem (tripeptide *versus* tetrapeptide) rather than upon the type of transpeptidase (PBPs *versus* YcbB). The observed kinetics may be accounted for by at least two explanations: The dimers containing tripeptide and tetrapeptide stems may be independently generated according to the one- and three-at-a-time models of insertion of new subunits depicted in supplementary Fig. S2A and S2C, respectively. Indeed, these models predict new→new to new→old ratios of 0 and 1, respectively, in agreement with the experimental data. Alternatively, all dimers may be generated by the two-at-a-time model of insertion of new subunits, which predicts a new→new to new→old ratio of 0.5. The new→new dimers do not contain a tripeptide in the acceptor position since tripeptide stems are slowly appearing in the newly synthesized material (above). There are several caveats in the previous analyses since they did not take into consideration (i) the fact that the mode of insertion of peptidoglycan subunits is likely to differ in the side-wall and in the septum, (ii) the complexity of the potential interconversions between dimers and monomers that involve not only the formation of cross-links by transpeptidases but also their hydrolysis by endopeptidases, and (iii) the conversion of tetrapeptide stems to tripeptide stems both in monomers and in the acceptor position of dimers (see Introduction section and Supplementary Fig. S10A).

For these reasons, our next objectives were to analyze the mode of insertion of peptidoglycan subunits (i) in strains exclusively relying on PBPs or YcbB for peptidoglycan cross-linking and (ii) in conditions in which synthesis of the side wall and the septum is blocked by selective inhibitors.

Mode of insertion of peptidoglycan subunits in the absence of any L,D-transpeptidase.

Kinetic analyses of the insertion of peptidoglycan subunits were performed in *E. coli* $\Delta 6ldt$, a derivative of strain BW25113 that does not harbor any of the six genes encoding L,D-transpeptidases in *E. coli*. The absence of these enzymes greatly simplifies both the metabolic scheme for peptidoglycan cross-linking (Supplementary Fig. S10B) and the muropeptide *rp*HPLC profile (Fig. 10A).

This profile contains only two main peaks, corresponding to the tetrapeptide monomer and the Tetra→Tetra dimer due to the absence of 3→3 cross-linked dimers (missing L,D-transpeptidase activity) and the absence of monomers or dimers containing tripeptide stems (L,D-carboxypeptidase activity). The medium switch led to the accumulation of the unlabeled tetrapeptide monomer and of hybrids h1, h2, and h3 (Fig. 10B and Fig. 10C - No Antibiotic). The majority of the Tetra→Tetra dimers of the $\Delta 6ldt$ strain were hybrids containing an unlabeled



Supplementary Figure S10: Peptidoglycan metabolism in *E. coli* M1.5 (A) and $\Delta 6ldt$ (B). The reactions catalyzed by transpeptidases (formation of cross-links), endopeptidases (hydrolysis of cross-links), and carboxypeptidases (hydrolysis of C-terminal D-Ala⁴ and D-Ala⁵) are indicated by black, red, and blue arrows, respectively. PG is polymerized from a single precursor, Lipid II, containing a disaccharide and a pentapeptide, which originates from *de novo* synthesis and from recycling.

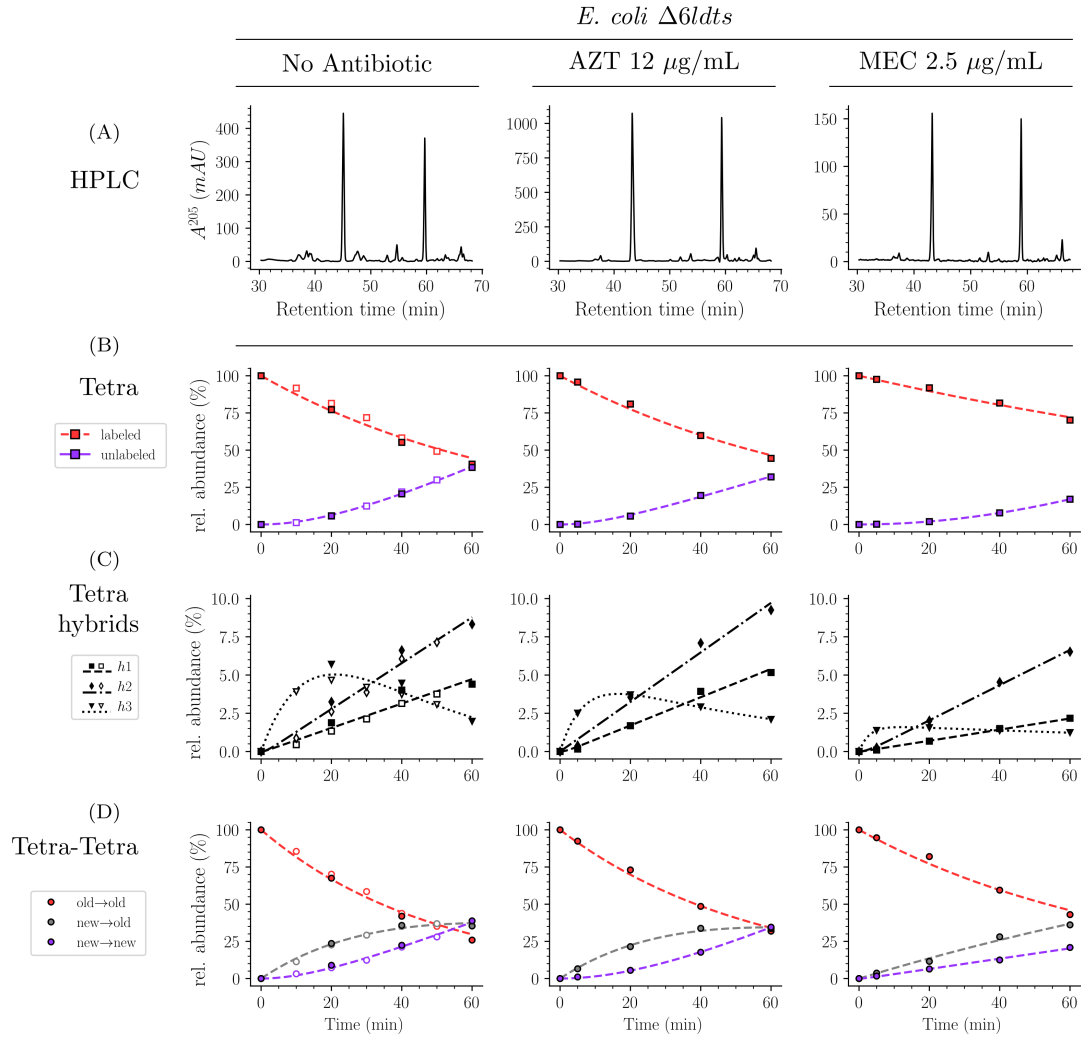


Figure 10: Mode of insertion of peptidoglycan subunits in the absence of L,D-transpeptidases and impact of the inhibition of PBPs by aztreonam and mecillinam. (A) Muropeptide *rp*HPLC profile of PG from *E. coli* strain $\Delta 6ldt$ grown in the absence of β -lactam or in the presence of aztreonam (AZT) or mecillinam (MEC). Kinetic data were collected for fully labeled (red), fully unlabeled (purple) tetrapeptide monomers (Tetra) (B) and hybrids (C) as defined in Figure 6. For the Tetra→Tetra dimer (D), the relative abundance (rel. abundance) was calculated for isotopologues originating from cross-linking of (i) two pre-existing stems (old→old; red), (ii) a new donor stem (*i.e.* a stem synthesized after the medium switch) and a pre-existing acceptor stem (new→old; grey), and (iii) two new stems (new→new; purple); see also Supp. Fig. 9. The calculations take into account the contribution of *de novo* synthesized stems originating from recycled moieties and from the labeled UDP-MurNAc-pentapeptide pool. The open and closed symbols correspond to data from two independent experiments.

beled (*de novo* synthesized) tetrapeptide stem at the donor position and a labeled tetrapeptide stem (preexisting peptidoglycan) at the acceptor position. This pattern mainly fits the one-at-a time mode of insertion of newly synthesized glycan strands.

Mode of insertion of peptidoglycan subunits into the septum and in the lateral wall.

In *E. coli*, two β -lactams, mecillinam and aztreonam, specifically inhibit the synthesis of the lateral cell wall and of the septum by inactivating the D,D-transpeptidase activity of PBP2 and PBP3, respectively. Mecillinam (2.5 $\mu\text{g/ml}$) and aztreonam (12 $\mu\text{g/ml}$) were added to the labeled culture medium of strain $\Delta 6ldt$ 5 min prior to the medium switch and to the unlabeled culture medium used to resuspend the bacteria at the medium switch. The kinetics of insertion of *de novo* synthesized subunits in the tetrapeptide monomers and in the Tetra \rightarrow Tetra dimers were similar in the cultures containing aztreonam or no drug (Fig. 10). The pattern corresponded to the one-at-a time mode of insertion of newly synthesized glycan strands since the new \rightarrow new dimer were not abundant at the beginning of the kinetics. In contrast, the new \rightarrow new and new \rightarrow old isotopologues dimers were both present in the cultures containing mecillinam indicating that formation of the septum involves insertion of multiple strands at a time.

Mode of insertion of peptidoglycan subunits in conditions in which YcbB is the only functional transpeptidase. In the presence of ampicillin (16 $\mu\text{g/ml}$), the peptidoglycan of strain M1.5 was predominantly (*ca.* 98.5%) cross-linked by YcbB since the D,D-transpeptidase activity of PBPs was inhibited by the drug (Fig. 11).

Inhibition of D,D-carboxypeptidases belonging to the PBP family prevented full hydrolysis of D-Ala⁵ since pentapeptide stems were detected both in monomers and in the acceptor position of dimers. Isotopologues of the new \rightarrow new type rather than of new \rightarrow old type were predominantly detected among dimers containing a tetrapeptide or a pentapeptide stem in the acceptor position. These dimers originate from neo-synthesized glycan chains cross-linked to each other. In contrast, the Tri \rightarrow Tetra dimers in the peptidoglycan of M1.5 grown in the absence of ampicillin contained both the new \rightarrow new and new \rightarrow old isotopologues (Fig. 9). This difference was not observed for the Tri \rightarrow Tri dimers since the new \rightarrow old isotopologues were prevalent for growth of M1.5 both in the presence or absence of ampicillin.

4 Discussion

Peptidoglycan labeling schemes. Initial studies of the expansion of the peptidoglycan macromolecule relied on labeling with [³H] or [¹⁴C]DAP [25]. Complementary imaging was

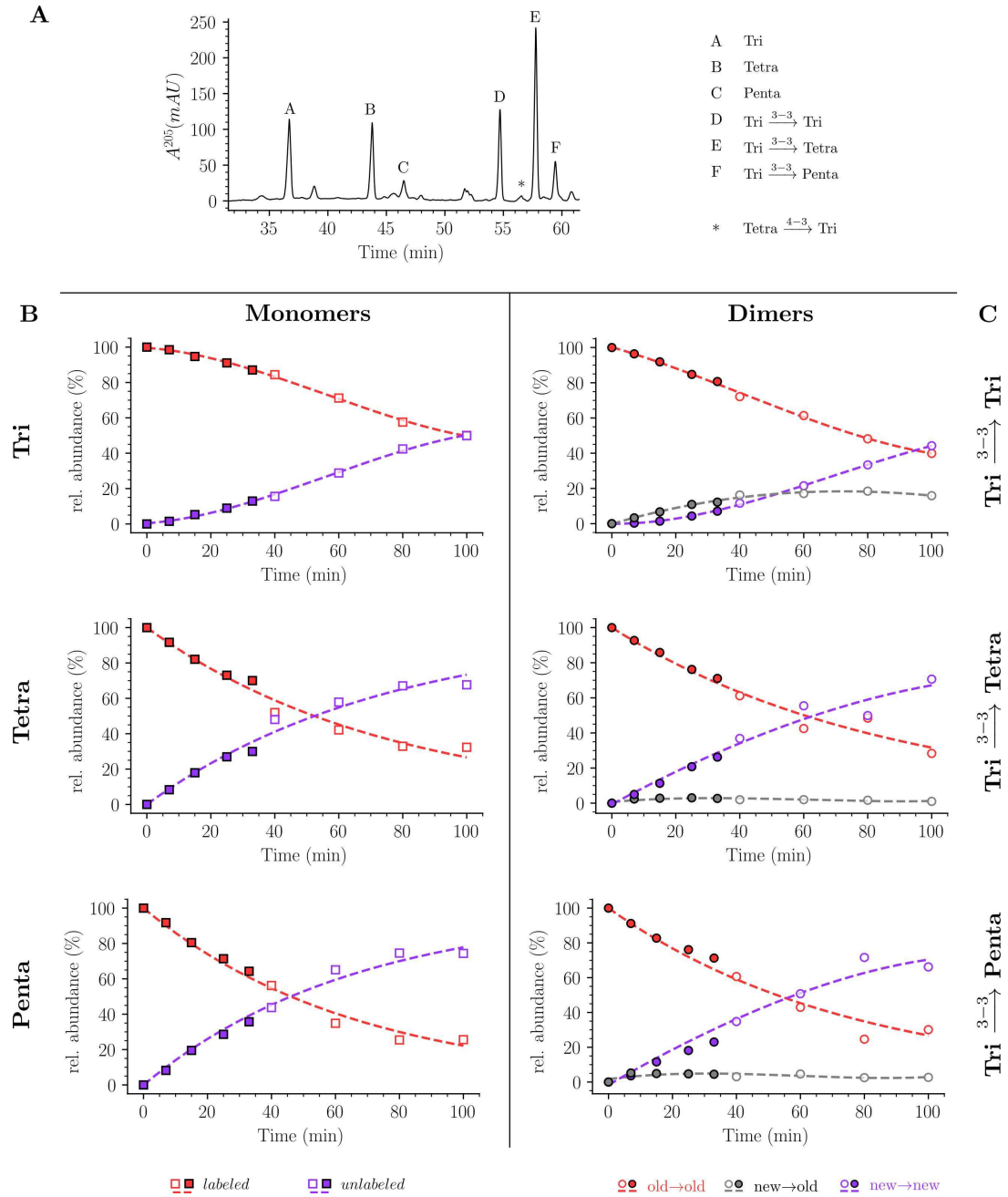


Figure 11: Mode of insertion of peptidoglycan subunits in conditions in which YcbB is the only functional transpeptidase following inhibitions of the D,D-transpeptidase activity of PBPs by ampicillin. (A) Muropeptide *rpHPLC* profile of PG from *E. coli* strain M1.5 grown in the presence of ampicillin (16 $\mu\text{g}/\text{ml}$). (B) Kinetic data were collected for neo-synthesized (new, red) and pre-existing (old, purple) monomers. (C) Kinetic data were also collected for dimers originating from cross-linking of (i) two pre-existing stems (old→old; red), (ii) a new donor stem (*i.e.* a stem synthesized after the medium switch) and a pre-existing acceptor stem (new→old; grey), and (iii) two new stems (new→new; purple). The calculations take into account the contribution of *de novo* synthesized stems originating from recycled moieties and from the labeled UDP-MurNAc-pentapeptide pool. The open and closed symbols correspond to data from two independent experiments. Rel. abundance, relative abundance of isotopologues. Disaccharide-peptide subunits contained a tripeptide (Tri), a tetrapeptide (Tetra), or a pentapeptide (Penta) stem.

based on the incorporation of D-cysteine at the fourth position of tetrapeptide stems by an enzymatic activity that was unknown at that time [39] and that most likely corresponds to the exchange activity of L,D-transpeptidases [7]. Free thiol groups of cysteine residues were biotinylated, enabling immunodetection by transmission electron microscopy. These approaches revealed single-strand and diffuse insertion of newly synthesized glycan chains into the lateral cell wall whereas synthesis of the septum relied on insertion of multiple strands at a time in sharply outlined growth zones [39]. Quantitatively, the number of glycan strands inserted at a time was previously estimated by determining the acceptor-donor radioactivity ratio (ADRR), *i.e.* the radioactivity ratio in the acceptor and donor positions of dimers (Supplementary Fig. S2) [40]. By analogy, we define here the acceptor-donor ratio in neo-synthesized stems (ADRNS), which is more accurate since it takes into account hybrid isotopologues containing unlabeled and labeled moieties (see below). ADRR determination was based on pulse labeling with radioactive DAP whereas ADRNS was based on determination of the incorporation of neo-synthesized subunits into the fully labeled pre-existing peptidoglycan. The latter strategy was chosen because of the ease of obtaining fully labeled cells with non-radioactive heavy isotopes thereby providing direct access to the absolute amount of isotopologues. Switching the medium from labelled to unlabelled was chosen since it facilitates the detection of neo-synthesized isotopologues present at a low abundance at early times after the medium switch. Indeed, the corresponding isotopic clusters do not appear in the region of the mass spectra containing the sodium adducts of the fully labeled isotopologues, which outnumber pre-existing isotopologues at the beginning of the kinetics. Preliminary experiments (data not shown) showed that this is paramount since the opposite labeling scheme involving an unlabeled-to-labelled medium switch resulted in the presence of neo-synthesized and pre-existing isotopologues in partially overlapping isotopic clusters.

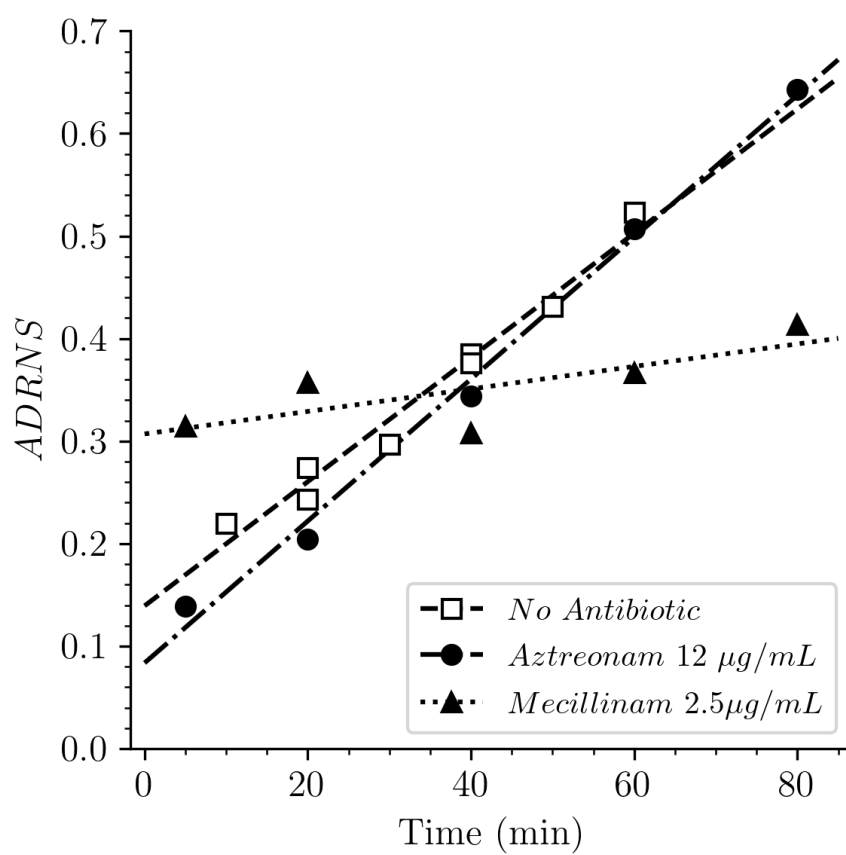
Mode of insertion of subunits into the growing peptidoglycan network by PBPs.

Since the mode of insertion of new peptidoglycan subunits into the growing peptidoglycan varies during the cell cycle various approaches were developed for specifically investigating expansion of the lateral cell wall and the synthesis of the septum. These approaches relied on the use of synchronized cells [25], specific inhibitors of proteins of the elongasome and of the divisome [41, 42], thermosensitive mutants deficient in cell elongation or cell division at the non-permissive temperature [40], and overproduction of the cell division inhibitor Sula [43, 44]. In our study, we used aztreonam and mecillinam to specifically inhibit synthesis of septal and lateral peptidoglycan, respectively, in strain BW25113 $\Delta 6ldt$, which exclusively relies on PBPs for cross-linking. In the presence of aztreonam, the acceptor-donor ratio of unlabeled (neo-synthesized) material (ADRNS) was 0.14 five minutes after the medium switch and increased to 0.20, 0.34, 0.50,

and 0.64 at 20, 40, 60, and 80 minutes, respectively (Supplementary Fig. S11). At this time scale, the pre-existing (labeled) disaccharide-peptides are gradually replaced by neo-synthesized (unlabeled) disaccharide-peptides accounting for the fact that neo-synthesized subunits are increasingly cross-linked to unlabeled disaccharide-peptide subunits generating dimers with an ADRNS of 1 (unlabeled donor and acceptor). The extrapolation of the ADRNS at $t=0$ (time of the medium switch) is therefore relevant to the evaluation of the mode of insertion of new subunits into the peptidoglycan. The extrapolated ADRNS value of 0.08 (Supplementary Fig. S11) was similar to the ADRR value of 0.10 reported in reference [25], in that case obtained by extrapolating data to a synchronized culture exclusively containing elongating cells. In the presence of mecillinam, the ADRNS values marginally increased over time, providing an extrapolated value of 0.31 for $t=0$. This value is lower than the ADRR of 0.64 reported by De Jonge *et al.* (1989) [25] by extrapolating data to a synchronized culture exclusively containing constricting cells. These values correspond to the insertion of approximately two or five strands at a time (calculated ADR of 0.33 and 0.67, respectively, see Introduction and Supplementary Figure S2). The origin of this difference is unknown but may involve multiple causes including the fact that blocking cell elongation by mecillinam may not fully prevent incorporation of newly synthesized subunits because mecillinam does not block the polymerization of glycan chains by the elongasome [43]. Together, our results are in agreement with the analysis reported by De Jonge *et al.* (1989) [25] showing single-strand insertion of neo-synthesized peptidoglycan in the side wall *versus* insertion of multiple strands for septal peptidoglycan synthesis. In the absence of mecillinam and aztreonam, the ADRNS value (0.14) was intermediate between the values observed in the presence of aztreonam (0.08) and mecillinam (0.31), as qualitatively expected for the combined contributions of cross-links located in the side wall and in the septum and the lower contribution of the latter to the cell surface.

Mode of insertion of subunits involving the combined cross-linking activity of PBPs and YcbB.

In the absence of β -lactam, *E. coli* M1.5 [8, 14] relies both on the D,D-transpeptidase activity of PBPs and the L,D-transpeptidase activity of YcbB for peptidoglycan cross-linking, leading to high proportions of 4 \rightarrow 3 (56%) and 3 \rightarrow 3 (44%) cross-linked dimers (Table S1). The proportions of dimers containing two neo-synthesized stems (new \rightarrow new) or one neo-synthesized and one pre-existing stem (new \rightarrow old) were similar for the two types of cross-links (Fig. 9). Thus, the D,D-transpeptidase activity of PBPs and the L,D-transpeptidase activity of YcbB were involved in similar modes of insertion of new strands into the preexisting peptidoglycan of strain M1.5. The ADRNS values were in the order of 0.17 and 0.22 for 4 \rightarrow 3 and 3 \rightarrow 3 crosslinks, respectively. These values indicate that the neo-synthesized glycan strands are predominantly but



Supplementary Figure S11: Acceptor to donor ratio of neo-synthesized stems (ADRNS) of *E. coli* $\Delta 6ldt$.

not exclusively cross-linked to the preexisting peptidoglycan for both types of transpeptidation. Peptidoglycan polymerization might involve single-strand insertion in the side-wall and insertion of multiple strands in the septum as discussed above for strain $\Delta 6ldt$. These observations suggest that the mode of insertion of new subunits is not determined by the transpeptidases but by other components of the peptidoglycan polymerization complexes, such as the scaffolding proteins.

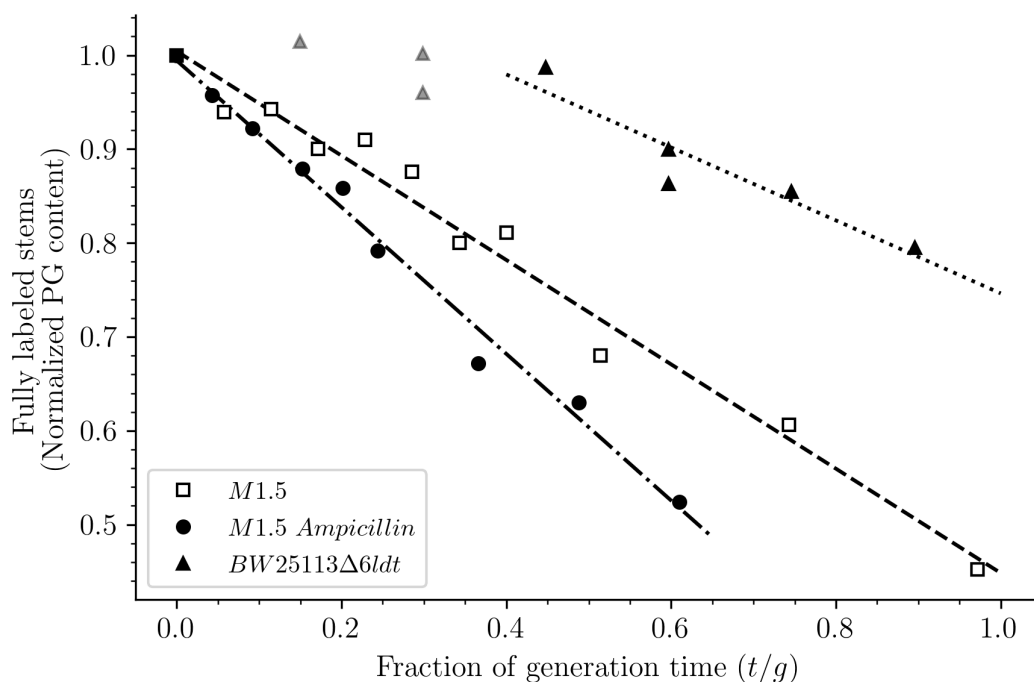
Mode of insertion of subunits involving exclusive cross-linking by the L,D-transpeptidase activity of YcbB.

Growth of *E. coli* M1.5 in the presence of 16 $\mu\text{g/mL}$ ampicillin resulted in a peptidoglycan almost exclusively cross-linked by YcbB due to the inhibition of the D,D-transpeptidase activity of PBPs (Fig. 11). Strikingly, the Tri \rightarrow Tetra and Tri \rightarrow Penta dimers were almost exclusively of the new \rightarrow new type. This mode of insertion was not found in strain M1.5 grown in the absence of ampicillin (Fig. 9) and in strain $\Delta 6ldt$ grown in the presence of aztreonam or in the absence of antibiotic (Fig. 10). The large proportion of new \rightarrow new dimers may originate from the inhibition of the transpeptidase activity of PBPs by ampicillin since inactivation of PBPs by β -lactams is known to result in the uncoupling of the cross-linking and transglycosylase reactions [43, 45]. This in turn results in the accumulation of linear glycan strands that might be cross-linked to each other by YcbB [14]. Accumulation of linear glycan strands potentially at the origin of the synthesis of the new \rightarrow new dimers formed by YcbB is also expected to be stimulated by a mutation present in M1.5 that impairs the activity of lytic transglycosylase SltY and prevents the degradation of uncross-linked glycan strands [14]. The new \rightarrow new pattern of insertion almost exclusively detected in the Tri \rightarrow Tetra and Tri \rightarrow Penta dimers (Fig. 11) corresponds to the insertion of multiple strands at a time. Thus, the neo-synthesized material was only connected to the preexisting peptidoglycan by the formation of Tri \rightarrow Tri dimers, which are the only new \rightarrow old dimers detected in the peptidoglycan. This implies that the acceptors of the cross-linking reactions in the preexisting peptidoglycan were almost exclusively tripeptides, whereas preexisting etrapeptides also acted as acceptors in the absence of ampicillin (Fig. 10). The exclusive use of pre-existing tripeptides as acceptors in the presence of ampicillin could be accounted for by the fact that these tripeptides originate from cleavage of 3 \rightarrow 3 cross-links liberating the tripeptide stems present in the donor position of the preexisting dimers. This model implies a cooperation between YcbB, which catalyzes the formation of the Tri \rightarrow Tri cross-links, and an endopeptidase activity, which provides the tripeptide acceptor substrate of this reaction by cleaving preexisting 3 \rightarrow 3 cross-links. This endopeptidase activity could correspond to that of MepK since this endopeptidase preferentially cleaves 3 \rightarrow 3 cross-links *in vitro*, is essential for bacterial growth only in strains overproducing YcbB, and is

not inhibited by ampicillin [14]. In the absence of ampicillin, the presence of 4→3 cross-links and of active endopeptidases belonging to the PBP family could contribute to the diversity of acceptors available for peptidoglycan cross-linking in mutant M1.5 leading to the formation of dimers containing both tripeptide and tetrapeptide stems in the acceptor position of dimers.

Extent of peptidoglycan recycling. In the absence of turnover and recycling, the number of fully labeled disaccharide-peptide subunits is expected to remain constant. Turnover, corresponding to a small proportion of peptidoglycan degradation products [46], results in a reduction in the content of fully labeled disaccharide-peptides through loss of peptidoglycan fragments in the external medium. Recycling also results in a reduction in the peptidoglycan content of fully labeled disaccharide-peptides since the recycled moieties are incorporated into peptidoglycan precursors in combination with neo-synthesized moieties according to the pathways depicted in Supplementary Fig. S1. These moieties include two glucosamine residues, two acetyl groups, one D-lactoyl residue, the L-Ala-D-iGlu-DAP tripeptide or its constitutive amino acids, and two D-Ala residues. Disaccharide-peptide units containing recycled fragments are therefore mixtures of labeled and unlabeled moieties. These neo-synthesized chimeric structures are easily distinguished from fully labeled disaccharide-peptide subunits originating from peptidoglycan polymerized before the medium switch. Thus, the decrease in the absolute number of fully labeled disaccharide-peptide subunits in one generation directly provides an estimate of the fraction of the preexisting peptidoglycan that is hydrolyzed during each generation. The decrease in the amount of fully labeled disaccharide-peptide subunits per generation was estimated to be 39% for strain $\Delta 6ldt$ and 56% or 78% for M1.5 grown in the absence or presence of ampicillin (Supplementary Figure S12).

These figures are rough estimates since they are collected over a fraction of a generation time (0.66 to 0.95). The extent of the release of fragments from the peptidoglycan macromolecule has been previously evaluated by several approaches based on determination of radiolabeled DAP. In mutants deficient in the production of the AmpG and Opp permeases, the peptidoglycan fragments are not recycled in the cytoplasm and released in the culture medium [47]. Using this approach, Jacobs *et al.* reported that *ca.* 44% of the peptidoglycan is released from the peptidoglycan layer each generation by the *E. coli* K-12 strain MC4100. This value is similar to that observed in our study for strain $\Delta 6ldt$ (39%). The extent of peptidoglycan degradation was higher in mutant M1.5, in particular in the presence of ampicillin (78%). This might result from the uncoupling of the transglycosylation and transpeptidation reactions (above), which was reported to lead to a futile cycle in which accumulation of uncross-linked glycan strands is associated with their partial degradation by autolysins [45].



Supplementary Figure S12: Loss of fully labeled disaccharide-peptide subunits from peptidoglycan. The relative amounts of fully labeled peptidoglycan disaccharide-peptides (normalized to 1.0 at the medium switch) decreased over time, which was normalized per strain to its respective generation time g (Supp. Table S2). The decrease was linear for M1.5 grown in the presence or absence of ampicillin. The extent of the combined turnover and recycling was estimated by linear regression of the full time course of the experiment. For BW25113 Δ 6ldt, a decrease in the content of fully labeled stems was only observed after 0.45 generation times potentially reflecting the assembly of peptidoglycan from labeled precursors pools. For this reason, regression analysis was performed for a portion of the kinetics (from 0.45 to 0.85 generation time; data points excluded from regression analysis are shown as grey triangles). The accuracy of the estimates of the combined peptidoglycan turnover and recycling provided by this analysis is limited by the absence of experimental evidence of the size of the putative preexisting precursors pools and data collection for a limited time (less than a generation).

Advantages and limitations of peptidoglycan analyses based on incorporation of radioactive DAP versus uniform labeling with stable isotopes. Most studies investigating PG metabolism based on labeling with radioactive DAP relied at least partially on *E. coli* strain W7, a derivative of K-12 strain MC4100, which is deficient in DAP synthesis and conversion of DAP to L-lysine due to deletions of the *lysA* and *dapF* genes, respectively [40, 48, 46, 23]. This strain is auxotroph for DAP and L-lysine and is generally grown in the presence of 2 µg/ml or more of DAP and, when grown in glucose minimal medium, 50 µg/ml of L-lysine. The intracellular DAP pool in *E. coli* W7 is larger than in wild-type *E. coli* K-12 strains (an estimated intracellular concentration of 31.5 mmol/l [49] vs. 0.6 mmol/l in *E. coli* K-12 [2]). For *E. coli* W7, the intracellular DAP pool exceeds the amount of DAP present in the peptidoglycan by a factor of five [49]. As discussed by Glauner and Höltje (1990), this limits the incorporation of radioactive DAP into the sacculi and induces a lag between the addition of DAP and its incorporation [48]. In order to improve the kinetics of incorporation of radiolabeled DAP, Burman *et al.* (1984) depleted the intracellular DAP pool by transferring cultures to DAP-free medium for about 25 minutes prior to the addition of radiolabeled DAP [40]. However, electron microscopy imaging of sacculi showed that this treatment compromises the integrity and stability of the PG layer before the onset of lysis [50]. The perturbations resulting from DAP starvation also include changes in cell morphology [51] and reduced turnover [50]. These perturbations were slowly and only partially reversed by the addition of DAP after the starvation period. Our procedure did not suffer from these limitations since uniform labeling of the PG with stable isotopes does not require use of *dapF* and *lysA* deficient mutants. In our conditions, the intracellular DAP pool did not limit the labeling efficacy since hybrid muropeptides containing a labeled DAP moiety were not detected after the medium switch. This is expected, since the intracellular DAP pool in wild-type K-12 strains represents 10% of the DAP content of PG and at least 50% of intracellular DAP is converted into L-lysine [49].

Another limitation of labeling procedures based on radioactive DAP is their inability to discriminate between muropeptides originating from pre-existing peptidoglycan, from recycling of the L-Ala-D-iGlu-DAP tripeptides, or from the preexisting UDP-MurNAc-pentapeptide pool. In contrast, our procedure based on uniform labeling with stable isotopes easily discriminates between these three types of muropeptides since they correspond to different isotopologues: uniformly labeled muropeptides for the preexisting peptidoglycan, hybrid h2 for recycled tripeptides (Fig. 7), and hybrid h3 for muropeptides issued from the intracellular pool of UDP-MurNAc-pentapeptide (Fig. 7). The latter type of muropeptides is likely to contribute to the lag phase observed for the incorporation of radioactive DAP into peptidoglycan. Accordingly, a lag phase

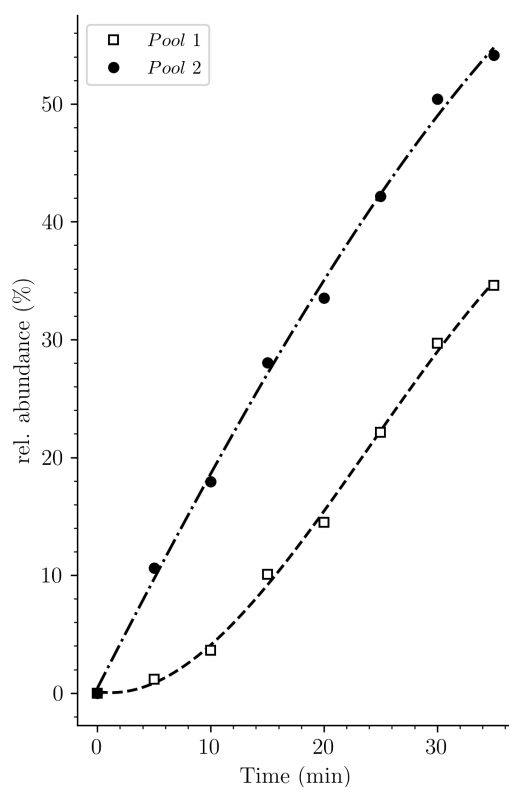
was observed in our study when hybrids containing an [^{13}C]- and [^{15}N]- labeled DAP were excluded from the data set (Supplementary Fig. S13).

The factors that limit the analysis of mucopeptides at early times after the medium switch differ for the labeling techniques based on radioactive DAP and stable isotopes. Purification of sacculi using the hot SDS procedure is prone to sample loss due to numerous washing and digestions steps [52]. According to the procedure implemented in our laboratory, the purification yield is severely impaired for extraction of peptidoglycan from culture volumes smaller than 200 mL. Methods based on DAP labeling offer the possibility to add unlabeled sacculi as carrier material [10] enabling experiments using small culture volumes (*e.g.* 25 mL [48] *versus* 200 mL in our study). In turn, small culture volumes grant access to labeling times as short as 20 seconds [48] based on filtration of an unlabeled culture, *in situ* labeling and immediate transfer of the filter to a boiling SDS solution. Our methodology is limited in this regard, since it is not compatible with the addition of unlabeled carrier sacculi and thus requires substantially larger sample volumes that cannot be easily filtrated. This introduces a delay originating from the necessity to recover labeled bacteria by centrifugation.

5 Conclusion and Perspectives

In conclusion, we report an innovative method for exploring of peptidoglycan metabolism, which does not depend on metabolic engineering for suitable labeling kinetics and is therefore applicable in various genetic backgrounds. The choice of uniform labeling of peptidoglycan with ^{13}C and ^{15}N enabled us to investigate peptidoglycan metabolism at a very fine level of detail since most isotopologues predicted by known recycling and biosynthesis pathways were detected and characterized. Our method was applied to the characterization of the modes of peptidoglycan cross-linking by D,D- and L,D-transpeptidases in the presence or absence of β -lactams revealing various modes of insertion of glycan strands into the pre-existing the expanding peptidoglycan macromolecule.

Further development of our method could involve the use specific tracer molecules, such as $^{13}\text{C}/^{15}\text{N}$ -labeled D-alanine instead of uniform labeling. This will diminish the resolving power for various aspects of peptidoglycan metabolic pathways, in particular for the recycling of aminosugars. However, this labeling scheme will result in markedly less complex mass spectra and improve the accuracy of the assignment of isotopologues. For example, only four isotopologues will have to be taken into consideration for the disaccharide-tetrapeptide following the addition of $^{13}\text{C}/^{15}\text{N}$ -labeled D-alanine to the culture medium: the fully unlabeled molecule and the isotopologues containing labeled alanine in either position 1 or 4 or both of the peptide stem (due



Supplementary Figure S13: Potential origin of the lag phase previously observed in experiments based on incorporation of radioactive DAP. Kinetics of accumulation of neo-synthesized disaccharide-tetrapeptide isotopologues containing unlabeled DAP (pool 1, squares) *versus* all neo-synthesized disaccharide-tetrapeptide isotopologues (pool 2, solid circles). Pool 1 comprises the fully unlabeled mucopeptide and hybrids h1 and hAla (see Fig. 8 and Supplementary Data for the structure and identification of these isotopologues). Pool 2 comprises all neo-synthesized isotopologues including those containing an unlabeled DAP (Pool 1, fully unlabeled, h1, and hAla) plus those containing a labeled DAP (h2, h1h2, h3, and h3Ala). Adding this set of mucopeptides, which are not identified as neo-synthesized by radioactive DAP labeling techniques, results in a kinetics devoid of any lag phase.

to the expected racemization of D-Ala by alanine racemases). Data obtained by this approach will be suitable for fitting differential equations describing a model for the interconversions of muropeptides (Supplementary Fig. S10A). This could provide estimates of the metabolic fluxes in the complex reaction network of muropeptides in the peptidoglycan layer.

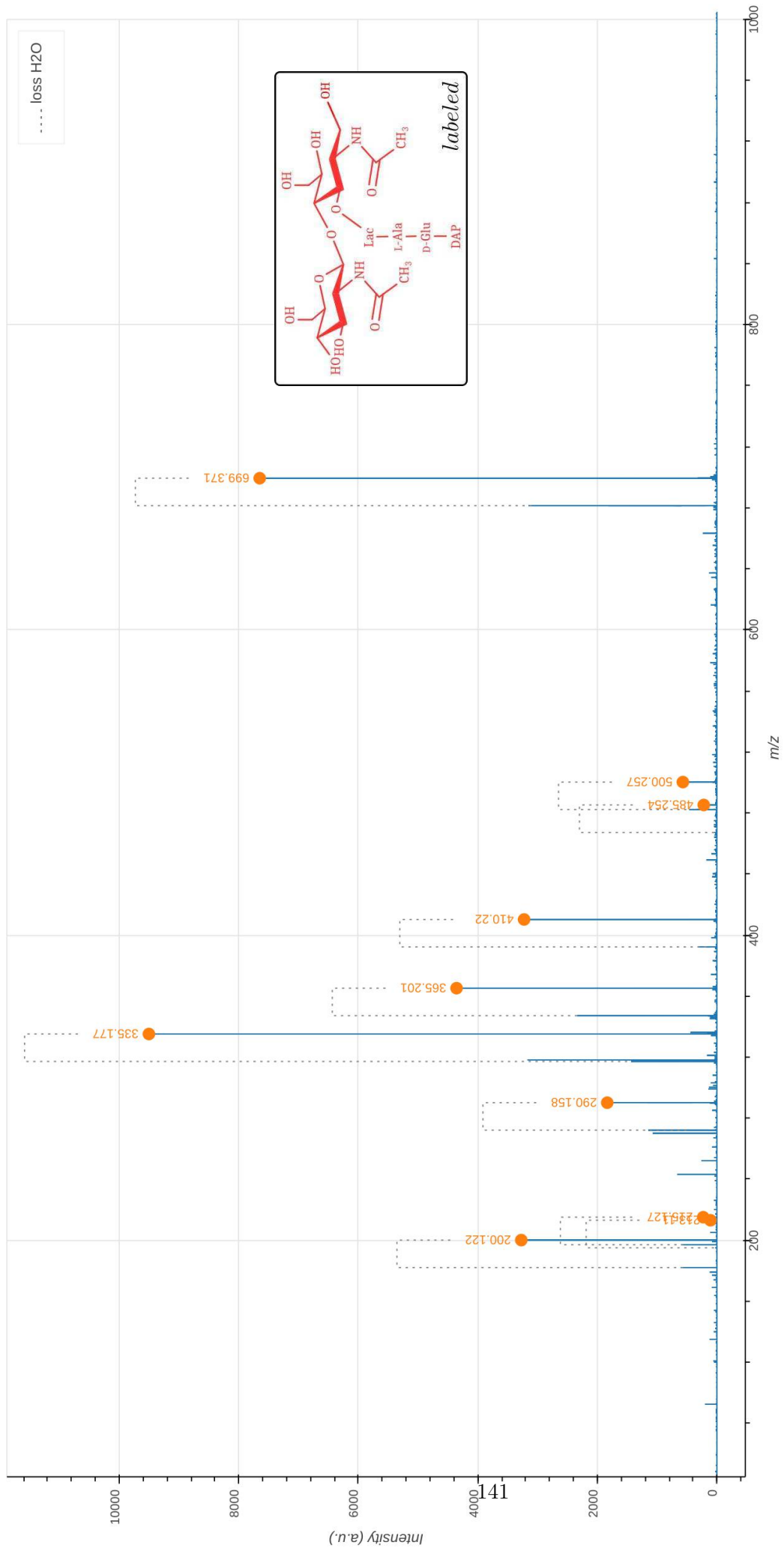
Supplementary Data

Tri - all heavy	2
Tri - h1	4
Tri - h2	6
Tri - h3	8
Tetra - all heavy	10
Tetra - h1	12
Tetra - h2	14
Tetra - h3	16
Tetra - hAla	18
Tetra - h1h2	20
Tetra - h3Ala	22
Additional monomer hybrids	24
Tri-Tri - labeled	25
Tri-Tri - unlabeled	27
Tri-Tri - Donor all light	29
Tetra-Tri - labeled	31
Tetra-Tri - unlabeled	33
Tetra-Tri - Donor all light	35
Tri-Tetra - labeled	37
Tri-Tetra - unlabeled	39
Tri-Tetra - Donor all light	41
Tetra-Tetra - labeled	43
Tetra-Tetra - unlabeled	45
Tetra-Tetra - Donor all light	47

Monomers

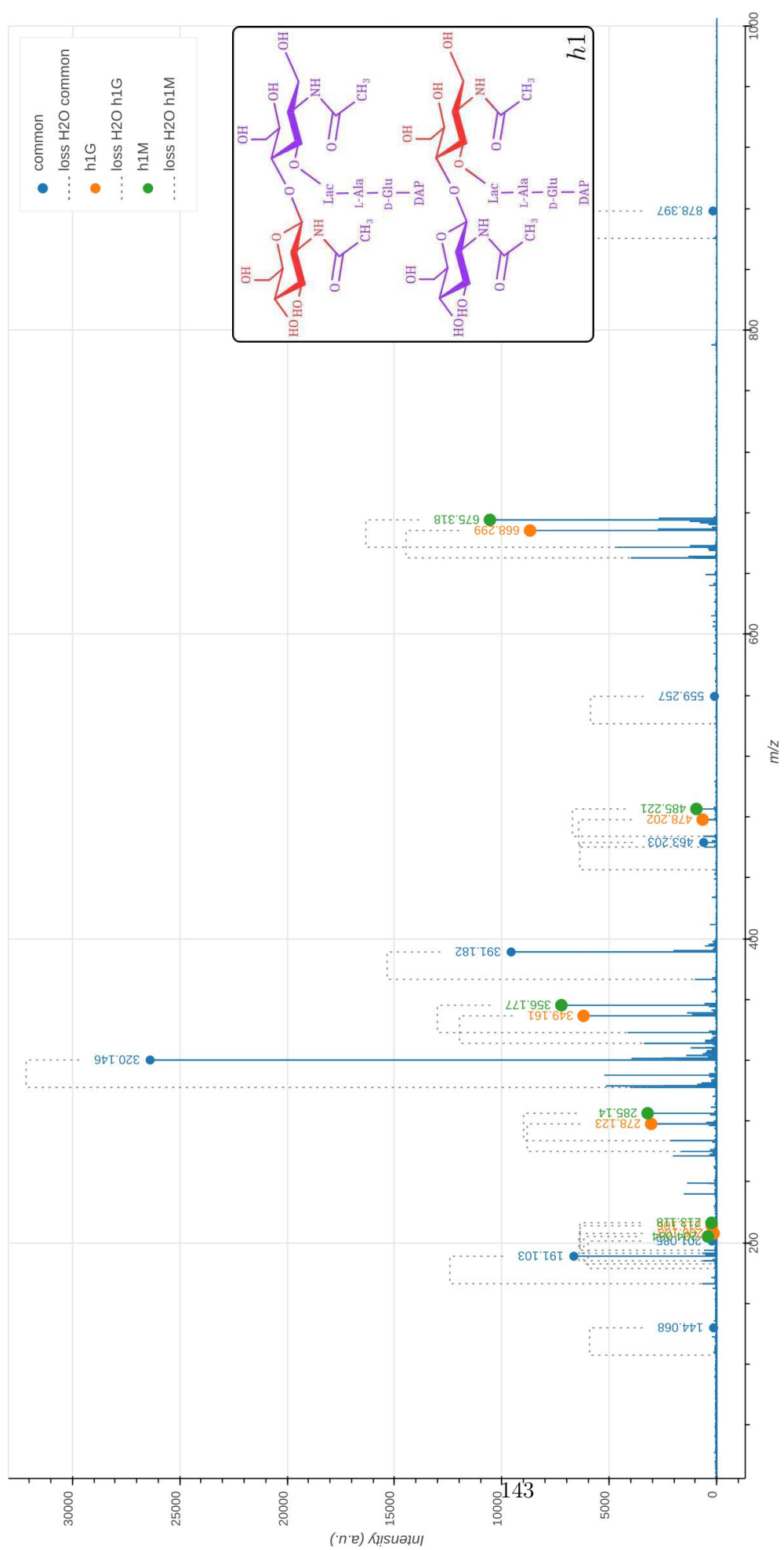
Supplementary Data 1.1: Tandem mass spectrometry analysis of the labeled disaccharide-tripeptide. The observed m/z_{obs} and calculated m/z_{cal} values of the parental ion, $[M+H]^+$, as determined in the absence of fragmentation (MS1), are indicated. The m/z_{calc} value was used to select the ion for fragmentation. The difference between the m/z_{obs} and m/z_{calc} values is indicated in ppm. The GlcNAc residue is indicated in two moieties, glucosamine (GlcN) and the acetyl group (Ac), since these moieties are potentially differentially labeled. For the same reason, the reduced (Red) MurNAc residue is indicated in three moieties, reduced glucosamine (GlcN^{Red}), the acetyl group (Ac), and the D-lactoyl group. Labeled and unlabeled moieties are represented in red and purple, respectively. The peaks corresponding to the list of fragments appearing in the table are highlighted by orange dots in the mass spectrum. In the mass spectrum, peaks differing by the loss of H₂O are connected by a dashed line. The tables only contain the m/z values for the fragments containing H₂O. An interactive report of the MS² analysis is available in Supplementary File F1.1 .

Precursor ion (MS1)	m/z_{obs}	m/z_{calc}	ppm		
GlcN(-Ac)-GlcN ^{Red} (-Ac)-Lac-Ala-Glu-DAP	911.475	911.475	0.3		
Product ion	m/z_{obs}	m/z_{calc}	ppm	Intensity (a.u.)	Isotopologue
GlcN ^{Red} (-Ac)-Lac-Ala-Glu-DAP	699.371	699.371	0.7	7650	all heavy
GlcN ^{Red} (-Ac)-Lac-Ala-Glu	500.257	500.259	2.7	570	all heavy
Lac-Ala-Glu-DAP	485.254	485.253	-2.7	220	all heavy
Ala-Glu-DAP	410.220	410.221	3.7	3226	all heavy
GlcN ^{Red} (-Ac)-Lac-Ala	365.201	365.202	2.5	4356	all heavy
Glu-DAP	335.177	335.177	0.3	9504	all heavy
GlcN ^{Red} (-Ac)-Lac	290.158	290.158	-1.0	1835	all heavy
GlcN ^{Red} (-Ac)	215.127	215.127	0.5	229	all heavy
GlcN(-Ac)	213.110	213.111	3.7	108	all heavy
DAP	200.122	200.121	-4.1	3273	all heavy



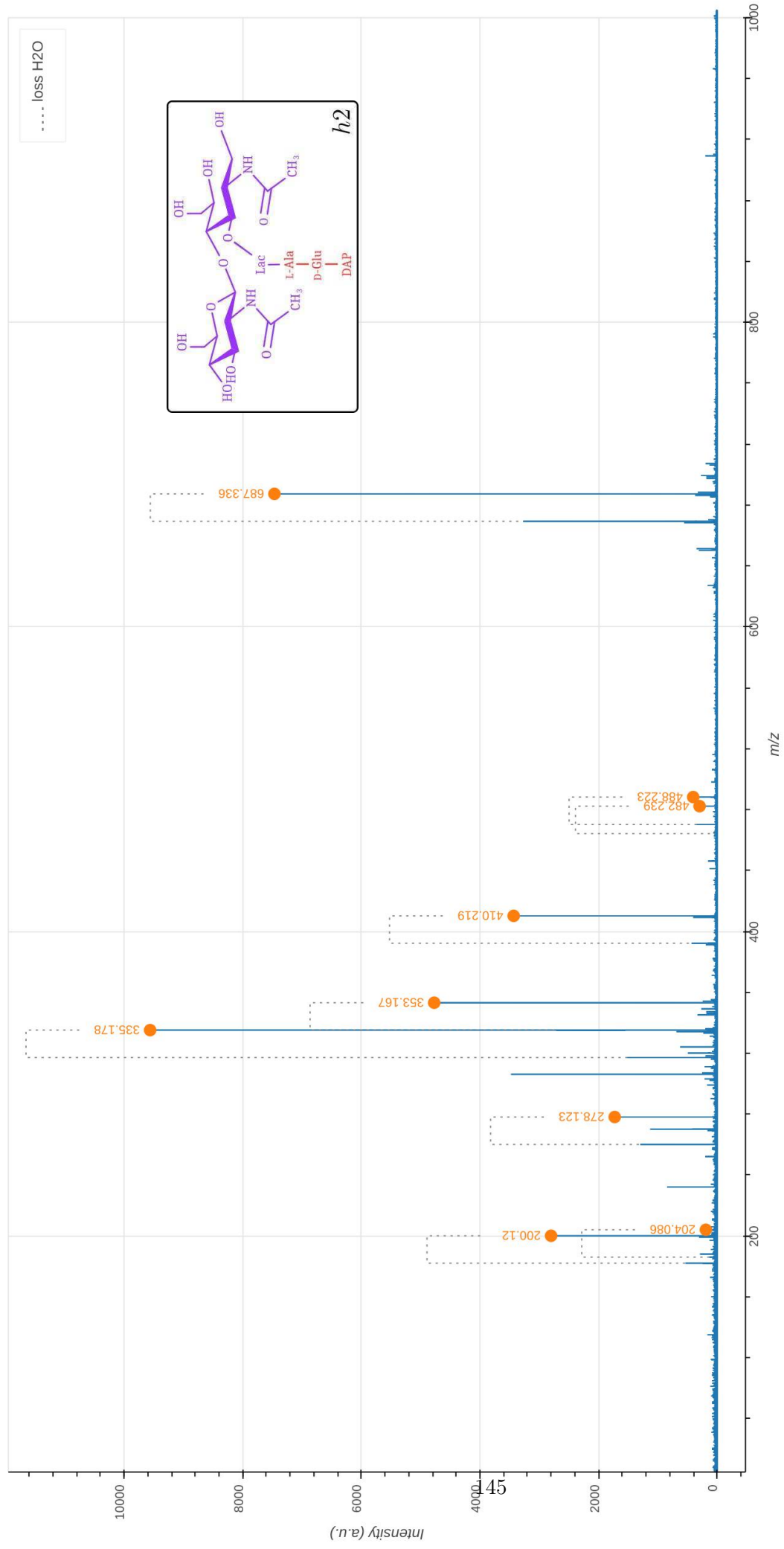
Supplementary Data 1.2: Tandem mass spectrometry analysis of the h1-type hybrid of the disaccharide-tripeptide. The molecule is fully unlabeled except for one of the two glucosamine moieties present in GlcNAc or MurNAc leading to the presence of two isotopomers. The observed m/z_{obs} and calculated m/z_{calc} values of the parental ion, $[M+H]^+$, as determined in the absence of fragmentation (MS^1), are indicated. The m/z_{cal} value was used to select the ion for fragmentation. The difference between the m/z_{obs} and m/z_{cal} values is indicated in ppm. The GlcNAc residue is indicated in two moieties, glucosamine (GlcN) and the acetyl group (Ac), since these moieties are potentially differentially labeled. For the same reason, the reduced (Red) MurNAc residue is indicated in three moieties, reduced glucosamine (GlcN^{Red}), the acetyl group (Ac), and the D-lactoyl group. Labeled and unlabeled moieties are represented in red and purple, respectively. The fragmentation led to two series of fragments specific of the isotopomers containing the unlabeled glucosamine moiety in the GlcNAc (h1G) or $\text{MurNAc}^{\text{Red}}$ (h1M) residues, respectively (discriminatory fragments). The fragments specific of h1G and of h1M are highlighted by orange and green dots in the mass spectrum. The other fragments are common to the fragmentation patterns of h1G and of h1M. The corresponding peaks are highlighted by blue dots in the mass spectrum. The mass spectrum indicates the presence of both isotopomers as expected from the recycling and synthesis pathways since UDP-MurNAc exclusively derives from UDP-GlcNAc. In the mass spectrum, peaks differing by the loss of H_2O are connected by a dashed line. The tables only contain the m/z values for the fragments containing H_2O . An interactive report of the MS^2 analysis is available in Supplementary File F1.2

Precursor Ion (MS^1)	m/z_{obs}	m/z_{calc}	ppm		
$\text{GlcN}(-\text{Ac})-\text{GlcN}^{\text{Red}}(-\text{Ac})-\text{Lac-Ala-Glu-DAP}$	878.392	878.396	-4.0		
$\text{GlcN}(-\text{Ac})-\text{GlcN}^{\text{Red}}(-\text{Ac})-\text{Lac-Ala-Glu-DAP}$	878.392	878.396	-4.0		
Discriminatory product ion	m/z_{obs}	m/z_{calc}	ppm	Intensity (a.u.)	Isotopomer
$\text{GlcN}^{\text{Red}}(-\text{Ac})-\text{Lac-Ala-Glu-DAP}$	675.318	675.316	-2.3	10563	h1M
$\text{GlcN}^{\text{Red}}(-\text{Ac})-\text{Lac-Ala-Glu-DAP}$	668.299	668.299	0.6	8694	h1G
$\text{GlcN}^{\text{Red}}(-\text{Ac})-\text{Lac-Ala-Glu}$	485.221	485.221	0.3	952	h1M
$\text{GlcN}^{\text{Red}}(-\text{Ac})-\text{Lac-Ala-Glu}$	478.202	478.204	3.4	662	h1G
$\text{GlcN}^{\text{Red}}(-\text{Ac})-\text{Lac-Ala}$	356.177	356.178	3.6	7236	h1M
$\text{GlcN}^{\text{Red}}(-\text{Ac})-\text{Lac-Ala}$	349.161	349.161	1.1	6203	h1G
$\text{GlcN}^{\text{Red}}(-\text{Ac})-\text{Lac}$	285.140	285.141	4.9	3223	h1M
$\text{GlcN}^{\text{Red}}(-\text{Ac})-\text{Lac}$	278.123	278.124	4.0	3059	h1G
$\text{GlcN}^{\text{Red}}(-\text{Ac})$	213.118	213.120	8.2	247	h1M
$\text{GlcN}(-\text{Ac})$	211.106	211.104	-6.8	238	h1G
$\text{GlcN}^{\text{Red}}(-\text{Ac})$	206.103	206.103	-0.5	148	h1G
$\text{GlcN}(-\text{Ac})$	204.084	204.087	15.1	419	h1M
Common product ion	m/z_{obs}	m/z_{calc}	ppm	Intensity (a.u.)	
$\text{GlcN}(-\text{Ac})-\text{GlcN}^{\text{Red}}(-\text{Ac})-\text{Lac-Ala-Glu-DAP}$	878.397	878.396	-2.1	178	
$\text{GlcN}(-\text{Ac})-\text{GlcN}^{\text{Red}}(-\text{Ac})-\text{Lac-Ala-Glu-DAP}$					
$\text{GlcN}(-\text{Ac})-\text{GlcN}^{\text{Red}}(-\text{Ac})-\text{Lac-Ala}$	559.257	559.258	0.8	112	
$\text{GlcN}(-\text{Ac})-\text{GlcN}^{\text{Red}}(-\text{Ac})-\text{Lac-Ala}$					
Lac-Ala-Glu-DAP	463.203	463.204	1.8	613	
Ala-Glu-DAP	391.182	391.183	2.0	9574	
Glu-DAP	320.146	320.146	0.3	26374	
Ala-Glu	201.085	201.088	13.5	227	
DAP	191.103	191.103	0.6	6654	
Lac-Ala	144.068	144.066	-10.4	154	



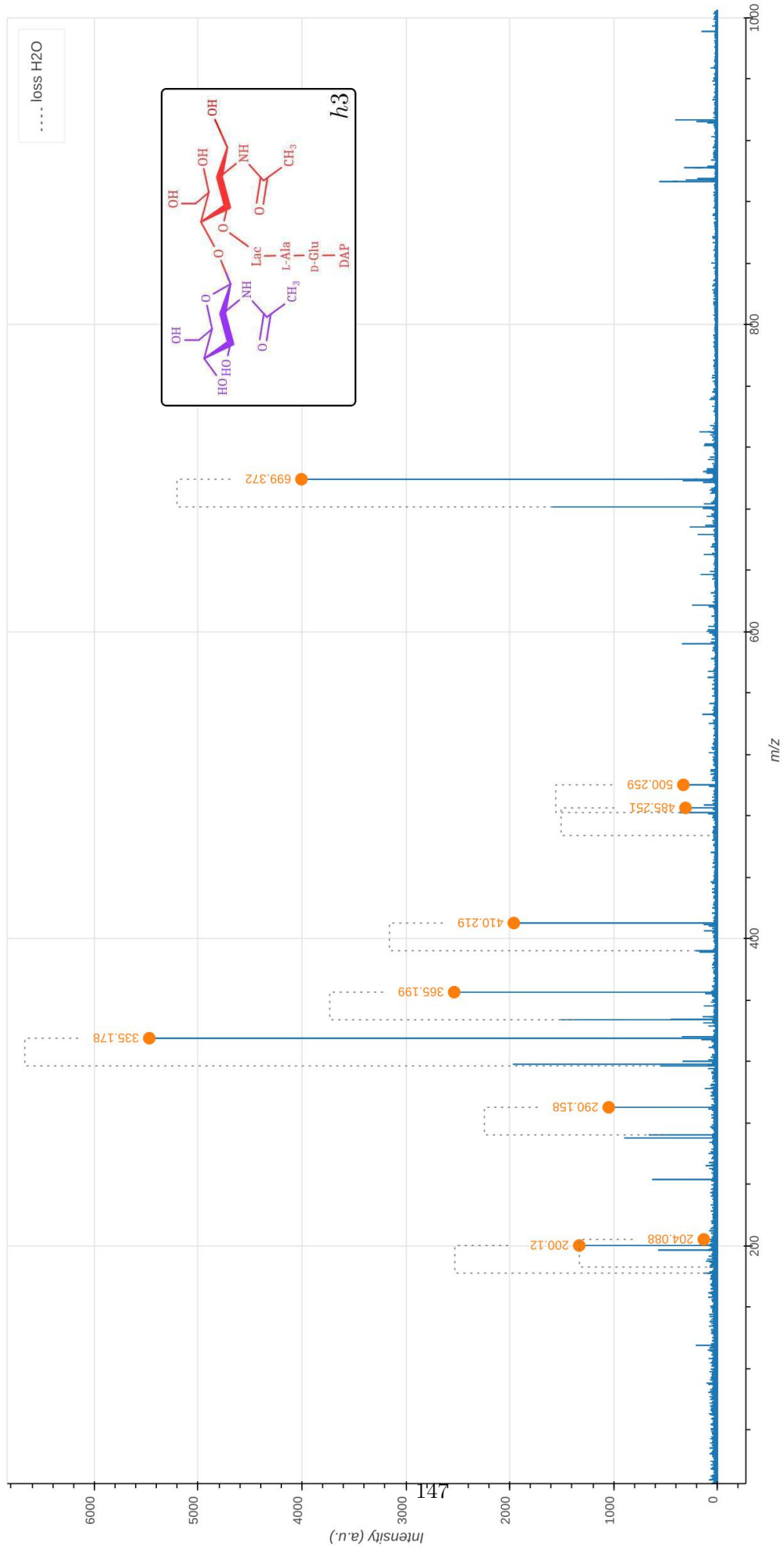
Supplementary Data 1.3: Tandem mass spectrometry analysis of the h2-type hybrid of the disaccharide-tripeptide. The observed m/z_{obs} and calculated m/z_{cal} values of the parental ion, $[M+H]^+$, as determined in the absence of fragmentation (MS1), are indicated. The m/z_{cal} value was used to select the ion for fragmentation. The difference between the m/z_{obs} and m/z_{cal} values is indicated in ppm. The GlcNAc residue is indicated in two moieties, glucosamine (GlcN) and the acetyl group (Ac), since these moieties are potentially differentially labeled. For the same reason, the reduced (Red) MurNAc residue is indicated in three moieties, reduced glucosamine (GlcN^{Red}), the acetyl group (Ac), and the D-lactoyl group. Labeled and unlabeled moieties are represented in red and purple, respectively. The peaks corresponding to the list of fragments appearing in the table are highlighted by orange dots in the mass spectrum. In the mass spectrum, peaks differing by the loss of H_2O are connected by a dashed line. The tables only contain the m/z values for the fragments containing H_2O . An interactive report of the MS² analysis is available in Supplementary File F1.3 .

Precursor ion (MS1)	m/z_{obs}	m/z_{cal}	ppm		
$\text{GlcN}^{\text{Red}}(-\text{Ac})-\text{GlcN}^{\text{Red}}(-\text{Ac})-\text{Lac}-\text{Ala}-\text{Glu}-\text{DAP}$	890.412	890.417	-5.7		
Product ion	m/z_{obs}	m/z_{cal}	ppm	Intensity (a.u.)	Isotopologue
$\text{GlcN}^{\text{Red}}(-\text{Ac})-\text{Lac}-\text{Ala}-\text{Glu}-\text{DAP}$	687.336	687.338	2.2	7465	h2
$\text{GlcN}^{\text{Red}}(-\text{Ac})-\text{Lac}-\text{Ala}-\text{Glu}$	488.223	488.225	3.1	404	h2
$\text{Lac}-\text{Ala}-\text{Glu}-\text{DAP}$	482.239	482.242	7.1	296	h2
$\text{Ala}-\text{Glu}-\text{DAP}$	410.219	410.221	5.5	3431	h2
$\text{GlcN}^{\text{Red}}(-\text{Ac})-\text{Lac}-\text{Ala}$	353.167	353.168	4.7	4771	h2
$\text{Glu}-\text{DAP}$	335.178	335.177	-2.4	9561	h2
$\text{GlcN}^{\text{Red}}(-\text{Ac})-\text{Lac}$	278.123	278.124	2.9	1727	h2
$\text{GlcN}(-\text{Ac})$	204.086	204.087	5.9	190	h2
DAP	200.120	200.121	4.2	2800	h2



Supplementary Data 1.4: Tandem mass spectrometry analysis of the h3-type hybrid of the disaccharide-tripeptide. The observed m/z_{obs} and calculated m/z_{cal} values of the parental ion, $[M+H]^+$, as determined in the absence of fragmentation (MS1), are indicated. The m/z_{calc} value was used to select the ion for fragmentation. The difference between the m/z_{obs} and m/z_{calc} values is indicated in ppm. The GlcNAc residue is indicated in two moieties, glucosamine (GlcN) and the acetyl group (Ac), since these moieties are potentially differentially labeled. For the same reason, the reduced (Red) MurNAc residue is indicated in three moieties, reduced glucosamine (GlcN^{Red}), the acetyl group (Ac), and the D-lactoyl group. Labeled and unlabeled moieties are represented in red and purple, respectively. The peaks corresponding to the list of fragments appearing in the table are highlighted by orange dots in the mass spectrum. In the mass spectrum, peaks differing by the loss of H_2O are connected by a dashed line. The tables only contain the m/z values for the fragments containing H_2O . The presence of the h3 isotopomer is expected since cells of *E. coli* contain the main PG precursor, UDP-MurNAc-pentapeptide in considerable amounts (about 2% compared to the total amount of disaccharide peptides in the cell wall). An interactive report of the MS² analysis is available in Supplementary File F1.4 .

Precursor ion (MS1)	m/z_{obs}	m/z_{calc}	ppm		
$\text{GlcN}(-\text{Ac})-\text{GlcN}^{\text{Red}}(-\text{Ac})-\text{Lac-Ala-Glu-DAP}$	902.447	902.451	-3.8		
Product ion	m/z_{obs}	m/z_{calc}	ppm	Intensity (a.u.)	Isotopomer
$\text{GlcN}^{\text{Red}}(-\text{Ac})-\text{Lac-Ala-Glu-DAP}$	699.372	699.371	-0.5	4005	h3
$\text{GlcN}^{\text{Red}}(-\text{Ac})-\text{Lac-Ala-Glu}$	500.259	500.259	-0.8	329	h3
Lac-Ala-Glu-DAP	485.251	485.253	3.1	308	h3
Ala-Glu-DAP	410.219	410.221	5.1	1961	h3
$\text{GlcN}^{\text{Red}}(-\text{Ac})-\text{Lac-Ala}$	365.199	365.202	8.5	2535	h3
Glu-DAP	335.178	335.177	-2.9	5470	h3
$\text{GlcN}^{\text{Red}}(-\text{Ac})-\text{Lac}$	290.158	290.158	0.2	1047	h3
$\text{GlcN}(-\text{Ac})$	204.088	204.087	-2.6	132	h3
DAP	200.120	200.121	3.8	1331	h3

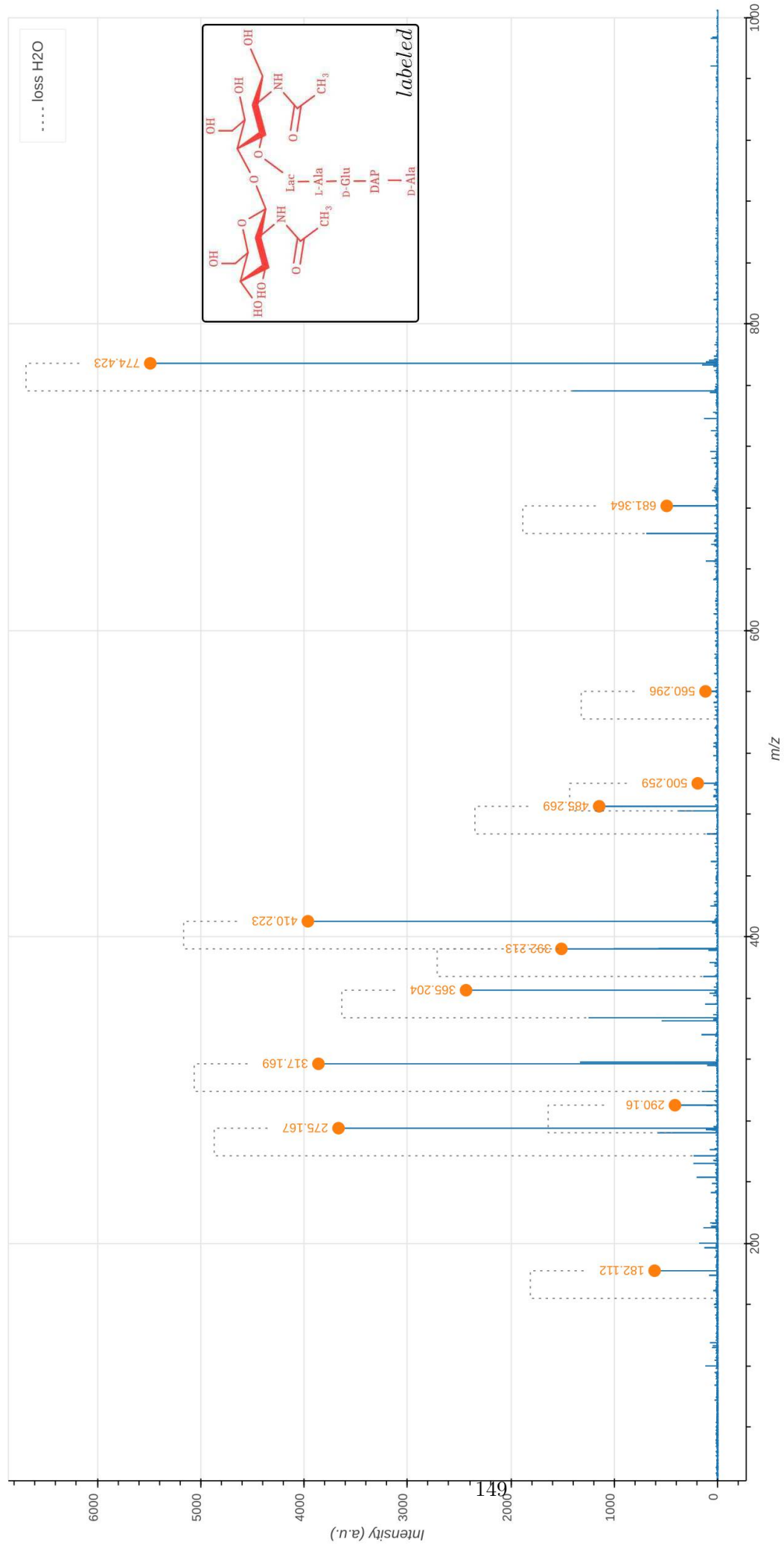


Supplementary Data 2.1: Supplementary Data D2.1 . Tandem mass spectrometry analysis of the labeled disaccharide-tetrapeptide.

The observed m/z_{obs} and calculated m/z_{calc} values of the parental ion, $[M+H]^+$, as determined in the absence of fragmentation (MS1), are indicated. The m/z_{calc} value was used to select the ion for fragmentation. The difference between the m/z_{obs} and m/z_{calc} values is indicated in ppm. The GlcNAc residue is indicated in two moieties, glucosamine (GlcN) and the acetyl group (Ac), since these moieties are potentially differentially labeled. For the same reason, the reduced (Red) MurNAc residue is indicated in three moieties, reduced glucosamine (GlcN^{Red}), the acetyl group (Ac), and the D-lactoyl group. Labeled and unlabeled moieties are represented in red and purple, respectively. The peaks corresponding to the list of fragments appearing in the table are highlighted by orange dots in the mass spectrum. In the mass spectrum, peaks differing by the loss of H₂O are connected by a dashed line. The tables only contain the m/z values for the fragments containing H₂O.

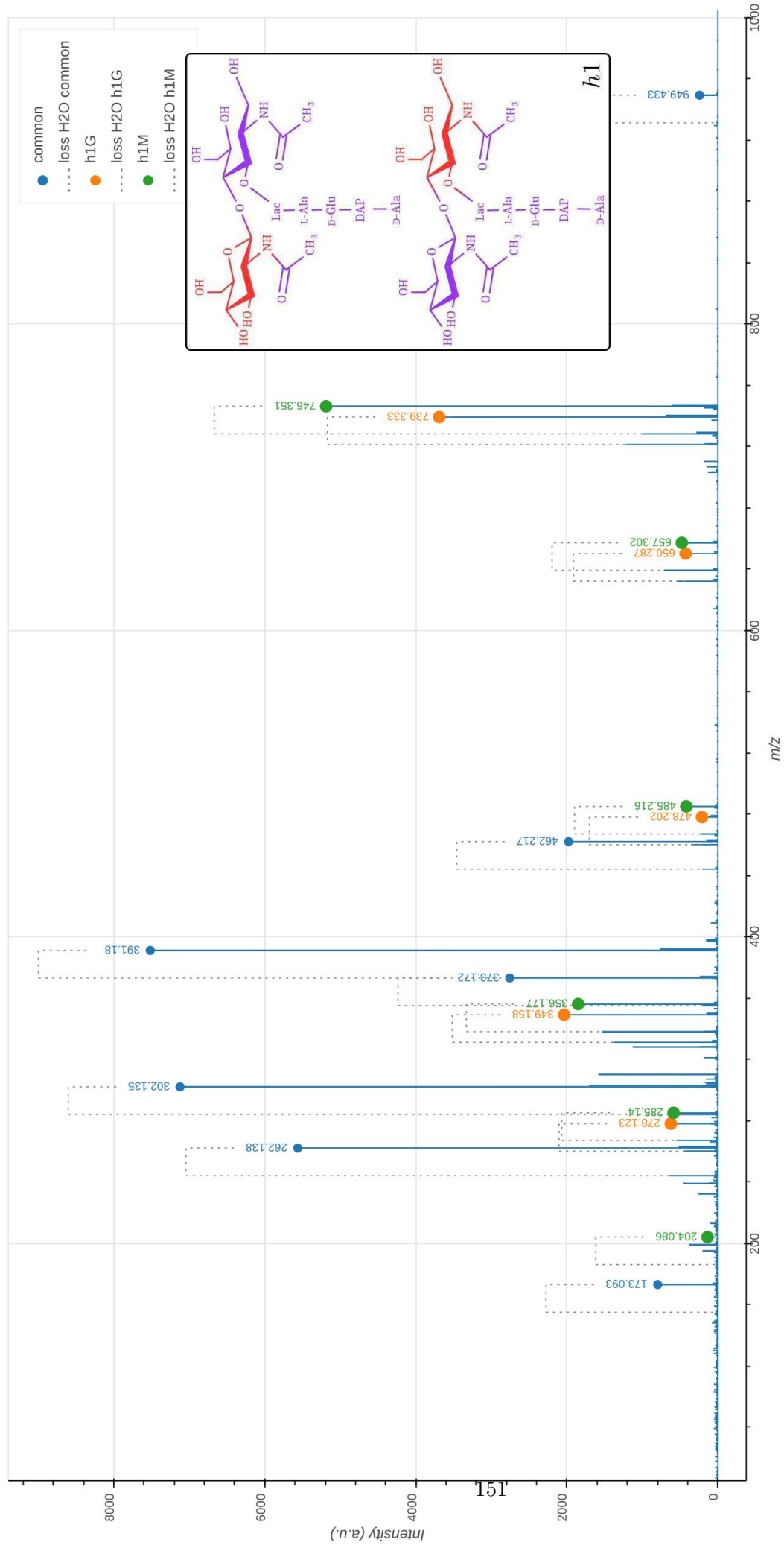
An interactive report of the MS2 analysis is available in Supplementary File F2.1.

Precursor ion (MS1)	m/z_{obs}	m/z_{calc}	ppm		
GlcN(-Ac)-GlcN ^{Red} (-Ac)-Lac-Ala-Glu-DAP-Ala	986.516	986.519	-3.1		
Product ion	m/z_{obs}	m/z_{calc}	ppm	Intensity (a.u.)	Isotopologue
GlcN ^{Red} (-Ac)-Lac-Ala-Glu-DAP-Ala	774.423	774.416	-9.3	5487	all heavy
GlcN ^{Red} (-Ac)-Lac-Ala-Glu-DAP	681.364	681.361	-5.1	494	all heavy
Lac-Ala-Glu-DAP-Ala	560.296	560.297	0.9	119	all heavy
GlcN ^{Red} (-Ac)-Lac-Ala-Glu	500.259	500.259	0.0	194	all heavy
Ala-Glu-DAP-Ala	485.269	485.266	-6.8	1147	all heavy
Glu-DAP-Ala	410.223	410.221	-3.9	3963	all heavy
Ala-Glu-DAP	392.213	392.211	-5.6	1512	all heavy
GlcN ^{Red} (-Ac)-Lac-Ala	365.204	365.202	-5.1	2434	all heavy
Glu-DAP	317.169	317.167	-8.5	3861	all heavy
GlcN ^{Red} (-Ac)-Lac	290.160	290.158	-7.3	414	all heavy
DAP-Ala	275.167	275.165	-6.2	3667	all heavy
DAP	182.112	182.110	-8.1	611	all heavy



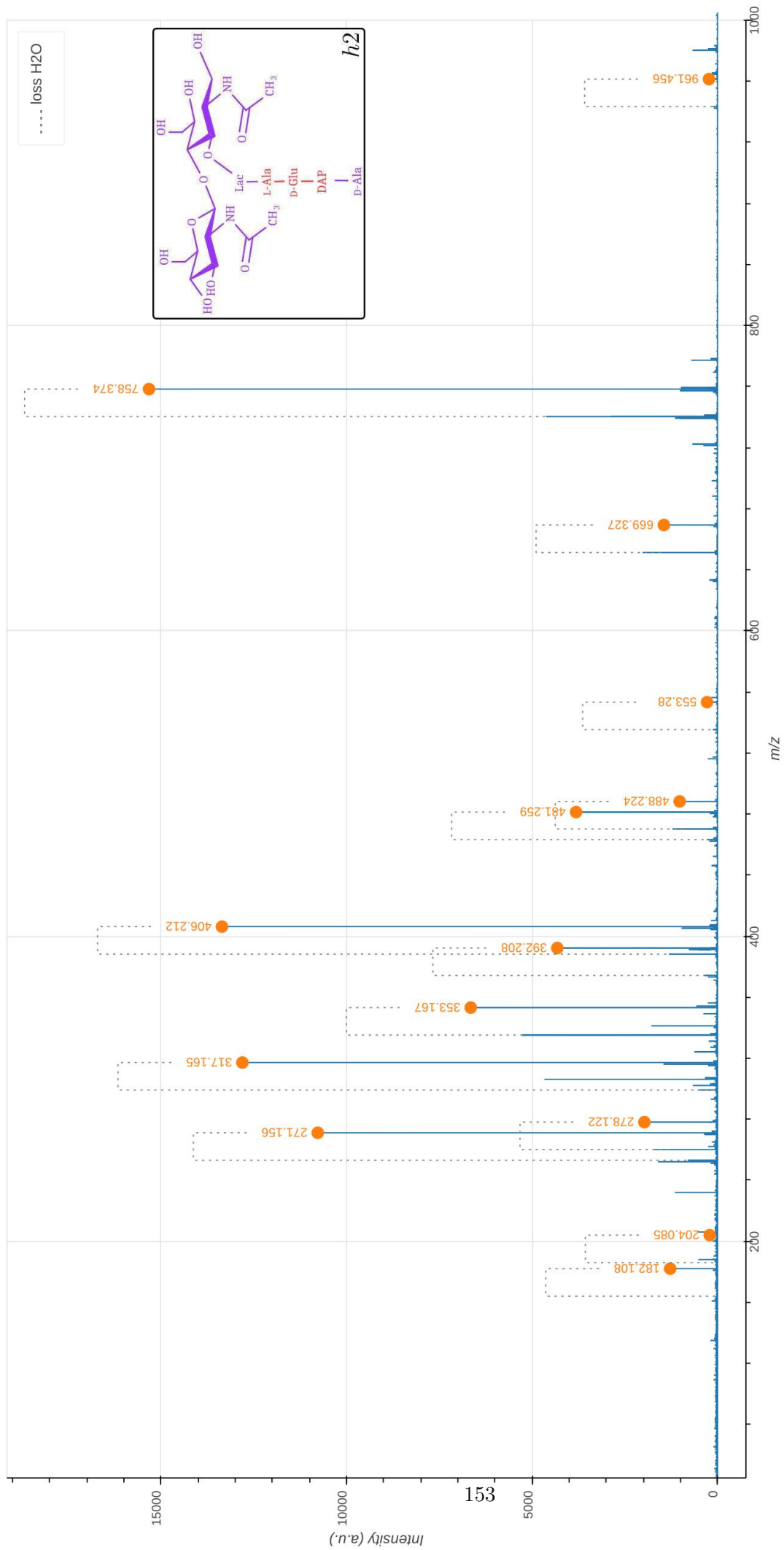
Supplementary Data 2.2: Tandem mass spectrometry analysis of the h1-type hybrid of the disaccharide-tetrapeptide. The molecule is fully unlabeled except for one of the two glucosamine moieties present in GlcNAc or MurNAc leading to the presence of two isotopomers. The observed m/z_{obs} and calculated m/z_{calc} values of the parental ion, $[M+H]^+$, as determined in the absence of fragmentation (MS^1), are indicated. The m/z_{cal} value was used to select the ion for fragmentation. The difference between the m/z_{obs} and m/z_{cal} values is indicated in ppm. The GlcNAc residue is indicated in two moieties, glucosamine (GlcN) and the acetyl group (Ac), since these moieties are potentially differentially labeled. For the same reason, the reduced (Red) MurNAc residue is indicated in three moieties, reduced glucosamine (GlcN^{Red}), the acetyl group (Ac), and the D-lactoyl group. Labeled and unlabeled moieties are represented in red and purple, respectively. The fragmentation led to two series of fragments specific of the isotopomers containing the unlabeled glucosamine moiety in the GlcNAc (h1G) or $\text{MurNAc}^{\text{Red}}$ (h1M) residues, respectively (discriminatory fragments). The fragments specific of h1G and of h1M are highlighted by orange and green dots in the mass spectrum. The other fragments are common to the fragmentation patterns of h1G and of h1M. The corresponding peaks are highlighted by blue dots in the mass spectrum. The mass spectrum indicates the presence of both isotopomers as expected from the recycling and synthesis pathways since UDP-MurNAc exclusively derives from UDP-GlcNAc. In the mass spectrum, peaks differing by the loss of H_2O are connected by a dashed line. The tables only contain the m/z values for the fragments containing H_2O . An interactive report of the MS^2 analysis is available in Supplementary File F2.2.

Precursor ion (MS^1)	m/z_{obs}	m/z_{calc}	ppm		
$\text{GlcN}^{\text{Red}}(-\text{Ac})-\text{GlcN}^{\text{Red}}(-\text{Ac})-\text{Lac}-\text{Ala}-\text{Glu}-\text{DAP}-\text{Ala}$	949.429	949.433	-4.0		
$\text{GlcN}(-\text{Ac})-\text{GlcN}^{\text{Red}}(-\text{Ac})-\text{Lac}-\text{Ala}-\text{Glu}-\text{DAP}-\text{Ala}$	949.429	949.433	-4.0		
Discriminatory product ions	m/z_{obs}	m/z_{calc}	ppm	Intensity (a.u.)	Isotopologue
$\text{GlcN}^{\text{Red}}(-\text{Ac})-\text{Lac}-\text{Ala}-\text{Glu}-\text{DAP}-\text{Ala}$	746.351	746.353	3.3	5188	h1M
$\text{GlcN}^{\text{Red}}(-\text{Ac})-\text{Lac}-\text{Ala}-\text{Glu}-\text{DAP}-\text{Ala}$	739.333	739.336	4.7	3690	h1G
$\text{GlcN}^{\text{Red}}(-\text{Ac})-\text{Lac}-\text{Ala}-\text{Glu}-\text{DAP}$	657.302	657.306	5.2	477	h1M
$\text{GlcN}^{\text{Red}}(-\text{Ac})-\text{Lac}-\text{Ala}-\text{Glu}-\text{DAP}$	650.287	650.288	2.7	427	h1G
$\text{GlcN}^{\text{Red}}(-\text{Ac})-\text{Lac}-\text{Ala}-\text{Glu}$	485.216	485.221	10.3	417	h1M
$\text{GlcN}^{\text{Red}}(-\text{Ac})-\text{Lac}-\text{Ala}-\text{Glu}$	478.202	478.204	3.3	210	h1G
$\text{GlcN}^{\text{Red}}(-\text{Ac})-\text{Lac}-\text{Ala}$	356.177	356.178	3.6	1850	h1M
$\text{GlcN}^{\text{Red}}(-\text{Ac})-\text{Lac}-\text{Ala}$	349.158	349.161	8.1	2036	h1G
$\text{GlcN}^{\text{Red}}(-\text{Ac})-\text{Lac}$	285.140	285.141	4.9	586	h1M
$\text{GlcN}^{\text{Red}}(-\text{Ac})-\text{Lac}$	278.123	278.124	4.0	622	h1G
$\text{GlcN}(-\text{Ac})$	204.086	204.087	7.2	137	h1M
Common product ion	m/z_{obs}	m/z_{calc}	ppm	Intensity (a.u.)	
$\text{GlcN}(-\text{Ac})-\text{GlcN}^{\text{Red}}(-\text{Ac})-\text{Lac}-\text{Ala}-\text{Glu}-\text{DAP}-\text{Ala}$	949.433	949.433	0.1	241	
$\text{GlcN}(-\text{Ac})-\text{GlcN}^{\text{Red}}(-\text{Ac})-\text{Lac}-\text{Ala}-\text{Glu}-\text{DAP}-\text{Ala}$	462.217	462.220	6.1	1977	
$\text{Ala}-\text{Glu}-\text{DAP}-\text{Ala}$	391.180	391.183	6.2	7517	
$\text{Glu}-\text{DAP}-\text{Ala}$	373.172	373.172	1.7	2756	
$\text{Ala}-\text{Glu}-\text{DAP}$	302.135	302.135	0.9	7122	
$\text{DAP}-\text{Ala}$	262.138	262.140	9.0	5564	
DAP	173.093	173.093	0.3	796	



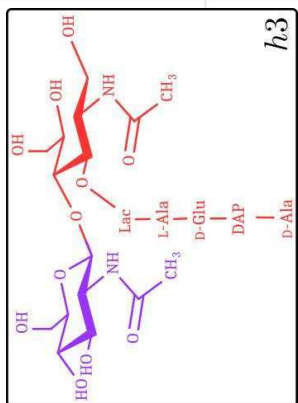
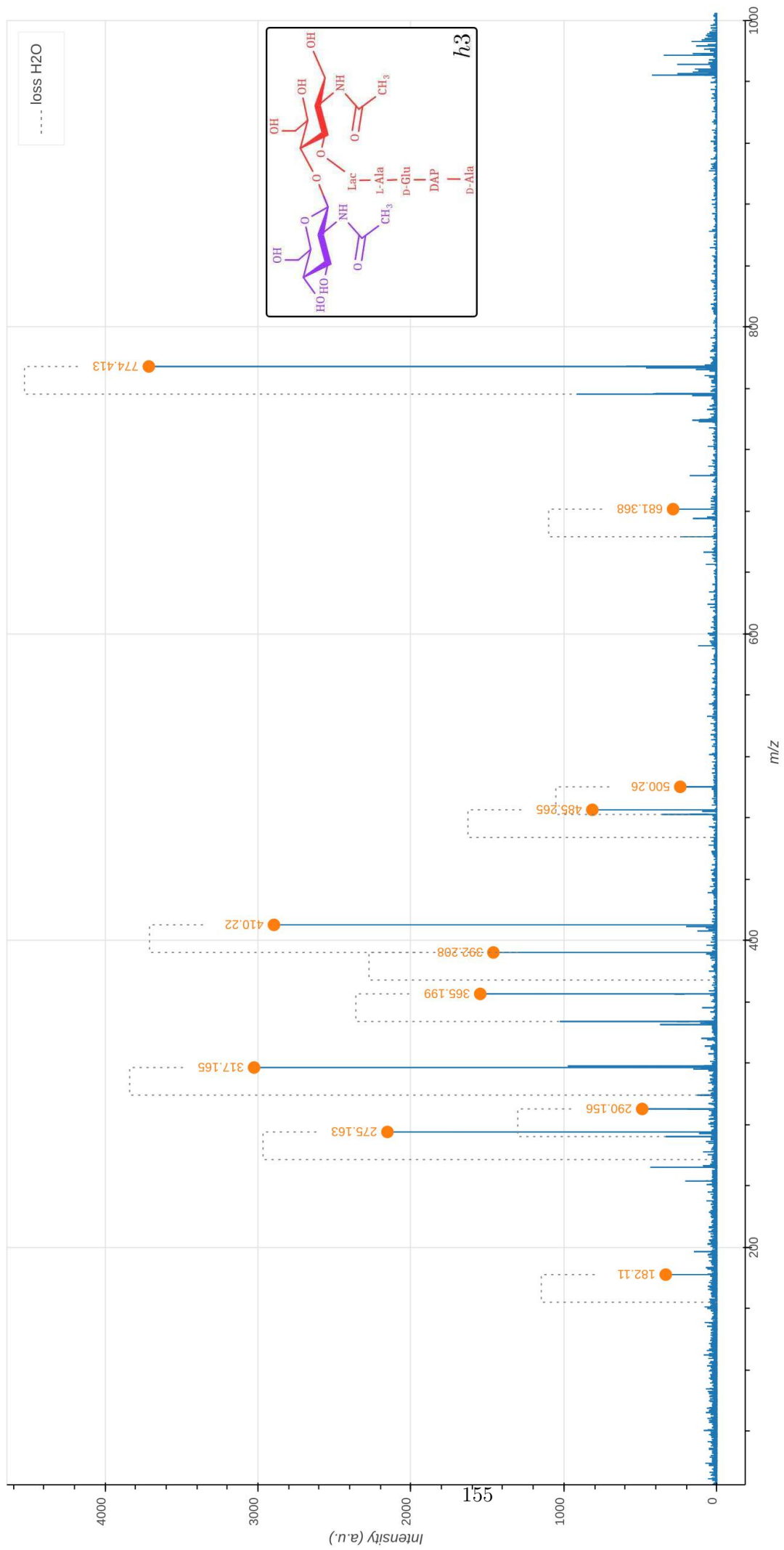
Supplementary Data 2.3: Tandem mass spectrometry analysis of the h2-type hybrid of the disaccharide-tetrapeptide. The observed m/z_{obs} and calculated m/z_{calc} values of the parental ion, $[M+H]^+$, as determined in the absence of fragmentation (MS1), are indicated. The m/z_{calc} value was used to select the ion for fragmentation. The difference between the m/z_{obs} and m/z_{calc} values is indicated in ppm. The GlcNAc residue is indicated in two moieties, glucosamine (GlcN) and the acetyl group (Ac), since these moieties are potentially differentially labeled. For the same reason, the reduced (Red) MurNAc residue is indicated in three moieties, reduced glucosamine (GlcN^{Red}), the acetyl group (Ac), and the D-lactoyl group. Labeled and unlabeled moieties are represented in red and purple, respectively. The peaks corresponding to the list of fragments appearing in the table are highlighted by orange dots in the mass spectrum. In the mass spectrum, peaks differing by the loss of H_2O are connected by a dashed line. The tables only contain the m/z values for the fragments containing H_2O . An interactive report of the MS² analysis is available in Supplementary File F2.3 .

Precursor ion (MS1)	m/z_{obs}	m/z_{calc}	ppm		
$\text{GlcN}(-\text{Ac})-\text{GlcN}^{\text{Red}}(-\text{Ac})-\text{Lac}-\text{Ala}-\text{Glu}-\text{DAP}-\text{Ala}$	961.451	961.454	-2.7		
Product ion	m/z_{obs}	m/z_{calc}	ppm	Intensity (a.u.)	Isotopologue
$\text{GlcN}(-\text{Ac})-\text{GlcN}^{\text{Red}}(-\text{Ac})-\text{Lac}-\text{Ala}-\text{Glu}-\text{DAP}-\text{Ala}$	961.456	961.454	-2.4	250	h2
$\text{GlcN}^{\text{Red}}(-\text{Ac})-\text{Lac}-\text{Ala}-\text{Glu}-\text{DAP}-\text{Ala}$	758.374	758.375	1.0	15348	h2
$\text{GlcN}^{\text{Red}}(-\text{Ac})-\text{Lac}-\text{Ala}-\text{Glu}-\text{DAP}$	669.327	669.327	-0.8	1466	h2
$\text{GlcN}(-\text{Ac})-\text{GlcN}^{\text{Red}}(-\text{Ac})-\text{Lac}-\text{Ala}$	556.244	556.248	7.1	191	h2
$\text{Lac}-\text{Ala}-\text{Glu}-\text{DAP}-\text{Ala}$	553.280	553.280	-0.4	302	h2
$\text{GlcN}^{\text{Red}}(-\text{Ac})-\text{Lac}-\text{Ala}-\text{Glu}$	488.224	488.225	1.8	1041	h2
$\text{Ala}-\text{Glu}-\text{DAP}-\text{Ala}$	481.259	481.258	-1.0	3833	h2
$\text{Lac}-\text{Ala}-\text{Glu}-\text{DAP}$	464.235	464.232	-6.3	133	h2
$\text{Glu}-\text{DAP}-\text{Ala}$	406.212	406.214	6.4	13380	h2
$\text{Ala}-\text{Glu}-\text{DAP}$	392.208	392.211	6.8	4340	h2
$\text{GlcN}^{\text{Red}}(-\text{Ac})-\text{Lac}-\text{Ala}$	353.167	353.168	3.4	6673	h2
$\text{Glu}-\text{DAP}$	317.165	317.167	3.8	12830	h2
$\text{GlcN}^{\text{Red}}(-\text{Ac})-\text{Lac}$	278.122	278.124	7.6	1991	h2
$\text{DAP}-\text{Ala}$	271.156	271.158	7.2	10798	h2
$\text{GlcN}^{\text{Red}}(-\text{Ac})$	206.103	206.103	-2.8	163	h2
$\text{GlcN}(-\text{Ac})$	204.085	204.087	12.7	229	h2
DAP	182.108	182.110	9.5	1297	h2



Supplementary Data 2.4: Tandem mass spectrometry analysis of the h3-type hybrid of the disaccharide-tetrapeptide. The observed m/z_{obs} and calculated m/z_{calc} values of the parental ion, $[M+H]^+$, as determined in the absence of fragmentation (MS1), are indicated. The m/z_{calc} value was used to select the ion for fragmentation. The difference between the m/z_{obs} and m/z_{calc} values is indicated in ppm. The GlcNAc residue is indicated in two moieties, glucosamine (GlcN) and the acetyl group (Ac), since these moieties are potentially differentially labeled. For the same reason, the reduced (Red) MurNAc residue is indicated in three moieties, reduced glucosamine (GlcN^{Red}), the acetyl group (Ac), and the D-lactoyl group. Labeled and unlabeled moieties are represented in red and purple, respectively. The peaks corresponding to the list of fragments appearing in the table are highlighted by orange dots in the mass spectrum. In the mass spectrum, peaks differing by the loss of H_2O are connected by a dashed line. The tables only contain the m/z values for the fragments containing H_2O . The presence of the h3 isotopomer is expected since cells of *E. coli* contain the main PG precursor, UDP-MurNAc-pentapeptide in considerable amounts (about 2% compared to the total amount of disaccharide peptides in the cell wall). An interactive report of the MS² analysis is available in Supplementary File F2.4 .

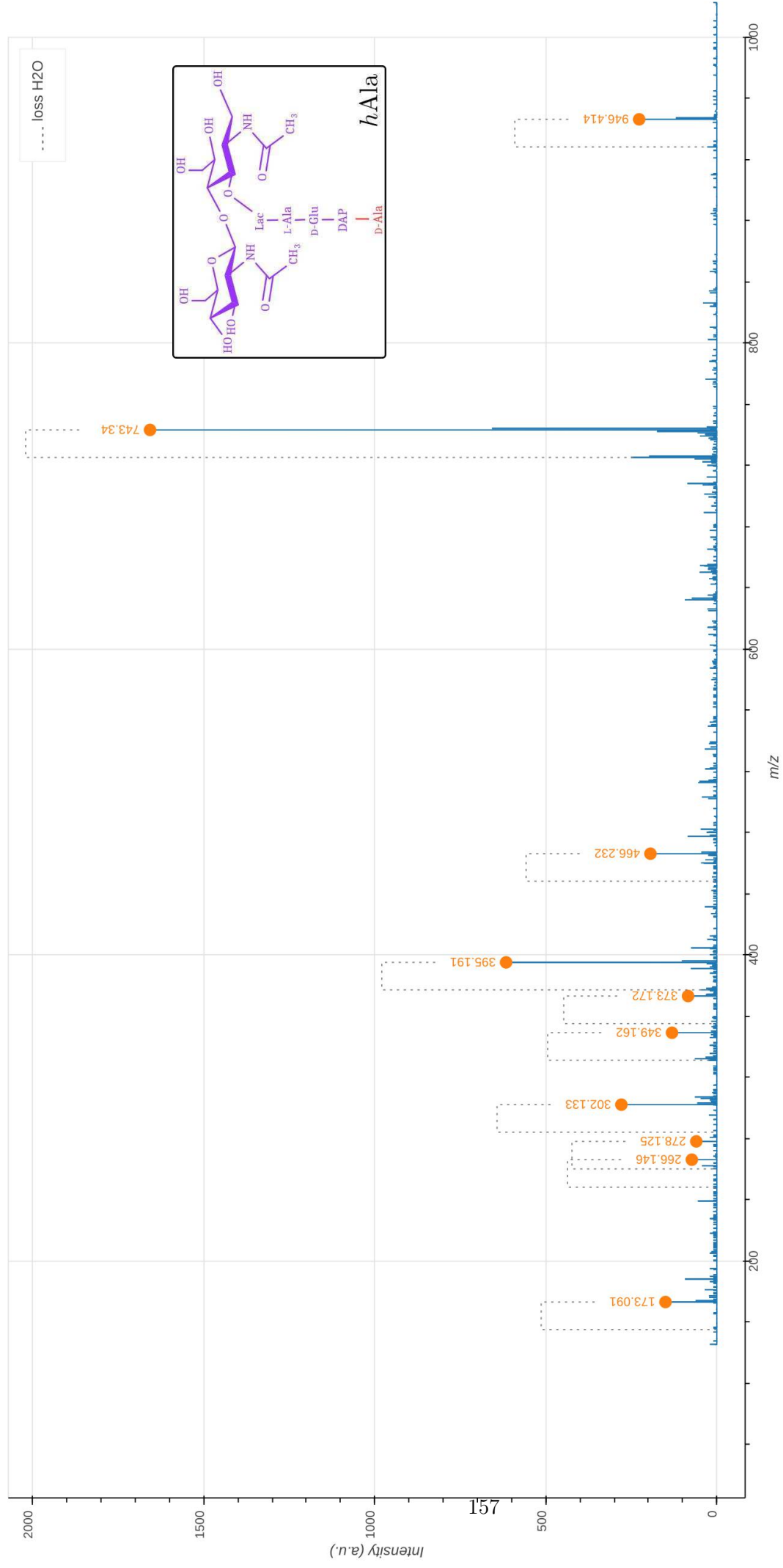
Precursor ion (MS1)	m/z_{obs}	m/z_{calc}	ppm		
$\text{GlcN}(-\text{Ac})-\text{GlcN}^{\text{Red}}(-\text{Ac})-\text{Lac-Ala-Glu-DAP-Ala}$	977.490	977.49	-5.0		
Product ion	m/z_{obs}	m/z_{calc}	ppm	Intensity (a.u.)	Isotopologue
$\text{GlcN}^{\text{Red}}(-\text{Ac})-\text{Lac-Ala-Glu-DAP-Ala}$	774.413	774.416	3.0	3734	h3
$\text{GlcN}^{\text{Red}}(-\text{Ac})-\text{Lac-Ala-Glu-DAP}$	681.368	681.361	-9.8	306	h3
$\text{GlcN}^{\text{Red}}(-\text{Ac})-\text{Lac-Ala-Glu}$	500.260	500.259	-2.0	259	h3
Ala-Glu-DAP-Ala	485.265	485.266	1.6	834	h3
Glu-DAP-Ala	410.220	410.221	3.9	2916	h3
Ala-Glu-DAP	392.208	392.211	6.4	1481	h3
$\text{GlcN}^{\text{Red}}(-\text{Ac})-\text{Lac-Ala}$	365.199	365.202	7.3	1567	h3
Glu-DAP	317.165	317.167	3.4	3046	h3
$\text{GlcN}^{\text{Red}}(-\text{Ac})-\text{Lac}$	290.156	290.158	7.5	508	h3
DAP-Ala	275.163	275.165	6.7	2174	h3
DAP	182.110	182.110	0.1	354	h3



Additional Monomer hybrids

Supplementary Data 2.5: Tandem mass spectrometry analysis of the hAla-type hybrid of the disaccharide-tetrapeptide. The observed m/z_{obs} and calculated m/z_{cal} values of the parental ion, $[M+H]^+$, as determined in the absence of fragmentation (MS1), are indicated. The m/z_{cal} value was used to select the ion for fragmentation. The difference between the m/z_{obs} and m/z_{cal} values is indicated in ppm. The GlcNAc residue is indicated in two moieties, glucosamine (GlcN) and the acetyl group (Ac), since these moieties are potentially differentially labeled. For the same reason, the reduced (Red) MurNAc residue is indicated in three moieties, reduced glucosamine (GlcN^{Red}), the acetyl group (Ac), and the D-lactoyl group. Labeled and unlabeled moieties are represented in red and purple, respectively. The peaks corresponding to the list of fragments appearing in the table are highlighted by orange dots in the mass spectrum. In the mass spectrum, peaks differing by the loss of H_2O are connected by a dashed line. The tables only contain the m/z values for the fragments containing H_2O . An interactive report of the MS2 analysis is available in Supplementary File F2.5.

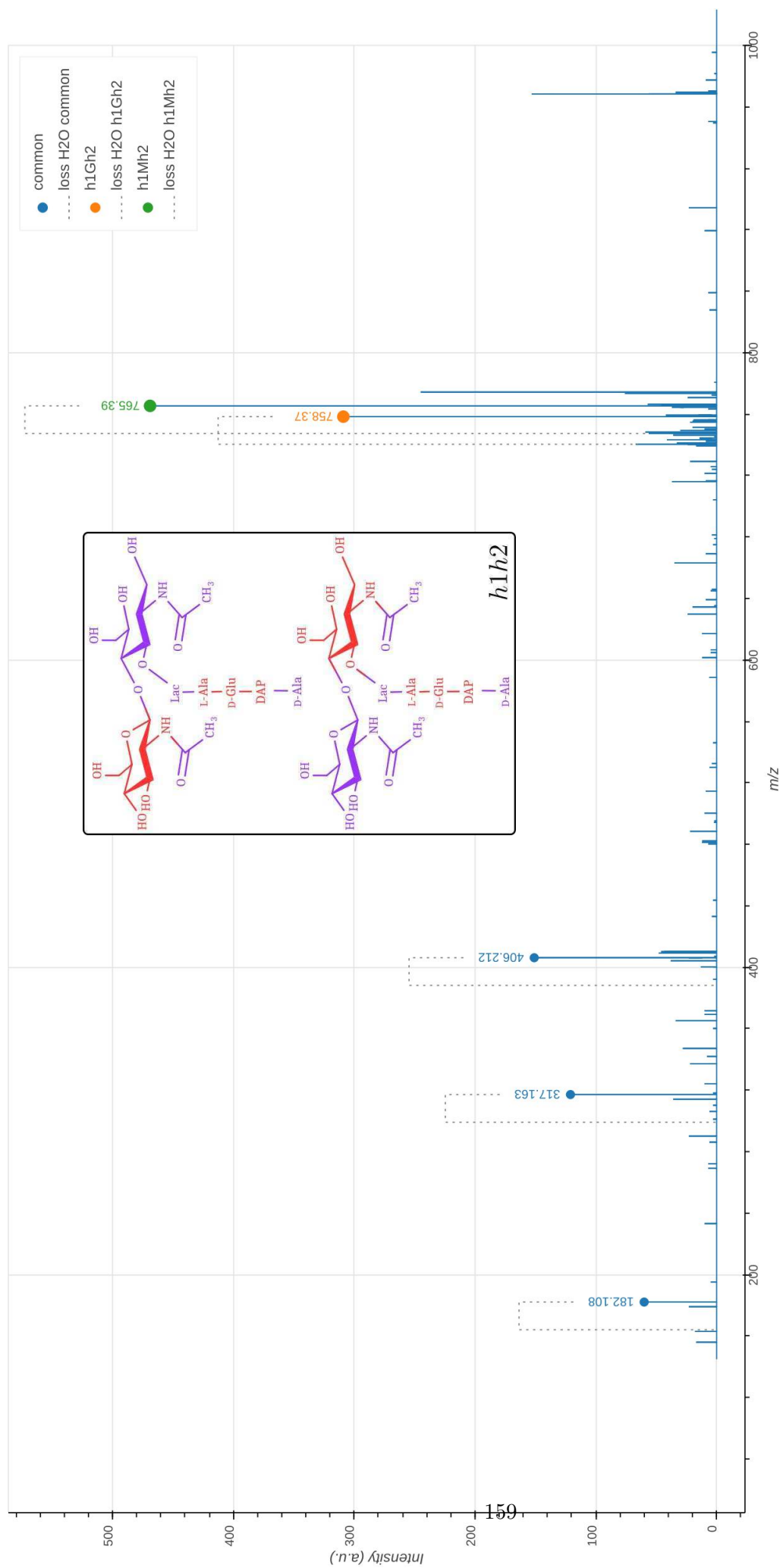
Parent (MS1)	m/z_{obs}	m/z_{calc}	ppm		
$\text{GlcN}(-\text{Ac})-\text{GlcN}^{\text{Red}}(-\text{Ac})-\text{Lac-Ala-Glu-DAP-Ala}$	946.420	946.423	-2.9		
Fragment	m/z_{obs}	m/z_{calc}	ppm	Intensity (a.u.)	Isotopologue
$\text{GlcN}(-\text{Ac})-\text{GlcN}^{\text{Red}}(-\text{Ac})-\text{Lac-Ala-Glu-DAP-Ala}$	946.414	946.423	8.8	227	hAla4
$\text{GlcN}^{\text{Red}}(-\text{Ac})-\text{Lac-Ala-Glu-DAP-Ala}$	743.340	743.343	4.3	1657	hAla4
Ala-Glu-DAP-Ala	466.232	466.227	-9.5	194	hAla4
Glu-DAP-Ala	395.191	395.190	-3.2	616	hAla4
Ala-Glu-DAP	373.172	373.172	0.3	84	hAla4
$\text{GlcN}^{\text{Red}}(-\text{Ac})-\text{Lac-Ala}$	349.162	349.161	-2.2	131	hAla4
Glu-DAP	302.133	302.135	7.2	279	hAla4
$\text{GlcN}^{\text{Red}}(-\text{Ac})-\text{Lac}$	278.125	278.124	-2.5	60	hAla4
DAP-Ala	266.146	266.147	4.3	73	hAla4
DAP	173.091	173.093	10.9	150	hAla4



Supplementary Data 2.6: Tandem mass spectrometry analysis of the h1h2-type hybrid of the disaccharide-tetrapeptide. The molecule is fully unlabeled except for one of the two glucosamine moieties present in GlcNAc or MurNAc leading to the presence of two isotopomers.

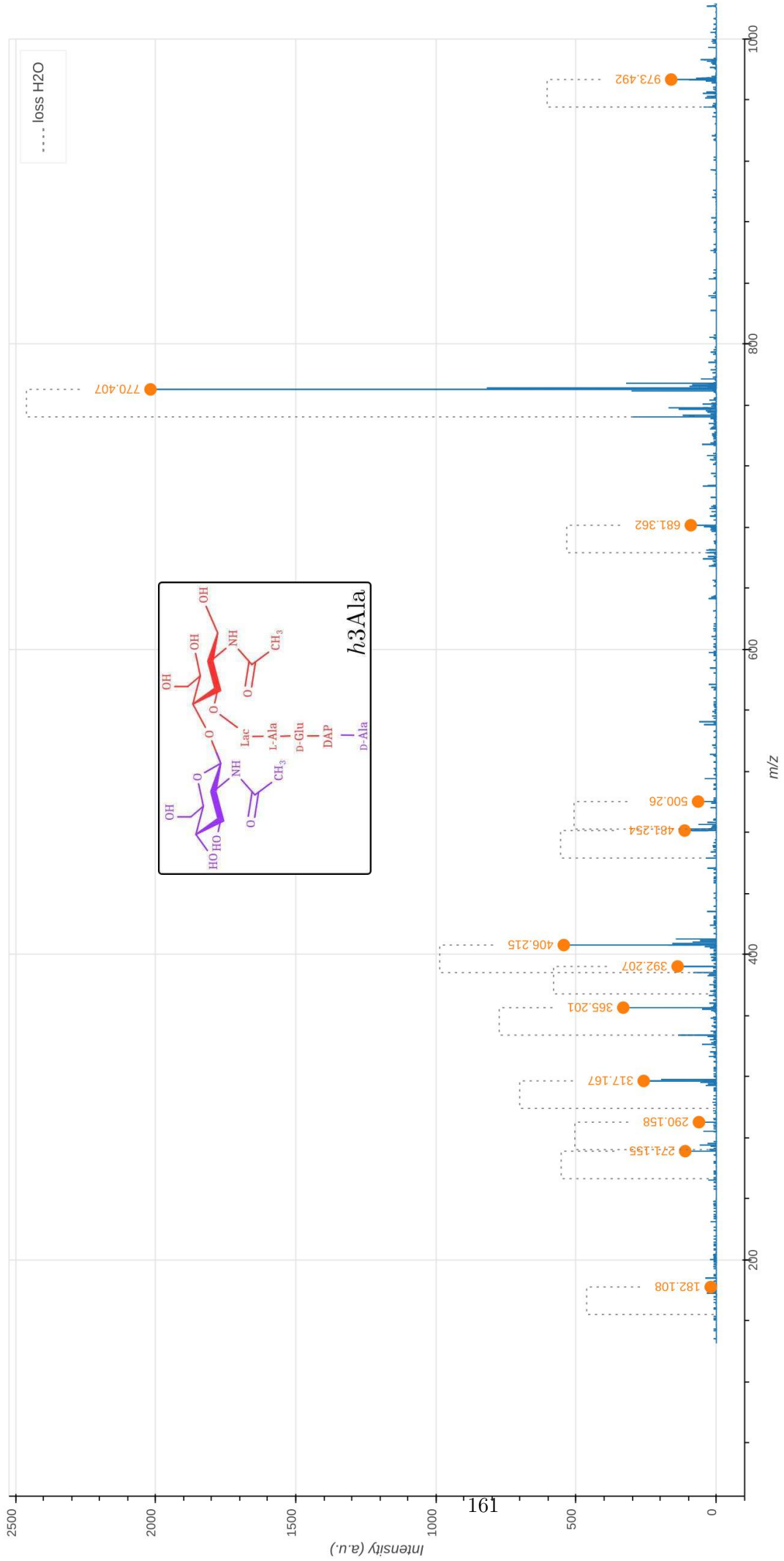
The observed m/z_{obs} and calculated m/z_{calc} values of the parental ion, $[M+H]^+$, as determined in the absence of fragmentation (MS^1), are indicated. The m/z_{cal} value was used to select the ion for fragmentation. The difference between the m/z_{obs} and m/z_{cal} values is indicated in ppm. The GlcNAc residue is indicated in two moieties, glucosamine (GlcN) and the acetyl group (Ac), since these moieties are potentially differentially labeled. For the same reason, the reduced (Red) MurNAc residue is indicated in three moieties, reduced glucosamine (GlcN^{Red}), the acetyl group (Ac), and the D-lactoyl group. Labeled and unlabeled moieties are represented in red and purple, respectively. The fragmentation led to two series of fragments specific of the isotopomers containing the unlabeled glucosamine moiety in the GlcNAc (h1Gh2) or MurNAc^{Red} (h1Mh2) residues, respectively (discriminatory fragments). The fragments specific of h1Gh2 and of h1Mh2 are highlighted by orange and green dots in the mass spectrum. The other fragments are common to the fragmentation patterns of h1Gh2 and of h1Mh2. The corresponding peaks are highlighted by blue dots in the mass spectrum. The mass spectrum indicates the presence of both isotopomers as expected from the recycling and synthesis pathways since UDP-MurNAc exclusively derives from UDP-GlcNAc. In the mass spectrum, peaks differing by the loss of H₂O are connected by a dashed line. The tables only contain the m/z values for the fragments containing H₂O. An interactive report of the MS2 analysis is available in Supplementary File F2.6.

Precursor ion (MS^1)	m/z_{obs}	m/z_{calc}	ppm		
GlcN(-Ac)-GlcN ^{Red} (-Ac)-Lac-Ala-Glu-DAP-Ala	968.471	968.471	0.2		
GlcN(-Ac)-GlcN ^{Red} (-Ac)-Lac-Ala-Glu-DAP-Ala	968.471	968.471	0.2		
Discriminatory product ions	m/z_{obs}	m/z_{calc}	ppm	Intensity (a.u.)	Isotopologue
GlcN ^{Red} (-Ac)-Lac-Ala-Glu-DAP-Ala	765.390	765.392	2.2	469	h1Mh2
GlcN ^{Red} (-Ac)-Lac-Ala-Glu-DAP-Ala	758.370	758.375	6.2	309	h1Gh2
Common product ions	m/z_{obs}	m/z_{calc}	ppm	Intensity (a.u.)	
Glu-DAP-Ala	406.212	406.214	5.8	151	
Glu-DAP	317.163	317.167	12.6	121	
DAP	182.108	182.110	11.6	60	

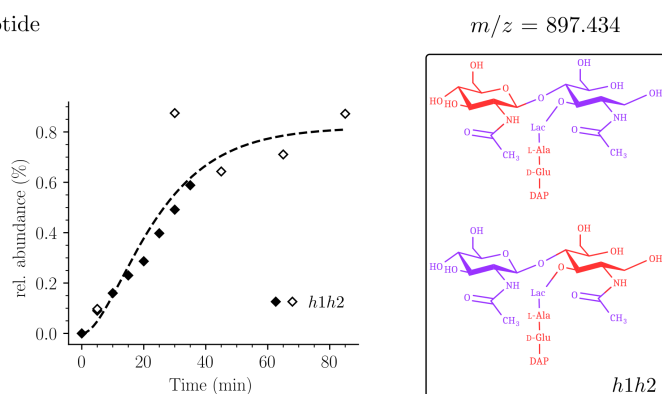


Supplementary Data 2.7: Tandem mass spectrometry analysis of the h3Ala-type hybrid of the disaccharide-tetrapeptide. The observed m/z_{obs} and calculated m/z_{calc} values of the parental ion, $[M+H]^+$, as determined in the absence of fragmentation (MS1), are indicated. The m/z_{calc} value was used to select the ion for fragmentation. The difference between the m/z_{obs} and m/z_{calc} values is indicated in ppm. The GlcNAc residue is indicated in two moieties, glucosamine (GlcN) and the acetyl group (Ac), since these moieties are potentially differentially labeled. For the same reason, the reduced (Red) MurNAc residue is indicated in three moieties, reduced glucosamine (GlcN^{Red}), the acetyl group (Ac), and the D-lactoyl group. Labeled and unlabeled moieties are represented in red and purple, respectively. The peaks corresponding to the list of fragments appearing in the table are highlighted by orange dots in the mass spectrum. In the mass spectrum, peaks differing by the loss of H_2O are connected by a dashed line. The tables only contain the m/z values for the fragments containing H_2O . An interactive report of the MS2 analysis is available in Supplementary File F2.7.

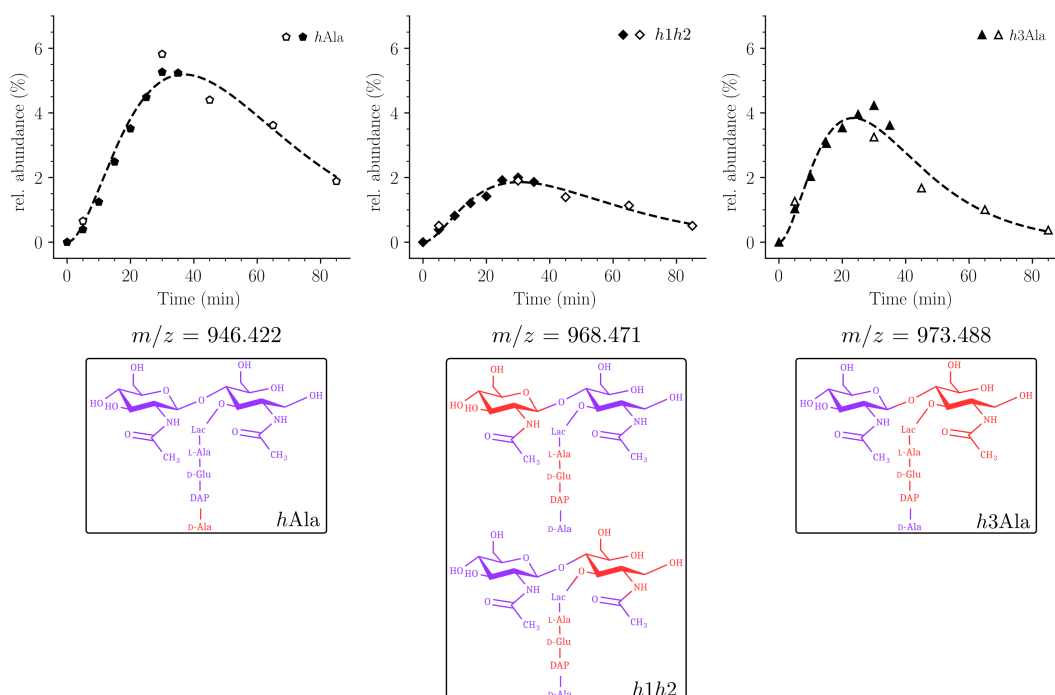
Precursor Ion (MS1)	m/z_{obs}	m/z_{calc}	ppm	
GlcN(-Ac)-GlcN^{Red}(-Ac)-Lac-Ala-Glu-DAP-Ala	973.484	973.488	-3.9	
Product ion	m/z_{obs}	m/z_{calc}	ppm	Intensity (a.u.)
GlcN(-Ac)-GlcN^{Red}(-Ac)-Lac-Ala-Glu-DAP-Ala	973.492	973.488	-3.7	161
GlcN^{Red}(-Ac)-Lac-Ala-Glu-DAP-Ala	770.407	770.409	2.1	2018
GlcN^{Red}(-Ac)-Lac-Ala-Glu-DAP	681.362	681.361	-1.4	91
GlcN^{Red}(-Ac)-Lac-Ala-Glu	500.260	500.259	-3.4	65
Ala-Glu-DAP-Ala	481.254	481.258	9.6	113
Glu-DAP-Ala	406.215	406.214	-2.1	544
Ala-Glu-DAP	392.207	392.211	10.6	138
GlcN^{Red}(-Ac)-Lac-Ala	365.201	365.202	2.0	332
Glu-DAP	317.167	317.167	-1.6	259
GlcN^{Red}(-Ac)-Lac	290.158	290.158	-0.3	62
DAP-Ala	271.155	271.158	11.1	111
DAP	182.108	182.110	12.8	20



A - GM-Tripeptide



B - GM-Tetrapeptide



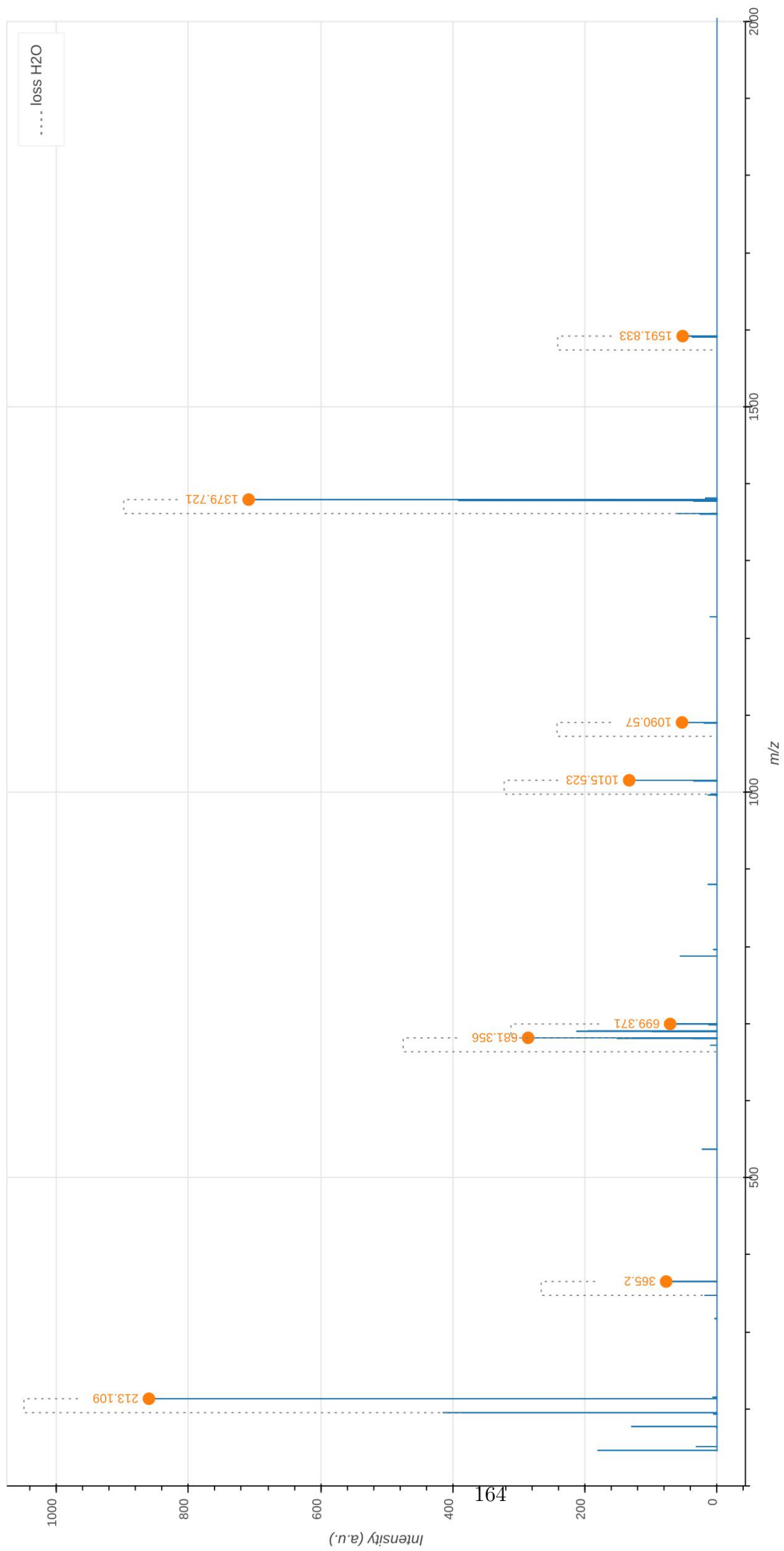
Supplementary Data 2.8: Timecourses and structures of additional monomer hybrids. (A) Structure and timecourse of the *h1h2* hybrid of the disaccharide tripeptide monomer combining a recycled tripeptide stem (*h2*) with a recycled glucosamine moiety (*h1*). (B) Additional hybrids of the disaccharide tetrapeptide comprise *hAla* (labeled C-terminal D-Ala⁴), *h1h2* (see (A)) and *h3Ala* (neo-synthesized GlcNAc and C-terminal D-Ala⁴). Since disaccharide tripeptides are issued from disaccharide tetrapeptides by removal of the C-terminal D-Ala⁴, *hAla* and *h3Ala* are not detected for the tripeptide as these are converted into the uniformly unlabeled and *h3* hybrid of the tripeptide, respectively. For structural characterization of the *hAla*, *h1h2*, and *h3Ala* hybrids see Supplementary Data above.

Dimers

Tri-Tri

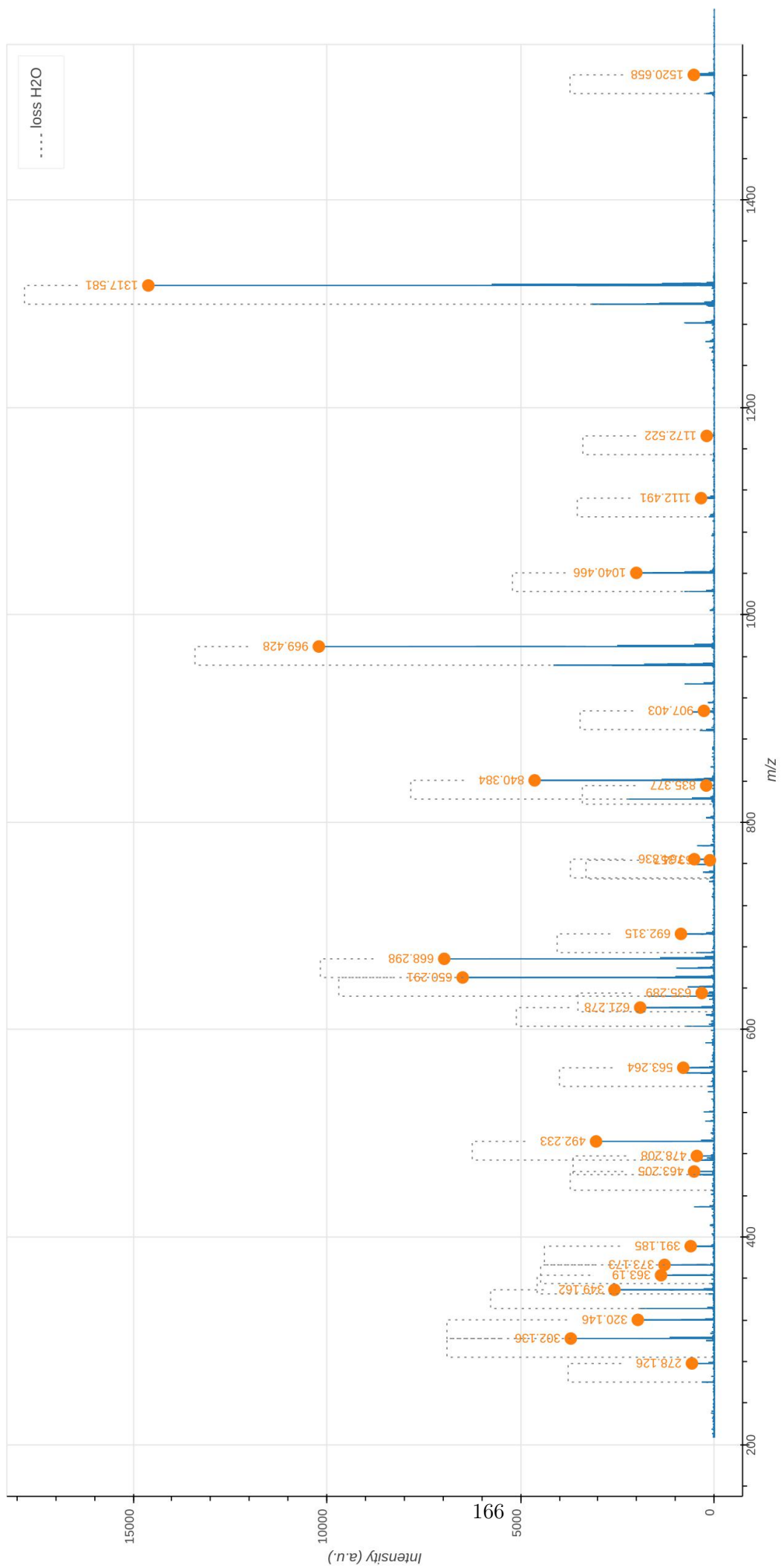
Supplementary Data 3.1: Tandem mass spectrometry analysis of the uniformly labeled Tri(3→3)Tri dimer. The observed m/z_{obs} and calculated m/z_{cal} values of the parental ion, $[M+2H]^{2+}$, as determined in the absence of fragmentation (MS1), are indicated. The m/z_{calc} value was used to select the ion for fragmentation. The difference between the m/z_{obs} and m/z_{calc} values is indicated in ppm. The GlcNAc residue is indicated in two moieties, glucosamine (GlcN) and the acetyl group (Ac), since these moieties are potentially differentially labeled. For the same reason, the reduced (Red) MurNAc residue is indicated in three moieties, reduced glucosamine (GlcN^{Red}), the acetyl group (Ac), and the D-lactoyl group. Labeled and unlabeled moieties are represented in red and purple, respectively. The peaks corresponding to the list of fragments appearing in the table are highlighted by orange dots in the mass spectrum. In the mass spectrum, peaks differing by the loss of H_2O are connected by a dashed line. The tables only contain the m/z values for the fragments containing H_2O . The arrows indicate the position of the 3→3 and 4→3 crosslinks. Residues in the acceptor are underlined. An interactive report of the MS2 analysis is available in Supplementary File F3.1.

Precursor ion (MS1)	$m/z_{\text{obs}} [M+2H]^{2+}$	$m/z_{\text{calc}} [M+2H]^{2+}$	ppm	
$\text{GlcN}(-\text{Ac})-\text{GlcN}^{\text{Red}}(-\text{Ac})-\text{Lac-Ala-Glu-DAP} \rightarrow \text{DAP-Glu-Ala-Lac-GlcN}^{\text{Red}}(-\text{Ac})-\text{GlcN}(-\text{Ac})$	902.464	902.469	-5.9	
Product ion	$m/z_{\text{obs}} [M+H]^{1+}$	$m/z_{\text{calc}} [M+H]^{1+}$	ppm	Intensity (a.u.)
$\text{GlcN}(-\text{Ac})-\text{GlcN}^{\text{Red}}(-\text{Ac})-\text{Lac-Ala-Glu-DAP} \rightarrow \text{DAP-Glu-Ala-Lac-GlcN}^{\text{Red}}(-\text{Ac})$	1591.833	1591.828	-3.4	52
$\text{GlcN}^{\text{Red}}(-\text{Ac})-\text{Lac-Ala-Glu-DAP} \rightarrow \text{DAP-Glu-Ala-Lac-GlcN}^{\text{Red}}(-\text{Ac})$	1379.721	1379.724	2.3	709
$\text{GlcN}^{\text{Red}}(-\text{Ac})-\text{Lac-Ala-Glu-DAP} \rightarrow \text{DAP-Glu-Ala}$	1090.570	1090.574	3.7	53
$\text{GlcN}^{\text{Red}}(-\text{Ac})-\text{Lac-Ala-Glu-DAP} \rightarrow \text{DAP-Glu}$	1015.523	1015.530	7.4	133
$\text{DAP-Glu-Ala-Lac-GlcN}^{\text{Red}}(-\text{Ac})$	699.371	699.371	1.1	71
$\text{GlcN}^{\text{Red}}(-\text{Ac})-\text{Lac-Ala-Glu-DAP}$	681.356	681.361	6.9	286
$\text{GlcN}^{\text{Red}}(-\text{Ac})-\text{Lac-Ala}$	365.200	365.202	5.6	77
$\text{GlcN}(-\text{Ac})$	213.109	213.111	7.8	860



Supplementary Data 3.2: Tandem mass spectrometry analysis of the uniformly unlabeled Tri(3→3)Tri dimer. The observed m/z_{obs} and calculated m/z_{calc} values of the parental ion, $[M+2H]^{2+}$, as determined in the absence of fragmentation (MS1), are indicated. The m/z_{calc} value was used to select the ion for fragmentation. The difference between the m/z_{obs} and m/z_{calc} values is indicated in ppm. The GlcNAc residue is indicated in two moieties, glucosamine (GlcN) and the acetyl group (Ac), since these moieties are potentially differentially labeled. For the same reason, the reduced (Red) MurNAc residue is indicated in three moieties, reduced glucosamine (GlcN^{Red}), the acetyl group (Ac), and the D-lactoyl group. Labeled and unlabeled moieties are represented in red and purple, respectively. The peaks corresponding to the list of fragments appearing in the table are highlighted by orange dots in the mass spectrum. In the mass spectrum, peaks differing by the loss of H₂O are connected by a dashed line. The tables only contain the m/z values for the fragments containing H₂O. The arrows indicate the position of the 3→3 and 4→3 crosslinks. Residues in the acceptor are underlined. An interactive report of the MS2 analysis is available in Supplementary File F3.2.

Precursor ion (MS1)	m/z_{obs} $[M+2H]^{2+}$	m/z_{calc} $[M+2H]^{2+}$	ppm	
GlcN(-Ac)-GlcN ^{Red} (-Ac)-Lac-Ala-Glu-DAP→DAP-Glu-Ala-Lac-GlcN ^{Red} (-Ac)-GlcN(-Ac)	862.373	862.373	0.0	
Product ion	m/z_{obs} $[M+H]^{1+}$	m/z_{calc} $[M+H]^{1+}$	ppm	Intensity (a.u.)
GlcN(-Ac)-GlcN ^{Red} (-Ac)-Lac-Ala-Glu-DAP→DAP-Glu-Ala-Lac-GlcN ^{Red} (-Ac)	1520.658	1520.659	0.9	528
GlcN ^{Red} (-Ac)-Lac-Ala-Glu-DAP→DAP-Glu-Ala-Lac-GlcN ^{Red} (-Ac)	1317.581	1317.580	-1.3	14608
GlcN(-Ac)-GlcN ^{Red} (-Ac)-Lac-Ala-Glu-DAP→DAP-Glu	1172.522	1172.506	-13.7	195
GlcN ^{Red} (-Ac)-Lac-Ala-Glu-DAP→DAP-Glu-Ala-Lac	1112.491	1112.485	-5.3	340
GlcN ^{Red} (-Ac)-Lac-Ala-Glu-DAP→DAP-Glu-Ala	1040.466	1040.464	-2.0	2012
GlcN ^{Red} (-Ac)-Lac-Ala-Glu-DAP→DAP-Glu	969.428	969.426	-1.3	10207
Lac-Ala-Glu-DAP→DAP-Glu-Ala-Lac	907.403	907.390	-14.5	267
GlcN ^{Red} (-Ac)-Lac-Ala-Glu-DAP→DAP	840.384	840.384	-0.5	4637
Lac-Ala-Glu-DAP→DAP-Glu-Ala	835.377	835.369	-10.5	208
Lac-Ala-Glu-DAP→DAP-Glu	764.336	764.331	-5.8	517
Ala-Glu-DAP→DAP-Glu-Ala	763.357	763.347	-12.3	114
Ala-Glu-DAP→DAP-Glu	692.315	692.310	-6.1	860
DAP-Glu-Ala-Lac-GlcN ^{Red} (-Ac)	668.298	668.299	1.6	6970
GlcN ^{Red} (-Ac)-Lac-Ala-Glu-DAP	650.291	650.288	-4.1	6495
Lac-Ala-Glu-DAP→DAP	635.289	635.289	-0.5	324
Glu-DAP→DAP-Glu	621.278	621.273	-7.6	1912
Ala-Glu-DAP→DAP	563.264	563.268	5.8	800
Glu-DAP→DAP	492.233	492.231	-4.0	3051
GlcN ^{Red} (-Ac)-Lac-Ala-Glu	478.208	478.204	-9.4	449
DAP-Glu-Ala-Lac	463.205	463.204	-2.7	521
DAP-Glu-Ala	391.185	391.183	-5.5	608
Ala-Glu-DAP	373.173	373.172	-0.8	1284
DAP→DAP	363.190	363.188	-4.9	1374
GlcN ^{Red} (-Ac)-Lac-Ala	349.162	349.161	-1.6	2576
DAP-Glu	320.146	320.146	-0.4	1973
Glu-DAP	302.136	302.135	-1.6	3703
GlcN ^{Red} (-Ac)-Lac	278.126	278.124	-6.0	576

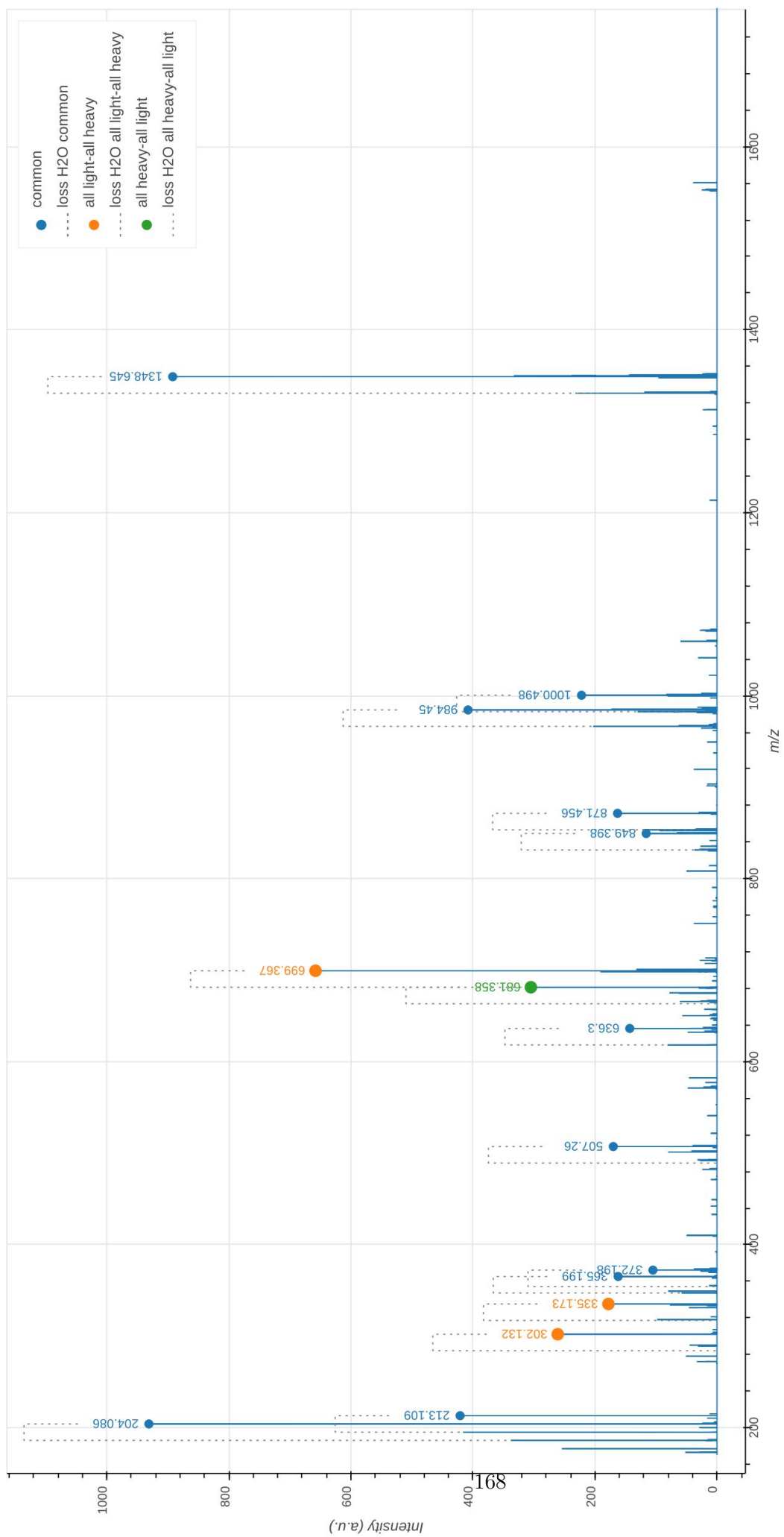


Supplementary Data 3.3: Tandem mass spectrometry analysis of the Tri→Tri dimer containing a uniformly labeled disaccharide-tripeptide cross-linked to a uniformly unlabeled disaccharide-tripeptide (3→3 cross-link). The observed m/z_{obs} and calculated m/z_{calc} values of the parental ion, $[M+2H]^{2+}$, as determined in the absence of fragmentation (MS1), are indicated. The m/z_{calc} value was used to select the ion for fragmentation. The difference between the m/z_{obs} and m/z_{calc} values is indicated in ppm. The GlcNAc residue is indicated in two moieties, glucosamine (GlcN) and the acetyl group (Ac), since these moieties are potentially differentially labeled. For the same reason, the reduced (Red) MurNAc residue is indicated in three moieties, reduced glucosamine (GlcN^{Red}), the acetyl group (Ac), and the D-lactoyl group. Labeled and unlabeled moieties are represented in red and purple, respectively. The fragmentation potentially leads to two series of fragments (discriminatory fragments) specific of the isotopomers containing the fully labeled disaccharide subunit in the donor (all heavy-all light) or acceptor position (all light-all heavy). These fragments are highlighted by green and orange dots in the mass spectrum, respectively. The other fragments are common to the fragmentation of the two isotopomers (highlighted by blue dots in the mass spectrum). The mass spectrum indicates the presence of the all light-all heavy isotopomers (orange dots). The peak at m/z_{obs} 681.358 (green dot) can also be accounted for by the loss of H₂O from the peak at 699.367 indicating that all peaks may be accounted for by the presence of the all light-all heavy isotopomer.

In the mass spectrum, peaks differing by the loss of H₂O are connected by a dashed line. The arrows indicate the position of the 3→3 and 4→3 crosslinks. Residues in the acceptor are underlined.

An interactive report of the MS2 analysis is available in Supplementary File F3.3.

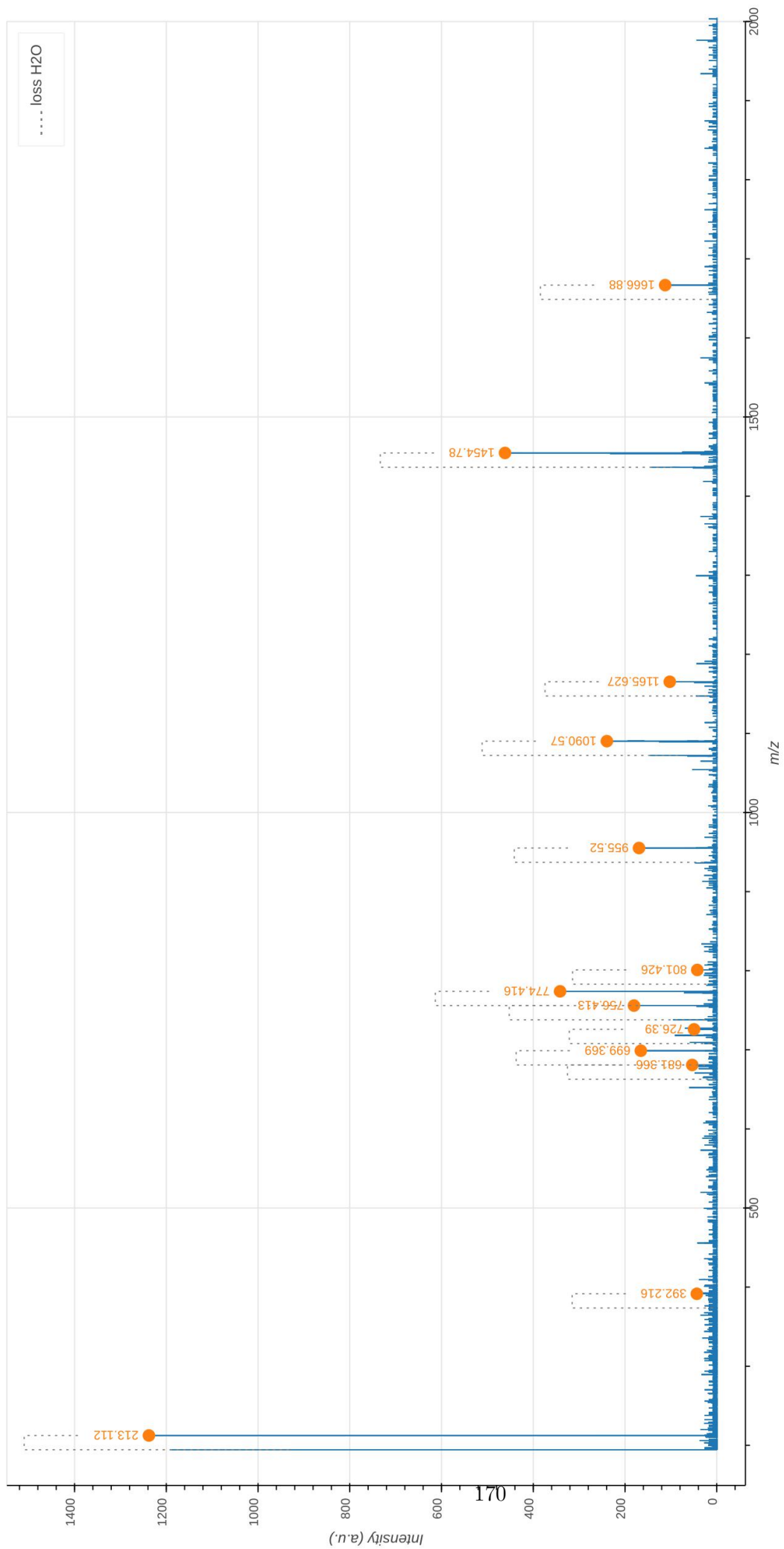
Precursor ion (MS1)	m/z_{obs} [M+2H] ²⁺	m/z_{calc} [M+2H] ²⁺	ppm		
GlcN(-Ac)-GlcN ^{Red} (-Ac)-Lac-Ala-Glu-DAP→DAP-Glu-Ala-Lac-GlcN ^{Red} (-Ac)-GlcN(-Ac)	882.421	882.421	-0.0		
GlcN(-Ac)-GlcN ^{Red} (-Ac)-Lac-Ala-Glu-DAP→DAP-Glu-Ala-Lac-GlcN ^{Red} (-Ac)-GlcN(-Ac)	882.421	882.421	-0.0		
Discriminatory product ions	m/z_{obs} [M+H] ¹⁺	m/z_{calc} [M+H] ¹⁺	ppm	Intensity (a.u.)	Isotopologue
DAP-Glu-Ala-Lac-GlcN ^{Red} (-Ac)	699.367	699.371	6.5	678	all light-all heavy
GlcN ^{Red} (-Ac)-Lac-Ala-Glu-DAP	681.358	681.361	4.8	325	all heavy-all light
DAP-Glu	335.173	335.177	13.8	198	all light-all heavy
Glu-DAP	302.132	302.135	11.5	281	all light-all heavy
Common product ions	m/z_{obs} [M+H] ¹⁺	m/z_{calc} [M+H] ¹⁺	ppm	Intensity (a.u.)	
GlcN ^{Red} (-Ac)-Lac-Ala-Glu-DAP→DAP-Glu-Ala-Lac-GlcN ^{Red} (-Ac)	1348.645	1348.652	5.6	912	
GlcN ^{Red} (-Ac)-Lac-Ala-Glu-DAP→DAP-Glu-Ala-Lac-GlcN ^{Red} (-Ac)					
GlcN ^{Red} (-Ac)-Lac-Ala-Glu-DAP→DAP-Glu	1000.498	1000.499	0.6	242	
Glu-DAP→DAP-Glu-Ala-Lac-GlcN ^{Red} (-Ac)					
GlcN ^{Red} (-Ac)-Lac-Ala-Glu-DAP→DAP-Glu	984.450	984.458	7.6	428	
Glu-DAP→DAP-Glu-Ala-Lac-GlcN ^{Red} (-Ac)					
GlcN ^{Red} (-Ac)-Lac-Ala-Glu-DAP→DAP	871.456	871.456	0.5	183	
DAP→DAP-Glu-Ala-Lac-GlcN ^{Red} (-Ac)					
DAP→DAP-Glu-Ala-Lac-GlcN ^{Red} (-Ac)	849.398	849.401	3.8	136	
GlcN ^{Red} (-Ac)-Lac-Ala-Glu-DAP→DAP					
Glu-DAP→DAP-Glu	636.300	636.305	7.0	163	
Glu-DAP→DAP-Glu					
DAP→DAP-Glu	507.260	507.262	3.0	190	
Glu-DAP→DAP					
DAP→DAP	372.198	372.206	19.4	125	
DAP→DAP					
GlcN ^{Red} (-Ac)-Lac-Ala	365.199	365.202	9.2	182	
Ala-Lac-GlcN ^{Red} (-Ac)					
GlcN(-Ac)	213.109	213.111	9.2	441	
GlcN(-Ac)					
GlcN(-Ac)	204.086	204.087	5.9	951	
GlcN(-Ac)					



Tetra-Tri

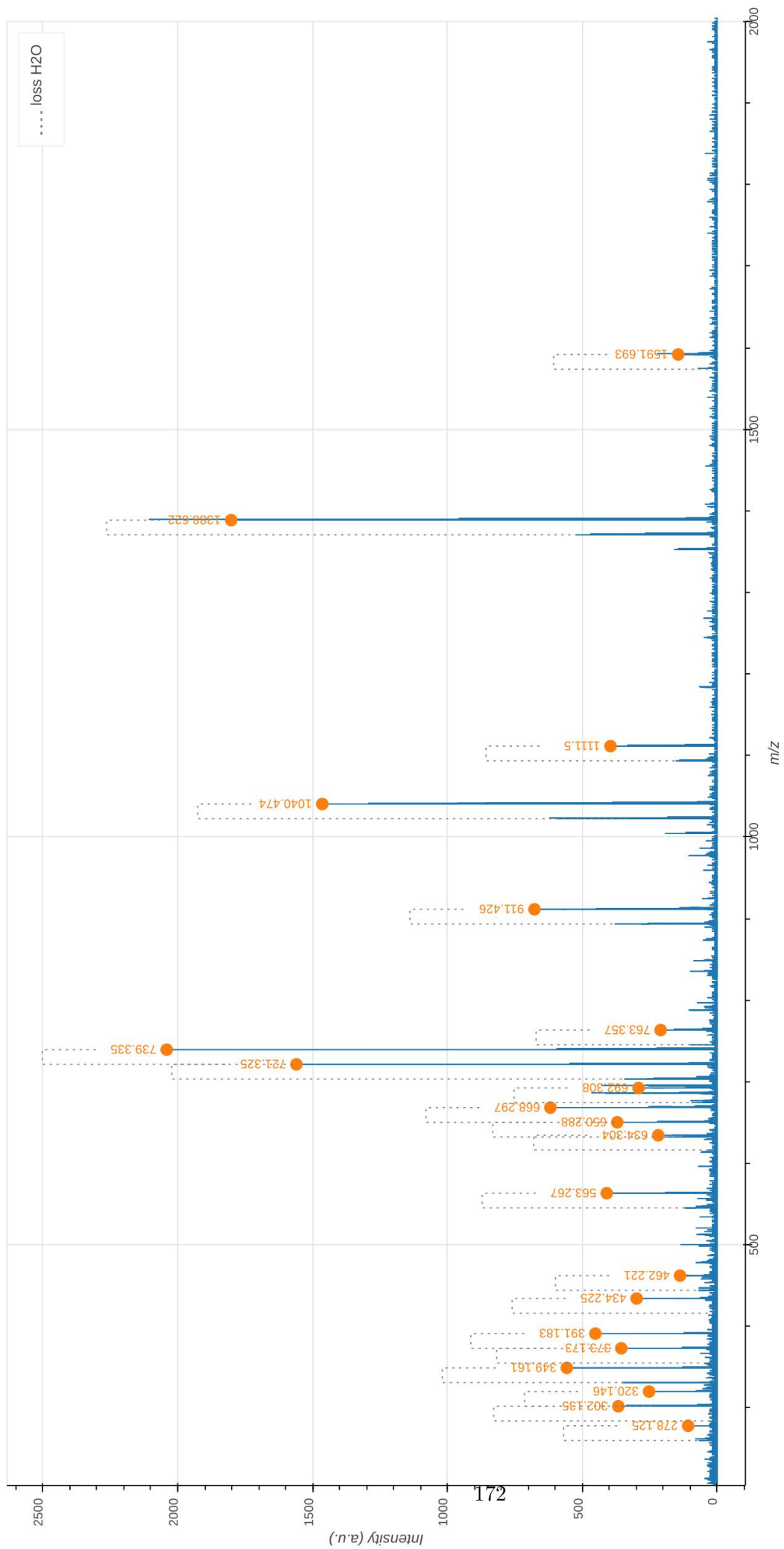
Supplementary Data 4.1: Tandem mass spectrometry analysis of the uniformly labeled Tetra(4→3)Tri dimer. The observed m/z_{obs} and calculated m/z_{cal} values of the parental ion, $[M+2H]^{2+}$, as determined in the absence of fragmentation (MS1), are indicated. The m/z_{cal} value was used to select the ion for fragmentation. The difference between the m/z_{obs} and m/z_{cal} values is indicated in ppm. The GlcNAc residue is indicated in two moieties, glucosamine (GlcN) and the acetyl group (Ac), since these moieties are potentially differentially labeled. For the same reason, the reduced (Red) MurNAc residue is indicated in three moieties, reduced glucosamine (GlcN^{Red}), the acetyl group (Ac), and the D-lactoyl group. Labeled and unlabeled moieties are represented in red and purple, respectively. The peaks corresponding to the list of fragments appearing in the table are highlighted by orange dots in the mass spectrum. In the mass spectrum, peaks differing by the loss of H₂O are connected by a dashed line. The tables only contain the m/z values for the fragments containing H₂O. The arrows indicate the position of the 3→3 and 4→3 crosslinks. Residues in the acceptor are underlined. An interactive report of the MS2 analysis is available in Supplementary File F4.1.

Precursor ion (MS1)	$m/z_{\text{obs}} [M+2H]^{2+}$	$m/z_{\text{calc}} [M+2H]^{2+}$	ppm	
GlcN(-Ac)-GlcN ^{Red} (-Ac)-Lac-Ala-Glu-DAP-Ala→ <u>DAP-Glu-Ala-Lac-GlcN^{Red}(-Ac)-GlcN(-Ac)</u>	939.992	939.992	0.1	
Product ion	$m/z_{\text{obs}} [M+H]^{1+}$	$m/z_{\text{calc}} [M+H]^{1+}$	ppm	Intensity (a.u.)
GlcN(-Ac)-GlcN ^{Red} (-Ac)-Lac-Ala-Glu-DAP-Ala→ <u>DAP-Glu-Ala-Lac-GlcN^{Red}(-Ac)</u>	1666.880	1666.872	-4.9	113
GlcN ^{Red} (-Ac)-Lac-Ala-Glu-DAP-Ala→ <u>DAP-Glu-Ala-Lac-GlcN^{Red}(-Ac)</u>	1454.780	1454.769	-7.6	462
GlcN ^{Red} (-Ac)-Lac-Ala-Glu-DAP-Ala→ <u>DAP-Glu-Ala</u>	1165.627	1165.619	-6.9	103
GlcN ^{Red} (-Ac)-Lac-Ala-Glu-DAP-Ala→ <u>DAP-Glu</u>	1090.570	1090.574	3.6	240
GlcN ^{Red} (-Ac)-Lac-Ala-Glu-DAP-Ala→ <u>DAP</u>	955.520	955.518	-2.5	170
Ala-Glu-DAP-Ala→ <u>DAP-Glu</u>	801.426	801.424	-2.3	43
Ala→ <u>DAP-Glu-Ala-Lac-GlcN^{Red}(-Ac)</u>	774.416	774.416	-0.7	342
GlcN ^{Red} (-Ac)-Lac-Ala-Glu-DAP-Ala	756.413	756.405	-11.1	181
Glu-DAP-Ala→ <u>DAP-Glu</u>	726.390	726.380	-13.5	50
<u>DAP-Glu-Ala-Lac-GlcN^{Red}(-Ac)</u>	699.369	699.371	2.9	166
GlcN ^{Red} (-Ac)-Lac-Ala-Glu-DAP	681.366	681.361	-6.8	54
Ala-Glu-DAP	392.216	392.211	-12.7	44
GlcN(-Ac)	213.112	213.111	-5.5	1238



Supplementary Data 4.2: Tandem mass spectrometry analysis of the uniformly unlabeled Tri(4→3)Tri dimer. The observed m/z_{obs} and calculated m/z_{cal} values of the parental ion, $[M+2H]^{2+}$, as determined in the absence of fragmentation (MS1), are indicated. The m/z_{cal} value was used to select the ion for fragmentation. The difference between the m/z_{obs} and m/z_{cal} values is indicated in ppm. The GlcNAc residue is indicated in two moieties, glucosamine (GlcN) and the acetyl group (Ac), since these moieties are potentially differentially labeled. For the same reason, the reduced (Red) MurNAc residue is indicated in three moieties, reduced glucosamine (GlcN^{Red}), the acetyl group (Ac), and the D-lactoyl group. Labeled and unlabeled moieties are represented in red and purple, respectively. The peaks corresponding to the list of fragments appearing in the table are highlighted by orange dots in the mass spectrum. In the mass spectrum, peaks differing by the loss of H₂O are connected by a dashed line. The tables only contain the m/z values for the fragments containing H₂O. The arrows indicate the position of the 3→3 and 4→3 crosslinks. Residues in the acceptor are underlined. An interactive report of the MS2 analysis is available in Supplementary File F4.2.

Precursor ion (MS1)	$m/z_{\text{obs}} [M+2H]^{2+}$	$m/z_{\text{calc}} [M+2H]^{2+}$	ppm	
GlcN(-Ac)-GlcN ^{Red} (-Ac)-Lac-Ala-Glu-DAP-Ala→ <u>DAP-Glu-Ala-Lac-GlcN^{Red}(-Ac)-GlcN(-Ac)</u>	897.889	897.892	-3.3	
Product ion	$m/z_{\text{obs}} [M+H]^{1+}$	$m/z_{\text{calc}} [M+H]^{1+}$	ppm	Intensity (a.u.)
GlcN(-Ac)-GlcN ^{Red} (-Ac)-Lac-Ala-Glu-DAP-Ala→ <u>DAP-Glu-Ala-Lac-GlcN^{Red}(-Ac)</u>	1591.693	1591.696	1.9	144
GlcN ^{Red} (-Ac)-Lac-Ala-Glu-DAP-Ala→ <u>DAP-Glu-Ala-Lac-GlcN^{Red}(-Ac)</u>	1388.622	1388.617	-3.4	1802
GlcN ^{Red} (-Ac)-Lac-Ala-Glu-DAP-Ala→ <u>DAP-Glu-Ala</u>	1111.500	1111.501	0.4	395
GlcN ^{Red} (-Ac)-Lac-Ala-Glu-DAP-Ala→ <u>DAP-Glu</u>	1040.474	1040.464	-10.3	1464
GlcN ^{Red} (-Ac)-Lac-Ala-Glu-DAP-Ala→ <u>DAP</u>	911.426	911.421	-5.8	677
Ala-Glu-DAP-Ala→ <u>DAP-Glu</u>	763.357	763.347	-13.1	209
Ala→ <u>DAP-Glu-Ala-Lac-GlcN^{Red}(-Ac)</u>	739.335	739.336	0.9	2041
GlcN ^{Red} (-Ac)-Lac-Ala-Glu-DAP-Ala	721.325	721.326	0.5	1560
Glu-DAP-Ala→ <u>DAP-Glu</u>	692.308	692.310	3.2	291
<u>DAP-Glu-Ala-Lac-GlcN^{Red}(-Ac)</u>	668.297	668.299	2.4	618
GlcN ^{Red} (-Ac)-Lac-Ala-Glu-DAP	650.288	650.288	1.3	370
Ala-Glu-DAP-Ala→ <u>DAP</u>	634.304	634.305	1.7	218
Glu-DAP-Ala→ <u>DAP</u>	563.267	563.268	1.2	409
Ala→ <u>DAP-Glu-Ala</u>	462.221	462.220	-1.1	137
DAP-Ala→ <u>DAP</u>	434.225	434.225	-0.2	298
Ala→ <u>DAP-Glu</u>	391.183	391.183	0.3	451
Ala-Glu-DAP	373.173	373.172	-2.5	355
GlcN ^{Red} (-Ac)-Lac-Ala	349.161	349.161	-1.1	557
<u>DAP-Glu</u>	320.146	320.146	-1.6	252
Glu-DAP	302.135	302.135	-0.7	366
GlcN ^{Red} (-Ac)-Lac	278.125	278.124	-5.0	107

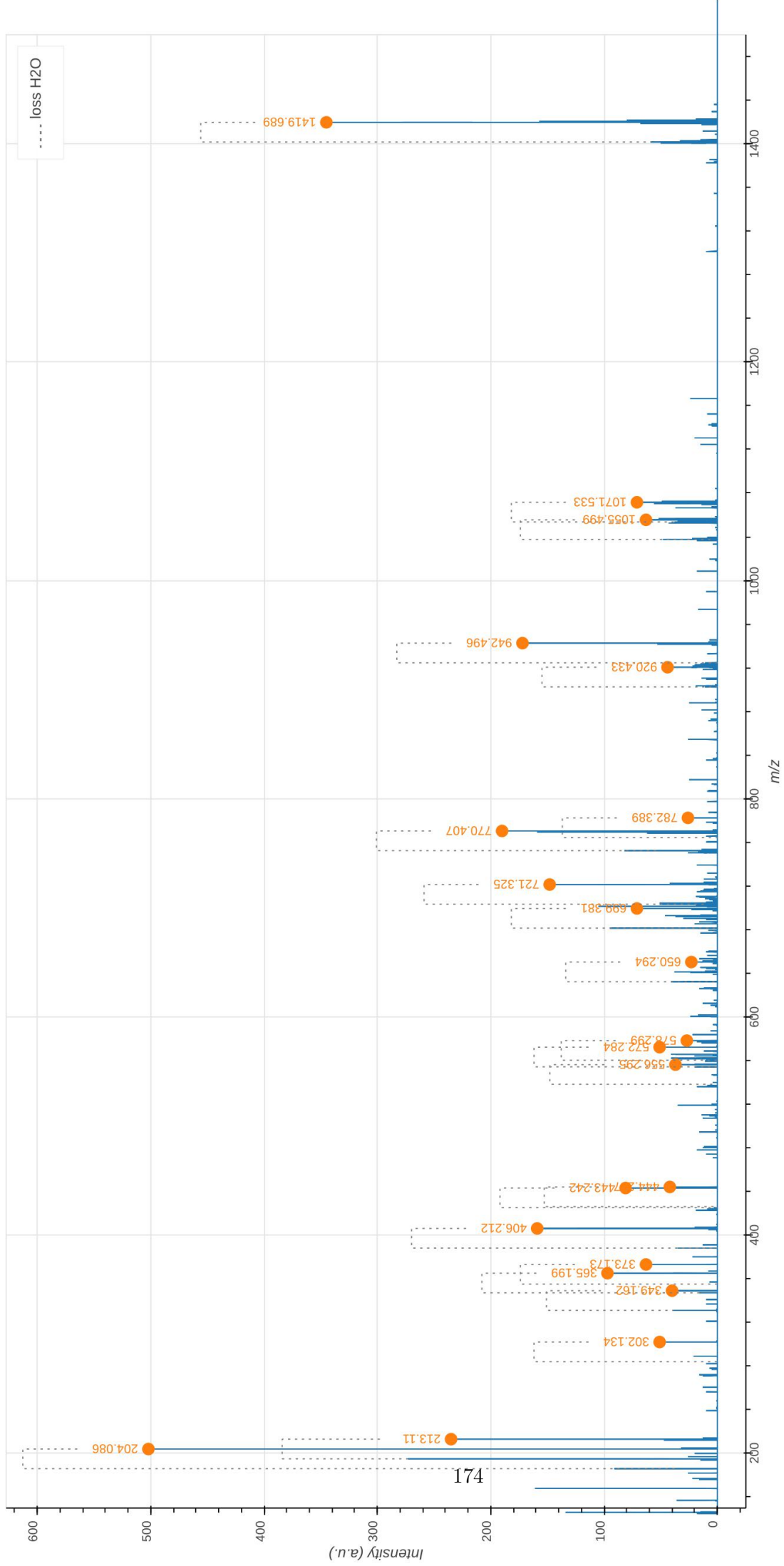


Supplementary Data 4.3: Tandem mass spectrometry analysis of the Tetra→Tri dimer containing a uniformly labeled disaccharide-tetrapeptide cross-linked to a uniformly unlabeled disaccharide-tripeptide (4→3 cross-link). The observed m/z_{obs} and calculated m/z_{calc} values of the parental ion, $[M+2H]^{2+}$, as determined in the absence of fragmentation (MS1), are indicated. The m/z_{calc} value was used to select the ion for fragmentation. The difference between the m/z_{obs} and m/z_{calc} values is indicated in ppm. The GlcNAc residue is indicated in two moieties, glucosamine (GlcN) and the acetyl group (Ac), since these moieties are potentially differentially labeled. For the same reason, the reduced (Red) MurNAc residue is indicated in three moieties, reduced glucosamine (GlcN^{Red}), the acetyl group (Ac), and the D-lactoyl group. Labeled and unlabeled moieties are represented in red and purple, respectively.

In the mass spectrum, peaks differing by the loss of H₂O are connected by a dashed line. The arrows indicate the position of the 3→3 and 4→3 crosslinks. Residues in the acceptor are underlined.

An interactive report of the MS2 analysis is available in Supplementary File F4.3.

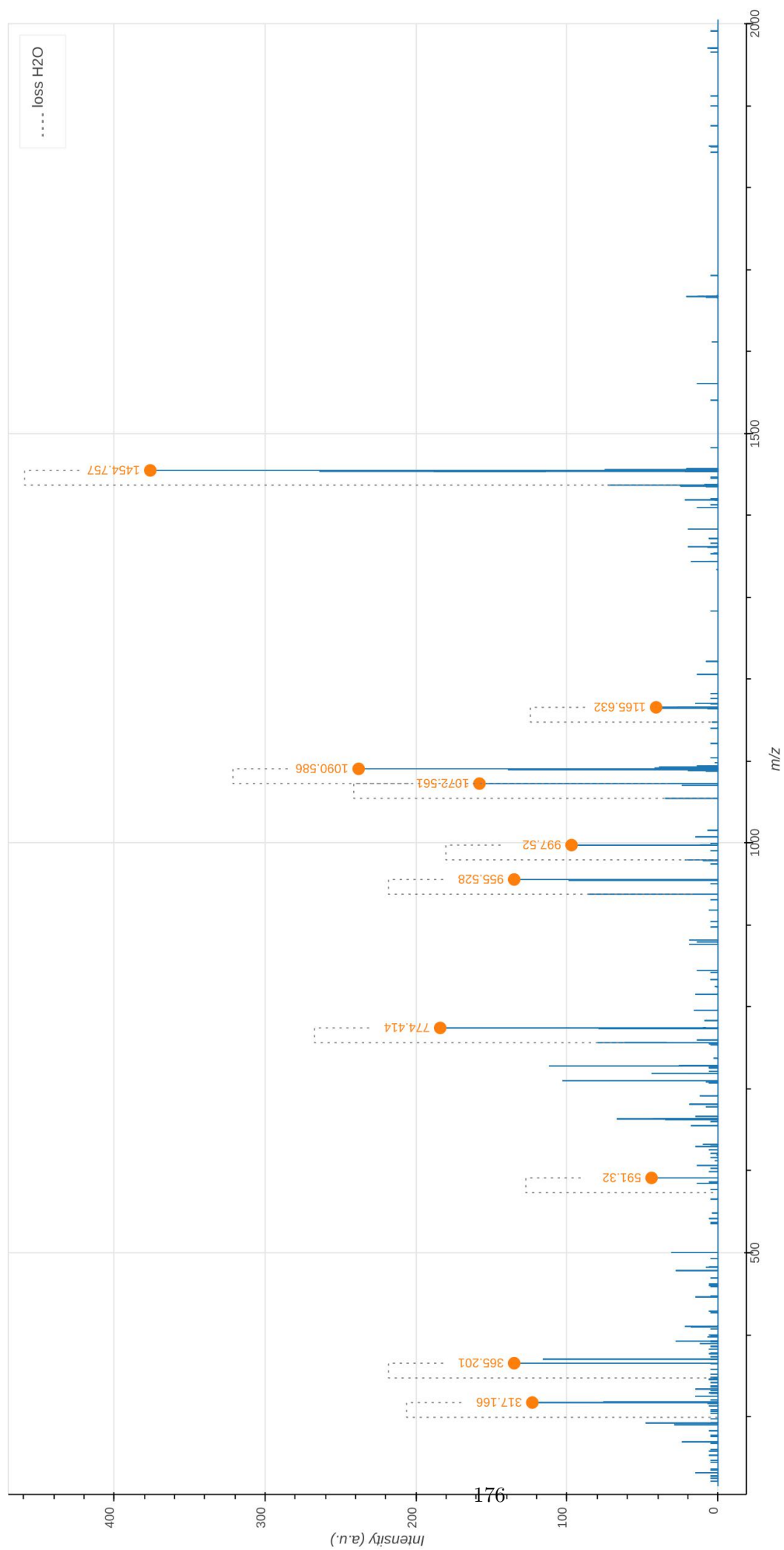
Precursor ion (MS1)	m/z_{obs} [M+2H] ²⁺	m/z_{calc} [M+2H] ²⁺	ppm	
GlcN(-Ac)-GlcN ^{Red} (-Ac)-Lac-Ala-Glu-DAP-Ala→ <u>DAP-Glu-Ala-Lac-GlcN^{Red}(-Ac)-GlcN(-Ac)</u>	917.936	917.940	-4.4	
Discriminatory product ion				
GlcN ^{Red} (-Ac)-Lac-Ala-Glu-DAP-Ala→ <u>DAP-Glu-Ala-Lac-GlcN^{Red}(-Ac)</u>	m/z_{obs} [M+H] ¹⁺	m/z_{calc} [M+H] ¹⁺	ppm	Intensity (a.u.)
Glu-DAP-Ala→ <u>DAP-Glu-Ala-Lac-GlcN^{Red}(-Ac)</u>	1419.689	1419.689	0.3	345
GlcN ^{Red} (-Ac)-Lac-Ala-Glu-DAP-Ala→ <u>DAP-Glu</u>	1071.533	1071.536	2.7	71
DAP-Ala→ <u>DAP-Glu-Ala-Lac-GlcN^{Red}(-Ac)</u>	1055.499	1055.495	-3.4	63
GlcN ^{Red} (-Ac)-Lac-Ala-Glu-DAP-Ala→ <u>DAP</u>	942.496	942.493	-3.2	172
Glu-DAP-Ala→ <u>DAP-Glu-Ala</u>	920.433	920.439	5.9	44
Ala→ <u>DAP-Glu-Ala-Lac-GlcN^{Red}(-Ac)</u>	782.389	782.386	-3.8	26
GlcN ^{Red} (-Ac)-Lac-Ala-Glu-DAP-Ala	770.407	770.409	1.4	190
<u>DAP-Glu-Ala-Lac-GlcN^{Red}(-Ac)</u>	721.325	721.326	0.7	148
GlcN ^{Red} (-Ac)-Lac-Ala-Glu-DAP	699.381	699.371	-14.3	71
DAP-Ala→ <u>DAP-Glu</u>	650.294	650.288	-8.5	23
Glu-DAP-Ala→ <u>DAP</u>	578.299	578.299	0.2	27
Ala→ <u>DAP-Glu-Ala-Lac</u>	572.284	572.285	2.7	51
Ala-Glu-DAP-Ala	556.295	556.290	-9.4	37
DAP-Ala→ <u>DAP</u>	444.207	444.209	6.0	42
Ala→ <u>DAP-Glu</u>	443.242	443.243	1.9	81
Ala-Glu-DAP	406.212	406.214	5.0	159
<u>Ala-Lac-GlcN^{Red}(-Ac)</u>	373.173	373.172	-0.5	63
GlcN ^{Red} (-Ac)-Lac-Ala	365.199	365.202	8.0	97
Glu-DAP	349.162	349.161	-1.4	40
<u>GlcN(-Ac)</u>	302.134	302.135	4.8	51
GlcN(-Ac)	213.110	213.111	6.5	235
	204.086	204.087	7.7	502



Tri-Tetra

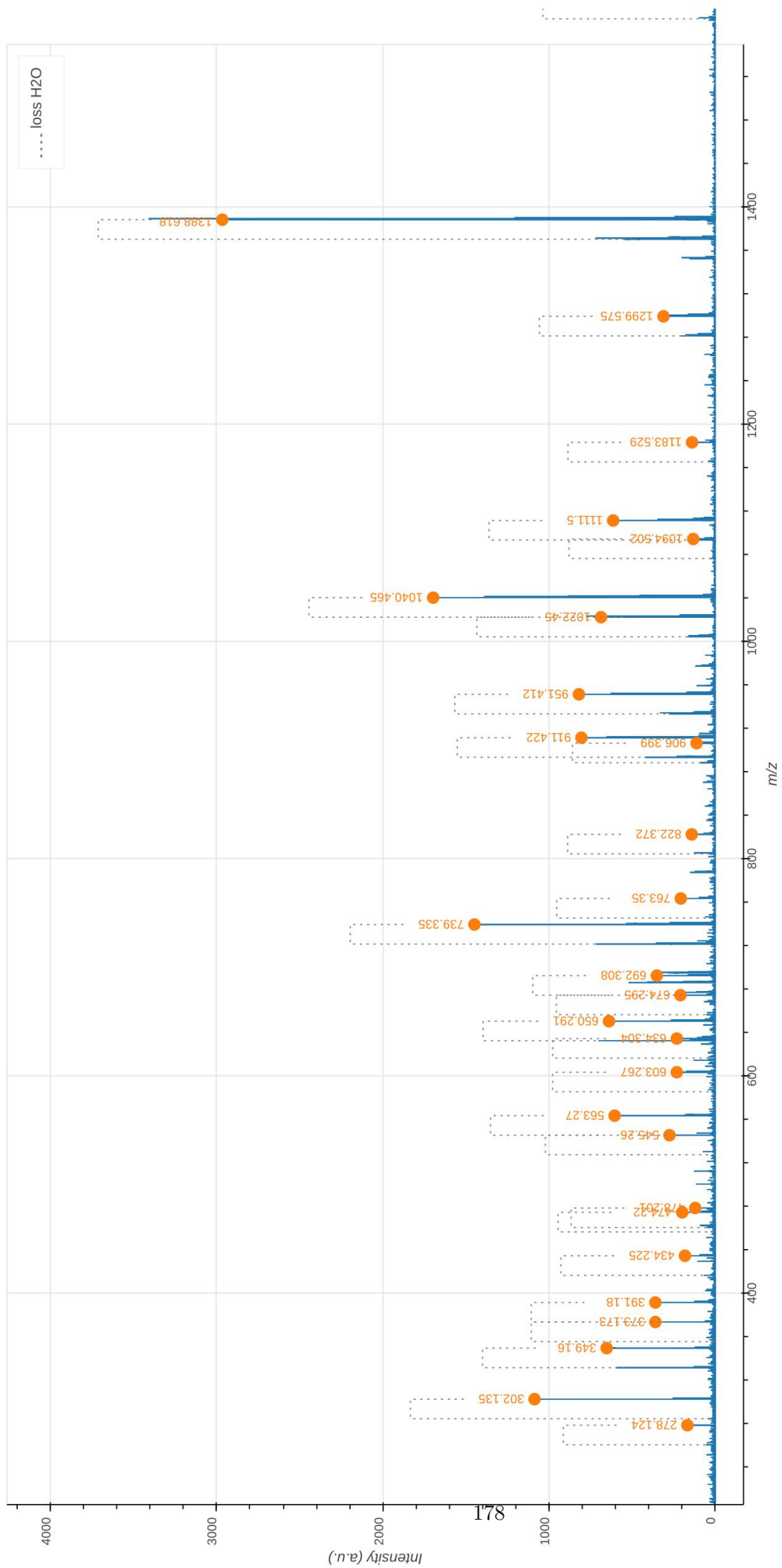
Supplementary Data 5.1: Tandem mass spectrometry analysis of the uniformly labeled Tri(4→3)Tetra dimer. The observed m/z_{obs} and calculated m/z_{cal} values of the parental ion, $[M+2H]^{2+}$, as determined in the absence of fragmentation (MS1), are indicated. The m/z_{cal} value was used to select the ion for fragmentation. The difference between the m/z_{obs} and m/z_{cal} values is indicated in ppm. The GlcNAc residue is indicated in two moieties, glucosamine (GlcN) and the acetyl group (Ac), since these moieties are potentially differentially labeled. For the same reason, the reduced (Red) MurNAc residue is indicated in three moieties, reduced glucosamine (GlcN^{Red}), the acetyl group (Ac), and the D-lactoyl group. Labeled and unlabeled moieties are represented in red and purple, respectively. The peaks corresponding to the list of fragments appearing in the table are highlighted by orange dots in the mass spectrum. In the mass spectrum, peaks differing by the loss of H₂O are connected by a dashed line. The tables only contain the m/z values for the fragments containing H₂O. The arrows indicate the position of the 3→3 and 4→3 crosslinks. Residues in the acceptor are underlined. An interactive report of the MS2 analysis is available in Supplementary File F5.1.

Precursor ion (MS1)	m/z_{obs} $[M+2H]^{2+}$	m/z_{calc} $[M+2H]^{2+}$	ppm	
GlcN(-Ac)-GlcN ^{Red} (-Ac)-Lac-Ala-Glu-DAP → <u>DAP(-Ala)-Glu-Ala-Lac-GlcN^{Red}(-Ac)-GlcN(-Ac)</u>	939.988	939.992	-3.3	
Product ion	m/z_{obs} $[M+H]^{1+}$	m/z_{calc} $[M+H]^{1+}$	ppm	Intensity (a.u.)
GlcN ^{Red} (-Ac)-Lac-Ala-Glu-DAP → <u>DAP(-Ala)-Glu-Ala-Lac-GlcN^{Red}(-Ac)</u>	1454.757	1454.769	8.0	376
GlcN ^{Red} (-Ac)-Lac-Ala-Glu-DAP → <u>DAP(-Ala)-Glu-Ala</u>	1165.632	1165.619	-11.3	41
GlcN ^{Red} (-Ac)-Lac-Ala-Glu-DAP → <u>DAP(-Ala)-Glu</u>	1090.586	1090.574	-10.9	238
GlcN ^{Red} (-Ac)-Lac-Ala-Glu-DAP → <u>DAP-Glu-Ala</u>	1072.561	1072.564	2.6	158
GlcN ^{Red} (-Ac)-Lac-Ala-Glu-DAP → <u>DAP-Glu</u>	997.520	997.520	-0.5	97
GlcN ^{Red} (-Ac)-Lac-Ala-Glu-DAP → <u>DAP(-Ala)</u>	955.528	955.518	-10.1	135
<u>DAP(-Ala)-Glu-Ala-Lac-GlcN^{Red}(-Ac)</u>	774.414	774.416	2.5	184
Glu-DAP → <u>DAP(-Ala)</u>	591.320	591.324	6.3	44
GlcN ^{Red} (-Ac)-Lac-Ala	365.201	365.202	1.9	135
Glu-DAP	317.166	317.167	3.2	123



Supplementary Data 5.2: Tandem mass spectrometry analysis of the uniformly unlabeled Tri(3→3)Tetra dimer. The observed m/z_{obs} and calculated m/z_{calc} values of the parental ion, $[M+2H]^{2+}$, as determined in the absence of fragmentation (MS1), are indicated. The m/z_{calc} value was used to select the ion for fragmentation. The difference between the m/z_{obs} and m/z_{calc} values is indicated in ppm. The GlcNAc residue is indicated in two moieties, glucosamine (GlcN) and the acetyl group (Ac), since these moieties are potentially differentially labeled. For the same reason, the reduced (Red) MurNAc residue is indicated in three moieties, reduced glucosamine (GlcN^{Red}), the acetyl group (Ac), and the D-lactoyl group. Labeled and unlabeled moieties are represented in red and purple, respectively. The peaks corresponding to the list of fragments appearing in the table are highlighted by orange dots in the mass spectrum. In the mass spectrum, peaks differing by the loss of H₂O are connected by a dashed line. The tables only contain the m/z values for the fragments containing H₂O. The arrows indicate the position of the 3→3 and 4→3 crosslinks. Residues in the acceptor are underlined. An interactive report of the MS2 analysis is available in Supplementary File F5.2.

Precursor ion (MS1)	$m/z_{\text{obs}} [M+2H]^{2+}$	$m/z_{\text{calc}} [M+2H]^{2+}$	ppm	
GlcN(-Ac)-GlcN ^{Red} (-Ac)-Lac-Ala-Glu-DAP→DAP(-Ala)-Glu-Ala-Lac-GlcN ^{Red} (-Ac)-GlcN(-Ac)	897.891	897.892	-0.9	
Product ion	$m/z_{\text{obs}} [M+H]^{1+}$	$m/z_{\text{calc}} [M+H]^{1+}$	ppm	Intensity (a.u.)
GlcN(-Ac)-GlcN ^{Red} (-Ac)-Lac-Ala-Glu-DAP→DAP(-Ala)-Glu-Ala-Lac-GlcN ^{Red} (-Ac)	1591.703	1591.696	-4.5	290
GlcN ^{Red} (-Ac)-Lac-Ala-Glu-DAP→DAP(-Ala)-Glu-Ala-Lac-GlcN ^{Red} (-Ac)	1388.618	1388.617	-0.8	2966
GlcN ^{Red} (-Ac)-Lac-Ala-Glu-DAP→DAP-Glu-Ala-Lac-GlcN ^{Red} (-Ac)	1299.575	1299.569	-4.2	311
GlcN ^{Red} (-Ac)-Lac-Ala-Glu-DAP→DAP(-Ala)-Glu-Ala-Lac	1183.529	1183.522	-5.7	139
GlcN ^{Red} (-Ac)-Lac-Ala-Glu-DAP→DAP(-Ala)-Glu-Ala	1111.500	1111.501	0.4	614
GlcN ^{Red} (-Ac)-Lac-Ala-Glu-DAP→DAP-Glu-Ala-Lac	1094.502	1094.474	-25.7	132
GlcN ^{Red} (-Ac)-Lac-Ala-Glu-DAP→DAP(-Ala)-Glu	1040.465	1040.464	-1.8	1697
GlcN ^{Red} (-Ac)-Lac-Ala-Glu-DAP→DAP-Glu-Ala	1022.450	1022.453	2.8	687
GlcN ^{Red} (-Ac)-Lac-Ala-Glu-DAP→DAP-Glu	951.412	951.416	4.5	820
GlcN ^{Red} (-Ac)-Lac-Ala-Glu-DAP→DAP(-Ala)	911.422	911.421	-0.9	805
Lac-Ala-Glu-DAP→DAP(-Ala)-Glu-Ala	906.399	906.406	7.8	112
GlcN ^{Red} (-Ac)-Lac-Ala-Glu-DAP→DAP	822.372	822.373	1.4	141
Ala-Glu-DAP→DAP(-Ala)-Glu	763.350	763.347	-3.4	207
DAP(-Ala)-Glu-Ala-Lac-GlcN ^{Red} (-Ac)	739.335	739.336	0.9	1449
Glu-DAP→DAP(-Ala)-Glu	692.308	692.310	3.2	351
Ala-Glu-DAP→DAP-Glu	674.295	674.300	6.8	209
GlcN ^{Red} (-Ac)-Lac-Ala-Glu-DAP	650.291	650.288	-3.1	639
Ala-Glu-DAP→DAP(-Ala)	634.304	634.305	1.8	231
Glu-DAP→DAP-Glu	603.267	603.263	-6.7	231
Glu-DAP→DAP(-Ala)	563.270	563.268	-4.0	605
Ala-Glu-DAP→DAP	545.260	545.257	-4.6	275
GlcN ^{Red} (-Ac)-Lac-Ala-Glu	478.201	478.204	5.9	120
Glu-DAP→DAP	474.220	474.220	-1.0	198
DAP→DAP(-Ala)	434.225	434.225	-0.2	182
DAP(-Ala)-Glu	391.180	391.183	7.9	360
Ala-Glu-DAP	373.173	373.172	-2.4	360
GlcN ^{Red} (-Ac)-Lac-Ala	349.160	349.161	3.2	653
Glu-DAP	302.135	302.135	-0.7	1087
GlcN ^{Red} (-Ac)-Lac	278.124	278.124	0.3	167

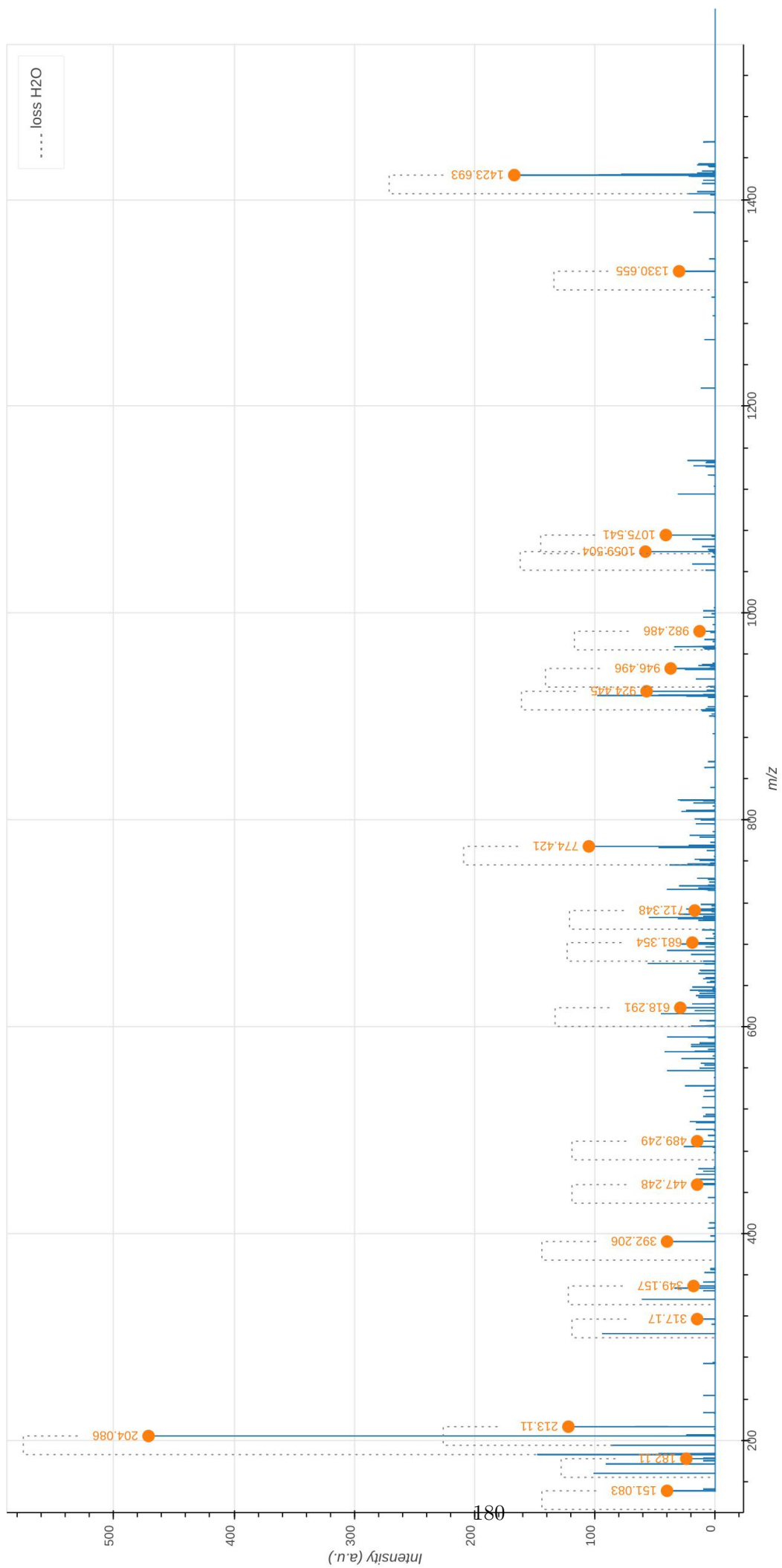


Supplementary Data 5.3: Tandem mass spectrometry analysis of the Tri→Tetra dimer containing a uniformly labeled disaccharide-tetrapeptide cross-linked to a uniformly unlabeled disaccharide-tripeptide (3→3 cross-link). The observed m/z_{obs} and calculated m/z_{calc} values of the parental ion, $[M+2H]^{2+}$, as determined in the absence of fragmentation (MS1), are indicated. The m/z_{calc} value was used to select the ion for fragmentation. The difference between the m/z_{obs} and m/z_{calc} values is indicated in ppm. The GlcNAc residue is indicated in two moieties, glucosamine (GlcN) and the acetyl group (Ac), since these moieties are potentially differentially labeled. For the same reason, the reduced (Red) MurNAc residue is indicated in three moieties, reduced glucosamine (GlcN^{Red}), the acetyl group (Ac), and the D-lactoyl group. Labeled and unlabeled moieties are represented in red and purple, respectively.

In the mass spectrum, peaks differing by the loss of H₂O are connected by a dashed line. The arrows indicate the position of the 3→3 and 4→3 crosslinks. Residues in the acceptor are underlined.

An interactive report of the MS2 analysis is available in Supplementary File F5.3.

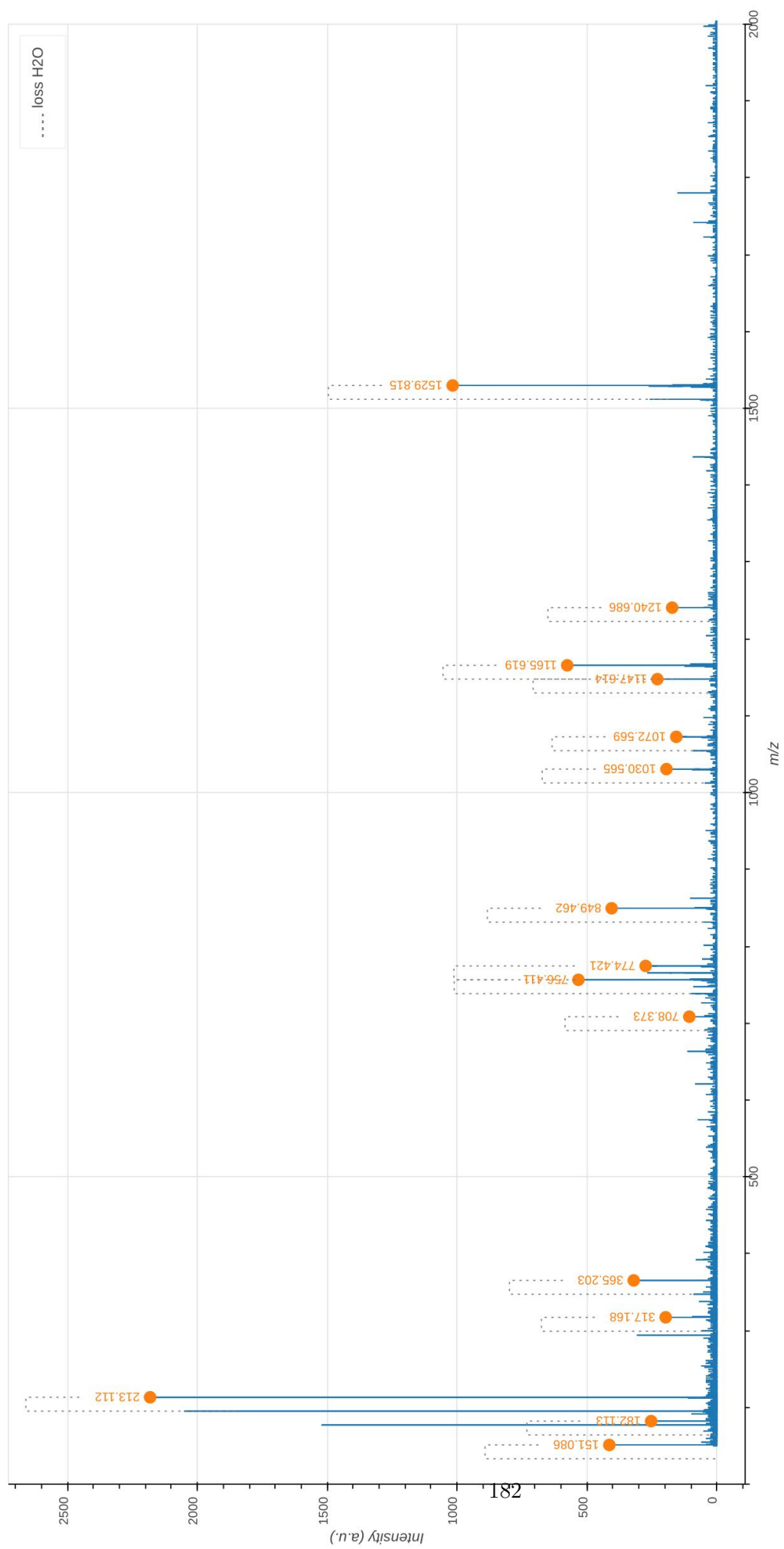
Precursor ion (MS1)	m/z_{obs} [M+2H] ²⁺	m/z_{calc} [M+2H] ²⁺	ppm	
GlcN(-Ac)-GlcN ^{Red} (-Ac)-Lac-Ala-Glu-DAP→ <u>DAP(-Ala)-Glu-Ala-Lac-GlcN^{Red}(-Ac)-GlcN(-Ac)</u>	919.942	919.943	-1.0	
Product ion	m/z_{obs} [M+H] ¹⁺	m/z_{calc} [M+H] ¹⁺	ppm	Intensity (a.u.)
GlcN ^{Red} (-Ac)-Lac-Ala-Glu-DAP→ <u>DAP(-Ala)-Glu-Ala-Lac-GlcN^{Red}(-Ac)</u>	1423.693	1423.696	2.4	167
GlcN ^{Red} (-Ac)-Lac-Ala-Glu-DAP→ <u>DAP-Glu-Ala-Lac-GlcN^{Red}(-Ac)</u>	1330.655	1330.642	-10.1	30
Glu-DAP→ <u>DAP(-Ala)-Glu-Ala-Lac-GlcN^{Red}(-Ac)</u>	1075.541	1075.543	2.3	41
GlcN ^{Red} (-Ac)-Lac-Ala-Glu-DAP→ <u>DAP(-Ala)-Glu</u>	1059.504	1059.502	-1.7	58
Glu-DAP→ <u>DAP-Glu-Ala-Lac-GlcN^{Red}(-Ac)</u>	982.486	982.488	2.8	13
DAP→ <u>DAP(-Ala)-Glu-Ala-Lac-GlcN^{Red}(-Ac)</u>	946.496	946.500	5.1	37
GlcN ^{Red} (-Ac)-Lac-Ala-Glu-DAP→ <u>DAP(-Ala)</u>	924.445	924.446	1.1	57
<u>DAP(-Ala)-Glu-Ala-Lac-GlcN^{Red}(-Ac)</u>	774.421	774.416	-7.2	105
<u>Glu-Ala-Lac-GlcN^{Red}(-Ac)-GlcN(-Ac)</u>	712.348	712.362	19.6	17
<u>DAP-Glu-Ala-Lac-GlcN^{Red}(-Ac)</u>	681.354	681.361	10.6	19
Glu-DAP→ <u>DAP-Glu</u>	618.291	618.294	4.1	29
DAP→ <u>DAP-Glu</u>	489.249	489.251	5.0	15
DAP→ <u>DAP(-Ala)</u>	447.248	447.250	4.1	15
<u>DAP-Glu-Ala</u>	392.206	392.211	13.2	40
GlcN ^{Red} (-Ac)-Lac-Ala	349.157	349.161	10.7	18
<u>DAP-Glu</u>	317.170	317.167	-9.7	15
<u>GlcN(-Ac)</u>	213.110	213.111	5.5	122
GlcN(-Ac)	204.086	204.087	6.8	471
<u>DAP</u>	182.110	182.110	0.8	24
<u>Ala-Lac</u>	151.083	151.083	-1.5	40



Tetra-Tetra

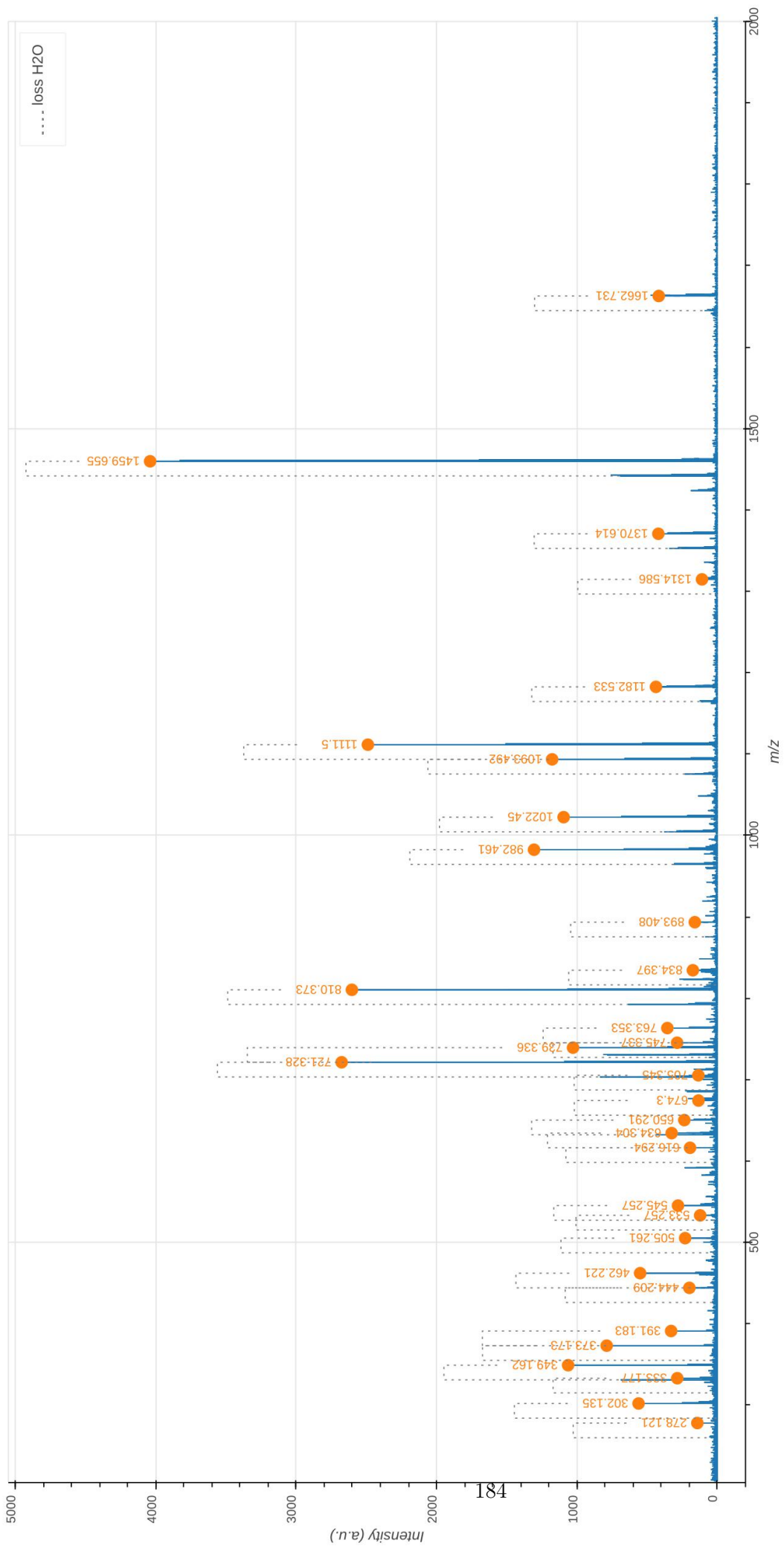
Supplementary Data 6.1: Tandem mass spectrometry analysis of the uniformly labeled Tetra(4→3)Tetra dimer. The observed m/z_{obs} and calculated m/z_{cal} values of the parental ion, $[M+2H]^{2+}$, as determined in the absence of fragmentation (MS1), are indicated. The m/z_{calc} value was used to select the ion for fragmentation. The difference between the m/z_{obs} and m/z_{calc} values is indicated in ppm. The GlcNAc residue is indicated in two moieties, glucosamine (GlcN) and the acetyl group (Ac), since these moieties are potentially differentially labeled. For the same reason, the reduced (Red) MurNAc residue is indicated in three moieties, reduced glucosamine (GlcN^{Red}), the acetyl group (Ac), and the D-lactoyl group. Labeled and unlabeled moieties are represented in red and purple, respectively. The peaks corresponding to the list of fragments appearing in the table are highlighted by orange dots in the mass spectrum. In the mass spectrum, peaks differing by the loss of H₂O are connected by a dashed line. The tables only contain the m/z values for the fragments containing H₂O. The arrows indicate the position of the 3→3 and 4→3 crosslinks. Residues in the acceptor are underlined. An interactive report of the MS2 analysis is available in Supplementary File F6.1.

Precursor ion (MS1)	m/z_{obs} $[M+2H]^{2+}$	m/z_{calc} $[M+2H]^{2+}$	ppm	
GlcN(-Ac)-GlcN ^{Red} (-Ac)-Lac-Ala-Glu-DAP-Ala → <u>DAP(-Ala)-Glu-Ala-Lac-GlcN^{Red}(-Ac)-GlcN(-Ac)</u>	977.512	977.514	-2.0	
Product ion	m/z_{obs} $[M+H]^{1+}$	m/z_{calc} $[M+H]^{1+}$	ppm	Intensity (a.u.)
GlcN ^{Red} (-Ac)-Lac-Ala-Glu-DAP-Ala → <u>DAP(-Ala)-Glu-Ala-Lac-GlcN^{Red}(-Ac)</u>	1529.815	1529.813	-1.7	1017
GlcN ^{Red} (-Ac)-Lac-Ala-Glu-DAP-Ala → <u>DAP(-Ala)-Glu-Ala</u>	1240.686	1240.663	-18.5	172
GlcN ^{Red} (-Ac)-Lac-Ala-Glu-DAP-Ala → <u>DAP(-Ala)-Glu</u>	1165.619	1165.619	-0.4	576
GlcN ^{Red} (-Ac)-Lac-Ala-Glu-DAP-Ala → <u>DAP-Glu-Ala</u>	1147.614	1147.608	-5.1	229
GlcN ^{Red} (-Ac)-Lac-Ala-Glu-DAP-Ala → <u>DAP-Glu</u>	1072.569	1072.564	-4.8	156
GlcN ^{Red} (-Ac)-Lac-Ala-Glu-DAP-Ala → <u>DAP(-Ala)</u>	1030.565	1030.562	-2.9	194
Ala → <u>DAP(-Ala)-Glu-Ala-Lac-GlcN^{Red}(-Ac)</u>	849.462	849.460	-2.4	405
<u>DAP(-Ala)-Glu-Ala-Lac-GlcN^{Red}(-Ac)</u>	774.421	774.416	-7.4	274
GlcN ^{Red} (-Ac)-Lac-Ala-Glu-DAP-Ala	756.411	756.405	-8.2	533
Glu-DAP-Ala → <u>DAP-Glu</u>	708.373	708.370	-5.4	106
GlcN ^{Red} (-Ac)-Lac-Ala	365.203	365.202	-1.1	320
Glu-DAP	317.168	317.167	-4.8	197
GlcN(-Ac)	213.112	213.111	-6.5	2182
DAP	182.113	182.110	-14.4	253
Lac-Ala	151.086	151.083	-19.2	414



Supplementary Data 6.2: Tandem mass spectrometry analysis of the uniformly unlabeled Tetra(4→3)Tetra dimer. The observed m/z_{obs} and calculated m/z_{cal} values of the parental ion, $[M+2H]^{2+}$, as determined in the absence of fragmentation (MS1), are indicated. The m/z_{cal} value was used to select the ion for fragmentation. The difference between the m/z_{obs} and m/z_{cal} values is indicated in ppm. The GlcNAc residue is indicated in two moieties, glucosamine (GlcN) and the acetyl group (Ac), since these moieties are potentially differentially labeled. For the same reason, the reduced (Red) MurNAc residue is indicated in three moieties, reduced glucosamine (GlcN^{Red}), the acetyl group (Ac), and the D-lactoyl group. Labeled and unlabeled moieties are represented in red and purple, respectively. The peaks corresponding to the list of fragments appearing in the table are highlighted by orange dots in the mass spectrum. In the mass spectrum, peaks differing by the loss of H₂O are connected by a dashed line. The tables only contain the m/z values for the fragments containing H₂O. The arrows indicate the position of the 3→3 and 4→3 crosslinks. Residues in the acceptor are underlined. An interactive report of the MS2 analysis is available in Supplementary File F6.2.

Precursor ion (MS1)	$m/z_{\text{obs}} [M+2H]^{2+}$	$m/z_{\text{calc}} [M+2H]^{2+}$	ppm	
GlcN(-Ac)-GlcN ^{Red} (-Ac)-Lac-Ala-Glu-DAP-Ala→ <u>DAP(-Ala)-Glu-Ala-Lac-GlcN^{Red}(-Ac)-GlcN(-Ac)</u>	933.409	933.410	-1.7	
Product ion	$m/z_{\text{obs}} [M+H]^{1+}$	$m/z_{\text{calc}} [M+H]^{1+}$	ppm	Intensity (a.u.)
GlcN(-Ac)-GlcN ^{Red} (-Ac)-Lac-Ala-Glu-DAP-Ala→ <u>DAP(-Ala)-Glu-Ala-Lac-GlcN^{Red}(-Ac)</u>	1662.731	1662.733	1.1	416
GlcN ^{Red} (-Ac)-Lac-Ala-Glu-DAP-Ala→ <u>DAP(-Ala)-Glu-Ala-Lac-GlcN^{Red}(-Ac)</u>	1459.655	1459.654	-0.9	4041
GlcN ^{Red} (-Ac)-Lac-Ala-Glu-DAP-Ala→ <u>DAP-Glu-Ala-Lac-GlcN^{Red}(-Ac)</u>	1370.614	1370.606	-5.8	419
GlcN(-Ac)-GlcN ^{Red} (-Ac)-Lac-Ala-Glu-DAP-Ala→ <u>DAP(-Ala)-Glu</u>	1314.586	1314.580	-4.8	108
GlcN ^{Red} (-Ac)-Lac-Ala-Glu-DAP-Ala→ <u>DAP(-Ala)-Glu-Ala</u>	1182.533	1182.538	4.2	436
GlcN ^{Red} (-Ac)-Lac-Ala-Glu-DAP-Ala→ <u>DAP(-Ala)-Glu</u>	1111.500	1111.501	0.3	2489
GlcN ^{Red} (-Ac)-Lac-Ala-Glu-DAP-Ala→ <u>DAP-Glu-Ala</u>	1093.492	1093.490	-1.8	1176
GlcN ^{Red} (-Ac)-Lac-Ala-Glu-DAP-Ala→ <u>DAP-Glu</u>	1022.450	1022.453	3.2	1094
GlcN ^{Red} (-Ac)-Lac-Ala-Glu-DAP-Ala→ <u>DAP(-Ala)</u>	982.461	982.458	-2.7	1305
GlcN ^{Red} (-Ac)-Lac-Ala-Glu-DAP-Ala→ <u>DAP</u>	893.408	893.410	3.2	159
Ala-Glu-DAP-Ala→ <u>DAP(-Ala)-Glu</u>	834.397	834.385	-14.7	173
Ala→ <u>DAP(-Ala)-Glu-Ala-Lac-GlcN^{Red}(-Ac)</u>	810.373	810.373	0.4	2603
Glu-DAP-Ala→ <u>DAP(-Ala)-Glu</u>	763.353	763.347	-7.3	355
Ala-Glu-DAP-Ala→ <u>DAP-Glu</u>	745.337	745.337	0.4	285
<u>DAP(-Ala)-Glu-Ala-Lac-GlcN^{Red}(-Ac)</u>	739.336	739.336	0.8	1027
GlcN ^{Red} (-Ac)-Lac-Ala-Glu-DAP-Ala	721.328	721.326	-3.7	2676
Ala-Glu-DAP-Ala→ <u>DAP(-Ala)</u>	705.345	705.342	-3.8	134
Glu-DAP-Ala→ <u>DAP-Glu</u>	674.300	674.300	0.1	133
GlcN ^{Red} (-Ac)-Lac-Ala-Glu-DAP	650.291	650.288	-3.3	234
Glu-DAP-Ala→ <u>DAP(-Ala)</u>	634.304	634.305	1.6	324
Ala-Glu-DAP-Ala→ <u>DAP</u>	616.294	616.294	-0.2	193
Glu-DAP-Ala→ <u>DAP</u>	545.257	545.257	0.6	279
Ala→ <u>DAP(-Ala)-Glu-Ala</u>	533.257	533.257	0.6	121
DAP-Ala→ <u>DAP(-Ala)</u>	505.261	505.262	2.2	228
Ala→ <u>DAP(-Ala)-Glu</u>	462.221	462.220	-1.2	549
Ala-Glu-DAP-Ala	444.209	444.209	0.1	198
<u>DAP(-Ala)-Glu</u>	391.183	391.183	0.2	328
Ala-Glu-DAP	373.173	373.172	-2.6	787
GlcN ^{Red} (-Ac)-Lac-Ala	349.162	349.161	-1.2	1062
Ala→ <u>DAP(-Ala)</u>	333.177	333.177	2.6	284
Glu-DAP	302.135	302.135	-0.9	560
GlcN ^{Red} (-Ac)-Lac	278.121	278.124	10.8	141

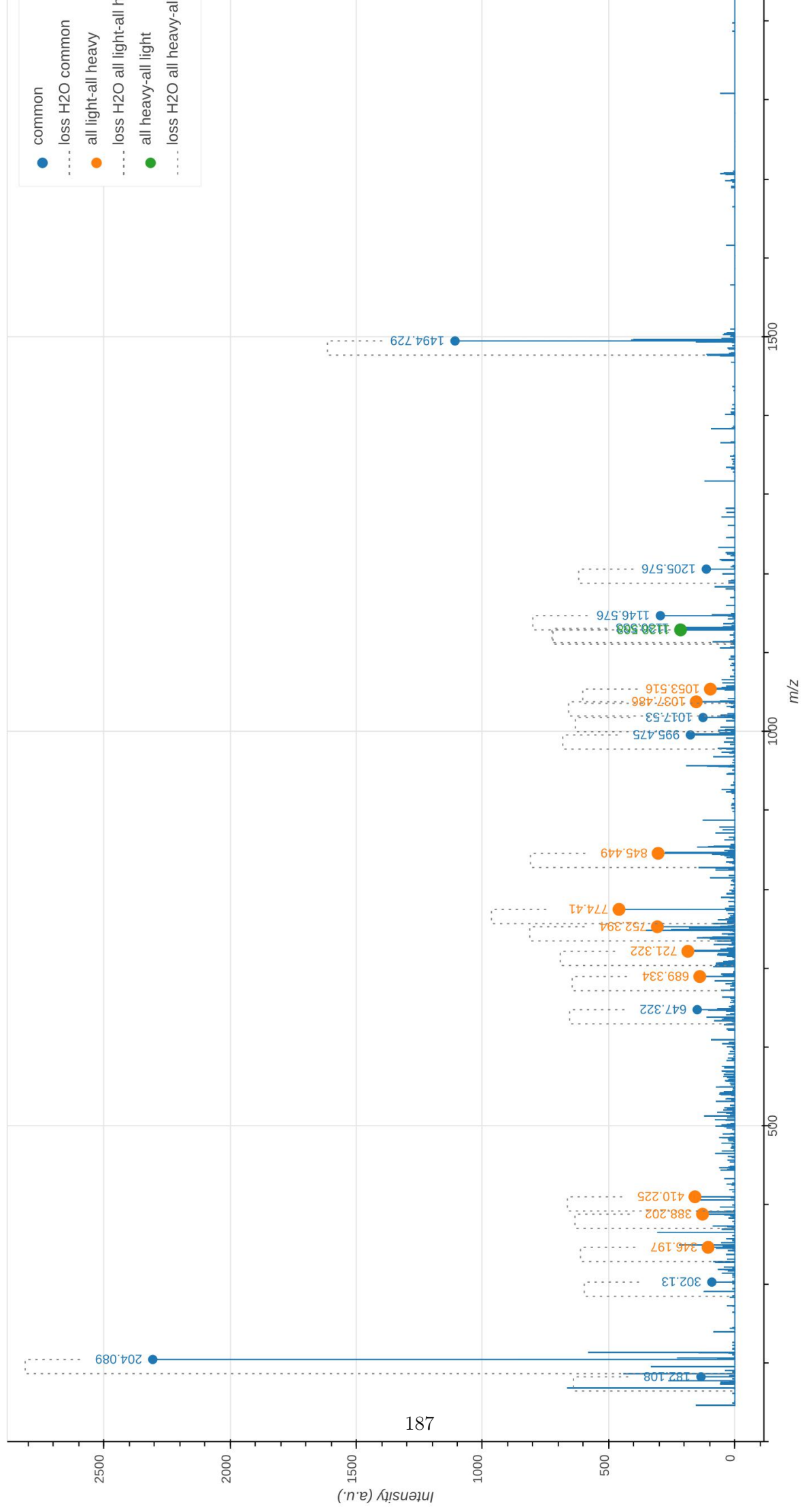


Supplementary Data 6.3: Tandem mass spectrometry analysis of the Tetra→Tetra dimer containing a uniformly labeled disaccharide-tripeptide cross-linked to a uniformly unlabeled disaccharide-tripeptide (4→3 cross-link). The observed m/z_{obs} and calculated m/z_{cal} values of the parental ion, $[M+2H]^{2+}$, as determined in the absence of fragmentation (MS1), are indicated. The m/z_{cal} value was used to select the ion for fragmentation. The difference between the m/z_{obs} and m/z_{cal} values is indicated in ppm. The GlcNAc residue is indicated in two moieties, glucosamine (GlcN) and the acetyl group (Ac), since these moieties are potentially differentially labeled. For the same reason, the reduced (Red) MurNAc residue is indicated in three moieties, reduced glucosamine (GlcN^{Red}), the acetyl group (Ac), and the D-lactoyl group. Labeled and unlabeled moieties are represented in red and purple, respectively. The fragmentation potentially leads to two series of fragments (discriminatory fragments) specific of the isotopomers containing the fully labeled disaccharide subunit in the donor (all heavy-all light) or acceptor position (all light-all heavy). These fragments are highlighted by green and orange dots in the mass spectrum, respectively. The other fragments are common to the fragmentation of the two isotopomers (highlighted by blue dots in the mass spectrum). The mass spectrum indicates the presence of the all light-all heavy isotopomers (orange dots). The peak at m/z_{obs} 1128.568 (green dot) can also be accounted for by the loss of H₂O from the peak at 1142.567 indicating that all peaks may be accounted for by the presence of the all light-all heavy isotopomer.

In the mass spectrum, peaks differing by the loss of H₂O are connected by a dashed line. The arrows indicate the position of the 3→3 and 4→3 crosslinks. Residues in the acceptor are underlined.

An interactive report of the MS2 analysis is available in Supplementary File F6.3.

Precursor ion (MS1)			m/z_{obs} [M+2H] ²⁺	m/z_{calc} [M+2H] ²⁺	ppm	
GlcN(-Ac)-GlcN ^{Red} (-Ac)-Lac-Ala-Glu-DAP-Ala	→ <u>DAP(-Ala)-Glu-Ala-Lac-GlcN^{Red}(-Ac)-GlcN(-Ac)</u>	955.459	955.462	-2.6		
GlcN(-Ac)-GlcN ^{Red} (-Ac)-Lac-Ala-Glu-DAP-Ala	→ <u>DAP(-Ala)-Glu-Ala-Lac-GlcN^{Red}(-Ac)-GlcN(-Ac)</u>	955.459	955.462	-2.6		
Discriminatory product ion						
	m/z_{obs} [M+H] ¹⁺	m/z_{calc} [M+H] ¹⁺	ppm	Intensity (a.u.)	Isotopologue	
GlcN ^{Red} (-Ac)-Lac-Ala-Glu-DAP-Ala	→ <u>DAP-Glu-Ala</u>	1128.568	1128.570	1.6	215	all heavy-all light
Glu-DAP-Ala	→ <u>DAP-Glu-Ala-Lac-GlcN^{Red}(-Ac)</u>	1053.516	1053.525	9.2	97	all light-all heavy
GlcN ^{Red} (-Ac)-Lac-Ala-Glu-DAP-Ala	→ <u>DAP-Glu</u>	1037.486	1037.484	-1.5	153	all light-all heavy
Ala	→ <u>DAP(-Ala)-Glu-Ala-Lac-GlcN^{Red}(-Ac)</u>	845.449	845.453	4.3	304	all light-all heavy
<u>DAP(-Ala)-Glu-Ala-Lac-GlcN^{Red}(-Ac)</u>	774.410	774.416	7.5	459	all light-all heavy	
Ala	→ <u>DAP-Glu-Ala-Lac-GlcN^{Red}(-Ac)</u>	752.394	752.398	5.1	307	all light-all heavy
GlcN ^{Red} (-Ac)-Lac-Ala-Glu-DAP-Ala	721.322	721.326	4.4	186	all light-all heavy	
Glu-DAP-Ala	→ <u>DAP-Glu</u>	689.334	689.331	-3.8	139	all light-all heavy
<u>DAP(-Ala)-Glu</u>	410.225	410.221	-9.5	158	all light-all heavy	
Ala	→ <u>DAP-Glu</u>	388.202	388.204	4.3	128	all light-all heavy
Ala	→ <u>DAP(-Ala)</u>	346.197	346.202	14.6	106	all light-all heavy
Common product ion						
	m/z_{obs} [M+H] ¹⁺	m/z_{calc} [M+H] ¹⁺	ppm	Intensity (a.u.)		
GlcN ^{Red} (-Ac)-Lac-Ala-Glu-DAP-Ala	→ <u>DAP(-Ala)-Glu-Ala-Lac-GlcN^{Red}(-Ac)</u>	1494.729	1494.733	2.8	1109	
GlcN ^{Red} (-Ac)-Lac-Ala-Glu-DAP-Ala	→ <u>DAP(-Ala)-Glu-Ala-Lac-GlcN^{Red}(-Ac)</u>					
GlcN ^{Red} (-Ac)-Lac-Ala-Glu-DAP-Ala	→ <u>DAP(-Ala)-Glu-Ala</u>	1205.576	1205.583	6.2	113	
Ala-Glu-DAP-Ala	→ <u>DAP(-Ala)-Glu-Ala-Lac-GlcN^{Red}(-Ac)</u>					
Glu-DAP-Ala	→ <u>DAP(-Ala)-Glu-Ala-Lac-GlcN^{Red}(-Ac)</u>	1146.576	1146.580	3.8	295	
GlcN ^{Red} (-Ac)-Lac-Ala-Glu-DAP-Ala	→ <u>DAP(-Ala)-Glu</u>					
Glu-DAP-Ala	→ <u>DAP(-Ala)-Glu-Ala-Lac-GlcN^{Red}(-Ac)</u>	1130.533	1130.539	5.7	219	
GlcN ^{Red} (-Ac)-Lac-Ala-Glu-DAP-Ala	→ <u>DAP(-Ala)-Glu</u>					
DAP-Ala	→ <u>DAP(-Ala)-Glu-Ala-Lac-GlcN^{Red}(-Ac)</u>	1017.530	1017.538	7.3	126	
GlcN ^{Red} (-Ac)-Lac-Ala-Glu-DAP-Ala	→ <u>DAP(-Ala)</u>					
DAP-Ala	→ <u>DAP(-Ala)-Glu-Ala-Lac-GlcN^{Red}(-Ac)</u>	995.475	995.483	7.4	176	
GlcN ^{Red} (-Ac)-Lac-Ala-Glu-DAP-Ala	→ <u>DAP(-Ala)</u>					
DAP-Ala	→ <u>DAP(-Ala)-Glu</u>	647.322	647.329	11.3	149	
Glu-DAP-Ala	→ <u>DAP(-Ala)</u>					
<u>DAP-Glu</u>	302.130	302.135	15.7	91		
Glu-DAP						
GlcN(-Ac)	204.089	204.087	-9.0	2307		
GlcN(-Ac)						
DAP	182.108	182.110	12.0	134		



References

- [1] W. Vollmer and U. Bertsche, “Murein (peptidoglycan) structure, architecture and biosynthesis in *Escherichia coli*,” *Biochimica et Biophysica Acta (BBA) - Biomembranes*, vol. 1778, pp. 1714–1734, sep 2008.
- [2] D. Mengin-Lecreulx, B. Flouret, and J. van Heijenoort, “Cytoplasmic steps of peptidoglycan synthesis in *Escherichia coli*,” *Journal of Bacteriology*, vol. 151, no. 3, pp. 1109–1117, 1982.
- [3] H. Barreteau, A. Kovač, A. Boniface, M. Sova, S. Gobec, and &. Didier Blanot, “Cytoplasmic steps of peptidoglycan biosynthesis,” 2008.
- [4] S. Biarrotte-Sorin, J.-E. Hugonnet, V. Delfosse, J.-L. Mainardi, L. Gutmann, M. Arthur, and C. Mayer, “Crystal Structure of a Novel β -Lactam-insensitive Peptidoglycan Transpeptidase,” *Journal of Molecular Biology*, vol. 359, pp. 533–538, jun 2006.
- [5] A. Zapun, C. Contreras-Martel, and T. Vernet, “Penicillin-binding proteins and β -lactam resistance,” *FEMS Microbiology Reviews*, vol. 32, pp. 361–385, mar 2008.
- [6] J.-L. Mainardi, R. Villet, T. D. Bugg, C. Mayer, and M. Arthur, “Evolution of peptidoglycan biosynthesis under the selective pressure of antibiotics in Gram-positive bacteria,” *FEMS Microbiology Reviews*, vol. 32, pp. 386–408, mar 2008.
- [7] J.-L. Mainardi, M. Fourgeaud, J.-E. Hugonnet, L. Dubost, J.-P. Brouard, J. Ouazzani, L. B. Rice, L. Gutmann, and M. Arthur, “A novel peptidoglycan cross-linking enzyme for a beta-lactam-resistant transpeptidation pathway,” *The Journal of biological chemistry*, vol. 280, pp. 38146–52, nov 2005.
- [8] J. E. Hugonnet, D. Mengin-Lecreulx, A. Monton, T. den Blaauwen, E. Carbonnelle, C. Veckérlé, V. B. Yves, M. van Nieuwenhze, C. Bouchier, K. Tu, L. B. Rice, and M. Arthur, “Factors essential for L,D-transpeptidase-mediated peptidoglycan cross-linking and β -lactam resistance in *Escherichia coli*,” *eLife*, vol. 5, no. OCTOBER2016, pp. 1–22, 2016.
- [9] S. Magnet, L. Dubost, A. Marie, M. Arthur, and L. Gutmann, “Identification of the l,d-Transpeptidases for Peptidoglycan Cross-Linking in *Escherichia coli*,” *Journal of Bacteriology*, vol. 190, pp. 4782–4785, jul 2008.
- [10] B. Glauner, “Separation and quantification of mucopeptides with high-performance liquid chromatography,” *Analytical Biochemistry*, vol. 172, pp. 451–464, aug 1988.
- [11] E. Sauvage, F. Kerff, M. Terrak, J. A. Ayala, P. Charlier, T. M, and B. TD, “The penicillin-binding proteins: structure and role in peptidoglycan biosynthesis,” *FEMS Microbiology Reviews*, vol. 32, pp. 234–258, mar 2008.
- [12] J.-L. Mainardi, V. Morel, M. Fourgeaud, J. Cremniter, D. Blanot, R. Legrand, C. Fréhel, M. Arthur, J. van Heijenoort, and L. Gutmann, “Balance between Two Transpeptidation Mechanisms Determines the Expression of β -Lactam Resistance in *Enterococcus faecium*,” *Journal of Biological Chemistry*, vol. 277, pp. 35801–35807, sep 2002.
- [13] S. K. Singh, L. SaiSree, R. N. Amrutha, and M. Reddy, “Three redundant murein endopeptidases catalyse an essential cleavage step in peptidoglycan synthesis of *Escherichia coli* K12,” *Molecular Microbiology*, vol. 86, pp. 1036–1051, dec 2012.
- [14] H. Voedts, D. Dorchène, A. Lodge, W. Vollmer, M. Arthur, and J.-E. Hugonnet, “Role of endopeptidases in peptidoglycan synthesis mediated by alternative cross-linking enzymes in *Escherichia coli*,” *bioRxiv*, vol. 3, p. 2021.02.12.430937, feb 2021.

- [15] T. Den Blaauwen, M. A. de Pedro, M. Nguyen-Distèche, and J. A. Ayala, “Morphogenesis of rod-shaped sacculi,” *FEMS Microbiology Reviews*, vol. 32, pp. 321–344, mar 2008.
- [16] W. Vollmer and J. V. Höltje, “Morphogenesis of *Escherichia coli*,” *Current Opinion in Microbiology*, vol. 4, no. 6, pp. 625–633, 2001.
- [17] J.-V. Holtje, “A hypothetical holoenzyme involved in the replication of the murein sacculus of *Escherichia coli*,” *Microbiology*, vol. 142, pp. 1911–1918, aug 1996.
- [18] A. Typas, M. Banzhaf, C. A. Gross, and W. Vollmer, “From the regulation of peptidoglycan synthesis to bacterial growth and morphology,” *Nature Publishing Group*, vol. 10, 2011.
- [19] S. O. Meroueh, K. Z. Bencze, D. Heseck, M. Lee, J. F. Fisher, T. L. Stemmler, and S. Mobashery, “Three-dimensional structure of the bacterial cell wall peptidoglycan,” *Proceedings of the National Academy of Sciences*, vol. 103, pp. 4404–4409, mar 2006.
- [20] B. A. Dmitriev, F. V. Toukach, K.-J. Schaper, O. Holst, E. T. Rietschel, and S. Ehlers, “Tertiary Structure of Bacterial Murein: the Scaffold Model,” *Journal of Bacteriology*, vol. 185, pp. 3458–3468, jun 2003.
- [21] T. Kern, S. Hediger, P. Müller, C. Giustini, B. Joris, C. Bougault, W. Vollmer, and J.-P. Simorre, “Toward the Characterization of Peptidoglycan Structure and Protein-Peptidoglycan Interactions by Solid-State NMR Spectroscopy,” *Journal of the American Chemical Society*, vol. 130, pp. 5618–5619, apr 2008.
- [22] X. Charpentier, C. Chalut, M. H. Rémy, and J. M. Masson, “Penicillin-binding proteins 1a and 1b form independent dimers in *Escherichia coli*,” *Journal of Bacteriology*, vol. 184, no. 13, pp. 3749–3752, 2002.
- [23] E. W. Goodell, “Recycling of murein by *Escherichia coli*,” *Journal of Bacteriology*, vol. 163, no. 1, pp. 305–310, 1985.
- [24] J. W. Johnson, J. F. Fisher, and S. Mobashery, “Bacterial cell-wall recycling,” *Annals of the New York Academy of Sciences*, vol. 1277, pp. 54–75, jan 2013.
- [25] B. L. de Jonge, F. B. Wientjes, I. Jurida, F. Driehuis, J. T. Wouters, and N. Nanninga, “Peptidoglycan synthesis during the cell cycle of *Escherichia coli*: composition and mode of insertion,” *Journal of Bacteriology*, vol. 171, no. 11, pp. 5783–5794, 1989.
- [26] K. A. Datsenko and B. L. Wanner, “One-step inactivation of chromosomal genes in *Escherichia coli* K-12 using PCR products,” *Proceedings of the National Academy of Sciences*, vol. 97, pp. 6640–6645, jun 2000.
- [27] S. Magnet, S. Bellais, L. Dubost, M. Fourgeaud, J.-L. Mainardi, S. Petit-Frere, A. Marie, D. Mengin-Lecreulx, M. Arthur, and L. Gutmann, “Identification of the l,d-Transpeptidases Responsible for Attachment of the Braun Lipoprotein to *Escherichia coli* Peptidoglycan,” *Journal of Bacteriology*, vol. 189, pp. 3927–3931, may 2007.
- [28] A. Montón Silva, C. Otten, J. Biboy, E. Breukink, M. VanNieuwenhze, W. Vollmer, and T. den Blaauwen, “The Fluorescent D-Amino Acid NADA as a Tool to Study the Conditional Activity of Transpeptidases in *Escherichia coli*,” *Frontiers in Microbiology*, vol. 9, sep 2018.
- [29] N. Morè, A. M. Martorana, J. Biboy, C. Otten, M. Winkle, C. K. G. Serrano, A. M. Silva, L. Atkinson, H. Yau, E. Breukink, T. Den Blaauwen, W. Vollmer, and A. Polissi, “Peptidoglycan Remodeling Enables *Escherichia coli* To Survive Severe Outer Membrane Assembly Defect,” 2019.

- [30] A. Arbeloa, J.-E. Hugonnet, A.-C. Sentilhes, N. Josseaume, L. Dubost, C. Monsempes, D. Blanot, J.-P. Brouard, and M. Arthur, "Synthesis of Mosaic Peptidoglycan Cross-bridges by Hybrid Peptidoglycan Assembly Pathways in Gram-positive Bacteria*," 2004.
- [31] R. Adusumilli and P. Mallick, "Data conversion with proteoWizard msConvert," in *Methods in Molecular Biology*, vol. 1550, pp. 339–368, 2017.
- [32] O. Langella and F. Rusconi, "mineXpert2 : Full-Depth Visualization and Exploration of MS n Mass Spectrometry Data," *Journal of the American Society for Mass Spectrometry*, vol. 32, pp. 1138–1141, apr 2021.
- [33] M. K. Lacki, M. Startek, D. Valkenborg, and A. Gambin, "IsoSpec: Hyperfast Fine Structure Calculator," *Analytical Chemistry*, vol. 89, no. 6, pp. 3272–3277, 2017.
- [34] M. Wang, G. Audi, A. Wapstra, F. Kondev, M. MacCormick, X. Xu, and B. Pfeiffer, "The Ame2012 atomic mass evaluation," *Chinese Physics C*, vol. 36, pp. 1603–2014, dec 2012.
- [35] J. Meija, T. B. Coplen, M. Berglund, W. A. Brand, P. De Bièvre, M. Gröning, N. E. Holden, J. Irrgeher, R. D. Loss, T. Walczyk, and T. Prohaska, "Atomic weights of the elements 2013 (IUPAC Technical Report)," *Pure and Applied Chemistry*, vol. 88, pp. 265–291, mar 2016.
- [36] K. M. Roberts and P. F. Fitzpatrick, "Measurement of Kinetic Isotope Effects in an Enzyme-Catalyzed Reaction by Continuous-Flow Mass Spectrometry," in *Methods in Enzymology*, vol. 596, pp. 149–161, Elsevier Inc., 1 ed., 2017.
- [37] D. Mengin-Lecreulx, J. van Heijenoort, and J. T. Park, "Identification of the mpl gene encoding UDP-N-acetylmuramate: L-alanyl-gamma-D-glutamyl-meso-diaminopimelate ligase in Escherichia coli and its role in recycling of cell wall peptidoglycan," *Journal of Bacteriology*, vol. 178, pp. 5347–5352, sep 1996.
- [38] M. F. Templin, A. Ursinus, and J. V. Höltje, "A defect in cell wall recycling triggers autolysis during the stationary growth phase of Escherichia coli," *EMBO Journal*, vol. 18, no. 15, pp. 4108–4117, 1999.
- [39] M. A. de Pedro, J. C. Quintela, J. V. Höltje, and H. Schwarz, "Murein segregation in Escherichia coli.," *Journal of bacteriology*, vol. 179, no. 9, pp. 2823–2834, 1997.
- [40] L. G. Burman and J. T. Park, "Molecular model for elongation of the murein sacculus of Escherichia coli," *Proceedings of the National Academy of Sciences of the United States of America*, vol. 81, pp. 1844–1848, mar 1984.
- [41] G. A. Botta and J. T. Park, "Evidence for involvement of penicillin-binding protein 3 in murein synthesis during septation but not during cell elongation.," *Journal of Bacteriology*, vol. 145, no. 1, pp. 333–340, 1981.
- [42] M. A. de Pedro and U. Schwarz, "Heterogeneity of newly inserted and preexisting murein in the sacculus of Escherichia coli.," *Proceedings of the National Academy of Sciences*, vol. 78, pp. 5856–5860, sep 1981.
- [43] T. Uehara and J. T. Park, "Growth of Escherichia coli: Significance of Peptidoglycan Degradation during Elongation and Septation," *JOURNAL OF BACTERIOLOGY*, vol. 190, no. 11, pp. 3914–3922, 2008.
- [44] H. Cho, C. N. Wivagg, M. Kapoor, Z. Barry, P. D. A. Rohs, H. Suh, J. A. Marto, E. C. Garner, and T. G. Bernhardt, "Bacterial cell wall biogenesis is mediated by SEDS and PBP polymerase families functioning semi-autonomously," *Nature Microbiology*, vol. 1, p. 16172, oct 2016.

- [45] H. Cho, T. Uehara, and T. G. Bernhardt, "Beta-lactam antibiotics induce a lethal malfunctioning of the bacterial cell wall synthesis machinery," *Cell*, vol. 159, no. 6, pp. 1300–1311, 2014.
- [46] E. W. Goodell and U. Schwarz, "Release of cell wall peptides into culture medium by exponentially growing *Escherichia coli*," *Journal of Bacteriology*, vol. 162, no. 1, pp. 391–397, 1985.
- [47] C. Jacobs, L. Huang, E. Bartowsky, S. Normark, and J. Park, "Bacterial cell wall recycling provides cytosolic muropeptides as effectors for beta-lactamase induction.," *The EMBO Journal*, vol. 13, pp. 4684–4694, oct 1994.
- [48] B. Glauner and J. V. Holtje, "Growth pattern of the murein sacculus of *Escherichia coli*," *The Journal of biological chemistry*, vol. 265, pp. 18988–96, nov 1990.
- [49] F. B. Wientjes, E. Pas, P. E. Taschner, and C. L. Woldringh, "Kinetics of uptake and incorporation of meso-diaminopimelic acid in different *Escherichia coli* strains," *Journal of Bacteriology*, vol. 164, pp. 331–337, oct 1985.
- [50] L. G. Burman, J. Raichler, and J. T. Park, "Evidence for diffuse growth of the cylindrical portion of the *Escherichia coli* murein sacculus.," *Journal of Bacteriology*, vol. 155, no. 3, pp. 983–988, 1983.
- [51] R. W. Verwer and N. Nanninga, "Pattern of meso-DL-2,6-diaminopimelic acid incorporation during the division cycle of *Escherichia coli*," *Journal of Bacteriology*, vol. 144, no. 1, pp. 327–336, 1980.
- [52] S. M. Desmarais, F. Cava, M. A. de Pedro, and K. C. Huang, "Isolation and preparation of bacterial cell walls for compositional analysis by ultra performance liquid chromatography," *Journal of Visualized Experiments*, p. 51183, jan 2014.

Annex

Publication IV

Triboulet, S.; Edoo, Z.; Compain, F.; Ourghanlian, C.; Dupuis, A.; Dubée, V.; Sutterlin, L.; **Atze, H.**; Etheve-Quelquejeu, M.; Hugonnet, J. E.; Arthur, M. Tryptophan Fluorescence Quenching in β -Lactam-Interacting Proteins Is Modulated by the Structure of Intermediates and Final Products of the Acylation Reaction. ACS Infect. Dis. 2019.
<https://doi.org/10.1021/acsinfecdis.9b00023>.

References

- [Abodakpi et al., 2019] Abodakpi, H., Wanger, A., and Tam, V. H. (2019). What the Clinical Microbiologist Should Know About Pharmacokinetics/Pharmacodynamics in the Era of Emerging Multidrug Resistance. *Clinics in Laboratory Medicine*, 39(3):473–485.
- [Abraham and Chain, 1940] Abraham, E. P. and Chain, E. (1940). An Enzyme from Bacteria able to Destroy Penicillin. *Nature*, 146(3713):837–837.
- [Alcorlo et al., 2017] Alcorlo, M., Martínez-Caballero, S., Molina, R., and Hermoso, J. A. (2017). Carbohydrate recognition and lysis by bacterial peptidoglycan hydrolases.
- [Ambler, 1980] Ambler, R. (1980). The structure of β -lactamases. *Philosophical Transactions of the Royal Society of London. B, Biological Sciences*, 289(1036):321–331.
- [Ambrose et al., 2017] Ambrose, P. G., VanScoy, B. D., Trang, M., McCauley-Miller, J., Conde, H., Bhavnani, S. M., Alexander, D. C., and Friedrich, L. V. (2017). Pharmacokinetics-pharmacodynamics of CB-618 in combination with cefepime, ceftazidime, ceftolozane, or meropenem: The pharmacological basis for a stand-alone β -lactamase inhibitor. *Antimicrobial Agents and Chemotherapy*, 61(12).
- [Anandakrishnan et al., 2012] Anandakrishnan, R., Aguilar, B., and Onufriev, A. V. (2012). H++ 3.0: Automating pK prediction and the preparation of biomolecular structures for atomistic molecular modeling and simulations. *Nucleic Acids Research*.
- [Andrei et al., 2019] Andrei, S., Droc, G., and Stefan, G. (2019). FDA approved antibacterial drugs: 2018-2019. *Discoveries*, 7(4):e102.
- [Andrei et al., 2018] Andrei, S., Valeanu, L., Chirvasuta, R., and Stefan, M.-G. (2018). New FDA approved antibacterial drugs: 2015-2017. *Discoveries*, 6(1):e81.
- [ARCAMONE et al., 2000] ARCAMONE, F. M., AURAMURA, M., PERROTTA, E., CREA, A., MANZINI, S., POMA, D., SALIMBENI, A., TRIOLO, A., and MAGGI, C. A. (2000). Synthesis and Biological Activity of the Penem Antibiotic MEN 10700 and Its Orally Absorbed Ester MEN 11505. *The Journal of Antibiotics*, 53(10):1086–1095.
- [Asli et al., 2016] Asli, A., Brouillette, E., Krause, K. M., Nichols, W. W., and Malouin, F. (2016). Distinctive binding of avibactam to penicillin-binding proteins of gram-negative and gram-positive bacteria. *Antimicrobial Agents and Chemotherapy*, 60(2):752–756.
- [Asmar et al., 2017] Asmar, A. T., Ferreira, J. L., Cohen, E. J., Cho, S. H., Beeby, M., Hughes, K. T., and Collet, J. F. (2017). Communication across the bacterial cell envelope depends on the size of the periplasm. *PLoS Biology*.
- [Atze, 2021] Atze, H. (2021). kantundpeterpan/IsoTool: Thesis.
- [Banzhaf et al., 2020] Banzhaf, M., Yau, H. C., Verheul, J., Lodge, A., Kritikos, G., Mateus, A., Cordier, B., Hov, A. K., Stein, F., Wartel, M., Pazos, M., Solovyova, A. S., Breukink, E., van Teeffelen, S., Savitski, M. M., den Blaauwen, T., Typas, A., and Vollmer, W. (2020). Outer membrane lipoprotein NlpI scaffolds peptidoglycan hydrolases within multi-enzyme complexes in Escherichia coli. *The EMBO Journal*, 39(5):e102246.
- [Barnes et al., 2019] Barnes, M. D., Kumar, V., Bethel, C. R., Moussa, S. H., O'Donnell, J., Rutter, J. D., Good, C. E., Hujer, K. M., Hujer, A. M., Marshall, S. H., Kreiswirth, B. N., Richter, S. S., Rather, P. N., Jacobs, M. R., Papp-Wallace, K. M., van den Akker, F., and Bonomo, R. A. (2019). Targeting Multidrug-Resistant Acinetobacter spp.: Sulbactam and the Diazabicyclooctenone β -Lactamase Inhibitor ETX2514 as a Novel Therapeutic Agent. *mBio*, 10(2).
- [Bayer, 1968] Bayer, M. E. (1968). Adsorption of Bacteriophages to Adhesions Between Wall and Membrane of Escherichia coli. *Journal of Virology*.
- [Bebrone, 2007] Bebrone, C. (2007). Metallo- β -lactamases (classification, activity, genetic organization, structure, zinc coordination) and their superfamily. *Biochemical Pharmacology*, 74(12):1686–1701.
- [Bhattacharjee, 2016] Bhattacharjee, M. K. (2016). *Chemistry of Antibiotics and Related Drugs*. Springer International Publishing, Cham.

- [Billaudeau et al., 2017] Billaudeau, C., Chastanet, A., Yao, Z., Cornilleau, C., Mirouze, N., Fromion, V., and Carballido-López, R. (2017). Contrasting mechanisms of growth in two model rod-shaped bacteria. *Nature Communications*, 8(1):15370.
- [Blizzard et al., 2014] Blizzard, T. A., Chen, H., Kim, S., Wu, J., Bodner, R., Gude, C., Imbriglio, J., Young, K., Park, Y. W., Ogawa, A., Raghoobar, S., Hairston, N., Painter, R. E., Wisniewski, D., Scapin, G., Fitzgerald, P., Sharma, N., Lu, J., Ha, S., Hermes, J., and Hammond, M. L. (2014). Discovery of MK-7655, a β -lactamase inhibitor for combination with Primaxin®. *Bioorganic and Medicinal Chemistry Letters*, 24(3):780–785.
- [Bogdanov et al., 2020] Bogdanov, M., Pyrshev, K., Yesylevskyy, S., Ryabichko, S., Boiko, V., Ivanchenko, P., Kiyamova, R., Guan, Z., Ramseyer, C., and Dowhan, W. (2020). Phospholipid distribution in the cytoplasmic membrane of Gram-negative bacteria is highly asymmetric, dynamic, and cell shape-dependent. *Science Advances*, 6(23):eaaz6333.
- [Bonnefoy, 2004] Bonnefoy, A. (2004). In vitro activity of AVE1330A, an innovative broad-spectrum non- β -lactamase inhibitor. *Journal of Antimicrobial Chemotherapy*, 54(2):410–417.
- [Boyd, 1979] Boyd, D. B. (1979). Conformational analogy between β -lactam antibiotics and tetrahedral transition states of dipeptide. *Journal of Medicinal Chemistry*, 22(5):533–537.
- [Boyle et al., 1997] Boyle, D. S., Khattar, M. M., Addinall, S. G., Lutkenhaus, J., and Donachie, W. D. (1997). *ftsW* is an essential cell-division gene in *Escherichia coli*. *Molecular Microbiology*, 24(6):1263–1273.
- [Bradley et al., 1999] Bradley, J. S., Garau, J., Lode, H., Rolston, K. V., Wilson, S. E., and Quinn, J. P. (1999). Carbapenems in clinical practice: A guide to their use in serious infection.
- [Braun and Hantke, 2019] Braun, V. and Hantke, K. (2019). Lipoproteins: Structure, Function, Biosynthesis. In *Subcellular Biochemistry*, volume 92, pages 39–77. Springer New York.
- [Bulychev et al., 1997] Bulychev, A., Massova, I., Miyashita, K., and Mobashery, S. (1997). Nuances of Mechanisms and Their Implications for Evolution of the Versatile β -Lactamase Activity: From Biosynthetic Enzymes to Drug Resistance Factors. *Journal of the American Chemical Society*, 119(33):7619–7625.
- [Burman and Park, 1984] Burman, L. G. and Park, J. T. (1984). Molecular model for elongation of the murein sacculus of *Escherichia coli*. *Proceedings of the National Academy of Sciences of the United States of America*, 81(6 I):1844–1848.
- [Burman et al., 1983] Burman, L. G., Raichler, J., and Park, J. T. (1983). Evidence for diffuse growth of the cylindrical portion of the *Escherichia coli* murein sacculus. *Journal of Bacteriology*, 155(3):983–988.
- [Bush, 1989] Bush, K. (1989). Characterization of β -lactamases. *Antimicrobial Agents and Chemotherapy*.
- [Bush, 2013] Bush, K. (2013). The ABCD’s of β -lactamase nomenclature. *Journal of Infection and Chemotherapy*, 19(4):549–559.
- [Bush, 2018] Bush, K. (2018). Past and Present Perspectives on β -Lactamases. *Antimicrobial Agents and Chemotherapy*, 62(10).
- [Bush and Bradford, 2016] Bush, K. and Bradford, P. A. (2016). β -Lactams and β -Lactamase Inhibitors: An Overview. *Cold Spring Harbor Perspectives in Medicine*, 6(8):a025247.
- [Bush and Bradford, 2019] Bush, K. and Bradford, P. A. (2019). Interplay between β -lactamases and new β -lactamase inhibitors. *Nature Reviews Microbiology*, 17(5):295–306.
- [Bush and Jacoby, 2010] Bush, K. and Jacoby, G. A. (2010). Updated Functional Classification of β -Lactamases. *Antimicrobial Agents and Chemotherapy*, 54(3):969–976.
- [Bush et al., 1995] Bush, K., Jacoby, G. A., and Medeiros, A. A. (1995). A functional classification scheme for β -lactamases and its correlation with molecular structure. *Antimicrobial Agents and Chemotherapy*, 39(6):1211–1233.
- [Carpenter et al., 2016] Carpenter, T. S., Parkin, J., and Khalid, S. (2016). The Free Energy of Small Solute Permeation through the *Escherichia coli* Outer Membrane Has a Distinctly Asymmetric Profile. *Journal of Physical Chemistry Letters*, 7(17):3446–3451.

- [Cayley et al., 2000] Cayley, D. S., Guttman, H. J., and Record, M. T. (2000). Biophysical characterization of changes in amounts and activity of *Escherichia coli* cell and compartment water and turgor pressure in response to osmotic stress. *Biophysical Journal*, 78(4):1748–1764.
- [Chambers and DeLeo, 2009] Chambers, H. F. and DeLeo, F. R. (2009). Waves of resistance: *Staphylococcus aureus* in the antibiotic era.
- [Chen et al., 2017] Chen, A. Y., Thomas, P. W., Stewart, A. C., Bergstrom, A., Cheng, Z., Miller, C., Bethel, C. R., Marshall, S. H., Credille, C. V., Riley, C. L., Page, R. C., Bonomo, R. A., Crowder, M. W., Tierney, D. L., Fast, W., and Cohen, S. M. (2017). Dipicolinic Acid Derivatives as Inhibitors of New Delhi Metallo- β -lactamase-1. *Journal of Medicinal Chemistry*, 60(17):7267–7283.
- [Chen and Herzberg, 2001] Chen, C. C. H. and Herzberg, O. (2001). Structures of the Acyl-Enzyme Complexes of the *Staphylococcus aureus* β -Lactamase Mutant Glu166Asp:Asn170Gln with Benzylpenicillin and Cephalexin. *Biochemistry*, 40(8):2351–2358.
- [Chen et al., 2007] Chen, Y., Bonnet, R., and Shoichet, B. K. (2007). The Acylation Mechanism of CTX-M β -Lactamase at 0.88 Å Resolution. *Journal of the American Chemical Society*, 129(17):5378–5380.
- [Chen et al., 2009] Chen, Y., McReynolds, A., and Shoichet, B. K. (2009). Re-examining the role of Lys67 in class C β -lactamase catalysis. *Protein Science*, pages NA–NA.
- [Chen et al., 2006] Chen, Y., Minasov, G., Roth, T. A., Prati, F., and Shoichet, B. K. (2006). The Deacylation Mechanism of AmpC β -Lactamase at Ultrahigh Resolution. *Journal of the American Chemical Society*, 128(9):2970–2976.
- [Chesnel et al., 2002] Chesnel, L., Zapun, A., Mouz, N., Dideberg, O., and Vernet, T. (2002). Increase of the deacylation rate of PBP2x from *Streptococcus pneumoniae* by single point mutations mimicking the class A β -lactamases. *European Journal of Biochemistry*, 269(6):1678–1683.
- [Cho et al., 2014] Cho, H., Uehara, T., and Bernhardt, T. G. (2014). Beta-lactam antibiotics induce a lethal malfunctioning of the bacterial cell wall synthesis machinery. *Cell*, 159(6):1300–1311.
- [Cho et al., 2016] Cho, H., Wivagg, C. N., Kapoor, M., Barry, Z., Rohs, P. D. A., Suh, H., Marto, J. A., Garner, E. C., and Bernhardt, T. G. (2016). Bacterial cell wall biogenesis is mediated by SEDS and PBP polymerase families functioning semi-autonomously. *Nature Microbiology*, 1(10):16172.
- [Chodisetti and Reddy, 2019] Chodisetti, P. K. and Reddy, M. (2019). Peptidoglycan hydrolase of an unusual cross-link cleavage specificity contributes to bacterial cell wall synthesis. *Proceedings of the National Academy of Sciences*, 116(16):7825–7830.
- [Choi et al., 2016] Choi, H., Paton, R. S., Park, H., and Schofield, C. J. (2016). Investigations on recycling and hydrolysis in avibactam mediated serine β -lactamase inhibition. *Organic & Biomolecular Chemistry*, 14(17):4116–4128.
- [Cohen et al., 2017] Cohen, E. J., Ferreira, J. L., Ladinsky, M. S., Beeby, M., and Hughes, K. T. (2017). Nanoscale-length control of the flagellar driveshaft requires hitting the tethered outer membrane. *Science*, 356(6334):197–200.
- [Collia et al., 2018] Collia, D., Bannister, T. D., Tan, H., Jin, S., Langae, T., Shumate, J., Scampavia, L., and Spicer, T. P. (2018). A Rapid Phenotypic Whole-Cell Screening Approach for the Identification of Small-Molecule Inhibitors That Counter β -Lactamase Resistance in *Pseudomonas aeruginosa*. *SLAS DISCOVERY: Advancing the Science of Drug Discovery*, 23(1):55–64.
- [Coltharp et al., 2016] Coltharp, C., Buss, J., Plumer, T. M., and Xiao, J. (2016). Defining the rate-limiting processes of bacterial cytokinesis. *Proceedings of the National Academy of Sciences*, 113(8):E1044–E1053.
- [Compain and Arthur, 2017] Compain, F. and Arthur, M. (2017). Impaired Inhibition by Avibactam and Resistance to the Ceftazidime-Avibactam Combination Due to the D179Y Substitution in the KPC-2 β -Lactamase. *Antimicrobial Agents and Chemotherapy*, 61(7).
- [Copeland, 2005] Copeland, R. (2005). *Evaluation of Enzyme Inhibitors in Drug Discovery: A Guide for Medicinal Chemists and Pharmacologists*. Wiley.

- [Crowfoot et al., 1949] Crowfoot, D., Bunn, C. W., Rogers-Low, B.-W., and Turner-Jones, A. (1949). The X-Ray Crystallographic Investigation of the Structure of Penicillin. In *Chemistry of Penicillin*, pages 310–366. Princeton University Press.
- [Dalbey and Kuhn, 2012] Dalbey, R. E. and Kuhn, A. (2012). Protein Traffic in Gram-negative bacteria – how exported and secreted proteins find their way. *FEMS Microbiology Reviews*, 36(6):1023–1045.
- [Daley et al., 2016] Daley, D. O., Skoglund, U., and Söderström, B. (2016). FtsZ does not initiate membrane constriction at the onset of division. *Scientific Reports*, 6(1):33138.
- [Davies et al., 2020a] Davies, D. T., Leiris, S., Sprynski, N., Castandet, J., Lozano, C., Bousquet, J., Zalacain, M., Vasa, S., Dasari, P. K., Pattipati, R., Vempala, N., Gujjewar, S., Godi, S., Jallala, R., Sathyap, R. R., Darshanoju, N. A., Ravu, V. R., Juvenhala, R. R., Pottabathini, N., Sharma, S., Pothukanuri, S., Holden, K., Warn, P., Marcoccia, F., Benvenuti, M., Pozzi, C., Mangani, S., Docquier, J.-D., Lemonnier, M., and Everett, M. (2020a). ANT2681: SAR Studies Leading to the Identification of a Metallo- β -lactamase Inhibitor with Potential for Clinical Use in Combination with Meropenem for the Treatment of Infections Caused by NDM-Producing Enterobacteriaceae. *ACS Infectious Diseases*, 6(9):2419–2430.
- [Davies et al., 2020b] Davies, D. T., Leiris, S., Zalacain, M., Sprynski, N., Castandet, J., Bousquet, J., Lozano, C., Llanos, A., Alibaud, L., Vasa, S., Pattipati, R., Valige, R., Kummari, B., Pothukanuri, S., De Piano, C., Morrissey, I., Holden, K., Warn, P., Marcoccia, F., Benvenuti, M., Pozzi, C., Tassone, G., Mangani, S., Docquier, J. D., Pallin, D., Elliot, R., Lemonnier, M., and Everett, M. (2020b). Discovery of ANT3310, a Novel Broad-Spectrum Serine β -Lactamase Inhibitor of the Diazabicyclooctane Class, Which Strongly Potentiates Meropenem Activity against Carbapenem-Resistant Enterobacterales and *Acinetobacter baumannii*. *Journal of Medicinal Chemistry*, 63(24):15802–15820.
- [de Pedro et al., 1997] de Pedro, M. A., Quintela, J. C., Höltje, J. V., and Schwarz, H. (1997). Murein segregation in *Escherichia coli*. *Journal of bacteriology*, 179(9):2823–2834.
- [Delhay et al., 2019] Delhay, A., Collet, J.-F., and Laloux, G. (2019). A Fly on the Wall: How Stress Response Systems Can Sense and Respond to Damage to Peptidoglycan. *Frontiers in Cellular and Infection Microbiology*, 9:380.
- [Derouaux et al., 2008] Derouaux, A., Wolf, B., Fraipont, C., Breukink, E., Nguyen-Diste, Che, M., and Terrak, M. (2008). The Monofunctional Glycosyltransferase of *Escherichia coli* Localizes to the Cell Division Site and Interacts with Penicillin-Binding Protein 3, FtsW, and FtsN. *Journal of Bacteriology*, 190(5):1831–1834.
- [Di Berardino et al., 1996] Di Berardino, M., Dijkstra, A., Stüber, D., Keck, W., and Gubler, M. (1996). The monofunctional glycosyltransferase of *Escherichia coli* is a member of a new class of peptidoglycan-synthesising enzymes. *FEBS Letters*, 392(2):184–188.
- [Díaz et al., 2006] Díaz, N., Suárez, D., and Sordo, T. L. (2006). Molecular Dynamics Simulations of Class C β -Lactamase from *Citrobacter freundii* : Insights into the Base Catalyst for Acylation. *Biochemistry*, 45(2):439–451.
- [Dik et al., 2018] Dik, D. A., Fisher, J. F., and Mobashery, S. (2018). Cell-Wall Recycling of the Gram-Negative Bacteria and the Nexus to Antibiotic Resistance. *Chemical Reviews*, 118(12):5952–5984.
- [Dmitriev et al., 1999] Dmitriev, B. A., Ehlers, S., and Rietschel, E. T. (1999). Layered murein revisited: a fundamentally new concept of bacterial cell wall structure, biogenesis and function. *Medical Microbiology and Immunology*, 187(3):173–181.
- [Drawz and Bonomo, 2010] Drawz, S. M. and Bonomo, R. A. (2010). Three Decades of β -Lactamase Inhibitors. *Clinical Microbiology Reviews*, 23(1):160–201.
- [Drawz et al., 2014] Drawz, S. M., Papp-Wallace, K. M., and Bonomo, R. A. (2014). New β -lactamase inhibitors: A therapeutic renaissance in an MDR world. *Antimicrobial Agents and Chemotherapy*, 58(4):1835–1846.
- [Du and Lutkenhaus, 2017] Du, S. and Lutkenhaus, J. (2017). Assembly and activation of the *Escherichia coli* divisome. *Molecular Microbiology*, 105(2):177–187.
- [Dufresne and Paradis-Bleau, 2015] Dufresne, K. and Paradis-Bleau, C. (2015). Biology and Assembly of the Bacterial Envelope. In *Advances in Experimental Medicine and Biology*, volume 883, pages 41–76.

- [Durand-Réville et al., 2017] Durand-Réville, T. F., Guler, S., Comita-Prevoir, J., Chen, B., Bifulco, N., Huynh, H., Lahiri, S., Shapiro, A. B., McLeod, S. M., Carter, N. M., Moussa, S. H., Velez-Vega, C., Olivier, N. B., McLaughlin, R., Gao, N., Thresher, J., Palmer, T., Andrews, B., Giacobbe, R. A., Newman, J. V., Ehmann, D. E., de Jonge, B., O'Donnell, J., Mueller, J. P., Tommasi, R. A., and Miller, A. A. (2017). ETX2514 is a broad-spectrum β -lactamase inhibitor for the treatment of drug-resistant Gram-negative bacteria including *Acinetobacter baumannii*. *Nature Microbiology*, 2(9):17104.
- [Eastman et al., 2017] Eastman, P., Swails, J., Chodera, J. D., McGibbon, R. T., Zhao, Y., Beauchamp, K. A., Wang, L. P., Simmonett, A. C., Harrigan, M. P., Stern, C. D., Wiewiora, R. P., Brooks, B. R., and Pande, V. S. (2017). OpenMM 7: Rapid development of high performance algorithms for molecular dynamics. *PLoS Computational Biology*.
- [Edoo et al., 2018] Edoo, Z., Iannazzo, L., Compain, F., Li de la Sierra Gallay, I., van Tilbeurgh, H., Fonvielle, M., Bouchet, F., Le Run, E., Mainardi, J.-L., Arthur, M., Ethève-Quelquejeu, M., and Hugonnet, J.-E. (2018). Synthesis of Avibactam Derivatives and Activity on β -Lactamases and Peptidoglycan Biosynthesis Enzymes of Mycobacteria. *Chemistry - A European Journal*, 24(32):8081–8086.
- [Egan et al., 2020] Egan, A. J. F., Errington, J., and Vollmer, W. (2020). Regulation of peptidoglycan synthesis and remodelling. *Nature Reviews Microbiology*, 18(8):446–460.
- [Egan and Vollmer, 2013] Egan, A. J. F. and Vollmer, W. (2013). The physiology of bacterial cell division. *Annals of the New York Academy of Sciences*, 1277(1):8–28.
- [Ehmann et al., 2013] Ehmann, D. E., Jahić, H., Ross, P. L., Gu, R.-F., Hu, J., Durand-Réville, T. F., Lahiri, S., Thresher, J., Livchak, S., Gao, N., Palmer, T., Walkup, G. K., and Fisher, S. L. (2013). Kinetics of Avibactam Inhibition against Class A, C, and D β -Lactamases. *Journal of Biological Chemistry*, 288(39):27960–27971.
- [Ehmann et al., 2012] Ehmann, D. E., Jahic, H., Ross, P. L., Gu, R.-F., Hu, J., Kern, G., Walkup, G. K., and Fisher, S. L. (2012). Avibactam is a covalent, reversible, non- β -lactam-lactamase inhibitor. *Proceedings of the National Academy of Sciences*, 109(29):11663–11668.
- [El Kharroubi et al., 1991] El Kharroubi, A., Jacques, P., Piras, G., Van Beeumen, J., Coyette, J., and Ghuysen, J. M. (1991). The *Enterococcus hirae* R40 penicillin-binding protein 5 and the methicillin-resistant *Staphylococcus aureus* penicillin-binding protein 2' are similar. *Biochemical Journal*.
- [Escobar et al., 1991] Escobar, W. A., Tan, A. K., and Fink, A. L. (1991). Site-directed mutagenesis of β -lactamase leading to accumulation of a catalytic intermediate. *Biochemistry*, 30(44):10783–10787.
- [Everett et al., 2018] Everett, M., Sprynski, N., Coelho, A., Castandet, J., Bayet, M., Bougnon, J., Lozano, C., Davies, D. T., Leiris, S., Zalacain, M., Morrissey, I., Magnet, S., Holden, K., Warn, P., De Luca, F., Docquier, J.-D., and Lemonnier, M. (2018). Discovery of a Novel Metallo- β -Lactamase Inhibitor That Potentiates Meropenem Activity against Carbapenem-Resistant Enterobacteriaceae. *Antimicrobial Agents and Chemotherapy*, 62(5).
- [Finlay, 2003] Finlay, J. (2003). A review of the antimicrobial activity of clavulanate. *Journal of Antimicrobial Chemotherapy*, 52(1):18–23.
- [Fisher and Mobashery, 2014] Fisher, J. F. and Mobashery, S. (2014). The sentinel role of peptidoglycan recycling in the β -lactam resistance of the Gram-negative Enterobacteriaceae and *Pseudomonas aeruginosa*. *Bioorganic Chemistry*, 56:41–48.
- [Floto et al., 2016] Floto, R. A., Olivier, K. N., Saiman, L., Daley, C. L., Herrmann, J. L., Nick, J. A., Noone, P. G., Bilton, D., Corris, P., Gibson, R. L., Hempstead, S. E., Koetz, K., Sabadosa, K. A., Sermet-Gaudelus, I., Smyth, A. R., van Ingen, J., Wallace, R. J., Winthrop, K. L., Marshall, B. C., and Haworth, C. S. (2016). US Cystic Fibrosis Foundation and European Cystic Fibrosis Society consensus recommendations for the management of non-tuberculous mycobacteria in individuals with cystic fibrosis. In *Thorax*, volume 71, pages i1–i22. BMJ Publishing Group.
- [Fuda et al., 2005] Fuda, C., Hessek, D., Lee, M., Morio, K.-I., Nowak, T., and Mobashery, S. (2005). Activation for Catalysis of Penicillin-Binding Protein 2a from Methicillin-Resistant *Staphylococcus aureus* by Bacterial Cell Wall. *Journal of the American Chemical Society*, 127(7):2056–2057.

- [Fujiu et al., 2020] Fujiu, M., Yokoo, K., Sato, J., Shibuya, S., Komano, K., Kusano, H., Sato, S., Aoki, T., Kohira, N., Miyagawa, S., Kawachi, T., and Yamawaki, K. (2020). Introduction of a Thio Functional Group to Diazabicyclooctane: An Effective Modification to Potentiate the Activity of β -Lactams against Gram-Negative Bacteria Producing Class A, C, and D Serine β -Lactamases. *ACS Infectious Diseases*, 6(11):3034–3047.
- [Garner et al., 2011] Garner, E. C., Bernard, R., Wang, W., Zhuang, X., Rudner, D. Z., and Mitchison, T. (2011). Coupled, Circumferential Motions of the Cell Wall Synthesis Machinery and MreB Filaments in *B. subtilis*. *Science*, 333(6039):222–225.
- [Gherman et al., 2004] Gherman, B. F., Goldberg, S. D., Cornish, V. W., and Friesner, R. A. (2004). Mixed Quantum Mechanical/Molecular Mechanical (QM/MM) Study of the Deacylation Reaction in a Penicillin Binding Protein (PBP) versus in a Class C β -Lactamase. *Journal of the American Chemical Society*, 126(24):7652–7664.
- [Glauner, 1988] Glauner, B. (1988). Separation and quantification of mucopeptides with high-performance liquid chromatography. *Analytical Biochemistry*, 172(2):451–464.
- [Glauner and Holtje, 1990] Glauner, B. and Holtje, J. V. (1990). Growth pattern of the murein sacculus of *Escherichia coli*. *The Journal of biological chemistry*, 265(31):18988–96.
- [Golemi et al., 2001] Golemi, D., Maveyraud, L., Vakulenko, S., Samama, J.-P., and Mobashery, S. (2001). Critical involvement of a carbamylated lysine in catalytic function of class D -lactamases. *Proceedings of the National Academy of Sciences*, 98(25):14280–14285.
- [González-Bello et al., 2020] González-Bello, C., Rodríguez, D., Pernas, M., Rodríguez, Á., and Colchón, E. (2020). β -Lactamase Inhibitors to Restore the Efficacy of Antibiotics against Superbugs. *Journal of Medicinal Chemistry*, 63(5):1859–1881.
- [Goodell, 1985] Goodell, E. W. (1985). Recycling of murein by *Escherichia coli*. *Journal of Bacteriology*, 163(1):305–310.
- [Gray et al., 2015] Gray, A. N., Egan, A. J., van’t Veer, I. L., Verheul, J., Colavin, A., Koumoutsis, A., Biboy, J., Altelaar, A. F. M., Damen, M. J., Huang, K. C., Simorre, J.-P., Breukink, E., den Blaauwen, T., Typas, A., Gross, C. A., and Vollmer, W. (2015). Coordination of peptidoglycan synthesis and outer membrane constriction during *Escherichia coli* cell division. *eLife*, 4.
- [Gumbart et al., 2014] Gumbart, J. C., Beeby, M., Jensen, G. J., and Roux, B. (2014). *Escherichia coli* Peptidoglycan Structure and Mechanics as Predicted by Atomic-Scale Simulations. *PLoS Computational Biology*, 10(2):e1003475.
- [Hakenbeck et al., 1991] Hakenbeck, R., Briese, T., Laible, G., Martin, C., and Schuster, C. (1991). Penicillin-binding proteins in *Streptococcus pneumoniae*: Alterations during development of intrinsic penicillin resistance. *Journal of Chemotherapy*.
- [Hall and Barlow, 2004] Hall, B. G. and Barlow, M. (2004). Evolution of the serine β -lactamases: past, present and future. *Drug Resistance Updates*, 7(2):111–123.
- [Hall and Schwarz, 2016] Hall, R. M. and Schwarz, S. (2016). Resistance gene naming and numbering: is it a new gene or not? *Journal of Antimicrobial Chemotherapy*, 71(3):569–571.
- [Hamilton-Miller, 2003] Hamilton-Miller, J. M. (2003). Chemical and Microbiologic Aspects of Penems, a Distinct Class of β -Lactams: Focus on Faropenem. *Pharmacotherapy*, 23(11):1497–1507.
- [Hamilton-Miller, 1979] Hamilton-Miller, J. M. T. (1979). An historical introduction to beta-lactamase.
- [Hara and Suzuki, 1984] Hara, H. and Suzuki, H. (1984). A novel glycan polymerase that synthesizes uncross-linked peptidoglycan in *Escherichia coli*. *FEBS Letters*, 168(1):155–160.
- [Harder et al., 1981] Harder, K. J., Nikaido, H., and Matsushashi, M. (1981). Mutants of *Escherichia coli* that are resistant to certain beta-lactam compounds lack the ompF porin. *Antimicrobial Agents and Chemotherapy*.
- [Hecker et al., 2020] Hecker, S. J., Reddy, K. R., Lomovskaya, O., Griffith, D. C., Rubio-Aparicio, D., Nelson, K., Tsivkovski, R., Sun, D., Sabet, M., Tarazi, Z., Parkinson, J., Totrov, M., Boyer, S. H., Glinka, T. W., Pemberton, O. A., Chen, Y., and Dudley, M. N. (2020). Discovery of Cyclic Boronic Acid QPX7728, an Ultrabroad-Spectrum Inhibitor of Serine and Metallo- β -lactamases. *Journal of Medicinal Chemistry*, 63(14):7491–7507.

- [Heidrich et al., 2001] Heidrich, C., Templin, M. F., Ursinus, A., Merdanovic, M., Berger, J., Schwarz, H., De Pedro, M. A., and Höltje, J.-V. (2001). Involvement of N-acetylmuramyl-L-alanine amidases in cell separation and antibiotic-induced autolysis of *Escherichia coli*. *Molecular Microbiology*, 41(1):167–178.
- [Heidrich et al., 2002] Heidrich, C., Ursinus, A., Berger, J., Schwarz, H., and Höltje, J.-V. (2002). Effects of Multiple Deletions of Murein Hydrolases on Viability, Septum Cleavage, and Sensitivity to Large Toxic Molecules in *Escherichia coli*. *Journal of Bacteriology*, 184(22):6093–6099.
- [Heijenoort, 2001] Heijenoort, J. v. (2001). Formation of the glycan chains in the synthesis of bacterial peptidoglycan. *Glycobiology*, 11(3):25R–36R.
- [Hermann et al., 2005] Hermann, J. C., Hensen, C., Ridder, L., Mulholland, A. J., and Höltje, H.-D. (2005). Mechanisms of Antibiotic Resistance: QM/MM Modeling of the Acylation Reaction of a Class A β -Lactamase with Benzylpenicillin. *Journal of the American Chemical Society*, 127(12):4454–4465.
- [Hermann et al., 2009] Hermann, J. C., Pradon, J., Harvey, J. N., and Mulholland, A. J. (2009). High Level QM/MM Modeling of the Formation of the Tetrahedral Intermediate in the Acylation of Wild Type and K73A Mutant TEM-1 Class A β -Lactamase †. *The Journal of Physical Chemistry A*, 113(43):11984–11994.
- [Hermann et al., 2003] Hermann, J. C., Ridder, L., Mulholland, A. J., and Höltje, H.-D. (2003). Identification of Glu166 as the General Base in the Acylation Reaction of Class A β -Lactamases through QM/MM Modeling. *Journal of the American Chemical Society*, 125(32):9590–9591.
- [Herve et al., 2007] Herve, M., Boniface, A., Gobec, S., Blanot, D., and Mengin-Lecreulx, D. (2007). Biochemical Characterization and Physiological Properties of *Escherichia coli* UDP-N-Acetylmuramate:1-Alanyl- γ -D-Glutamyl-meso-Diaminopimelate Ligase. *Journal of Bacteriology*, 189(11):3987–3995.
- [Holden, 1984] Holden, K. (1984). Cephalosporins. In *Comprehensive Heterocyclic Chemistry*, pages 285–298. Elsevier.
- [Holst, 2007] Holst, O. (2007). The structures of core regions from enterobacterial lipopolysaccharides an update. *FEMS Microbiology Letters*, 271(1):3–11.
- [Höltje, 1998] Höltje, J. V. (1998). Growth of the stress-bearing and shape-maintaining murein sacculus of *Escherichia coli*. *Microbiology and molecular biology reviews : MMBR*, 62(1):181–203.
- [Honoré et al., 1986] Honoré, N., Nicolas, M., and Cole, S. (1986). Inducible cephalosporinase production in clinical isolates of *Enterobacter cloacae* is controlled by a regulatory gene that has been deleted from *Escherichia coli*. *The EMBO Journal*, 5(13):3709–3714.
- [Hubschwerlen, 2007] Hubschwerlen, C. (2007). β -Lactam Antibiotics. In *Comprehensive Medicinal Chemistry II*, pages 479–518. Elsevier.
- [Hugonnet et al., 2016] Hugonnet, J. E., Mengin-Lecreulx, D., Monton, A., den Blaauwen, T., Carbonnelle, E., Veckerlé, C., Yves, V. B., van Nieuwenhze, M., Bouchier, C., Tu, K., Rice, L. B., and Arthur, M. (2016). Factors essential for L,D-transpeptidase-mediated peptidoglycan cross-linking and β -lactam resistance in *Escherichia coli*. *eLife*, 5(OCTOBER2016):1–22.
- [Indelicato et al., 1974] Indelicato, J. M., Norvilas, T. T., Pfeiffer, R. R., Wheeler, W. J., and Wilham, W. L. (1974). Substituent effects upon the base hydrolysis of penicillins and cephalosporins. Competitive intramolecular nucleophilic amino attack in cephalosporins. *Journal of Medicinal Chemistry*, 17(5):523–527.
- [Ishino et al., 1986] Ishino, F., Park, W., Tomioka, S., Tamaki, S., Takase, I., Kunugita, K., Matsuzawa, H., Asoh, S., Ohta, T., and Spratt, B. G. (1986). Peptidoglycan synthetic activities in membranes of *Escherichia coli* caused by overproduction of penicillin-binding protein 2 and rodA protein. *Journal of Biological Chemistry*, 261(15):7024–7031.
- [Jacob et al., 1990] Jacob, F., Joris, B., Lepage, S., Dusart, J., and Frère, J. M. (1990). Role of the conserved amino acids of the ‘SDN’ loop (Ser130, Asp131 and Asn132) in a class A β -lactamase studied by site-directed mutagenesis. *Biochemical Journal*, 271(2):399–406.
- [Jacobs et al., 1997] Jacobs, C., Frère, J.-M., and Normark, S. (1997). Cytosolic Intermediates for Cell Wall Biosynthesis and Degradation Control Inducible β -Lactam Resistance in Gram-Negative Bacteria. *Cell*, 88(6):823–832.

- [Jacobs et al., 1994] Jacobs, C., Huang, L., Bartowsky, E., Normark, S., and Park, J. (1994). Bacterial cell wall recycling provides cytosolic muropeptides as effectors for beta-lactamase induction. *The EMBO Journal*, 13(19):4684–4694.
- [Jacoby, 2009] Jacoby, G. A. (2009). AmpC β -Lactamases. *Clinical Microbiology Reviews*, 22(1):161–182.
- [Jae et al., 2005] Jae, S. S., Jeong, H. J., Jung, H. L., Seok, H. J., Byeong, C. J., Kim, S. J., Lee, J. H., and Sang, H. L. (2005). Molecular characterization of TEM-type β -lactamases identified in cold-seep sediments of edison seamount (South of Lihir Island, Papua New Guinea). *Journal of Microbiology*.
- [Johnson et al., 2013] Johnson, J. W., Fisher, J. F., and Mobashery, S. (2013). Bacterial cell-wall recycling. *Annals of the New York Academy of Sciences*, 1277(1):54–75.
- [Kahan et al., 1983] Kahan, F. M., Kropp, H., Sundelof, J. G., and Birnbaum, J. (1983). Thienamycin: development of imipenem-cilastatin. *Journal of Antimicrobial Chemotherapy*, 12(suppl D):1–35.
- [Kahan et al., 1979] Kahan, J. S., Kahan, F. M., Goegelman, R., Currie, S. A., Jackson, M., Stapley, E. O., Miller, T. W., Miller, A. K., Hendlin, D., Woodruff, H. B., Birnbaum, J., Mochales, S., and Hernandez, S. (1979). Thienamycin, a new β -lactam antibiotic i. discovery, taxonomy, isolation and physical properties. *The Journal of Antibiotics*.
- [Kaneko et al., 2005] Kaneko, K., Okamoto, R., Nakano, R., Kawakami, S., and Inoue, M. (2005). Gene mutations responsible for overexpression of AmpC β -lactamase in some clinical isolates of *Enterobacter cloacae*. *Journal of Clinical Microbiology*, 43(6):2955–2958.
- [KATO-TOMA et al., 2003] KATO-TOMA, Y., IWASHITA, T., MASUDA, K., OYAMA, Y., and ISHIGURO, M. (2003). pKa measurements from nuclear magnetic resonance of tyrosine-150 in class C beta-lactamase. *Biochemical Journal*, 371(1):175–181.
- [Kawai et al., 2009] Kawai, Y., Daniel, R. A., and Errington, J. (2009). Regulation of cell wall morphogenesis in *Bacillus subtilis* by recruitment of PBP1 to the MreB helix. *Molecular Microbiology*, 71(5):1131–1144.
- [Kawazura et al., 2017] Kawazura, T., Matsumoto, K., Kojima, K., Kato, F., Kanai, T., Niki, H., and Shiomi, D. (2017). Exclusion of assembled MreB by anionic phospholipids at cell poles confers cell polarity for bidirectional growth. *Molecular Microbiology*, 104(3):472–486.
- [Ke et al., 2012] Ke, W., Rodkey, E. A., Sampson, J. M., Skalweit, M. J., Sheri, A., Pagadala, S. R. R., Nottingham, M. D., Buynak, J. D., Bonomo, R. A., and van den Akker, F. (2012). The Importance of the trans-Enamine Intermediate as a β -Lactamase Inhibition Strategy Probed in Inhibitor-Resistant SHV β -Lactamase Variants. *ChemMedChem*, 7(6):1002–1008.
- [Keighley, 2011] Keighley, W. (2011). The Need for High Throughput Kinetics Early in the Drug Discovery Process.
- [King et al., 2016a] King, A. M., King, D. T., French, S., Brouillette, E., Asli, A., Alexander, J. A. N., Vuckovic, M., Maiti, S. N., Parr, T. R., Brown, E. D., Malouin, F., Strynadka, N. C., and Wright, G. D. (2016a). Structural and Kinetic Characterization of Diazabicyclooctanes as Dual Inhibitors of Both Serine- β -Lactamases and Penicillin-Binding Proteins. *ACS Chemical Biology*, 11(4):864–868.
- [King et al., 2016b] King, D. T., King, A. M., Lal, S. M., Wright, G. D., and Strynadka, N. C. (2016b). Molecular Mechanism of Avibactam-Mediated β -Lactamase Inhibition. *ACS Infectious Diseases*, 1(4):175–184.
- [King et al., 2017a] King, D. T., Sobhanifar, S., and Strynadka, N. C. J. (2017a). The Mechanisms of Resistance to β -Lactam Antibiotics. In *Handbook of Antimicrobial Resistance*, pages 177–201. Springer New York, New York, NY.
- [King et al., 2017b] King, D. T., Wasney, G. A., Nosella, M., Fong, A., and Strynadka, N. C. (2017b). Structural Insights into Inhibition of *Escherichia coli* Penicillin-binding Protein 1B. *Journal of Biological Chemistry*, 292(3):979–993.
- [Klare et al., 1992] Klare, I., Rodloff, A. C., Wagner, J., Witte, W., and Hakenbeck, R. (1992). Overproduction of a penicillin-binding protein is not the only mechanism of penicillin resistance in *Enterococcus faecium*. *Antimicrobial Agents and Chemotherapy*.

- [Kocaoglu and Carlson, 2015] Kocaoglu, O. and Carlson, E. E. (2015). Profiling of β -lactam selectivity for penicillin-binding proteins in *Escherichia coli* strain DC2. *Antimicrobial Agents and Chemotherapy*, 59(5):2785–2790.
- [KONG et al., 2010] KONG, K.-F., SCHNEPER, L., and MATHEE, K. (2010). Beta-lactam antibiotics: from antibiosis to resistance and bacteriology. *APMIS*, 118(1):1–36.
- [Konovalova and Silhavy, 2015] Konovalova, A. and Silhavy, T. J. (2015). Outer membrane lipoprotein biogenesis: Lol is not the end. *Philosophical Transactions of the Royal Society B: Biological Sciences*, 370(1679):20150030.
- [Kourtesi et al., 2013] Kourtesi, C., Ball, A. R., Huang, Y.-Y., Jachak, S. M., Vera, D. M. A., Khondkar, P., Gibbons, S., Hamblin, M. R., and Tegos, G. P. (2013). Microbial Efflux Systems and Inhibitors: Approaches to Drug Discovery and the Challenge of Clinical Implementation. *The Open Microbiology Journal*.
- [Krajnc et al., 2019] Krajnc, A., Brem, J., Hinchliffe, P., Calvopiña, K., Panduwawala, T. D., Lang, P. A., Kamps, J. J. A. G., Tyrrell, J. M., Widlake, E., Seward, B. G., Walsh, T. R., Spencer, J., and Schofield, C. J. (2019). Bicyclic Boronate VNRX-5133 Inhibits Metallo- and Serine- β -Lactamases. *Journal of Medicinal Chemistry*, 62(18):8544–8556.
- [Kruse et al., 2005] Kruse, T., Bork-Jensen, J., and Gerdes, K. (2005). The morphogenetic MreBCD proteins of *Escherichia coli* form an essential membrane-bound complex. *Molecular Microbiology*, 55(1):78–89.
- [Labischinski et al., 1991] Labischinski, H., Goodell, E. W., Goodell, A., and Hochberg, M. L. (1991). Direct proof of a 'more-than-single-layered' peptidoglycan architecture of *Escherichia coli* W7: A neutron small-angle scattering study. *Journal of Bacteriology*, 173(2):751–756.
- [Lacki et al., 2017] Lacki, M. K., Startek, M., Valkenborg, D., and Gambin, A. (2017). IsoSpec: Hyper-fast Fine Structure Calculator. *Analytical Chemistry*, 89(6):3272–3277.
- [Lahiri et al., 2016] Lahiri, S. D., Bradford, P. A., Nichols, W. W., and Alm, R. A. (2016). Structural and sequence analysis of class A β -lactamases with respect to avibactam inhibition: impact of Ω -loop variations. *Journal of Antimicrobial Chemotherapy*, 71(10):2848–2855.
- [Lahiri et al., 2013] Lahiri, S. D., Mangani, S., Durand-Reville, T., Benvenuti, M., De Luca, F., Sanyal, G., and Docquier, J.-D. (2013). Structural Insight into Potent Broad-Spectrum Inhibition with Reversible Recyclization Mechanism: Avibactam in Complex with CTX-M-15 and *Pseudomonas aeruginosa* AmpC β -Lactamases. *Antimicrobial Agents and Chemotherapy*, 57(6):2496–2505.
- [Lahiri et al., 2015] Lahiri, S. D., Mangani, S., Jahić, H., Benvenuti, M., Durand-Reville, T. F., De Luca, F., Ehmann, D. E., Rossolini, G. M., Alm, R. A., and Docquier, J.-D. (2015). Molecular Basis of Selective Inhibition and Slow Reversibility of Avibactam against Class D Carbapenemases: A Structure-Guided Study of OXA-24 and OXA-48. *ACS Chemical Biology*, 10(2):591–600.
- [Lambert, 2005] Lambert, P. A. (2005). Bacterial resistance to antibiotics: Modified target sites. *Advanced Drug Delivery Reviews*, 57(10):1471–1485.
- [Langan et al., 2018] Langan, P. S., Vandavasi, V. G., Cooper, S. J., Weiss, K. L., Ginell, S. L., Parks, J. M., and Coates, L. (2018). Substrate Binding Induces Conformational Changes in a Class A β -lactamase That Prime It for Catalysis. *ACS Catalysis*, 8(3):2428–2437.
- [Lapuebla et al., 2015] Lapuebla, A., Abdallah, M., Olafisoye, O., Cortes, C., Urban, C., Landman, D., and Quale, J. (2015). Activity of imipenem with relebactam against gram-negative pathogens from New York City. *Antimicrobial Agents and Chemotherapy*, 59(8):5029–5031.
- [Lara et al., 2005] Lara, B., Mengin-Lecreulx, D., Ayala, J. A., and Van Heijenoort, J. (2005). Peptidoglycan precursor pools associated with MraY and FtsW deficiencies or antibiotic treatments. *FEMS Microbiology Letters*, 250(2):195–200.
- [Lavollay et al., 2008] Lavollay, M., Arthur, M., Fourgeaud, M., Dubost, L., Marie, A., Veziris, N., Blanot, D., Gutmann, L., and Mainardi, J.-L. (2008). The Peptidoglycan of Stationary-Phase *Mycobacterium tuberculosis* Predominantly Contains Cross-Links Generated by L,D-Transpeptidation. *Journal of Bacteriology*, 190(12):4360–4366.

- [Lebeaux et al., 2019] Lebeaux, D., Ourghanlian, C., Dorcène, D., Soroka, D., Edoo, Z., Compain, F., and Arthur, M. (2019). Inhibition Activity of Avibactam against *Nocardia farcinica* β -Lactamase FAR IFM10152. *Antimicrobial Agents and Chemotherapy*, 64(2).
- [Lee et al., 2013] Lee, M., Heseck, D., Llarrull, L. I., Lastochkin, E., Pi, H., Boggess, B., and Mobashery, S. (2013). Reactions of All *Escherichia coli* Lytic Transglycosylases with Bacterial Cell Wall.
- [Lee et al., 2014] Lee, T. K., Tropini, C., Hsin, J., Desmarais, S. M., Ursell, T. S., Gong, E., Gitai, Z., Monds, R. D., and Huang, K. C. (2014). A dynamically assembled cell wall synthesis machinery buffers cell growth. *Proceedings of the National Academy of Sciences*, 111(12):4554–4559.
- [Leiris et al., 2019] Leiris, S., Coelho, A., Castandet, J., Bayet, M., Lozano, C., Bougnon, J., Bousquet, J., Everett, M., Lemonnier, M., Sprynski, N., Zalacain, M., Pallin, T. D., Cramp, M. C., Jennings, N., Raphy, G., Jones, M. W., Pattipati, R., Shankar, B., Sivasubrahmanyam, R., Soodhagani, A. K., Juvenhala, R. R., Pottabathini, N., Pothukanuri, S., Benvenuti, M., Pozzi, C., Mangani, S., De Luca, F., Cerboni, G., Docquier, J.-D., and Davies, D. T. (2019). SAR Studies Leading to the Identification of a Novel Series of Metallo- β -lactamase Inhibitors for the Treatment of Carbapenem-Resistant Enterobacteriaceae Infections That Display Efficacy in an Animal Infection Model. *ACS Infectious Diseases*, 5(1):131–140.
- [Leonard et al., 2013] Leonard, D. A., Bonomo, R. A., and Powers, R. A. (2013). Class D β -Lactamases: A Reappraisal after Five Decades. *Accounts of Chemical Research*, 46(11):2407–2415.
- [Levy et al., 2019] Levy, N., Bruneau, J.-M., Le Rouzic, E., Bonnard, D., Le Strat, F., Caravano, A., Chevreuil, F., Barbion, J., Chasset, S., Ledoussal, B., Moreau, F., and Ruff, M. (2019). Structural Basis for *E. coli* Penicillin Binding Protein (PBP) 2 Inhibition, a Platform for Drug Design. *Journal of Medicinal Chemistry*, 62(9):4742–4754.
- [Lim and Strynadka, 2002] Lim, D. and Strynadka, N. C. (2002). Structural basis for the β lactam resistance of PBP2a from methicillin-resistant *Staphylococcus aureus*. *Nature Structural Biology*.
- [Lindberg et al., 1985] Lindberg, F., Westman, L., and Normark, S. (1985). Regulatory components in *Citrobacter freundii* ampC beta-lactamase induction. *Proceedings of the National Academy of Sciences*, 82(14):4620–4624.
- [Livermore et al., 2018] Livermore, D. M., Meunier, D., Hopkins, K. L., Doumith, M., Hill, R., Pike, R., Staves, P., and Woodford, N. (2018). Activity of ceftazidime/avibactam against problem Enterobacteriaceae and *Pseudomonas aeruginosa* in the UK, 2015–16. *Journal of Antimicrobial Chemotherapy*, 73(3):648–657.
- [Llarrull et al., 2008] Llarrull, L. I., Tioni, M. F., and Vila, A. J. (2008). Metal Content and Localization during Turnover in *B. cereus* Metallo- β -lactamase. *Journal of the American Chemical Society*, 130(47):15842–15851.
- [Lou et al., 2011] Lou, H., Chen, M., Black, S. S., Bushell, S. R., Ceccarelli, M., Mach, T., Beis, K., Low, A. S., Bamford, V. A., Booth, I. R., Bayley, H., and Naismith, J. H. (2011). Altered antibiotic transport in OmpC mutants isolated from a series of clinical strains of multi-drug resistant *E. coli*. *PLoS ONE*.
- [Lu et al., 2001] Lu, W.-P., Kincaid, E., Sun, Y., and Bauer, M. D. (2001). Kinetics of β -Lactam Interactions with Penicillin-susceptible and -resistant Penicillin-binding Protein 2x Proteins from *Streptococcus pneumoniae*. *Journal of Biological Chemistry*, 276(34):31494–31501.
- [Madoori and Thunnissen, 2010] Madoori, P. K. and Thunnissen, A.-M. W. H. (2010). Purification, crystallization and preliminary X-ray diffraction analysis of the lytic transglycosylase MltF from *Escherichia coli*. *Acta Crystallographica Section F Structural Biology and Crystallization Communications*, 66(5):534–538.
- [Maeshima and Fernandez, 2013] Maeshima, N. and Fernandez, R. C. (2013). Recognition of lipid A variants by the TLR4-MD-2 receptor complex. *Frontiers in Cellular and Infection Microbiology*, 4(FEB):1–13.
- [Magnet et al., 2007] Magnet, S., Bellais, S., Dubost, L., Fourgeaud, M., Mainardi, J.-L., Petit-Frere, S., Marie, A., Mengin-Lecreulx, D., Arthur, M., and Gutmann, L. (2007). Identification of the L,d-Transpeptidases Responsible for Attachment of the Braun Lipoprotein to *Escherichia coli* Peptidoglycan. *Journal of Bacteriology*, 189(10):3927–3931.

- [Magnet et al., 2008] Magnet, S., Dubost, L., Marie, A., Arthur, M., and Gutmann, L. (2008). Identification of the 1,d-Transpeptidases for Peptidoglycan Cross-Linking in *Escherichia coli*. *Journal of Bacteriology*, 190(13):4782–4785.
- [Maier et al., 2015] Maier, J. A., Martinez, C., Kasavajhala, K., Wickstrom, L., Hauser, K. E., and Simmerling, C. (2015). ff14SB: Improving the Accuracy of Protein Side Chain and Backbone Parameters from ff99SB. *Journal of Chemical Theory and Computation*.
- [Mainardi et al., 2005] Mainardi, J.-L., Fourgeaud, M., Hugonnet, J.-E., Dubost, L., Brouard, J.-P., Ouazzani, J., Rice, L. B., Gutmann, L., and Arthur, M. (2005). A novel peptidoglycan cross-linking enzyme for a beta-lactam-resistant transpeptidation pathway. *The Journal of biological chemistry*, 280(46):38146–52.
- [Marchand-Brynaert and Brulé, 2008] Marchand-Brynaert, J. and Brulé, C. (2008). Penicillins. In *Comprehensive Heterocyclic Chemistry III*, pages 173–237. Elsevier.
- [Marrero et al., 2006] Marrero, A., Mallorquí-Fernández, G., Guevara, T., García-Castellanos, R., and Gomis-Rüth, F. X. (2006). Unbound and Acylated Structures of the MecR1 Extracellular Antibiotic-sensor Domain Provide Insights into the Signal-transduction System that Triggers Methicillin Resistance. *Journal of Molecular Biology*, 361(3):506–521.
- [Marshall et al., 2017] Marshall, S., Hujer, A. M., Rojas, L. J., Papp-Wallace, K. M., Humphries, R. M., Spellberg, B., Hujer, K. M., Marshall, E. K., Rudin, S. D., Perez, F., Wilson, B. M., Wasserman, R. B., Chikowski, L., Paterson, D. L., Vila, A. J., van Duin, D., Kreiswirth, B. N., Chambers, H. F., Fowler, V. G., Jacobs, M. R., Pulse, M. E., Weiss, W. J., and Bonomo, R. A. (2017). Can Ceftazidime-Avibactam and Aztreonam Overcome β -Lactam Resistance Conferred by Metallo- β -Lactamases in Enterobacteriaceae? *Antimicrobial Agents and Chemotherapy*, 61(4).
- [Martin and Jones, 1995] Martin, R. and Jones, J. B. (1995). Rational design and synthesis of a highly effective transition state analog inhibitor of the RTEM-1 β -lactamase. *Tetrahedron Letters*, 36(46):8399–8402.
- [Massova and Mobashery, 1998] Massova, I. and Mobashery, S. (1998). Kinship and Diversification of Bacterial Penicillin-Binding Proteins and β -Lactamases. *Antimicrobial Agents and Chemotherapy*, 42(1):1–17.
- [Matias et al., 2003] Matias, V. R. F., Al-Amoudi, A., Dubochet, J., and Beveridge, T. J. (2003). Cryo-Transmission Electron Microscopy of Frozen-Hydrated Sections of *Escherichia coli* and *Pseudomonas aeruginosa*. *JOURNAL OF BACTERIOLOGY*, 185(20):6112–6118.
- [Matsuzawa et al., 1973] Matsuzawa, H., Hayakawa, K., Sato, T., and Imahori, K. (1973). Characterization and Genetic Analysis of a Mutant of *Escherichia coli* K-12 with Rounded Morphology. *Journal of Bacteriology*, 115(1):436–442.
- [Maveyraud et al., 2002] Maveyraud, L., Golemi-Kotra, D., Ishiwata, A., Meroueh, O., Mobashery, S., and Samama, J.-P. (2002). High-Resolution X-ray Structure of an Acyl-Enzyme Species for the Class D OXA-10 β -Lactamase. *Journal of the American Chemical Society*, 124(11):2461–2465.
- [Maveyraud et al., 1998] Maveyraud, L., Pratt, R. F., and Samama, J. P. (1998). Crystal structure of an acylation transition-state analog of the TEM-1 β -lactamase. Mechanistic implications for class A β -lactamases. *Biochemistry*, 37(8):2622–2628.
- [McPherson and Popham, 2003] McPherson, D. C. and Popham, D. L. (2003). Peptidoglycan Synthesis in the Absence of Class A Penicillin-Binding Proteins in *Bacillus subtilis*. *Journal of Bacteriology*, 185(4):1423–1431.
- [Meeske et al., 2016] Meeske, A. J., Riley, E. P., Robins, W. P., Uehara, T., Mekalanos, J. J., Kahne, D., Walker, S., Kruse, A. C., Bernhardt, T. G., and Rudner, D. Z. (2016). SEDS proteins are a widespread family of bacterial cell wall polymerases. *Nature*, 537(7622):634–638.
- [Meini et al., 2015] Meini, M.-R., Llarrull, L. I., and Vila, A. J. (2015). Overcoming differences: The catalytic mechanism of metallo- β -lactamases. *FEBS Letters*, 589(22):3419–3432.
- [Meroueh et al., 2006] Meroueh, S. O., Bencze, K. Z., Heseck, D., Lee, M., Fisher, J. F., Stemmler, T. L., and Mobashery, S. (2006). Three-dimensional structure of the bacterial cell wall peptidoglycan. *Proceedings of the National Academy of Sciences*, 103(12):4404–4409.

- [Meroueh et al., 2005] Meroueh, S. O., Fisher, J. F., Schlegel, H. B., and Mobashery, S. (2005). Ab Initio QM/MM Study of Class A β -Lactamase Acylation: Dual Participation of Glu166 and Lys73 in a Concerted Base Promotion of Ser70. *Journal of the American Chemical Society*, 127(44):15397–15407.
- [Meroueh et al., 2003] Meroueh, S. O., Minasov, G., Lee, W., Shoichet, B. K., and Mobashery, S. (2003). Structural Aspects for Evolution of β -Lactamases from Penicillin-Binding Proteins. *Journal of the American Chemical Society*, 125(32):9612–9618.
- [Miller and Salama, 2018] Miller, S. I. and Salama, N. R. (2018). The gram-negative bacterial periplasm: Size matters. In *PLOS Biology*, volume 16, page e2004935. Public Library of Science.
- [Mobley, 2019] Mobley, D. (2019). The Open Force Field 1.0 (Parsley).
- [Mohammadi et al., 2011] Mohammadi, T., Van Dam, V., Sijbrandi, R., Vernet, T., Zapun, A., Bouhss, A., Diepeveen-De Bruin, M., Nguyen-Distè Che, M., De Kruijff, B., and Breukink, E. (2011). Identification of FtsW as a transporter of lipid-linked cell wall precursors across the membrane. *The EMBO Journal*, 30:1425–1432.
- [Moon et al., 2018] Moon, T. M., D’Andréa, É. D., Lee, C. W., Soares, A., Jakoncic, J., Desbonnet, C., Garcia-Solache, M., Rice, L. B., Page, R., and Peti, W. (2018). The structures of penicillin-binding protein 4 (PBP4) and PBP5 from Enterococci provide structural insights into β -lactam resistance. *Journal of Biological Chemistry*, 293(48):18574–18584.
- [Morè et al., 2019] Morè, N., Martorana, A. M., Biboy, J., Otten, C., Winkle, M., Serrano, C. K. G., Silva, A. M., Atkinson, L., Yau, H., Breukink, E., Den Blaauwen, T., Vollmer, W., and Polissi, A. (2019). Peptidoglycan Remodeling Enables Escherichia coli To Survive Severe Outer Membrane Assembly Defect.
- [Morgenstein et al., 2015] Morgenstein, R. M., Bratton, B. P., Nguyen, J. P., Ouzounov, N., Shaevitz, J. W., and Gitai, Z. (2015). RodZ links MreB to cell wall synthesis to mediate MreB rotation and robust morphogenesis. *Proceedings of the National Academy of Sciences*, 112(40):12510–12515.
- [Morinaka et al., 2015] Morinaka, A., Tsutsumi, Y., Yamada, M., Suzuki, K., Watanabe, T., Abe, T., Furuuchi, T., Inamura, S., Sakamaki, Y., Mitsuhashi, N., Ida, T., and Livermore, D. M. (2015). OP0595, a new diazabicyclooctane: mode of action as a serine β -lactamase inhibitor, antibiotic and β -lactam ‘enhancer’. *Journal of Antimicrobial Chemotherapy*, 70(10):2779–2786.
- [Moya et al., 2017] Moya, B., Barcelo, I. M., Bhagwat, S., Patel, M., Bou, G., Papp-Wallace, K. M., Bonomo, R. A., and Oliver, A. (2017). Potent β -Lactam Enhancer Activity of Zidebactam and WCK 5153 against Acinetobacter baumannii, Including Carbapenemase-Producing Clinical Isolates. *Antimicrobial agents and chemotherapy*, 61(11):e01238–17.
- [Munnik et al., 2020] Munnik, M., Lohans, C. T., Langley, G. W., Bon, C., Brem, J., and Schofield, C. J. (2020). A Fluorescence-Based Assay for Screening β -Lactams Targeting the Mycobacterium tuberculosis Transpeptidase Ldt Mt2. *ChemBioChem*, 21(3):368–372.
- [Naas et al., 2017] Naas, T., Oueslati, S., Bonnin, R. A., Dabos, M. L., Zavala, A., Dortet, L., Retailleau, P., and Iorga, B. I. (2017). Beta-lactamase database (BLDB) – structure and function. *Journal of Enzyme Inhibition and Medicinal Chemistry*, 32(1):917–919.
- [Nayler, 1991] Nayler, J. H. (1991). Semi-synthetic approaches to novel penicillins. *Trends in Biochemical Sciences*.
- [Nikaido, 2003] Nikaido, H. (2003). Molecular Basis of Bacterial Outer Membrane Permeability Revisited. *Microbiology and Molecular Biology Reviews*, 67(4):593–656.
- [Nikaido and Takatsuka, 2009] Nikaido, H. and Takatsuka, Y. (2009). Mechanisms of RND multidrug efflux pumps.
- [Oefner et al., 1990] Oefner, C., D’Arcy, A., Daly, J. J., Gubernator, K., Charnas, R. L., Heinze, I., Hub-schwerlen, C., and Winkler, F. K. (1990). Refined crystal structure of β -lactamase from Citrobacter freundii indicates a mechanism for β -lactam hydrolysis. *Nature*, 343(6255):284–288.
- [Ogawara, 2016] Ogawara, H. (2016). Self-resistance in Streptomyces, with Special Reference to β -Lactam Antibiotics. *Molecules*, 21(5):605.

- [Otero et al., 2013] Otero, L. H., Rojas-Altuve, A., Llarrull, L. I., Carrasco-López, C., Kumarasiri, M., Lastochkin, E., Fishovitz, J., Dawley, M., Hesek, D., Lee, M., Johnson, J. W., Fisher, J. F., Chang, M., Mobashery, S., and Hermoso, J. A. (2013). How allosteric control of *Staphylococcus aureus* penicillin binding protein 2a enables methicillin resistance and physiological function. *Proceedings of the National Academy of Sciences of the United States of America*.
- [Ourghanlian et al., 2017] Ourghanlian, C., Soroka, D., and Arthur, M. (2017). Inhibition by Avibactam and Clavulanate of the β -Lactamases KPC-2 and CTX-M-15 Harboring the Substitution N132G in the Conserved SDN Motif. *Antimicrobial Agents and Chemotherapy*, 61(3).
- [Ozbaykal et al., 2020] Ozbaykal, G., Wollrab, E., Simon, F., Vigouroux, A., Cordier, B., Aristov, A., Chaze, T., Matondo, M., and van Teeffelen, S. (2020). The transpeptidase PBP2 governs initial localization and activity of the major cell-wall synthesis machinery in *E. coli*. *eLife*, 9:1–37.
- [Page et al., 2010] Page, M. G., Dantier, C., and Desarbres, E. (2010). In vitro properties of BAL30072, a novel siderophore sulfactam with activity against multiresistant gram-negative bacilli. *Antimicrobial Agents and Chemotherapy*.
- [Page, 2012] Page, M. G. P. (2012). Beta-Lactam Antibiotics. In *Antibiotic Discovery and Development*, pages 79–117. Springer US, Boston, MA.
- [Palzkill, 2013] Palzkill, T. (2013). Metallo- β -lactamase structure and function. *Annals of the New York Academy of Sciences*, 1277(1):91–104.
- [Papp-Wallace, 2019] Papp-Wallace, K. M. (2019). The latest advances in β -lactam/ β -lactamase inhibitor combinations for the treatment of Gram-negative bacterial infections. *Expert Opinion on Pharmacotherapy*, 20(17):2169–2184.
- [Park and Olivier, 2015] Park, I. K. and Olivier, K. N. (2015). Nontuberculous mycobacteria in cystic fibrosis and non-cystic fibrosis bronchiectasis. *Seminars in Respiratory and Critical Care Medicine*, 36(2):217–224.
- [Park and Uehara, 2008] Park, J. T. and Uehara, T. (2008). How Bacteria Consume Their Own Exoskeletons (Turnover and Recycling of Cell Wall Peptidoglycan). *Microbiology and Molecular Biology Reviews*, 72(2):211–227.
- [Patera et al., 2000] Patera, A., Blaszczyk, L. C., and Shoichet, B. K. (2000). Crystal Structures of Substrate and Inhibitor Complexes with AmpC β -Lactamase: Possible Implications for Substrate-Assisted Catalysis. *Journal of the American Chemical Society*, 122(43):10504–10512.
- [Patrick, 2013] Patrick, G. L. (2013). *An Introduction to Medicinal Chemistry*. Oxford University Press.
- [Pazos and Peters, 2019] Pazos, M. and Peters, K. (2019). Peptidoglycan. pages 127–168.
- [Pemberton et al., 2020] Pemberton, O. A., Noor, R. E., Kumar M. V., V., Sanishvili, R., Kemp, M. T., Kearns, F. L., Woodcock, H. L., Gelis, I., and Chen, Y. (2020). Mechanism of proton transfer in class A β -lactamase catalysis and inhibition by avibactam. *Proceedings of the National Academy of Sciences*, 117(11):5818–5825.
- [Penwell et al., 2015] Penwell, W. F., Shapiro, A. B., Giacobbe, R. A., Gu, R.-F., Gao, N., Thresher, J., McLaughlin, R. E., Huband, M. D., DeJonge, B. L. M., Ehmann, D. E., and Miller, A. A. (2015). Molecular Mechanisms of Sulbactam Antibacterial Activity and Resistance Determinants in *Acinetobacter baumannii*. *Antimicrobial Agents and Chemotherapy*, 59(3):1680–1689.
- [Perlstein et al., 2007] Perlstein, D. L., Zhang, Y., Wang, T. S., Kahne, D. E., and Walker, S. (2007). The direction of glycan chain elongation by peptidoglycan glycosyltransferases. *Journal of the American Chemical Society*, 129(42):12674–12675.
- [Peters et al., 2011] Peters, N. T., Dinh, T., and Bernhardt, T. G. (2011). A Fail-Safe Mechanism in the Septal Ring Assembly Pathway Generated by the Sequential Recruitment of Cell Separation Amidases and Their Activators. *Journal of Bacteriology*, 193(18):4973–4983.
- [Peterson and Kaur, 2018] Peterson, E. and Kaur, P. (2018). Antibiotic Resistance Mechanisms in Bacteria: Relationships Between Resistance Determinants of Antibiotic Producers, Environmental Bacteria, and Clinical Pathogens. *Frontiers in Microbiology*, 9(NOV).

- [Plackett, 2020] Plackett, B. (2020). Why big pharma has abandoned antibiotics. *Nature*, 586(7830):S50–S52.
- [Poirel et al., 2010] Poirel, L., Naas, T., and Nordmann, P. (2010). Diversity, Epidemiology, and Genetics of Class D β -Lactamases. *Antimicrobial Agents and Chemotherapy*, 54(1):24–38.
- [Potluri et al., 2010] Potluri, L., Karczmarek, A., Verheul, J., Piette, A., Wilkin, J.-M., Werth, N., Banzhaf, M., Vollmer, W., Young, K. D., Nguyen-Distèche, M., and Den Blaauwen, T. (2010). Septal and lateral wall localization of PBP5, the major D,D-carboxypeptidase of *Escherichia coli*, requires substrate recognition and membrane attachment. *Molecular Microbiology*, 77(2):300–323.
- [Potluri et al., 2012] Potluri, L.-P., Kannan, S., and Young, K. D. (2012). ZipA Is Required for FtsZ-Dependent Preseptal Peptidoglycan Synthesis prior to Invagination during Cell Division. *Journal of Bacteriology*, 194(19):5334–5342.
- [Quintela et al., 1995] Quintela, J. C., Caparros, M., and de Pedro, M. A. (1995). Variability of peptidoglycan structural parameters in Gram-negative bacteria. *FEMS Microbiology Letters*, 125(1):95–100.
- [Raetz and Whitfield, 2002] Raetz, C. R. and Whitfield, C. (2002). Lipopolysaccharide endotoxins.
- [Reading and Cole, 1977] Reading, C. and Cole, M. (1977). Clavulanic Acid: a Beta-Lactamase-Inhibiting Beta-Lactam from *Streptomyces clavuligerus*. *Antimicrobial Agents and Chemotherapy*, 11(5):852–857.
- [Rice et al., 2018] Rice, L. B., Desbonnet, C., Tait-Kamradt, A., Garcia-Solache, M., Lonks, J., Moon, T. M., D’Andréa, É. D., Page, R., and Peti, W. (2018). Structural and regulatory changes in PBP4 trigger decreased β -lactam susceptibility in *Enterococcus faecalis*. *mBio*.
- [Richter et al., 2017] Richter, M. F., Drown, B. S., Riley, A. P., Garcia, A., Shirai, T., Svec, R. L., and Hergenrother, P. J. (2017). Predictive compound accumulation rules yield a broad-spectrum antibiotic. *Nature*, 545(7654):299–304.
- [Rietmeyer et al., 2021] Rietmeyer, L., Fix-Boulier, N., Le Fournis, C., Iannazzo, L., Kitoun, C., Patin, D., Mengin-Lecreulx, D., Ethève-Quelquejeu, M., Arthur, M., and Fonvielle, M. (2021). Partition of tRNAGly isoacceptors between protein and cell-wall peptidoglycan synthesis in *Staphylococcus aureus*. *Nucleic Acids Research*, 49(2):684–699.
- [Rohde, 2019] Rohde, M. (2019). The Gram-Positive Bacterial Cell Wall. *Microbiology Spectrum*, 7(3):1–21.
- [Rohs et al., 2018] Rohs, P. D. A., Buss, J., Sim, S. I., Squyres, G. R., Srisuknimit, V., Smith, M., Cho, H., Sjodt, M., Kruse, A. C., Garner, E. C., Walker, S., Kahne, D. E., and Bernhardt, T. G. (2018). A central role for PBP2 in the activation of peptidoglycan polymerization by the bacterial cell elongation machinery. *PLOS Genetics*, 14(10):e1007726.
- [Ruggiero et al., 2017] Ruggiero, M., Papp-Wallace, K. M., Taracila, M. A., Mojica, M. F., Bethel, C. R., Rudin, S. D., Zeiser, E. T., Gutkind, G., Bonomo, R. A., and Power, P. (2017). Exploring the landscape of diazabicyclooctane (DBO) inhibition: Avibactam inactivation of PER-2 β -Lactamase. *Antimicrobial Agents and Chemotherapy*, 61(6).
- [Ruiz, 2008] Ruiz, N. (2008). Bioinformatics identification of MurJ (MviN) as the peptidoglycan lipid II flippase in *Escherichia coli*. *Proceedings of the National Academy of Sciences*, 105(40):15553–15557.
- [Rybkin et al., 1998] Rybkin, T., Mainardi, J. L., Sougakoff, W., Collatz, E., and Gutmann, L. (1998). Penicillin-binding protein 5 sequence alterations in clinical isolates of *Enterococcus faecium* with different levels of β -lactam resistance. *Journal of Infectious Diseases*.
- [Salje et al., 2011] Salje, J., van den Ent, F., de Boer, P., and Löwe, J. (2011). Direct Membrane Binding by Bacterial Actin MreB. *Molecular Cell*, 43(3):478–487.
- [Sanders and Pavelka, 2013] Sanders, A. N. and Pavelka, M. S. (2013). Phenotypic analysis of *Escherichia coli* mutants lacking l,d-transpeptidases. *Microbiology*, 159(Pt_9):1842–1852.
- [Sari et al., 2011] Sari, R., D’Costa, V. M., King, C. E., Kalan, L., Morar, M., Sung, W. W. L., Schwarz, C., Froese, D., Zazula, G., Calmels, F., Debruyne, R., Golding, G. B., Poinar, H. N., and Wright, G. D. (2011). Antibiotic resistance is ancient. *Nature*.

- [Sauvage et al., 2008] Sauvage, E., Kerff, F., Terrak, M., Ayala, J. A., Charlier, P., M, T., and TD, B. (2008). The penicillin-binding proteins: structure and role in peptidoglycan biosynthesis. *FEMS Microbiology Reviews*, 32(2):234–258.
- [Schiffer and Höltje, 1999] Schiffer, G. and Höltje, J. V. (1999). Cloning and characterization of PBP 1C, a third member of the multimodular class A penicillin-binding proteins of *Escherichia coli*. *Journal of Biological Chemistry*, 274(45):32031–32039.
- [Schrödinger, 2015] Schrödinger, L. (2015). The PyMol Molecular Graphics System, Version 2.4.
- [Segawa et al., 2013] Segawa, T., Takeuchi, N., Rivera, A., Yamada, A., Yoshimura, Y., Barcaza, G., Shinbori, K., Motoyama, H., Kohshima, S., and Ushida, K. (2013). Distribution of antibiotic resistance genes in glacier environments. *Environmental Microbiology Reports*.
- [Seltmann and Holst, 2002] Seltmann, G. and Holst, O. (2002). Periplasmic Space and Rigid Layer. In *The Bacterial Cell Wall*, pages 103–132. Springer Berlin Heidelberg, Berlin, Heidelberg.
- [Sgrignani et al., 2014] Sgrignani, J., Grazioso, G., De Amici, M., and Colombo, G. (2014). Inactivation of TEM-1 by Avibactam (NXL-104): Insights from Quantum Mechanics/Molecular Mechanics Metadynamics Simulations.
- [Sham et al., 2014] Sham, L.-T., Butler, E. K., Lebar, M. D., Kahne, D., Bernhardt, T. G., and Ruiz, N. (2014). MurJ is the flippase of lipid-linked precursors for peptidoglycan biogenesis. *Science*, 345(6193):220–222.
- [Shields et al., 2017] Shields, R. K., Chen, L., Cheng, S., Chavda, K. D., Press, E. G., Snyder, A., Pandey, R., Doi, Y., Kreiswirth, B. N., Nguyen, M. H., and Clancy, C. J. (2017). Emergence of Ceftazidime-Avibactam Resistance Due to Plasmid-Borne blaKPC-3 Mutations during Treatment of Carbapenem-Resistant *Klebsiella pneumoniae* Infections. *Antimicrobial Agents and Chemotherapy*, 61(3).
- [Shields et al., 2016] Shields, R. K., Potoski, B. A., Haidar, G., Hao, B., Doi, Y., Chen, L., Press, E. G., Kreiswirth, B. N., Clancy, C. J., and Nguyen, M. H. (2016). Clinical Outcomes, Drug Toxicity, and Emergence of Ceftazidime-Avibactam Resistance Among Patients Treated for Carbapenem-Resistant Enterobacteriaceae Infections: Table 1. *Clinical Infectious Diseases*, 63(12):1615–1618.
- [Shih et al., 2003] Shih, Y.-L., Le, T., and Rothfield, L. (2003). Division site selection in *Escherichia coli* involves dynamic redistribution of Min proteins within coiled structures that extend between the two cell poles. *Proceedings of the National Academy of Sciences*, 100(13):7865–7870.
- [Shiomi et al., 2013] Shiomi, D., Toyoda, A., Aizu, T., Ejima, F., Fujiyama, A., Shini, T., Kohara, Y., and Niki, H. (2013). Mutations in cell elongation genes *mreB*, *mrdA* and *mrdB* suppress the shape defect of *RodZ*-deficient cells. *Molecular Microbiology*, 87(5):1029–1044.
- [Silhavy et al., 2010] Silhavy, T. J., Kahne, D., and Walker, S. (2010). The Bacterial Cell Envelope. *Cold Spring Harbor Perspectives in Biology*, 2(5):a000414–a000414.
- [Singh et al., 2012] Singh, S. K., SaiSree, L., Amrutha, R. N., and Reddy, M. (2012). Three redundant murein endopeptidases catalyse an essential cleavage step in peptidoglycan synthesis of *Escherichia coli* K12. *Molecular Microbiology*, 86(5):1036–1051.
- [Sjodt et al., 2018] Sjodt, M., Brock, K., Dobihal, G., Rohs, P. D. A., Green, A. G., Hopf, T. A., Meeske, A. J., Srisuknimit, V., Kahne, D., Walker, S., Marks, D. S., Bernhardt, T. G., Rudner, D. Z., and Kruse, A. C. (2018). Structure of the peptidoglycan polymerase RodA resolved by evolutionary coupling analysis. *Nature*, 556(7699):118–121.
- [Sjodt et al., 2020] Sjodt, M., Rohs, P. D. A., Gilman, M. S. A., Erlandson, S. C., Zheng, S., Green, A. G., Brock, K. P., Taguchi, A., Kahne, D., Walker, S., Marks, D. S., Rudner, D. Z., Bernhardt, T. G., and Kruse, A. C. (2020). Structural coordination of polymerization and crosslinking by a SEDS-bPBP peptidoglycan synthase complex. *Nature Microbiology*, 5(6):813–820.
- [Smoum et al., 2012] Smoum, R., Rubinstein, A., Dembitsky, V. M., and Srebnik, M. (2012). Boron Containing Compounds as Protease Inhibitors. *Chemical Reviews*, 112(7):4156–4220.

- [Söderström et al., 2016] Söderström, B., Mirzadeh, K., Toddo, S., von Heijne, G., Skoglund, U., and Daley, D. O. (2016). Coordinated disassembly of the divisome complex in *Escherichia coli*. *Molecular Microbiology*, 101(3):425–438.
- [Söderström et al., 2014] Söderström, B., Skoog, K., Blom, H., Weiss, D. S., von Heijne, G., and Daley, D. O. (2014). Disassembly of the divisome in *Escherichia coli*: Evidence that FtsZ dissociates before compartmentalization. *Molecular Microbiology*, 92(1):1–9.
- [Soroka et al., 2014] Soroka, D., Dubée, V., Soulier-Escrihuela, O., Cuinet, G., Hugonnet, J. E., Gutmann, L., Mainardi, J. L., and Arthur, M. (2014). Characterization of broad-spectrum mycobacterium abscessus class A β -lactamase. *Journal of Antimicrobial Chemotherapy*.
- [Soroka et al., 2016] Soroka, D., Ourghanlian, C., Compain, F., Fichini, M., Dubée, V., Mainardi, J.-L., Hugonnet, J.-E., and Arthur, M. (2016). Inhibition of β -lactamases of mycobacteria by avibactam and clavulanate. *Journal of Antimicrobial Chemotherapy*, page dkw546.
- [Spratt, 1975] Spratt, B. G. (1975). Distinct penicillin binding proteins involved in the division, elongation, and shape of *Escherichia coli* K12. *Proceedings of the National Academy of Sciences*, 72(8):2999–3003.
- [Strynadka et al., 1996] Strynadka, N. C., Martin, R., Jensen, S., Gold, M., and Jones, J. B. (1996). Structure-based design of a potent transition state analogue for TEM-1 β -lactamase. *Nature Structural & Molecular Biology*, 3(8):688–695.
- [Strynadka et al., 1992] Strynadka, N. C. J., Adachi, H., Jensen, S. E., Johns, K., Sielecki, A., Betzel, C., Sutoh, K., and James, M. N. G. (1992). Molecular structure of the acyl-enzyme intermediate in β -lactam hydrolysis at 1.7 Å resolution. *Nature*, 359(6397):700–705.
- [Sun, 2003] Sun, T. (2003). Comparison of β -lactamases of classes A and D: 1.5-Å crystallographic structure of the class D OXA-1 oxacillinase. *Protein Science*, 12(1):82–91.
- [Tacconelli et al., 2017] Tacconelli, E., Carrara, E., Savoldi, A., Kattula, D., and Burkert, F. (2017). GLOBAL PRIORITY LIST OF ANTIBIOTIC-RESISTANT BACTERIA TO GUIDE RESEARCH, DISCOVERY, AND DEVELOPMENT OF NEW ANTIBIOTICS. Technical report, WHO.
- [Taguchi et al., 2019] Taguchi, A., Welsh, M. A., Marmont, L. S., Lee, W., Sjødt, M., Kruse, A. C., Kahne, D., Bernhardt, T. G., and Walker, S. (2019). FtsW is a peptidoglycan polymerase that is functional only in complex with its cognate penicillin-binding protein. *Nature Microbiology*, 4(4):587–594.
- [Tamma et al., 2019] Tamma, P. D., Doi, Y., Bonomo, R. A., Johnson, J. K., Simner, P. J., Tamma, P. D., Doi, Y., and Bonomo, R. A. (2019). A Primer on AmpC β -Lactamases: Necessary Knowledge for an Increasingly Multidrug-resistant World. *Clinical Infectious Diseases*, 69(8):1446–1455.
- [Templin et al., 1992] Templin, M., Edwards, D., and Höltje, J. (1992). A murein hydrolase is the specific target of bulgecin in *Escherichia coli*. *Journal of Biological Chemistry*, 267(28):20039–20043.
- [Templin et al., 1999] Templin, M. F., Ursinus, A., and Höltje, J. V. (1999). A defect in cell wall recycling triggers autolysis during the stationary growth phase of *Escherichia coli*. *EMBO Journal*, 18(15):4108–4117.
- [Tipper and Strominger, 1965] Tipper, D. J. and Strominger, J. L. (1965). Mechanism of action of penicillins: a proposal based on their structural similarity to acyl-D-alanyl-D-alanine. *Proceedings of the National Academy of Sciences of the United States of America*, 54(4):1133–1141.
- [Tomanicek et al., 2011] Tomanicek, S. J., Wang, K. K., Weiss, K. L., Blakeley, M. P., Cooper, J., Chen, Y., and Coates, L. (2011). The active site protonation states of perdeuterated Toho-1 β -lactamase determined by neutron diffraction support a role for Glu166 as the general base in acylation. *FEBS Letters*, 585(2):364–368.
- [Tonge, 2018] Tonge, P. J. (2018). Drug–Target Kinetics in Drug Discovery. *ACS Chemical Neuroscience*, 9(1):29–39.
- [Tooke et al., 2019] Tooke, C. L., Hinchliffe, P., Bragginton, E. C., Colenso, C. K., Hirvonen, V. H., Takebayashi, Y., and Spencer, J. (2019). β -Lactamases and β -Lactamase Inhibitors in the 21st Century. *Journal of Molecular Biology*, 431(18):3472–3500.

- [Tremblay et al., 2010] Tremblay, L. W., Xu, H., and Blanchard, J. S. (2010). Structures of the Michaelis Complex (1.2 Å) and the Covalent Acyl Intermediate (2.0 Å) of Cefamandole Bound in the Active Sites of the Mycobacterium tuberculosis β -Lactamase K73A and E166A Mutants,. *Biochemistry*, 49(45):9685–9687.
- [Tripathi and Nair, 2013] Tripathi, R. and Nair, N. N. (2013). Mechanism of Acyl–Enzyme Complex Formation from the Henry–Michaelis Complex of Class C β -Lactamases with β -Lactam Antibiotics. *Journal of the American Chemical Society*, 135(39):14679–14690.
- [Tsivkovski et al., 2020] Tsivkovski, R., Totrov, M., and Lomovskaya, O. (2020). Biochemical Characterization of QPX7728, a New Ultrabroad-Spectrum Beta-Lactamase Inhibitor of Serine and Metallo-Beta-Lactamases. *Antimicrobial Agents and Chemotherapy*, 64(6).
- [Turck, 1982] Turck, M. (1982). Extended-spectrum cephalosporins and related lactams. *Journal of Antimicrobial Chemotherapy*.
- [Uehara and Park, 2008] Uehara, T. and Park, J. T. (2008). Growth of Escherichia coli: Significance of Peptidoglycan Degradation during Elongation and Septation. *JOURNAL OF BACTERIOLOGY*, 190(11):3914–3922.
- [Uehara et al., 2010] Uehara, T., Parzych, K. R., Dinh, T., and Bernhardt, T. G. (2010). Daughter cell separation is controlled by cytokinetic ring-activated cell wall hydrolysis. *The EMBO Journal*, 29(8):1412–1422.
- [van den Akker and Bonomo, 2018] van den Akker, F. and Bonomo, R. A. (2018). Exploring Additional Dimensions of Complexity in Inhibitor Design for Serine β -Lactamases: Mechanistic and Intra- and Inter-molecular Chemistry Approaches. *Frontiers in Microbiology*, 9(APR):1–10.
- [van den Ent et al., 2014] van den Ent, F., Izoré, T., Bharat, T. A., Johnson, C. M., and Löwe, J. (2014). Bacterial actin MreB forms antiparallel double filaments. *eLife*, 3:2634.
- [van Heijenoort, 2011] van Heijenoort, J. (2011). Peptidoglycan Hydrolases of Escherichia coli. *Microbiology and Molecular Biology Reviews*, 75(4):636–663.
- [van Teeffelen et al., 2011] van Teeffelen, S., Wang, S., Furchtgott, L., Huang, K. C., Wingreen, N. S., Shaevitz, J. W., and Gitai, Z. (2011). The bacterial actin MreB rotates, and rotation depends on cell-wall assembly. *Proceedings of the National Academy of Sciences*, 108(38):15822–15827.
- [Varma et al., 2007] Varma, A., de Pedro, M. A., and Young, K. D. (2007). FtsZ Directs a Second Mode of Peptidoglycan Synthesis in Escherichia coli. *Journal of Bacteriology*, 189(15):5692–5704.
- [Vázquez-Ucha et al., 2020] Vázquez-Ucha, J. C., Arca-Suárez, J., Bou, G., and Beceiro, A. (2020). New carbapenemase inhibitors: Clearing the way for the β -lactams. *International Journal of Molecular Sciences*, 21(23):1–32.
- [Vollmer, 2008] Vollmer, W. (2008). Structural variation in the glycan strands of bacterial peptidoglycan. *FEMS Microbiology Reviews*, 32(2):287–306.
- [Vollmer and Bertsche, 2008] Vollmer, W. and Bertsche, U. (2008). Murein (peptidoglycan) structure, architecture and biosynthesis in Escherichia coli. *Biochimica et Biophysica Acta (BBA) - Biomembranes*, 1778(9):1714–1734.
- [Vollmer et al., 2008] Vollmer, W., Blanot, D., and De Pedro, M. A. (2008). Peptidoglycan structure and architecture.
- [Vollmer and Seligman, 2010] Vollmer, W. and Seligman, S. J. (2010). Architecture of peptidoglycan: more data and more models. *Trends in Microbiology*, 18(2):59–66.
- [von Rechenberg et al., 1996] von Rechenberg, MORITZ, Ursinus, A., and Holtje, J.-V. (1996). Affinity Chromatography as a Means to Study Multienzyme Complexes Involved in Murein Synthesis. *Microbial Drug Resistance*, 2(1):155–157.
- [Walkup et al., 2015] Walkup, G. K., You, Z., Ross, P. L., Allen, E. K. H., Daryaei, F., Hale, M. R., O’Donnell, J., Ehmann, D. E., Schuck, V. J. A., Buurman, E. T., Choy, A. L., Hajec, L., Murphy-Benenato, K., Marone, V., Patey, S. A., Grosser, L. A., Johnstone, M., Walker, S. G., Tonge, p. J., and Fisher, S. L. (2015). Translating slow-binding inhibition kinetics into cellular and in vivo effects. *Nature Chemical Biology*, 11(6):416–423.

- [Wang et al., 2016] Wang, D. Y., Abboud, M. I., Markoulides, M. S., Brem, J., and Schofield, C. J. (2016). The road to avibactam: the first clinically useful non- β -lactam working somewhat like a β -lactam. *Future Medicinal Chemistry*.
- [Weiner et al., 2001] Weiner, J. H., Sambasivarao, D., and Rothery, R. A. (2001). Bacterial Cytoplasmic Membrane. In *Encyclopedia of Life Sciences*. John Wiley & Sons, Ltd, Chichester.
- [Welsh et al., 2019] Welsh, M. A., Schaefer, K., Taguchi, A., Kahne, D., and Walker, S. (2019). Direction of Chain Growth and Substrate Preferences of Shape, Elongation, Division, and Sporulation-Family Peptidoglycan Glycosyltransferases. *Journal of the American Chemical Society*, 141(33):12994–12997.
- [Wientjes and Nanninga, 1989] Wientjes, F. B. and Nanninga, N. (1989). Rate and topography of peptidoglycan synthesis during cell division in *Escherichia coli*: concept of a leading edge. *Journal of Bacteriology*, 171(6):3412–3419.
- [Wientjes et al., 1985] Wientjes, F. B., Pas, E., Taschner, P. E., and Woldringh, C. L. (1985). Kinetics of uptake and incorporation of meso-diaminopimelic acid in different *Escherichia coli* strains. *Journal of Bacteriology*, 164(1):331–337.
- [WOLDRINGH et al., 1987] WOLDRINGH, C. L., HULS, P., PAS, E., BRAKENHOFF, G. J., and NANNINGA, N. (1987). Topography of Peptidoglycan Synthesis during Elongation and Polar Cap Formation in a Cell Division Mutant of *Escherichia coli* MC4100. *Microbiology*, 133(3):575–586.
- [Woodward, 1980] Woodward, R. B. (1980). Penems and related substances. *Philosophical Transactions of the Royal Society of London. B, Biological Sciences*, 289(1036):239–250.
- [Yahav et al., 2020] Yahav, D., Giske, C. G., Grāmatniece, A., Abodakpi, H., Tam, V. H., and Leibovici, L. (2020). New β -Lactam- β -Lactamase Inhibitor Combinations. *Clinical Microbiology Reviews*, 34(1).
- [Yang et al., 2011] Yang, D. C., Peters, N. T., Parzych, K. R., Uehara, T., Markovski, M., and Bernhardt, T. G. (2011). An ATP-binding cassette transporter-like complex governs cell-wall hydrolysis at the bacterial cytokinetic ring. *Proceedings of the National Academy of Sciences*, 108(45):E1052–E1060.
- [Yang et al., 2017] Yang, X., Lyu, Z., Miguel, A., McQuillen, R., Huang, K. C., and Xiao, J. (2017). GTPase activity-coupled treadmilling of the bacterial tubulin FtsZ organizes septal cell wall synthesis. *Science*, 355(6326):744–747.
- [Young et al., 2019] Young, K., Painter, R. E., Raghoobar, S. L., Hairston, N. N., Racine, F., Wisniewski, D., Balibar, C. J., Villafania, A., Zhang, R., Sahm, D. F., Blizzard, T., Murgolo, N., Hammond, M. L., and Motyl, M. R. (2019). In vitro studies evaluating the activity of imipenem in combination with relebactam against *Pseudomonas aeruginosa*. *BMC Microbiology*, 19(1):150.
- [Yousif et al., 1985] Yousif, S. Y., BROOME-SMITH, J. K., and SPRATT, B. G. (1985). Lysis of *Escherichia coli* by β -Lactam Antibiotics: Deletion Analysis of the Role of Penicillin-binding Proteins 1A and 1B. *Microbiology*, 131(10):2839–2845.
- [Yunck et al., 2016] Yunck, R., Cho, H., and Bernhardt, T. G. (2016). Identification of MltG as a potential terminase for peptidoglycan polymerization in bacteria. *Molecular Microbiology*, 99(4):700–718.
- [Zapun et al., 2008] Zapun, A., Contreras-Martel, C., and Vernet, T. (2008). Penicillin-binding proteins and β -lactam resistance. *FEMS Microbiology Reviews*, 32(2):361–385.
- [Zerbib, 2017] Zerbib, D. (2017). Bacterial Cell Envelopes: Composition, Architecture, and Origin. In *Handbook of Electroporation*, volume 1, pages 417–436. Springer International Publishing, Cham.
- [Zhang et al., 2010] Zhang, Y., Bao, Q., Gagnon, L. A., Huletsky, A., Oliver, A., Jin, S., and Langae, T. (2010). ampG Gene of *Pseudomonas aeruginosa* and Its Role in β -Lactamase Expression. *Antimicrobial Agents and Chemotherapy*, 54(11):4772–4779.
- [Zhao et al., 2017] Zhao, H., Patel, V., Helmann, J. D., and Dörr, T. (2017). Don’t let sleeping dogmas lie: new views of peptidoglycan synthesis and its regulation. *Molecular Microbiology*, 106(6):847–860.

Summary

Bacterial peptidoglycan (PG) is a mesh like structure comprising glycan strands cross-linked by peptide stems. Since PG is a specific and essential component of bacterial cells it is an attractive and validated target for antibacterial agents. Indeed, the first antibiotic in clinical use - the β -lactam penicillin - targets the enzymes catalyzing the final transpeptidation step of PG synthesis - the Penicillin-Binding-Proteins (PBPs). A prevalent mechanism of resistance to β -lactams is the production of β -lactamases (β Ls) that inactivate the drugs. A first generation of β -lactamase inhibitors (BLIs) was based on the β -lactam core followed by diazabicyclooctanes (DBOs), which entered the market in 2015 with avibactam. Emergence of mutations compromising the efficacy of DBOs prompted us to study a series of triazole-substituted DBOs that were obtained by click chemistry. The triazole ring was found to be disfavored due to the absence of a hydrogen bond connecting the carboxamide of marketed DBOs to a conserved asparagine residue (N132) of β Ls. However, functionalization of the triazole partially restored inhibition efficacy without impairing drug penetration. Besides the major cross-links formed by PBPs, alternative cross-links are formed by the structurally distinct L,D-transpeptidases (LDTs) mediating resistance to several β -lactams. We investigated the mechanisms of insertion of new subunits into the expanding PG mesh by developing a method based on labeling with heavy isotopes and mass spectrometry. We report the modes of PG polymerization and the extent of combined recycling and turnover in strains relying either on both PBPs and an LDTs or on a single LDT for PG cross-linking.

Keywords: Antimicrobial resistance; β -lactamase; β -lactamase inhibitor; Diazabicyclooctane; peptidoglycan metabolism; peptidoglycan polymerization.

Résumé

Le peptidoglycane (PG) forme un réseau covalent comprenant des chaînes glycanes reliées par des peptides. Le PG est une cible validée pour développer de nouveaux antibiotiques parce que c'est un composant spécifique et essentiel des bactéries. En effet, les antibiotiques appartenant à la famille des β -lactamines inactivent les protéines de liaisons à la pénicilline (PLP) qui catalysent la dernière étape de polymérisation du PG. Un mécanisme de résistance répandu de résistance est la production de β -lactamases (β L) qui inactivent les β -lactamines. Une première génération d'inhibiteurs de β L a été basée sur le noyau β -lactame suivi par les diazabicyclooctanes (DBO) entrés sur le marché en 2015 avec l'avibactam. L'émergence de mutations compromettant l'efficacité des DBO nous a incités à étudier une série de dérivés obtenus par chimie click qui contenaient un groupement triazole. Ce dernier s'est avéré défavorable en raison de l'absence de la liaison hydrogène reliant le carboxamide des DBO commercialisés à un résidu asparagine conservé (N132) des β L. La fonctionnalisation du triazole a partiellement restauré l'efficacité des DBO sans altérer leur pénétration. Les PLP peuvent être remplacées par des L,D-transpeptidases (LDT) entraînant une résistance aux β -lactamines. Nous avons étudié le mode d'insertion de nouvelles sous-unités dans le PG en expansion en développant une nouvelle méthode basée sur le marquage avec des isotopes lourds et la spectrométrie de masse. Nous rapportons les modes de polymérisation du PG dans des souches utilisant des PBP et une LDT, seules ou en combinaison, et en présence ou en absence de β -lactamine, ainsi que la participation du recyclage au métabolisme du PG.

Mots-clés : β -lactamase; Diazabicyclooctane; Inhibiteur de β -lactamase; Métabolisme du peptidoglycane; Polymérisation du peptidoglycane; Résistance aux antimicrobiens.